Syntheses of novel tris(pyrid-2-yl) and tris(2,2'-bipyrid-6-yl) methanol derivatives and their coordination chemistries

Neha Singh

ProQuest LLC
789 East Eisenhower Parkway
P.O. Box 1346
Ann Arbor, MI 48106-1346

DECLARATION

This work has not previously been accepted in substance for any degree and is not concurrently submitted in candidature for any degree.

Signed .....N. Singh..... (candidate) Date ...09 June 08.....

STATEMENT 1

This thesis is being submitted in partial fulfillment of the requirements for the degree of .....Ph.D.....(insert MCh, MD, MPhil, PhD etc, as appropriate)

Signed ...N. Singh..... (candidate) Date ...09 June 08.....

STATEMENT 2

This thesis is the result of my own independent work/investigation, except where otherwise stated. Other sources are acknowledged by explicit references.

Signed .....N. Singh..... (candidate) Date ...09 June 08.....

STATEMENT 3

I hereby give consent for my thesis, if accepted, to be available for photocopying and for inter-library loan, and for the title and summary to be made available to outside organisations.

Signed .....N. Singh..... (candidate) Date ...09 June 08.....

STATEMENT 4: PREVIOUSLY APPROVED BAR ON ACCESS

I hereby give consent for my thesis, if accepted, to be available for photocopying and for inter-library loans **after expiry of a bar on access previously approved by the Graduate Development Committee.**

Signed .....N. Singh..... (candidate) Date ...09 June 08.....

Abstract

The work presented in this thesis describes the synthesis, structure and stability of a range of tris(2-pyrid-2-yl) and tris(2,2'-bipyrid-6-yl)methanol derivatives and their coordination chemistries with some divalent transition metals. A number of different synthetic strategies are investigated in order to synthesise these tripodal ligands in reasonable yields. The routes that proved to be most successful involved the carbonylation and Stille coupling of 6-bromopyrid-2-yl derivatives in the presence of a palladium catalyst, tetrakis triphenylphosphine palladium(0) ($Pd(PPh_3)_4$).

By adapting the method published by Peng and Aguilar, mono, bis and tris(6-sodium carboxylate pyrid-2-yl)methanol derivatives were successfully synthesised. These led to the introduction of a number of novel mono, bis and tris(6-methylcarboxypyrid-2-yl)methanol intermediates that were also successfully characterised by crystallographic studies. The solid-state structures reveal some interesting topologies of the ligand due to the flexibility introduced to the coordination sphere by the methyl ester groups. Further spectroscopic analyses involve ultra-violet, infra-red, nuclear magnetic resonance spectroscopy, mass spectrometry, elemental analysis and electrochemisty.

The work presented by Leize *et al.* led to the syntheses of mono, bis and tris(2,2'-bipyrid-6-yl)methanol derivatives. Again some interesting topologies are revealed from their crystallographic data of their metal complexes. A number of geometries are identified throughout this study. Interestingly, these tripodal ligands reveal trigonal prismatic coordination with Zn and Fe metal centres whereas the Cu(II) ion of d^9 configuration only exhibits one Jahn-Teller distortion (a distorted octahedron) with only one of the ligands synthesised, the (2,2'-bipyrid-6-yl)bis(pyrid-2-yl)methanol. The other Cu geometries discussed are square pyramidal or trigonal bipyramidal. Typically the Ni(II) complexes characterised exhibit pseudo-octahedral coordination with solvent molecules occupying the apical position.

Acknowledgements

Firstly, I would like to thank my supervisors, Dr Angelo Amoroso and Professor Peter Edwards for their help and support throughout this project. Also thanks to Dr Simon Aldridge for the many discussions and advice.

Thanks to Dr Li-Ling and Dr Tom Tatchell for crystallography, also to Swansea Mass Spectrometry service and to the technical staff at Cardiff University especially Rob Jenkins and Robin.

Many Thanks to the members of Lab. 1.124 and 1.125, in particular Mark, Debs and Bres for passing on their much appreciated advice and techniques. To Cerys for being a great friend throughout, Mini for keeping me entertained, Tom, Bunn, Becky, Ruth, Jo and Dan. Also I would like to thank my boyfriend Darragh, for his love and encouragement to help complete this thesis.

Finally and most importantly I would like to thank my family especially Mum and Papa for their love, support and encouragement throughout my life. My sisters, Rashmi and Radha and my brother Rahul.

Glossary / Abbreviations

Å	Angstrom, 1 x 10^{-10} metre
ACS	American Chemical Society
amtp	tris(2-(1-pyrazolyl)methyl) amine
bipy	2,2'-bipyridine
BOX	bisoxazolines
Bp	dihydrobis(pyrazolyl)borate
b	broad
ca.	circa
cc	clathro chelate
cm^{-1}	wavenumber, unit of frequency (= ν/c)
cm^3	cubic centimetre
δ	chemical shift
$CDCl_3$	deuterated chloroform
$CHCl_3$	chloroform
CH_2Cl_2	dichloromethane
CH_3CN	acetonitrile
CT	charge transfer
CV	cyclic voltammetry
d	doublet
dd	doublet of doublets
DCM	dichloromethane
DMF	dimethylformamide
DMSO	dimethylsulfoxide
DMSO-d_6	deuterated dimethylsulfoxide
D_2O	deuterated water
dota	tetraazacyclododecane –N,N',N",N"'-tetraacetic acid
dpk	di-2-pyridyl ketone
dtpa	diethylenetriamine-pentaacetic acid
ε	extinction coefficient in $M^{-1}cm^{-1}$
EIMS	electron ionisation mass spectrometry
en	ethylenediamine
ESMS	electrospray mass spectrometry

Et_2O	diethyl ether
Etpy	ethylpyridine
FAB	fast atom bombardment
Fc/Fc^+	ferrocene/ferricinium
FTIR	Fourier Transform Infra Red
HOMO	highest occupied molecular orbital
H_3tpaa	α,α',α"nitrilotri(6-methyl-1-pyridinecarboxylic acid)
Hz	hertz, s^{-1}
IR	infrared
Im	imidazolyl
i-Pr	isopropyl
J	coupling constant in Hertz
KBr	potassium bromide
λ	wavelength in nm
LMCT	ligand to metal charge transfer
LUMO	lowest unoccupied molecular orbital
M	a general metal or molar (mol dm^{-3})
M^+	molecular ion
m	multiplet or medium
mcpba	*meta*-chloroperbenzooic acid
me	methyl
MeOH	methanol
MLCT	metal to ligand charge transfer
m/z	mass / charge ratio
n-BuLi	*n*-butyl lithium
nm	nanometres
NMR	Nuclear Magnetic Resonance spectroscopy
ntb	tris(2-benzimidazolylmethyl) amine
Oh	octahedral
PA	picolinic acid
$P(bipy)_3$	tris(6(2,2'-bipyridyl))phosphine
PccBF	fluoroborotris(2-carboxaldimino-6-pyridyl)phosphine
$Pd(PPh_3)_4$	tetrakistriphenylphosphine palladium (II)
Ph	phenyl

$P(Mepox)_3$	tris(2-*O*-methylcarboxaldimino-6-pyridyl)phosphine
ppm	parts per million
py	pyridine
$(py)_3tach$	*cis,cis*-1,3,5-tris(pyridine-2-carboxaldimino)cyclohexene
$(py)_3tame$	1,1',1''-tris(pyridine-2-carboxaldimino)ethane
$(py)_3tren$	1,1',1''-tris(pyridine-2-carboxaldimino)nitrilotriethane
pz	pyrazolyl
q	quartet
RSC	Royal Society of Chemistry
s	singlet or strong
SBP	square based pyramidal / square pyramidal
sh	sharp
SP	square planar
spa	N^3-Salicycloylpyridine-2-carboxamidrazonato
t	triplet
TAP	trigonal antiprismatic
TBP	trigonal bipyramidal
TCPM	tris(6-carboxypyrid-2-yl)methanol
Td	tetrahedral
terpy	terpyridine
THF	tetrahydrofuran
tmima	tris(2-(1-methtlimidazolyl)methyl)amine
tmqa	tris(2-quinolylmethyl)amine
TMS	trimethylsilane
TOX	trisoxazolines
TP	trigonal prismatic
Tp	hydrotris(pyrazolyl)borate
tpa	tris(2-pyridylmethyl)amine
tpAs	tris (2-pyridyl)arsenic
tpb	tris(pyrazolyl)borate
tpmOH	tris(2-pyridyl)methanol
tpN	tris(2-pyridyl)amine
tpm	tris(2-pyridylmethyl)methane
tqtaea	tris-8-quinolyl-tris(2-aminoethyl)amine

tren	tris(2-aminoethyl)amine
trioxma	tris[4,4-dimethyl-2-(4,5-dihyrooxazolyl)]methylamine
T4IA	tris(4-(1-methylimidazolyl)methylamine
UV	ultra violet
ν	frequency in hertz
Vis.	Visible
VSEPR	valence shell electron pair repulsion
w	weak
w/w	weight / weight
X	a general halide

Contents

Chapter One

Introduction into Tripodal Ligands

1.1 Introduction

Numerous chemists have previously carried out work into the synthesis of tripodal ligands. They have shown that these ligands are typically facially coordinating, tridentate chelates which have received a great deal of interest in both coordination and organometallic chemistry. Over the last three decades, there have been hundreds of published articles and reviews reporting a wide variety of metal complexes that contain tripodal ligands. Mainly the reports concentrate on polypyrazolylborate ligands[1-5] but in this thesis, the main interests are tripod ligands, which contain pyridine donors such as tris(2-pyridyl) or tris(2,2'-bipyridyl). Previous literature has noted that pyridine donors are better σ donors than pyrazoles and tend to be better π-acidic ligands, hence transition metal complexes that use tris(pyridyl) ligands, show a sufficient amount of variation in overall charge, solubility, and redox properties compared to complexes that contain tris(pyrazolyl) ligands.[6]

The contents of this chapter aim to summarise the literature reports that are most relevant to the chemistry presented within this thesis; firstly a brief overview of the appropriate background to transition metal coordination chemistry in tripod systems is discussed and secondly, some well known tripodal nitrogen donor ligand reports are highlighted, together with a summary of their coordination chemistry with some transition metals.

1.2 A brief overview of transition metal coordination numbers

A d-block metal has a total of nine atomic valence orbitals. Some of these are used to form bonds with ligands, while others are nonbonding. The nonbonding electrons are lone pairs; these exert much less influence on geometry of transition metal complexes than the compounds in the main group, which tend to be directional (hence the VSEPR Rules).[7] Coordination numbers in the transition metal complexes of polydentate tripodal systems (some of which are discussed later) are mainly four (very few), five, and six being the most common, however two, three and seven are also seen.

1.2.1 Four coordinate complexes

Four is the least common of the three coordination numbers, but contains two of the most important geometries, tetrahedral (T_d being the most common) and square planar (SP), however there are many examples of intermediate or distorted geometries. These geometries can easily be determined by the use of X-ray crystallography, angles around a metal atom can instantly distinguish between square planar and tetrahedral complexes. Typically, square planar geometries possess four 90° *cis* angles around a metal atom (4 *cis* angles add up to 360° in a perfect SP geometry) and tetrahedral coordination have three 109.4° angles around the central metal atom.[8] Deviations from typical geometries can often occur due to the steric constraints of a ligand and can therefore be calculated, it is an important factor to consider when characterising novel complexes.

The size of a metal ion is important in determining whether the adopted configuration will be tetrahedral or some higher coordination number. If the metal cation is small, or the ligands are large, then steric effects might compensate for the advantage

found in forming more metal-ligand bonds.[9,10] It is also important to note that the number of d electrons in the central transition metal determines whether a four-coordinate transition metal complex is tetrahedral or square planar; it is energetically advantageous for d^8 metal ions (e.g. Pt^{2+}, Pd^{2+} Ni^{2+} and Rh^{+}) to adopt a square planar geometry, the eight d-electrons achieve some stabilization in energy by occupying the dzx, dyz, dz^2, and dxy orbitals (see Figure 1.4 for splitting diagram).[9,10]

1.2.2 Five coordinate complexes

There are two important five coordinate geometries of complexes; trigonal bipyramidal (TBP) and square based pyramidal (SBP, Figure 1.1).

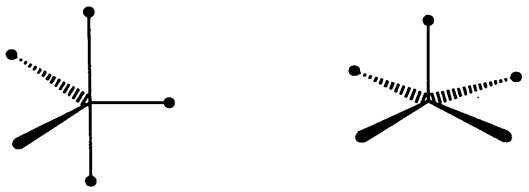

Figure 1.1 trigonal bipyramidal (left), square pyramidal (right).

An analysis of the two geometries suggests that the energy difference between the trigonal bipyramidal and square pyramidal structures are marginal. It is therefore relatively easy to interconvert between these two structures with relatively small movements of the five ligands. Consequently many of the above structures exist with geometries intermediate between the two limiting coordination geometries. It is also common for the ligands physically to exchange between the sites, in which case the compound is referred to as fluxional.[7,9,10] Interestingly, for a five coordinate system the degree of trigonal bipyramidal or square based pyramidal character can be measured by the τ value (also known as Berry Pseudo Rotation),[11] a useful parameter introduced by

Reedijk *et al.*[12] The parameter is dependent upon the two angles, α and β, where α is the smaller of the two basal plane angles and β is therefore the larger; for example are labelled as follows:

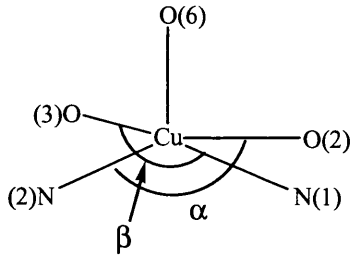

The parameter τ is defined as (β – α) / 60, and the values are reported from 0 in square pyramidal systems to 1 in trigonal bipyramidal.

1.2.3 Six coordinate complexes

The most common coordination number for d-block metal complexes with tripodal systems is six. For several decades, all six coordinate metal complexes were assumed to be octahedral (O_h) including the first tris(dithiolene) metal complex to be prepared, namely $Mo[S_2C_2(CF_3)_2]_3$ obtained in 1963.[13] However, the structural information on such metal tris(dithiolene) became available through X-ray diffraction, this assumption was shown to be false. The first demonstration of a non-octahedral structure for a metal tris(dithiolene) was the discovery of a trigonal prismatic (TP) structure for the rhenium complex $Re(S_2C_2Ph_2)_3$ in 1965.[14,15] Since then theoretical studies in order to rationalise this unusual trigonal prismatic geometry have been reported and typically occur in ML_6 complexes in which the electronic configuration of the metal is $d^{0,6,8,10}$.[16-18] There are many instances of structural distortions brought about by the metal's electronic configuration or by the ligands involved. Coordination geometries intermediate between the trigonal prismatic (TP) and octahedron (O_h) limit have been demonstrated for a

number of tris-chelate species.[19,20] The Baliar twist illustrated in Figure 1.2 shows the stages from a trigonal prism to the octahedron is measured by the twist angle θ where, θ = 0° and θ = 60° respectively. Intermediate stages of the Bailar twist (e.g. θ = 30°) have only C_3 symmetry rather than the higher D_{3h} and O_h symmetries of the trigonal prism and octahedron respectively.[21]

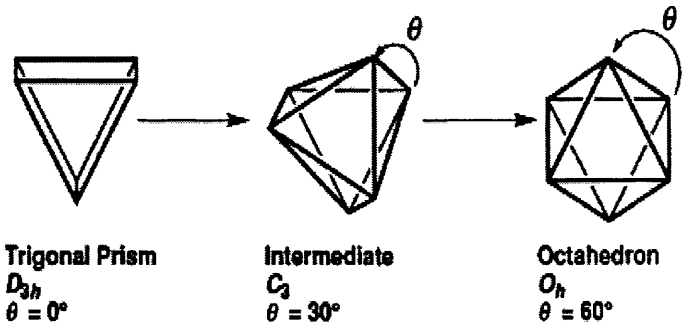

Figure 1.2 The 'Baliar twist' interconverting the octahedron and trigonal prism through C_3 intermediate shows the definition of the angle θ.[22]

In addition, close inspection of donor-metal-donor bond angles obtained from X-ray data can also help distinguish between the two geometries. That is, for an octahedral complex one would expect twelve L-M-L 90° angles and three 180° angles.[21] However, the applications of a Bailar twist to this polyhedron results in a trigonal prism, which has six 90° angles (A-M-B, three for each triangular face), three 70.5° angles (A-M-C) and six 131.7° angles (A-M-D) (see Figure 1.3).[21]

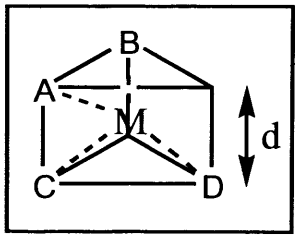

Figure 1.3 Bond angles associated with trigonal prismatic metal centres.

1.2.4 The chelate effect

Complexes of polydentate ligands tend to be more stable than those with comparable monodentate ligands.[7,9] For example, the following reaction is favourable:

$$[Ni(NH_3)_6]^{2+} + 3en \rightleftharpoons [Ni(en)_3]^{2+} + 6NH_3$$

en is ethylenediamine, $H_2NCH_2CH_2NH_2$

This is purely a thermodynamic phenomenon where two factors are considered:

i) In the above equilibrium the entropy of the system increases from left to right since more free molecules are produced. $\Delta G = \Delta H - T\Delta S$ and $\Delta G = -RT\ln K$, assuming enthalpy change is approximately equal for NH_3 and en, ΔG is more favourable for formation of the en complex and therefore the equilibrium lies to the right.

ii) Once one end of the chelating ligand is coordinated it is more favourable to coordinate the other end than to bring in an external ligand. This is because, with one end of the ligand attached to the metal the other end is relatively constrained, i.e. it does not have full freedom of movement, therefore not so much entropy is lost as would be in the case if another ligand is brought in from the solution.

The size of the resulting chelate ring in a complex is also a factor in the chelate effect. Three chelate rings in a complex represent a more stable situation than two chelate rings, and in turn this is a more stable situation than one ring.

Planar five membered chelate rings are closest to the tetrahedral, sp^3, value of 109°. For rings with more than five members, puckering occurs to give suitable bond angles. For rings with less than five members the bond angle are significantly smaller than

the tetrahedral value and there is a large amount of strain in the ring and therefore tend to be unfavourable.[7,9]

1.2.5 Crystal field splitting diagrams seen in tripodal systems

Although the octahedral arrangement of six ligands around a metal centre is the most prevalent for transition metal complexes, distorted octahedral, tetrahedral, square planar and trigonal prismatic geometries are also seen in tripodal systems. In the case of a tetrahedral complex the arrangement of ligands and orbitals is such that there will be lesser electrostatic interaction between the ligands and the dz^2 and dx^2-y^2 orbitals than with the dxy, dxz, dyz orbitals. The opposite splitting pattern is observed for complexes with octahedral symmetry and is shown in Figure 1.4.

The degree of interaction between the ligands and orbitals is less in the tetrahedral case, the reason being that only four ligands are causing the splitting rather than six. The symmetry labels for these sets of orbitals are e and t_2 and reflect the fact that the tetrahedral point group does not have a centre of symmetry, thus removing the distinction between gerade and ungerade. The energy gap between the two sets of orbitals is labelled as Δ_t and it is just under half the size of the octahedral gap Δ_o as given below;[7,9]

$$\Delta_t = \frac{4}{9} \Delta_o$$

The four coordinate square planar shape adopted, mainly, by a number of the heavy, late-transition metal complexes (d^8 electronic configuration). The energy level diagram for this system is obtained by considering an octahedral complex and then removing two *trans*-ligands, which maybe the two on the z-axis. As these ligands are pulled away from the metal centre, the interaction with the metal d-orbitals possessing a z-

component will decrease resulting in a lowering of the energy of the dz^2 and, to a lesser extent, of the dxz and dyz. To counter this the energy of the remaining orbitals will increase. As these two ligands are pulled further away along the z-axis, the energies of the orbitals are affected further until the ligands are completely removed resulting in a square planar complex and the energy level diagram resembles that shown in Figure 1.4.[23]

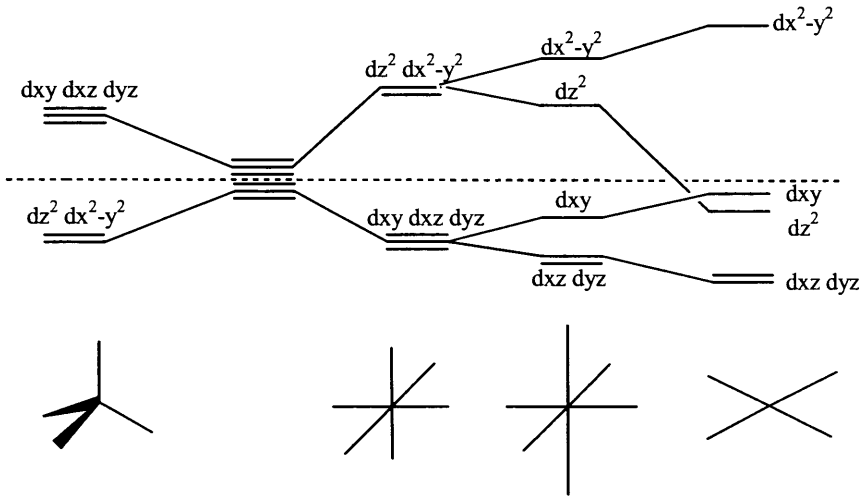

Figure 1.4 Energy level diagrams for (in order from left to right); tetrahedral, octahedral, distorted octahedral, and square planar geometry.

1.2.5.1 Second order Jahn-Teller distortion of an octahedron to a trigonal prism

The distortion of an octahedron to a trigonal prism in six-coordinate complexes of $d^{<4}$ early transition metals can result from a second-order Jahn-Teller effect involving the splitting of the t_{1u} HOMO and the t_{2g} LUMO in order to allow mixing of the resulting e' orbitals in the trigonal prismatic geometry (see Figure 1.5). This effect causes a small $t_{1u} - t_{2g}$ energy gap and is favoured when the ligands are strong σ-donors but weak π-donors and the metal is not too electropositive such as is the case with many tris(dithiolenes) d^0 metal complexes.[22]

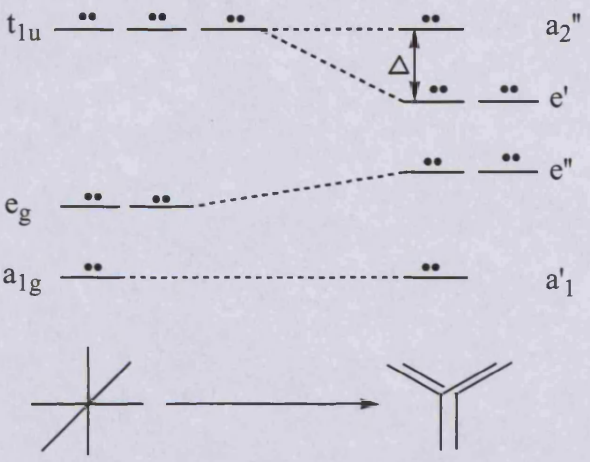

Figure 1.5 Changes in molecular orbitals in going from an octahedron to a trigonal prism for a d^0 metal complex.[22]

1.2.5.2 Significance of Crystal Field Theory (CFT)

Crystal Field Theory (CFT) has proved to be an extremely simple but useful method of introducing the bonding, spectra and magnetism of first-row transition metal complexes.

In the interpretation of spectra, it is usual to start with an octahedral Ti^{3+} complex with a d^1 electronic configuration. CFT predicts that because of the different spatial distribution of charge arising from the filling of the five d-orbitals, those orbitals pointing towards bond axes will be destabilised and those pointing between axes will be stabilised.

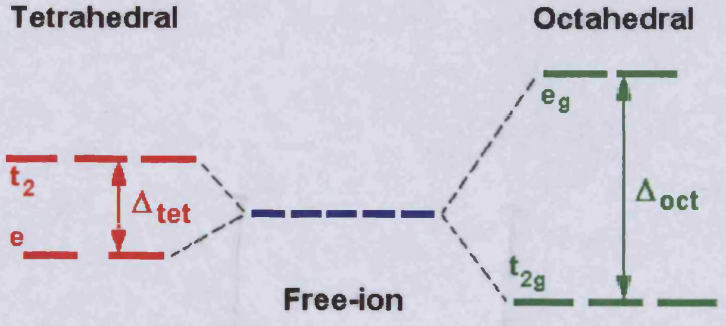

Figure 1.6 Energy separation of the two subsets in Tetrahedral (T_d) and Octahedral (O_h) complexes.

The t_{2g} and e_g subsets are then populated from the lower level first, which for d^1 gives a final configuration of $t_{2g}^1\ e_g^0$. Figure 1.6 shows the energy separation of the two subsets equals the splitting value Δ (or D_q) and ligands can be arranged in order of increasing Δ, which is called the spectrochemical series and is essentially independent of metal ion. For all octahedral complexes except high spin d^5, simple CFT would therefore predict that only 1 band should appear in the electronic spectrum corresponding to the absorption of energy equivalent to Δ. If we ignore spin-forbidden lines, this is borne out by d^1, d^9 as well as to d^4, d^6. The observation of 2 or 3 peaks in the electronic spectra of d^2, d^3, d^7 and d^8 high spin octahedral complexes requires further treatment involving electron-electron interactions. [7,9]

Tanabe-Sugano diagrams (an example is shown in Figure 1.7) have been extensively used to interpret the spectra of octahedral complexes and will be used herein. The procedure involves finding the ratio of the energies of the second to first absorption peak (i.e. v2/v1) and from this locate the position along the X-axis from which Δ/B can be determined. B is the Racah parameter, its a measure of electron-electron repulsion and relates to the free ion. The apparent value B in a complex is always less than the free ion value because electrons on the metal can be delocalised into molecular orbitals covering both the metal and the ligands. Having found the Δ/B value, tracing a vertical line up the diagram will give the values (in E/B units) of all spin-allowed and spin-forbidden transitions from which B for the complex can be calculated and subsequently the third band can also be predicted (E/B (of the third band) x B).[7,9]

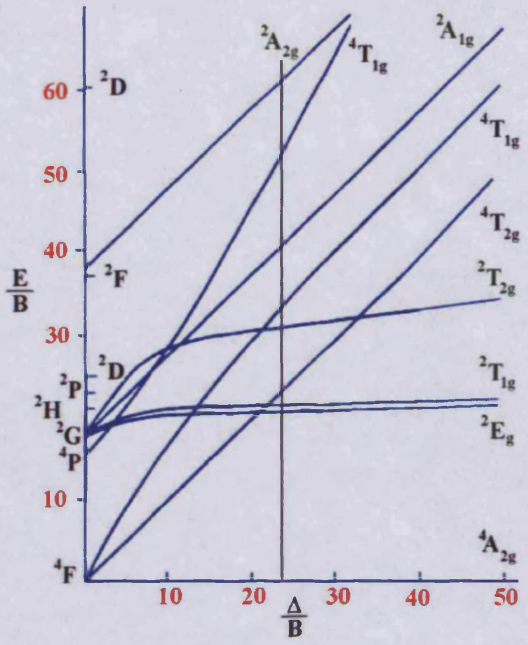

Figure 1.7 Tanabe Sugano Diagram, for O_h d^8 Complexes.[7,9]

A number of known octahedral complexes have been characterised this way, their Δ (or D_q) and B values are useful in characterising complexes and determining the degree of distortions from the ideal geometry, these will be discussed in detail later.

1.3 Coordination chemistries of tridentate tripodal ligands

1.3.1 Tris(2-pyridyl) tripod ligands

In this thesis there are a series of tripodal ligands that all contain aromatic nitrogen donors. In particular the work has been dominated by the tris(2-pyridyl)methanol (tpmOH) frame work and the ligands synthesised in chapters 2 and 4 are derivatives.

A review by Szczepura *et al.*[24] describes the chemistry of carbon-bridged tris(2-pyridyl) tripod ligands as well as an examination of recent studies involving nitrogen-bridged, phosphorus-bridged, and arsenic-bridged analogues to the carbon-bridged ligands (Figure 1.8). Those tripods that are more relevant to this thesis will be discussed along

with the coordination of these derivatives with transition metals (in particular first row) are included for discussion and comparison with future chapters.

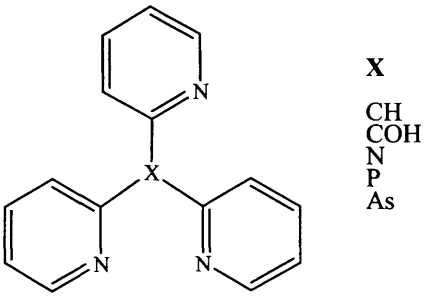

Figure 1.8 Tris(2-pyridyl) tripodal derivatives.[24]

1.3.1.1 Tripod ligands with nitrogen as the bridgehead atom

Tris(2-pyridyl) amine, tpN, which is the pyridine analogue of triphenylamine, was first prepared by Wibaut and La Batside in 1933.[25] This tertiary amine was synthesised by the condensation of 2-halopyridine with 2-aminopyridine. The first condensation generates the secondary amine, di(2-pyridyl) amine and this intermediate is then further reacted with excess 2-halopyridine to give the desired product.

The coordination of tpN to transition metals is shown in Figure 1.9, it was first reported by McWhinnie *et al.* in 1966, establishing the ability of tpN to coordinate to $Mo(CO)_6$ to form $Mo(tpN)(CO)_3$.[26]

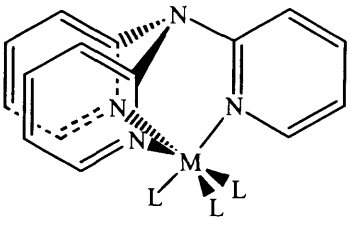

Figure 1.9 The basic structure of octahedral transition metal complexes containing a single tris(2-pyridyl) tripod ligand.[26]

Later, work by Kaizaki and Legg reported the synthesis of $[Cr(tpN)Cl_3]$ in their structural characterisation of octahedral metal complexes of the type $[MX_3(py\text{-}d_5)_3]$ (M = Cr(III), Mo(III); X = Cl^-, Br^-, F^-, NCS^-) by H^1 NMR spectroscopy.[27] Not long after $[W(tpN)Cl_4]$ was prepared by Monsy and Crabtree in 1996.[28] TpN was proposed to coordinate in a tridentate fashion, but no ^1H NMR spectroscopic data could be obtained due to the complex being paramagnetic and no crystallographic analysis could be performed due to unsuitable crystals. When $Fe(ClO_4)_2$ was reacted with tpN, the spectroscopy and diamagnetism indicated the formation of $[Fe(tpN)_2](ClO_4)_2$. Crystallographic data implied the structure to be only slightly distorted from octahedral geometry.[29] Further work by Lancaster and McWhinnie reported the reaction of 4- and 5-methyl-2-pyridyldi(pyrid-2-yl)amine (4- and 5-npdpN) with $Fe(ClO_4)_2$, yielded the octahedral bis(tripod) complexes, $[Fe(L)_2](ClO_4)_2$ (L = 4- or 5-mpdpN). McWhinnie *et al.* also investigated the reaction of one equivalent of ligand with various nickel / zinc(II) salts. Ni / ZnX_2 (X = Cl^-, Br^- or NO_3^-) would form octahedral complexes $[Ni(tpN)(H_2O)_2X]X$, while the combination of NiX_2 (where X = ClO_4^- or NO_3^-) with two equivalents of tpN results in the formation of octahedral complexes $[Ni(tpN)_2]X_2$. The tpN coordinates in a tridentate fashion in both cases. However, the zinc would form tetrahedral complexes $[Zn(tpN)X_2]$, containing bidentate tpN.[30]

Reactions of $Co(ClO_4)_2$ with the tripod ligands tpN, tpP, tpP=O, or tpAs results in the formation of the sandwiched complexes, $[Co(tripod)_2](ClO_4)_2$, where the tripod ligands are coordinated in a tridentate fashion to the metal centre. Crystallographic analysis of $[Co(tpN)_2](ClO_4)_2$ was performed and, unlike the iron(II) analogue which was reported to deviate only slightly from the octahedral geometry, the cobalt(II) species was

found to show greater deviations. Similarly, the reactions of $Co(NO_3)_2$ with tpN results in the formation of $[Co(tpN)_2](NO_3)_2$. $[Co(tpN)_2X_2]$ complexes (X = Br^-, Cl^- or NCS^-) have been prepared and the ligand coordinates in a bidentate fashion. These complexes readily isomerise to form the $[Co(tpN)_2](CoX_4)$ complexes, where the tripod ligand now binds in a tridentate fashion. It was not until 1982 that the bidentate coordination of tpN with Cu(II) ions was demonstrated using X-ray crystallography. Complexes prepared by Iber and Marks *et al.* as models of the active site in certain copper containing proteins were characterised.[31,32] In 1992 Boys *et al.* confirmed through X-ray crystal structure analysis the structure predicted by McWhinnie *et al.* for the complex of $[Cu(tpN)_2(ClO_4)_2]$.[33] The coordination geometry was a tetragonally distorted octahedron. The tpN were coordinated along the equatorial positions while the two perchlorates anions were weakly coordinated along the axial positions.

1.3.1.2 Tripod ligands with carbon as the bridgehead atom

The preparation of the pyridyl-based tripod ligands with carbon bridgeheads are based on a reaction developed by the group of Wibaut *et al.* in 1951 where lithiopyridine reacts with dipyridyl ketone.[34] During the ongoing investigation into the utility of 2- and 3-lithiopyridine as reagents in organic synthesis, the pyridine-based analogue to triphenylcarbinol, tris(2-pyridyl) methanol (tpmOH), was prepared as illustrated in Scheme 1.1. It was noted that in strongly acidic solutions tpmOH did not undergo spectroscopic changes similar to triphenylcarbinol. The change in this behaviour was possibly due to the high electronegativity of nitrogen (in pyridine), which inductively caused the central carbon bridgehead atom to become partially positive, thus

strengthening the bond between the carbon and the hydroxy group. This enhanced interaction caused the dissociation of the hydroxy group to become less favourable in tpmOH than in triphenylmethanol.

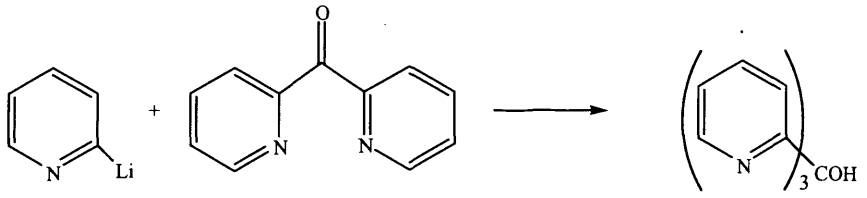

Scheme 1.1 Synthesis of tpmOH adapted from Wibaut *et al.*[34]

Several tpmOH derivatives have been synthesised while designing a new series of chelating ligands by White and Faller.[36] In their preparations, tpmOH was converted to tris(2-pyridyl) bromomethane which was then reacted with *n*-BuLi. Subsequent reaction with water yielded tpm in a 55% yield. The authors went on to report the synthesis of the following chelates: tris(2-pyridyl)bromomethane, tris(2-pyridyl)chloromethane, tris(2-pyridyl)ethoxymethane, tris(2-pyridyl)methylacetate, tris(2-pyridyl)methoxyl-$_k$*N*,$_k$*O*](difluoroborne), and *n*-[tris(2-pyridyl)methyl]analine. This series of compounds demonstrates the richness of the chemistry associated with the tpm core structure. By changing substituents on the bridgehead carbon, properties such as solubility, overall charge of the complexes, and the potential modes of attachment to supports were varied, demonstrating the potential use of the tpm structure in a variety of applications.

Various authors have extensively studied coordination modes of tpmOH with first row transition metals. Typically these tripod ligands coordinate in a tridentate fashion through the pyridyl nitrogens as shown in Figure 1.10, however examples of other modes of coordination has been observed, such as bidentate coordination through two pyridyl groups or one pyridyl group plus the bridgehead heteroatom have been reported. Of all the

ligands mentioned in this section, only tpmOH has shown to coordinate in a tridentate manner through two pyridyl groups and the bridgehead group to a single transition metal centre (see Figure 1.10, *N, N', O*-tpmOH and *N, N', O*-tpmO$^-$ coordination modes).[24]

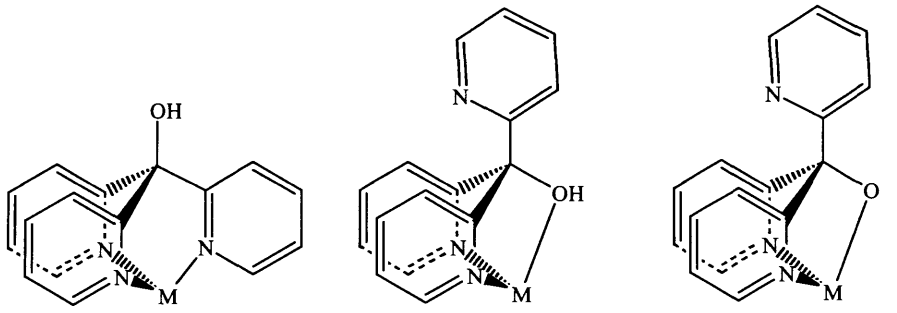

N, N', N''-tpmOH *N, N', O*-tpmOH *N, N', O*-tpmO$^-$

Figure 1.10 The observed charges and binding modes of the tris(2-pyridyl)methanol ligand.

The synthesis and characterisation of transition metal complexes containing two tpmOH ligands was first reported by Boggess and Boberg.[39] The coordination modes were based on spectroscopic data as structural data could not be obtained. Later, Boggess *et al.* clarified the coordination modes of each of the tpmOH ligands by further spectral studies.[40] The transition metals which were studied included, Ni(II), Fe(II), Mn(II), Cu(II) and Zn(II). $[Cu(tpmOH)_2](ClO_4)_2$ is paramagnetic and its UV-vis spectrum is similar to $[Cu(tpN)_2]^{2+}$ indicating a symmetric (*N, N', N''*-tpmOH) coordination mode for both tpmOH ligands.[45] The zinc(II) complex was proposed to have a similar coordination mode based on ^{1}H NMR spectroscopy.[45] Three different iron(II) complexes were isolated and identified as [Fe(*N, N', N''*-tpmOH)(*N, N', N''*-tpmOH)]$^{2+}$, [Fe(*N, N', N''*-tpmOH)(*N, N', O*-tpmOH)]$^{2+}$, and [Fe(*N, N', N''*-tpmOH)(*N, N', O*-tpmO$^-$)]$^+$. The preparation of these complexes depends on the method used.[41] The manganese(II) and

nickel(II) complexes have coordination sphere similar to the above unsymmetrical iron(II) complex.[41]

In addition to the above complexes, Boggess and Boberg went on to report the preparation of a bis(tpmOH) cobalt complex.[39] Although the crystal structure data was not obtained the coordination mode as (*N, N', N''*-tpmOH)(*N, N', O*-tpmO$^-$), was based on spectroscopic (IR and electronic) data.[39] The coordination of tpmOH to cobalt was investigated by Szalda and Keene.[41] Depending on the solvent in which the reaction was conducted, two complexes were prepared, the symmetrical [Co(III)(*N, N', N''*-tpmOH)$_2$](ClO$_4$)$_3$ complex and the unsymmetrical [Co(III)(*N, N', N''*-tpmOH)(*N, N', O*-tpmO$^-$)](ClO$_4$)$_2$ complex. A crystal structure of the symmetric complex, [Li(*N, N', N''*-tpmOH)$_2$](S$_2$O$_6$)$_3$·10H$_2$O was obtained, proving the (*N, N', N''*-tpmOH)(*N, N', N''*-tpmOH) coordination mode.

Later, Canty *et al.* discovered another mode of coordination for tpmOH. Reaction of [InMe$_2$](NO$_3$) with tpmOH resulted in the isolation of monomethylindium(III) complex containing a bimetallic cation.[42] The [(InMe)$_2${tpmO}$_2$(NO$_3$)(H$_2$O)]NO$_3$ complex is the first and only report of tpmO$^-$ acting as a bridging ligand between two metal centres and has a proposed structure as shown in Figure 1.11.

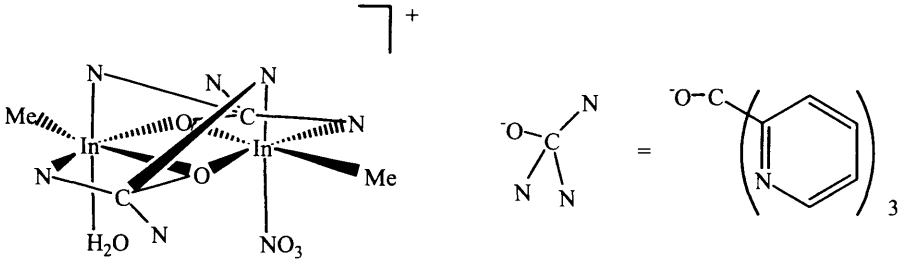

Figure 1.11 The first complex containing a bridging tris(2-pyridyl)tripod ligand, [(InMe)$_2${tpmO}$_2$(NO$_3$)(H$_2$O)]$^+$.[42]

1.3.1.3 Applications of tris(2-pyridyl) tripod ligands

1.3.1.3.1 Modelling biological systems

The use of tpmOH and other tridentate tripodal ligands were studied by Brown and Huguet.[43] They prepared a number of zinc(II) complexes which were investigated as possible models for the active sites of carbonic anhydrase enzyme. The p*K*a values and the binding abilities (pK_M^{2+}) for a number of ligands complexed to Zn(II), Co(II), Ni(II) and Cu(II) were determined. The order of binding constants is Cu(II)>Zn(II)>Ni(II)>Co(II), and while the tpmOH and substituted analogues resulted in the hightest binding affinity for Cu(II), only one ligand displayed exactly the same trend with all the metals as carbonic anhydrase. The Zn(II) complex did not catalyse the hydrolysis of of *p*-nitrophenol or the hydration of acetaldehyde. The tpmOH complexes were shown not to be good structural models for carbonic anhydrase.

Other ions such as molybdenum(III) and tungsten(III) were of much interest to Cote who investigated the stabilisation of these metal centres due to their possible involvement in biological systems. These stable M(III) complexes were very rare in 1983 since most of them were oxidised to yield M(IV) species. It was found that the tridentate tris(pyrazolyl)borate (tpb) ligand stabilised the monomeric M(III). Therefore, the ability of tpN to stabilise these metal centres were investigated by Cote.[44]

Kodera *et al.* prepared viable hemerythrin models using tpm based tripod ligands (see Figure 1.12). This ligand stabilised oxo-bridged di-iron species that were synthesised as models for the active sites of non-heme iron proteins.[45]

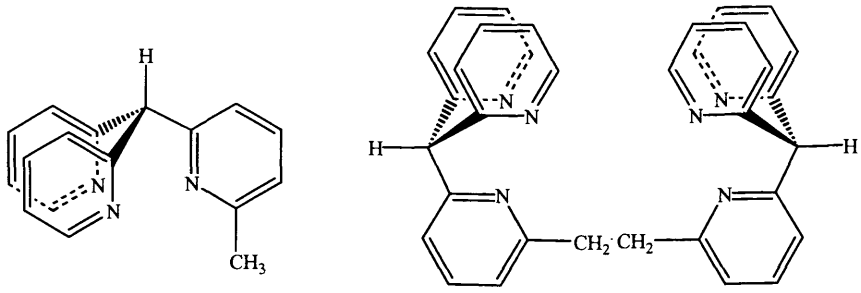

Figure 1.12 Tris(2-pyridyl) tripod ligands used to prepare models of non-heme iron proteins.

Copper based products obtained as a result of the oxidation of Cu(I) to Cu(II) were of much interest to Marks and Iber.[46] Firstly, because Cu(I) ions are commonly used as catalysts in a variety of oxidation-based enzymatic and non-enzymatic reactions and secondly, Cu(I) ions are readily oxidised aerobically. They utilised tpN ligands and synthesised the copper cluster $[Cu_4(OH)_4(SO_3CF_3)(tpN)_4][(SO_3CF_3)]_2$ from the oxidation of $[Cu(tpN)(SO_3CF_3)]$ complex, its crystal structure showed a cubane-like cluster with four copper atoms at alternating vertices and oxygen from hydroxy groups at the remaining four vertice. This cluster was structurally reminiscent of the iron cubane-type clusters, which are often associated with biological processes.

1.3.1.3.2 Catalysis

Faller and Ma prepared $[(tpm)M(CO)(NO)_2](SbF_6)_2$ (M = Mo or W).[47] These complexes readily lose CO to give $[(tpm)M(NO)_2]^{2+}$, which catalyse Diels-Alder reactions between methyl vinyl ketone and 1,3-butadiene. Faller and Gundersen further investigated the catalytic properties. They reported $[(tpm)W(NO)_2(CO)](SbF_6)_2$ catalyses the addition of silylated *C*-nucleophiles to carbonyl compounds as well as the addition of TMS-CN to carbonyl compounds (Scheme 1.2). The catalyst is recovered easily and can be reused in further reactions with high percentage yields.[48]

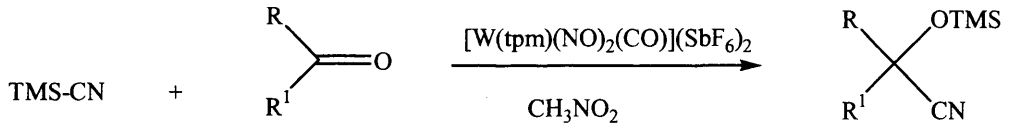

Scheme 1.2 $[(tpm)W(NO)_2(CO)](SbF_6)_2$ readily loses CO and is an active catalyst in the above reaction.

Moberg *et al.* investigated ways of attaching complexes containing tpmOH onto polymeric supports to yield heterogeneous catalysts.[49] One of the polymeric materials synthesised displayed catalytic activity towards the ring opening of epoxides (such as styrene oxide) by methanol. The polymer could be reused, although the reactivity decreased after each cycle.

1.3.1.4 Tris(2-pyridylmethyl)methane (tpm)

Tris(2-pyridylmethyl)methane, tpm was first reported by Clavereul *et al.* in 1987. It was synthesised by a simple reaction involving the addition of formyl acetate to the lithium carbanion of 2-picoline in THF followed by protonation, affording the tripodal ligand (Scheme 1.3).[50]

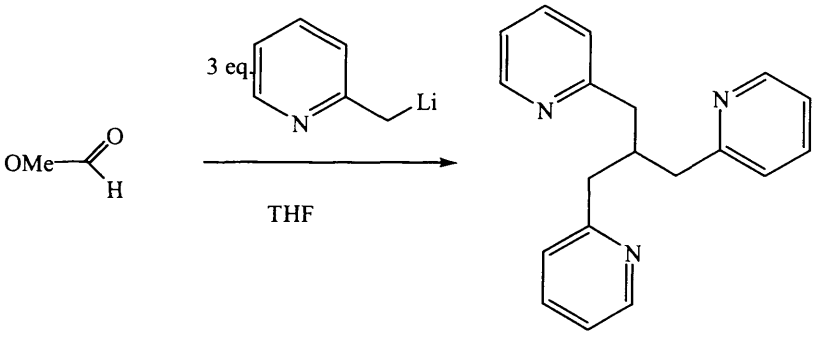

Scheme 1.3 Synthesis of Tris(2-pyridylmethyl)methane, tpm.

Coordination chemistry of first row transition metals with the tpm ligand has not been investigated to the extent of tpN and tpmOH, although other metals such as Mo, W, Rh, Ru, Pd and Pt has been researched thoroughly over the last couple of decades. In 1995 Astely *et al.* reported the synthesis and characterisation of $[Cu(tpm)_2](NO_3)_2$.[37] The crystallographic analysis showed that all six Cu-N bonds were equivalent, which is unusual because Cu(II) complexes with a coordination number of six usually display a tetragonally distorted octahedral geometry. Despite the crystal structure, other spectroscopic data confirmed that the Cu(II) centre was a tetragonally distorted octahedron. Also, around this time Zvargulis *et al.* isolated and characterised the zinc complex, $[Zn(tpm)_2]^{2+}$.[38]

Owing to the flexible nature of their spacer, they may be able to adopt various conformations in solutions. A recent publication by Lee *et al.* investigated a series of ligands and their complexation to $AgClO_4$.[51] One of the complexes reported and structurally characterised was $[Ag_3(tpm)_2](ClO_4)_2$ (Figure 1.13).

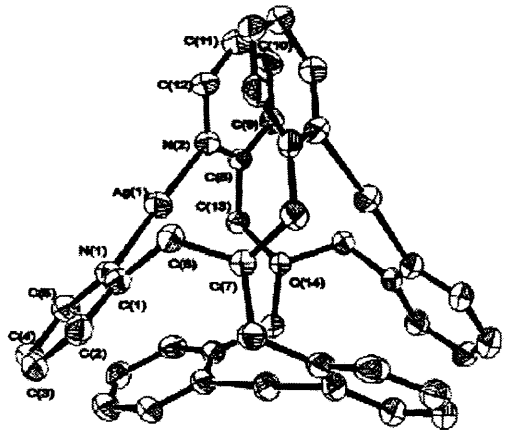

Figure 1.13 View of the cage structure of complex $[Ag_3(tpm)_2](ClO_4)_2$.[51]

Figure 1.13 shows the discrete trinuclear supramolecular cage structure of the complex. The M_3L_2 type cagelike complexes are not well documented up to now. Two

tripodal ligands (tpm) are aggregated by the simultaneous coordination of their pyridine nitrogen atoms to three silver ions to form a C_3 symmetric cage structure.

1.3.2 Ligands containing three aromatic N-donor atoms.

1.3.2.1 Polypyrazolyl Borates

Poly(pyrazolyl)borate ligands are versatile ligands in physio-chemical, bio-inorganic and structurally oriented coordination chemistry. The parent compounds are dihydrobis(pyrazolyl)borate (Bp) and hydrotris(pyrazolyl)borate (Tp) (Figure 1.14).

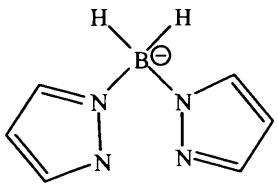

Bp

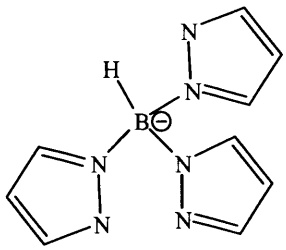

Tp

Figure 1.14 Examples of Poly(pyrazolyl)borates.

This class of ligands, also known as scorpionate ligands, were first discovered by Trofimenko in the mid 1960s,[52,53] their coodination chemistry has been extensively developed with particular interest arising out of the ability of these ligands to modify or control the steric and electronic environment about the metal centre by variation of the pyrazolyl group. The term "scorpionate ligand" specifically refers to tris(pyrazolyl)borate, a BH unit bound to three pyrazolyl arms, the "pincers" of the compound refer to two of the pyrazolyl groups ($C_3H_4N_2$) that can bind a metal, where the third pyrazolyl group, the tail, can move forward to "sting" the metal, holding it more firmly in place via tridentate coordination (Figure 1.15). The R group attached to the boron centre is usually hydrogen but can also be phenyl and alkyl groups. When the "stinger" is the same as the "pincers,"

then the compound is considered a homoscorpionate, but when the stinger is different from the pincers, it is considered to be heteroscorpionate.[54]

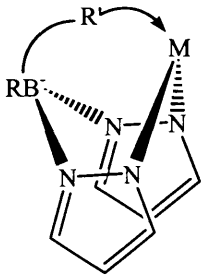

Figure 1.15 The pinch and sting of the Scorpionate Ligands.

These ligands are usually synthesised by reacting pyrazole with alkali-metal borohydrides, such as sodium borohydride $NaBH_4$, under reflux. H_2 is evolved as the borohydride is sequentially converted first to pyrazolylborate $[H_3B(C_3N_2H_3)]^-$, then to dipyrazolyborate $[H_2B(C_3N_2H_3)_2]^-$, and finally to tris(pyrazoly)borate $[HB(C_3N_2H_3)_3]^-$. Bulky pyrazolyl borates can be prepared from 3,5-disubstituted pyrazoles, such as the dimethyl dervative.[55] These bulky pyrazolyl borates have proven especially valuable in the preparation of catalysts and models for enzyme active sites. Utilising scorpionate ligands in the syntheses of metal catalysts may allow simpler and more accurate methods to be developed. The ligand allows for good shielding of the bound metal while strong sigma bonds between the nitrogens and the metal stabilise the complex.[56] The unsubstituted Tp ligand forms bis-ligand Tp_2M complexes (M = Fe(II), Co(II), Ni(II), Cu(II), Zn(II)) even in the presence of excess metal ion.[52]

In general, however, the pyrazolylborates are tripodal ligands that include a diverse set of structures as shown in Figure 1.16.[55] The ligands can also be tetradentate, bidentate, or monodentate, depending on the number of donor substituents on the boron and the steric congestion around the metal. Nitrogen heterocycles other than pyrazole can be used,

such as pyrrole, imidazole, indole, indazole and triazole.[57-61] In addition, tripodal pyrazole based ligands can have central atoms other than boron, such as carbon, phosphorus, or gallium. Similar ligands can also bind metals through sulphur, phosphorus, or other donor atoms. Other modifications include having a methylene between the central atom and the donor group as seen in Figure 1.16.

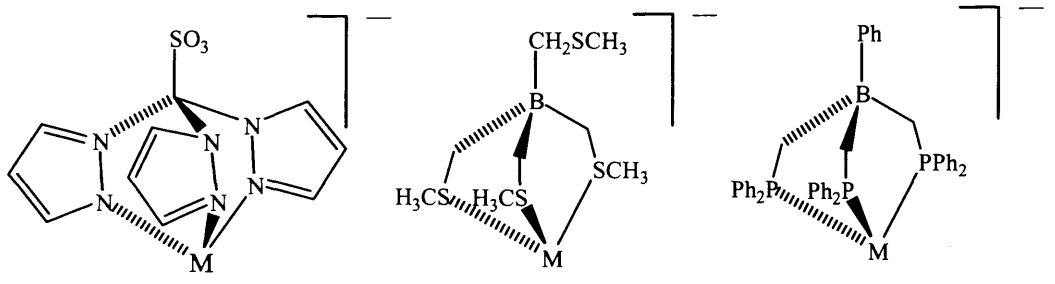

Tris(pyarzolyl)methane-sulfonate

Tris[(methylthio) methyl]borate

Tris[diphenyl phosphinomethyl] borate

Figure 1.16 VARIATIONS Tripodal ligands include a diverse set of structures that can be multidentate with N, S, or P donor atoms.[55]

1.3.2.2 Tris(pyrazolyl)alkane

Poly(pyrazolylalkanes remained unexplored for a long time, mainly due to difficulties in the preparation of large quantity of these ligands. Only recently several researchers have contrasted the chemistry of the neutral poly(pyrazolyl)alkanes with that previously developed for anionic poly(pyrazolyl)borates.[52-55]

Tris(pyrazolyl)alkanes constitutes a family of stable and flexible polydentate ligands isoelectronic and isosteric with poly(pyrazolyl)borates. These donors can be prepared readily and various substituents may replace each hydrogen atom, so that electronic and steric effects can be varied easily. These molecules contain azole rings,

which are generally very stable towards chemical attack, for example against both oxidising and reducing agents.[62,63]

The simplest member of this family, the tris(pyrazolyl)methane (Scheme 1.4), was firstly prepared by the reaction of sodium pyrazolate with chloroform in benzene. Two analogous methods were reported in 1970 and in 1990.[62,63] A solid-liquid phase transfer procedure involving heating a mixture of the appropriate pyrazole, chloroform, potassium carbonate and tetrabutylammonium hydrogen sulfate at reflux overnight has been described.

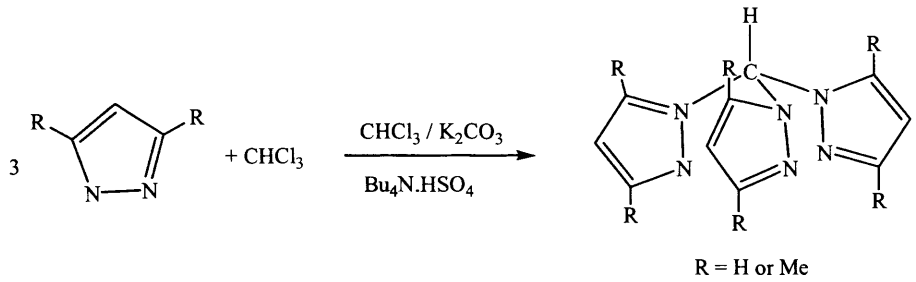

Scheme 1.4 Synthesis of tris(pyrazolyl)methanes.[62,63]

In 1999, Reger reviewed some procedures for the synthesis of tris(pyrazolyl)methanes and also reported a summary of their coordination chemistry towards Cu(I), silver(I), cadmium(II), lead(II) and thallium.[64] Later Pettinari *et al.* reviewed results obtained with tris and tetrakis-(pyrazolyl)alkanes from 1970 to 2003.[42] They discussed coordination chemistries of tris(pyrazolyl)methane with some groups I, II, IV, V, VI, VII and VIII metal ions. A few of them will be mentioned herein.

Trofimenko first reported the complexes $[Fe\{HC(pz)_3\}_2]_3$, $[Co\{HC(pz)_3\}_2]X_2$ (X = NO_3, I, PF_6 or $X_2 = SiF_6$) and $[Ni\{HC(pz)_3\}_2]X_2$ (X = NO_3, I_2, PF_6) in 1970.[62] Since the early work of Trofimenko, several other research groups have explored the coordination

chemistries of this ligand. More recently, Charbonniere and Ziessel reported and characterised by single-crystal X-ray diffraction and electronic spectroscopy of $[M\{HC(pz)_3\}_2][NO_3]_2$ (M = Co or Ni), (See Figure 1.17).[65]

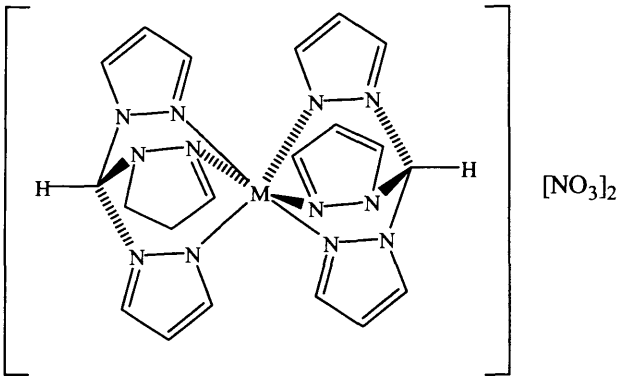

Figure 1.17 Structure of sandwich type complexes of formula $[M\{HC(pz)_3\}_2]$.

Further investigations by Mani *et al.*,[66] led to the synthesis and the characterisation of the octahedral mononuclear $[Fe\{HC(pz)_3\}_2]Br_2$ and poly(pyrazolyl) $[Fe\{HC(pz)_3\}(NCS)_2]$. A range of other iron complexes has been prepared with other iron salts with slightly different characterisations.

1.3.3 Trisoxazolines

In the last decade there has been rapid growth in the development and application of bisoxazolines (BOX). They have been widely used in metal-catalysed asymmetric synthesis.[67]

Inspired by the versatility of bisoxazolines, trisoxazolines (TOX) first emerged in 1993, when Sorrell *et al.* reported the synthesis of achiral trisoxazoline (Scheme 1.5).[68] Later, Katsuki *et al.*[69] synthesised a chiral analogue (where the bridgehead N atom was

replaced by CH; as shown in Figure 1.18, **I**), this was accomplished by an asymmetric Kharash-Sonavsky reaction.

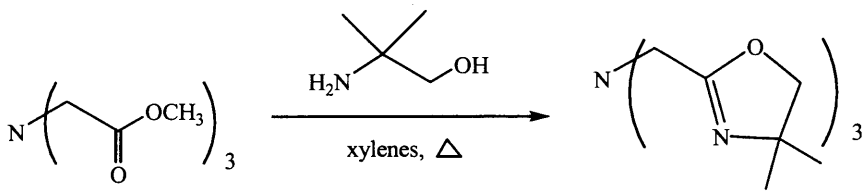

Scheme 1.5 Synthesis of tris[4,4-dimethyl-2-(4,5-dihyrooxazolyl)]methylamine (trioxma).

Since then, several types of trisoxazolines, including C_3-symmetric and pseduo-C_3-symmetric, homochiral and heterochiral, have been developed. These ligands are utilised in asymmetric catalysis and molecular recognition. To date they are only partially mentioned in recent reviews[70-73] dealing with oxazoline-containing ligands, but further investigation by Zhou and Tang reported a summary of the synthetic strategies and methods for the preparation of trisoxazoline derivatives and their application in asymmetric catalysis.[74] Some of the recent derivatives mentioned are illustrated in Figure 1.18.

Since the ligand, tris[4,4-dimethyl-2-(4,5-dihyrooxazolyl)]methylamine (trioxma) was first employed in asymmetric allylic oxidations, trisoxazolines with different structures have already found utility in several asymmetric reactions such as Kharash-Sosnovsky, Friedal-Crafts, Michael addition, Diels-Alder reaction, cyclopropanation and kinetic resolution of racemic chiral esters by transesterification. Excellent results have been achieved in some of these reactions. Most importantly, TOX proved to be superior to BOX in some cases, which demonstrates that the catalyst property (both electronic and steric) of TOX is, indeed, different from that of BOX.[70-73]

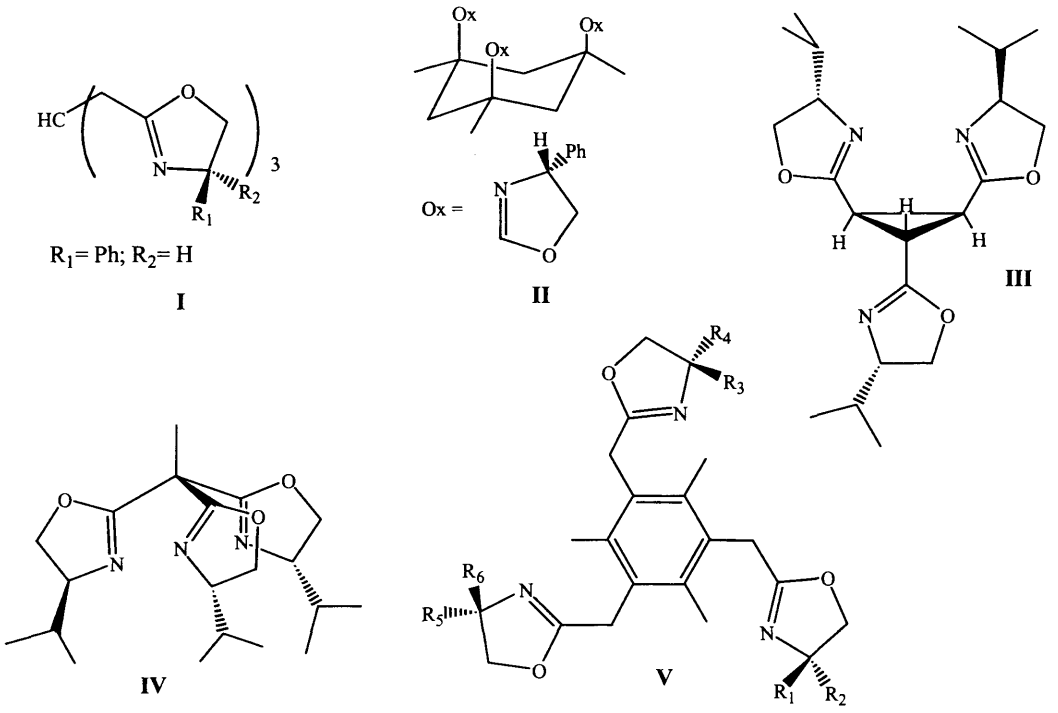

Figure 1.18 Some examples of trisoxazoline derivatives; tris[4,4-dimethyl-2-(4,5-dihydrooxazolyl)]methane; **I**, cyclohexene-trisoxazoline; **II**, *trans*-tris(oxazolinyl)cyclopropane; **III**, 1,1,1-tris{2-[(*S*)-4-isopropyl]oxazolyl}ethane; **IV**, C_1-symmetric benzene-based tripodal oxazolines (C_1-BTOs); **V**.

Transition metal complexes of these three-fold symmetric ligands have been of interest over the last decade due to their three open coordination sites that can be occupied. Coordination of trioxma with Cu(I) was first reported by Sorrell *et al.* The synthesis of $[Cu(\mu\text{-trioxma})]_2[BF_4]_2$ was structurally characterised by x-ray crystallography.[68] A three coordinate Cu(I) dimer utilising two trioxma ligands was obtained. Each Cu(I) is ligated by two oxazoline groups from one ligand and one oxazoline from the second ligand. The geometry about the metal ion was described as distorted trigonal. Complexes with other transition metals have not been explored with this particular ligand. Unlike ligand, 1,1,1-tris{2-[(*S*)-4-isopropyl]oxazolylethane (Figure

1.16, **IV**) has been efficiently prepared by coupling of a bis(oxazoline) derivative with a preformed activated mono(oxazoline) ring. Coordination chemistry of these ligands has been investigated with scandium, molybdenum, iron, cobalt, rhodium, nickel, palladium, copper and zinc. The binding capabilities of the trisoxazoline tripods are facially coordinating tridentate ligands and have been established in all cases (except with copper and palladium). X-ray diffraction studies demonstrate these systems are chiral meaning they are enantiomers in the solid state. The chiral *i*Pr-trisox-Zn complex (Figure 1.19) was synthesised by the reaction of 1,1,1-tris{2-[(S)-4-isopropyl]oxazolyl}ethane with $Zn(Otf)_2$ in dry methanol.[75]

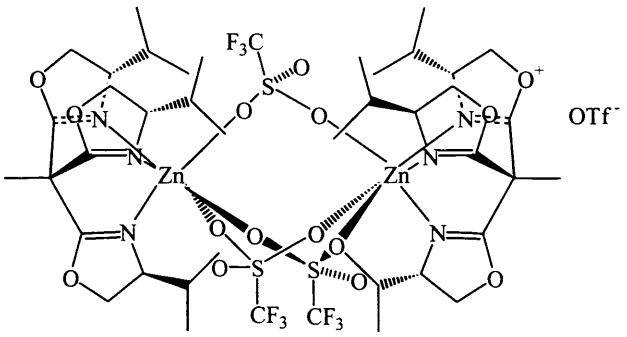

Figure 1.19 Structure of the dinuclear complex $[(i\text{Pr-trisox})_2Zn_2(\mu\text{-Otf})_3]$Otf.

Both metal centres in the dinuclear zinc complex are coordinated by the tripodal TOX ligand and are symmetrically linked by three triflato ligands. The structural constraints imposed by the relatively rigid tripod ligand lead to a trigonal antiprismatic elongation of the {(*i*Pr-trisox-Zn)} unit in the distorted $\{ZnN_3O_3\}$ octahedron. The chiral complex showed significant enantioselectivity in the kinetic resolution of various phenyl ester derivatives of *N*-protected amino-acids by transesterification with methanol.

1.3.4 Tris(4-imidazolyl)carbinol

Recently, Collman *et al.* succeeded in the synthesis of tris(4-imidazolyl)carbinol, by nucleophilic addition of 4-magnesio-1-tritlimidazole to methyl chloroformate as shown in Scheme 1.6.[76]

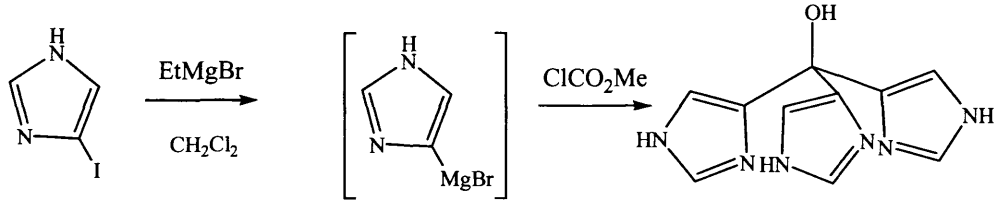

Scheme 1.6 Synthesis of tris(4-imidazolyl)carbinol.[76]

Later, this method was modified by the group of Fujii *et al.* they synthesised a series of tris(4-imidazolyl)carbinol derivatives.[77] The NH group was chemically stabilised by a methyl-protecting group and a bulky substituent (isopropyl or phenyl, Figure 1.20), which resulted in the stabilisation of the reactive species bound to the metal centre. The copper complexes prepared from these ligands mimics the metal active site of copper enzymes and were suitable for biomimetic studies.

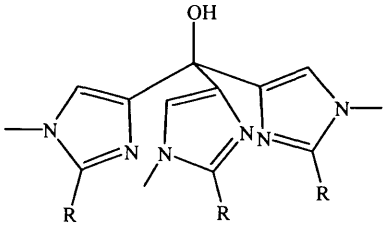

R = *i*-Pr, Ph

Figure 1.20 Structure of $HOC(Im^{i\text{-}Pr})_3$ and $HOC(Im^{Ph})_3$.

Copper complexes of these ligands were prepared by the reaction of $Cu(MeCN)_4ClO_4$ with one equivalent of ligand ($HOC(Im^{i\text{-}Pr})_3$ or $HOC(Im^{Ph})_3$) in CH_2Cl_2. They formed

monomeric complexes with distorted tetrahedral geometries with the three-imidazolyl groups of the ligand and an acetonitrile molecule coordinating to the central metal. It was reported by Sorrell *et al.* that a non-substituted tripodal ligand such as tris(4-imidazolyl) carbinol does not form the monomeric complex but the intermolecular Cu(I) dimer bridged by the ligand,[78] suggesting the formation of the monomeric complexes are a result of the steric effect of the isopropyl or the phenyl groups in each ligand.

1.4 Co-ordination chemistries of tetradentate tripodal ligands

1.4.1 Tris(2-pyridylmethyl)amine (tpa)

A review by Blackman summarises a series of tripodal tetraamine ligands and their coordination chemistry with transition and lanthanide metal ions.[79] Some of the ligands are discussed here on. Anderegg and Wenk first prepared tris(2-pyridylmethyl)amine, (tpa, Figure 1.21)[80] in 1967 from the reaction of 2-(aminomethyl)pyridine with two equivalents of 2-(chloromethyl)pyridine in aqueous solution and this, or a slight modification, seems to be the method of choice for the synthesis of this ligand to the present day. Derivatives of tpa substituted on either the pyridine rings or at a methylene carbon can be prepared by adaption of this method and use of appropriately substituted starting materials.

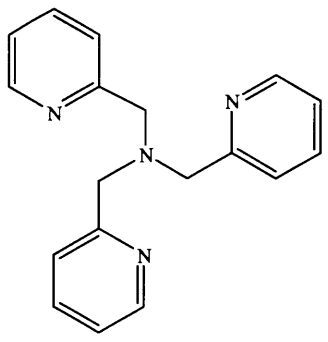

Figure 1.21 Structure of tris(2-pyridylmethyl)amine (tpa).

Tpa is one of the two most studied tripodal tetradentate amine ligands (tren being the other), with complexes of all first row metals except titanium having been reported, along with most second and third row metals, as well as the majority of lanthanide ions. A study of these complexes has shown that the ionic radius of the metal ion is crucial in determining the stoichiometry of the complexes obtained from the reaction of metal ion with tpa. A 1:2 complex is formed for metal ions having ionic radii greater than 0.9 Å, while smaller ions give 1:1 complexes.[81] There are no crystallographically characterised examples of four-coordinate transition metal complexes of the type $[M(tpa)]^{n+}$, although the thallium complex $[Tl(tpa)]_2(H_3O)(NO_3)_3$ has been shown to contain a $[Tl(tpa)]^+$ cation. Monomeric five-coordinate complexes containing tetradentate tpa are relatively common, some examples of those that have been structurally characterised are $[Cu(tpa)CN]^{n+}$, $[Co(tpa)Cl]^{n+}$ and $[Zn(tpa)Cl]^{n+}$.[82]

Typically these complexes possess trigonal bipyramidal geometries in which the aliphatic nitrogen atom occupies an axial site, with the smallest τ value being 0.74 (being closer to a trigonal bipyramidal geometry rather than a square based pyramidal).[21]

A number of six-coordinate complexes have been structurally characterised, while there are very few examples of seven and eight coordinate structurally characterised tpa complexes. Iron complexes of tpa have received particular attention, most notably due to their reactivity in alkane hydroxylation reactions. Thus, complexes such as $[Fe(tpa)Cl_2]ClO_4$, $[Fe(tpa)Br_2]ClO_4$ and $[Fe_2O(tpa)_2(H_2O)_2](CF_3SO_3)_4$ have been found to catalyse alkane functionalisation reactions in the presence of *t*-BuOOH, via a mechanism involving production of a high valent Fe(IV)-oxo species. An alternative mechanism

involving H-atom abstraction by hydroperoxide-derived alkoyl radicals has also been proposed.[83]

1.4.2 Tris(2-quinolylmethyl)amine (tmqa)

Tmqa (Figure 1.22) was first reported in 1994, the ligand was synthesised from the reaction of 2-(bromomethyl)quinoline and ammonium hydroxide in THF.[84] The coodination chemistry of this ligand has so far been limited to some copper complexes. [Cu(tmqa)]X (X = PF_6, ClO_4). The complex adopts a trigonal bipyramidal geometry with the tertiary N atom occupying the apical position, and the three quinolyl units provide a binding pocket for another axial ligand. [Cu(tmqa)Cl]PF_6·MeCN·0.5Et_2O was also formed is nearly perfectly square pyramidal. Its geometry has been rationalised on the basis that adoption of a trigonal bipyramidal structure would lead to unfavourable steric interactions between the Cl^- ligand and the protons at the 8-position of the three quinolyl rings.[85]

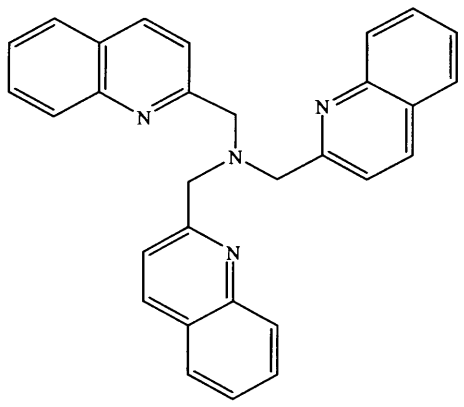

Figure 1.22 Structure of tris(2-quinolylmethyl)amine (tmqa).

Later in 2002, a series of quinolyl derivatives were synthesised by Stratford.[86] Tris-8-quinolyl-tris(2-aminoethyl)amine (tqtaea, Figure 1.23), was prepared by the

reaction of tren with three equivalents of 8-hydroxylquinoline and sodium metabisulfite. They were refluxed together in water, and the ligand was purified from hot ethanol and fully characterised.

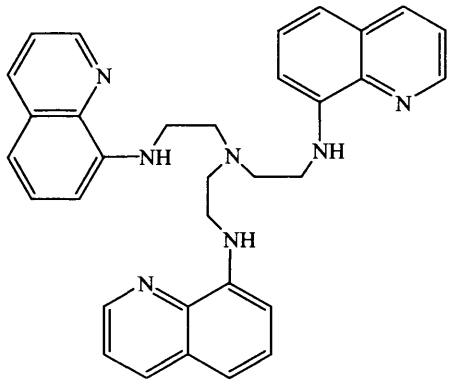

Figure 1.23 Structure of Tris-8-quinolyl-tris(2-aminoethyl)amine (tqtaea).[86]

The coordination chemistry of this ligand was explored with some transition metal ions Co, Zn and Cd. A six coordinate zinc complex, $[Zn(tqtaea)][ClO_4]_2$ was synthesised, its crystal structure gave a distorted octahedral geometry. It was noted that one of the quinoline groups was not associated to the metal centre. When a larger ion, Cd was complexed to the ligand a seven coordinate complex was formed enabling all quinoline groups to bind to the metal ion. The structure has a mono-capped octahedral core.[86]

1.4.3 Tris(2-(1-pyrazolyl)methyl)amine (amtp)

The 3,5-dimethylpyrazolyl derivative of amtp was first prepared in 1980 from the reaction of potassium 3,5-dimethylpyrazolate with $N(CH_2Cl)_3$ in THF[87] while amtp (Figure 1.24) itself was first reported in 1982 as the product of the reaction of 1-hydroxymethylpyrazole with ammonium acetate, this latter method has also been adapted for the synthesis of the 3,5-dimethylethylpyrazolyl derivative.[88] Complexations of the

amtp ligand with hydrated MX_2 salts (M = Co, Cu, Zn, X = Cl, NCS) in ethanol gives 5-coordinate [M(amtp)X]-X· $n$$H_2O$ or six-coordinate [M(amtp)X_2] · $n$$H_2O$ when excess ligand is used, whereas five-coordinate [M(amtp)X]$_2$(MX_4) complexes are obtained under conditions of excess metal salts.[89] The amtp ligand is found to hydrolyse in the presence of some metal salts, with loss of a pyrazolylmethyl arm resulting in formation of a tridentate ligand, and this reactivity has been ascribed to the three small bite angles of the amtp ligand (~80°) which leads to highly strained complexes on coordination of a metal ion to all four N donor atoms.[90]

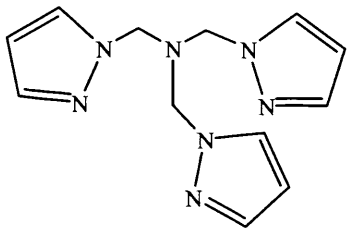

Figure 1.24 Structure of Tris(2-(1-pyrazolyl)methyl)amine (amtp).

1.4.4 Tris (Imidazolyl) derivatives

1.4.4.1 Tris(2-(1-methtlimidazolyl)methyl)amine (tmima)

Tris(2-(1-methtlimidazolyl)methyl)amine (tmima, Figure 1.25) was first referenced in 1990 in a study of alkane functionalisation by iron complexes in the presence of H_2O_2. The ligand was synthesised from 1-methyl-2-aminomethylimidazole with two equivalents of 2-chloromethyl-1-methylimidazole.[91]

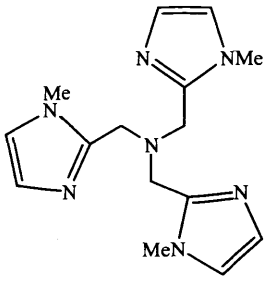

Figure 1.25 Structure of tris(2-(1-methtlimidazolyl)methyl)amine (tmima).

Tmima gives a five coordinate copper complex, $[Cu(tmima)Cl]PF_6 \cdot MeCN$, taking a trigonal bipyramidal geometry.[91] This ligand reacts with $FeCl_3$ and $NaClO_4$ in an ethanolic solution to give a monomeric six-coordinate complex, $[Fe(tmima)Cl_2]ClO_4 \cdot 0.5MeCN$ while a dimeric species is obtained with $Fe(ClO_4)_3 \cdot 9H_2O$, $[\{Fe(timima)(OH_2)\}_2(\mu\text{-}O)](ClO_4)_4$.[92] Mn(III) has also formed dimeric species, $[(tmima)Mn(O)(OAc)Mn(tmima)](ClO_4)_3 \cdot 2MeCN$. Other complexes of tmima include three Hg(II) complexes that possess eight and five coordinate geometries, the latter displaying a trigonal bipyramidal coordination mode. The ligand has also shown to bind strongly with Zn^{2+} to give a 1:1 complex in an aqueous solution, $[Zn(tmima)(OH_2)]^{2+}$.[93]

Later another isomer of tmima, tris(4-(1-methylimidazolyl)methylamine (T4IA, Figure 1.26) was reported in 2003, from the reaction of 1-methylimidazole-4-carboxaldehyde with ammonium chloride and subsequent hydrogenation (Pd/C).[93] The only complex thus far reported is $[Zn(T4IA)(OH_2)]^{2+}$ generated in aqueous solution.

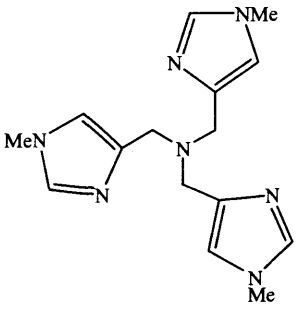

Figure 1.26 Structure of tris(4-(1-methylimidazolyl)methylamine (T4IA).

1.4.4.2 Tris(2-benzimidazolylmethyl)amine (ntb)

The benzimidazole derived ligand tris(2-benzimidazolylmethyl)amine (ntb, Figure 1.27) was first prepared in 1977.[94] Since then extensive research have been carried out on the ligand with regards to its synthesis and coordination chemistry .

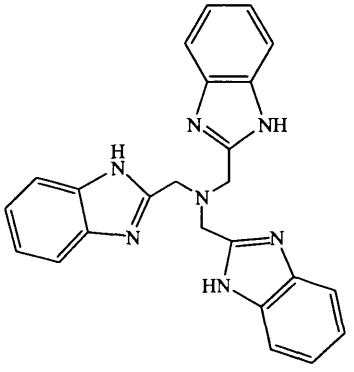

Figure 1.27 Structure of tris(2-benzimidazolylmethyl)amine (ntb).

The ligand can be deprotonated with potassium, and subsequent reaction with alkylating agents gives the tris-alkylated products. Thus, many derivatives of ntb have been prepared by this method. Ntb can also be selectively alkylated at a benzimidazole N atom and the mono(*N*-carboxymethyl) derivative HAcntb has been reported. Similarly, ntb derivatives having a methyl, isobutyl or isopropyl group in place of a methylene proton on only one of the tripodal arms can be prepared by condensation of *o*-phenylenediamine with an

asymmetric nitrilotriacetic acid derivative, which itself prepared from the reaction of analine, leucine or valine with two equivalents of chloroacetic acid.[95]

Five and six coordinate complexes are favoured by the ntb ligand, a number of which have been structurally characterised. Some examples of mononuclear five coordinate complexes of ntb are $[Co(ntb)ClO_4]^+$, $[Cu(ntb)Cl]^+$, $[Zn(ntb)OH_2]^{2+}$, and $[Hg(ntb)Cl]^+$. It can be seen that almost exclusively, they exhibit trigonal bipyramidal geometries about the metal ion.[96-98]

First row, from vanadium to zinc, and some second and third row transition metal complexes of ntb have been reported. A number of lanthanide and actinide complexes of ntb have also been synthesised and investigated. The eight coordinate lanthanide complex has the stoichiometry $[Ln(ntb)_2]^{3+}$ (Ln = Eu, Pr, Tb, La, Nd, Lu) when prepared by reaction of the metal perchlorate with ligand, even in the presence of excess metal ion, it has been known to have strong intramolecular π-π interactions between the two ntb ligands both in the solid state and in solution.[99]

1.5 Coordination chemistries of pentadentate tripodal ligands

1.5.1 Pentadentate amino pyridine ligands

Pentadentate ligands are rare but interest has emerged recently, and a growing number of five-coordinate Cu(II) complexes with such ligands have been synthesised.[100-102] Five coordinate Cu(II) was also found in its complexes with bleomycin, an antibiotic and anti-cancer drug,[103] and with bleomycin models.[102,104] Rybak *et. al.* have reported the synthesise and characterisation of a series of Cu(II) complexes with pentadentate amino pyridine ligands (Figure 1.28).[8] Additional interest in such ligands bearing aminopyridine

arms lie in their applications, for example, peroxide activation at five coordinate iron centres.[105-107]

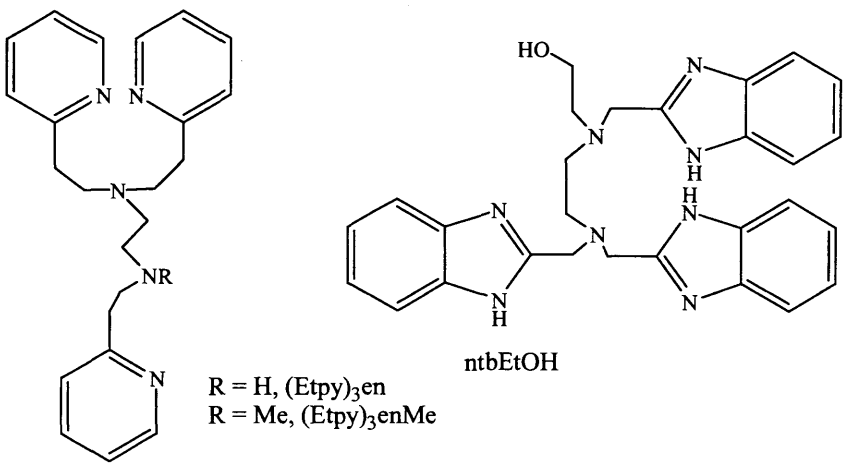

Figure 1.28 Pentadentate aminopyridine ligand derivatives; $(Etpy)_3en$ where, Etpy is ethylpyridine and en is ethylenediamine; $(Etpy)_3enMe$, tris(2-benzimidazolylmethyl)amine ethanol (ntbEtOH).

$(Etpy)_3en$ was prepared using a variation of the procedure outlined by Phillip *et. al.*[108] Ethylene diimine and 0.5 molar equivalent of vinyl pyridine in ethanol (100ml) and glacial acetic acid (3g) were refluxed under nitrogen for 20 hrs. The resulting solution was mixed with $CuCl_2$ x H_2O in 60 ml of water, and a small excess of NH_4PF_6 (14g) was added to form the complex $[Cu((Etpy)_3en)](PF_6)_2$. Its crystal structure revealed the coordination of all five nitrogen atoms to Cu(II) ion, in a distorted square-pyramidal fashion. The structural deviation of the Cu(II) five coordinate complexes from ideal SBP or TBP geometries can be described by applying the Berry pathway, it indicates only a slight distortion from an ideal square pyramidal geometry ($\tau = 10.3^{\circ}$). Similarly, the five coordinate complex $[Cu((Etpy)_3enMe)](PF_6)_2$ was also prepared.[8] The electronic properties of this complex was characteristic of distorted square-pyramidal Cu(II) complexes (see Table 1.1 for electronic spectra).

Complex	Solvent	λ_{max} (nm) (ε, $M^{-1}dm^3$)
$[Cu((Etpy)_3en)](PF_6)_2$	CH_3CN	598 (220); ~ 850 shoulder (~30)
$[Cu((Etpy)_3enMe)](PF_6)_2$	CH_3CN	604 (250); ~ 850 shoulder (~20)
$[Cu(ntbEtOH)](ClO_4)_2$	CH_3OH	690 (103); 1075 (40)

Table 1.1 Electronic spectra of the solutions of five coordinate Cu(II) complexes with aminopyridine ligands.[8]

Typically five coordinate complexes display two-band visible spectra, with the intensity of the higher energy band (ε of about 220) being significantly higher than the intensity of the lower energy shoulder (ε of about 30). The opposite ratio of intensities is typical of trigonal pyramidal geometry.[100,108] Hence the $[Cu(ntbEtOH)](ClO_4)_2$ complex also has a distorted square-pyramidal geometry.[101]

1.6 Coordination chemistries of hexadentate tripodal ligands

1.6.1 *Cis, cis*-1,3,5-Tris(pyridine-2-carboxalimino)cyclohexane derivatives

Examples of trigonal prismatic coordination are relatively few although it has been seen in a number of tripodal complexes synthesised by Wentworth *et al.*[109] They have investigated electronic properties of the generalised tris chelate $M(L\text{-}L)_3$, whose structures are described in part by a twist angle θ of the two L_3 donor atom triangles whose planes are normal to the threefold axis. The report describes the synthesise of the ligands and their respective complexes shown in Figure 1.29.[109,110] X-ray structural results have established trigonal prismatic (TP), trigonal antiprismatic (TAP or O_h) and some cases of intermediate stereochemistry.

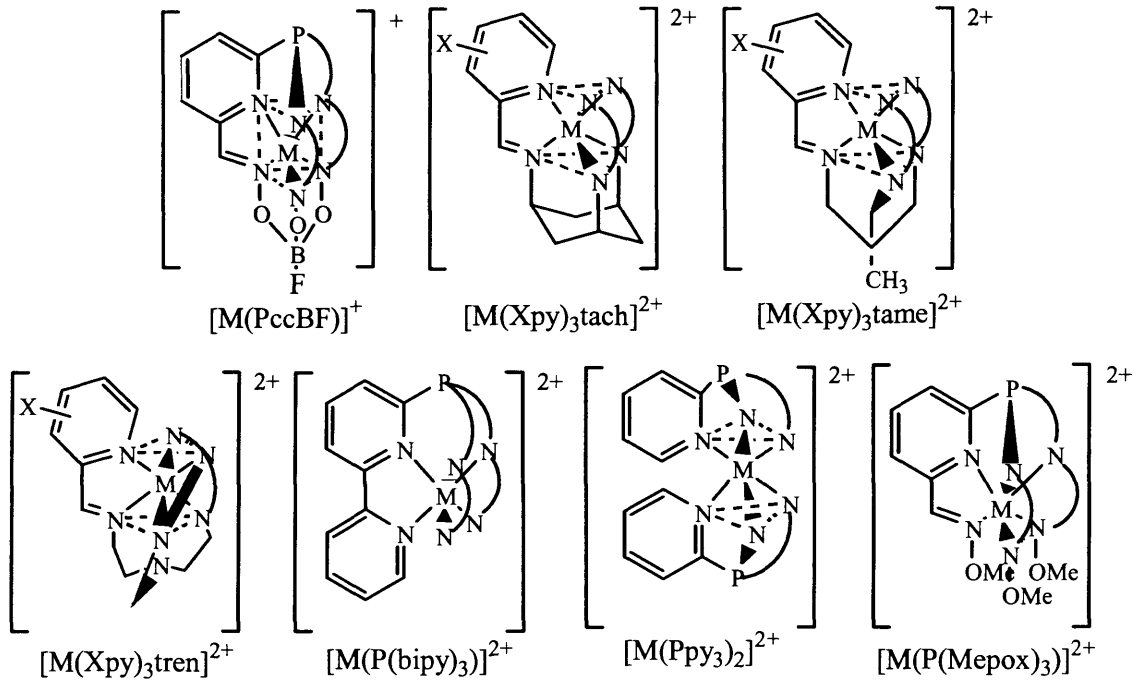

Figure 1.29 Schematic structural formulas for hexadentate and bis(tridentate) metal(II) complexes. (M = Co(II), Ni(II), Zn(II), Cu(II) and Fe(II)).

Results obtained in the last several years have clearly revealed that octahedral, TP, and intermediate geometries may be stabilised by the use of hexadentate ligands, which contain a common binding group, pyridine-2-carboxaldimine, but differ in the extent of twist which occurs upon coordination to a given metal ion. The complexes of type $[M(PccBF)]^+$ contain a bicyclic ligand which encapsulates the metal ion and forms a "clathro chelate" (cc).[111] Rigidity and dimensions of the ligand framework stabilises TP geometry, as found in Ni(II) complex, or to constrain an ion such as Fe(II), which is notably unstable in this geometry from approaching near octahedral coordination.

$[M((py)_3tach)]^{2+/3+}$ species were first reported by Lions and Martin.[112] X-ray data demonstrate that the $[Zn((py)_3tach)](ClO_4)_2$ complex where $(py)_3tach$ is *cis,cis*-1,3,5-tris(pyridine-2-carboxaldimino)cyclohexene very closely approaches TP geometry and the

Ni(II) derivative has an intermediate geometry (θ = *ca.* 32°).[109,110] Structural studies by Fleischer *et al.* have since demonstrated that the Zn(II)[19] and Fe(II)[20] complexes of the $[M((py)_3tame)]^{2+}$ species to possess coordination geometries intermediate between the trigonal prismatic (TP) and octahedron (O_h) limit. The complete series of $[M((py)_3tren)]^{2+}$ complexes where M = Mn(II) – Zn(II), has been prepared by Wilson and Rose[113] reveal structures that closely approaches TAP.

Because the above complexes effectively span the structural limits (TP, TAP) of six-coordination and include a number of examples of intermediate geometries, they constitute a unique structural series. Consequently this series provided the opportunity to examine the effects of varying stereochemistry on the electronic properties of complexes containing a common coordinating group.[110] Reported herein are the electronic spectra for only some of the Ni(II) complexes for comparison with results obtained in later chapters.

1.6.1.1 Electronic properties of TP, TAP and intermediate stereochemistry

The solution spectrum of some of the Ni(II) complexes are shown in Figure 1.30.[110] Near-TP chromophore $[Ni(PccBF)](BF_4)$ gives rise to three features whose intensities suggest identification as ligand-field bands. Those at 9380 (1066 nm) and 11,000 cm^{-1} (909 nm) are both polarized perpendicular to the molecular pseudo-C_3 axis in the single crystal spectrum, consistent with the assignments $^3A_2' \rightarrow {}^3E'$, $^1E'$ transition in D_{3h} symmetry. The higher energy feature is the spin-forbidden transition, which presumably has borrowed intensity from the spin-allowed transition. The unpolarised shoulder at ~20,500 cm^{-1} (488 nm) is tentatively assigned to the $^3A_2' \rightarrow {}^3E''$ and / or $^3A_2''$ transition (s), both of which are Laporte forbidden.[110]

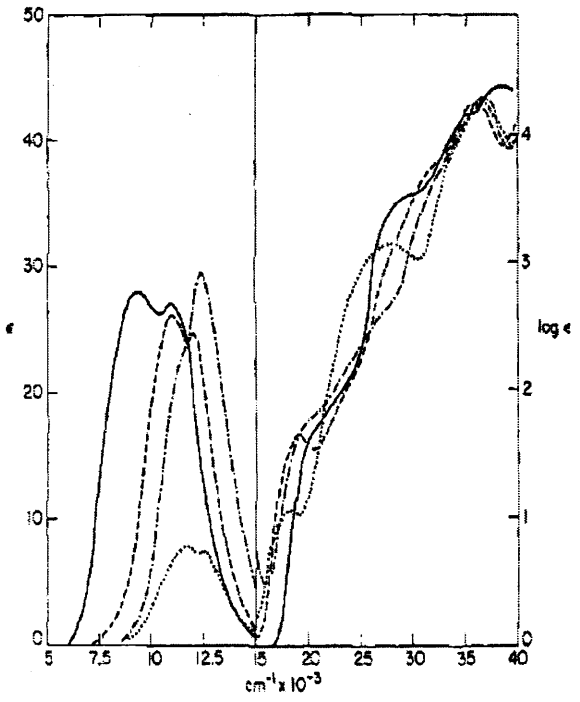

Figure 1.30 Electronic absorption spectra of the following Ni(II) complexes in CH_3CN. ___ $[Ni(PccBF)](BF_4)$, —— $[Ni((py)_3tach)](ClO_4)_2$, _. _. $[Ni((py)_3tame)](ClO_4)_2$, ... $Ni((py)_3tren)](ClO_4)_2$.[110]

Each complex exhibits a band in the narrow 11,000 – 11,700 cm^{-1} region that is assigned to the $^3A_2' \rightarrow {}^1E'$ transition. The spectral features most clearly affected by structural changes are the energies and the intensities of the spin-allowed bands in the 9000 -13,000 cm^{-1} region. The energies show a blue shift, with those of $[Ni((py)_3tach)]^{2+}$ (12,000 cm^{-1}) and $[Ni((py)_3tame)]^{2+}$ (12,400 cm^{-1}) intermediate between the values of TAP and TP species. Intensities are two or three times smaller in TAP complexes of effective octahedral symmetry than in complexes of TP or intermediate stereochemistry. This is indicated by the spectral comparison of $[Ni((py)_3tach)]^{2+}$ and $[Ni(bipy)_3]^{2+}$ in Figure 1.31. For the octahedral (or near TAP) bipyridine derivative, *Dq* is 1280 cm^{-1} while *B* is 710 cm^{-1} and is somewhat different from the TP $[Ni((py)_3tach)]^{2+}$ complex, where *Dq* is 1210 cm^{-1} and *B* is 980 cm^{-1}. Similarly the spectrum of $[Ni((py)_3tren)]^{2+}$ can be

analysed assuming octahedral symmetry, the bands observed are; $^3A_{2g} \rightarrow {}^3T_{2g}$ (v_1), 12,550 cm^{-1}; $^3A_{2g} \rightarrow {}^3T_{1g}(F)$ (v_2), 18,300 cm^{-1} and $^3A_{2g} \rightarrow {}^1E_g(^1D)$, 11,630 cm^{-1}; where *Dq* value is 1255 cm^{-1} and *B* is 710 cm^{-1}. Intense absorptions at higher energies usually obscure the octahedral v_3 band ($^3A_{2g} \rightarrow {}^3T_{1g}(P)$). The spectrum of $[Ni(P(py)_3)_2]^{2+}$ can also be similarly assigned octahedral, with *Dq* of 1260 cm^{-1} and B = 690 cm^{-1}.[109,110]

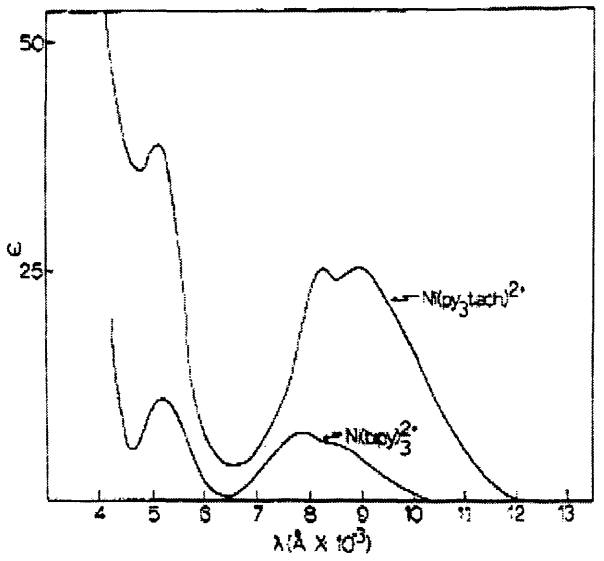

Figure 1.31 A comparison of the electronic spectra of aqueous $[Ni((py)_3tach)]^{2+}$ and aqueous $[Ni(bipy)_3]^{2+}$.[110]

1.7 Aims of the current research

The objectives for the research described in this thesis were as follows:

(i) Firstly, to design and synthesise a range of novel tripodal ligands for potential use within the bio-inorganic chemistry field. Secondly, to centre the design of the novel ligands based on the tpmOH ligand backbone.

ii) To complex these novel ligands to transition metals and investigate their coordination chemistry.

iii) To compare and contrast the results obtained within this thesis and also with previous literature reports on similar species.

1.8 References s

1. S. Trofimenko, *Chem. Rev.*, 1993, **93**, 943.
2. N. Kitajitna, W.B. Tolman, *Progress in Inorg. Chem.*, 1995, **43**, 419.
3. G. Parkin, *Adv. Inorg. Chem.*, 1995, **42**, 292.
4. M. Etienne, *Coord. Chem. Rev.*, 1996, **156**, 201.
5. J. Elguero, *Comprehensive Heterocycl. Chem. II*, 1996, **3**, 1.
6. D.L. Jameson, J.K. Blaho, K.T. Kruger, K.A. Golsby, *Inorg. Chem.*, 1989, **28**, 4312.
7. M.J. Winter, "d-Block Chemistry" (oxford chem. primer), published in1994, 26.
8. For a review of the coordination chemistry of Cu(II) , see: B.J. Hathaway, G. Wilkinson, R.D. Gillard, J.A. McClevarty, "In Comprehensive Coordination Chemistry", Pergamon Press: Oxford, 1989, **5**, pp 533-750.
9. S.M. Owen, A.T. Brooker, "A guide to modern inorganic chemistry", published in 1991, 146.
10. J.D. Lee, "Concise Inorganic Chemistry", 1996, 5th edition, 196.
11. S. Berry, *J. Chem. Phys.*, 1960, **32**, 933.
12. A.W. Addison, T.N. Rao, J. Reedijk, J. van Rijn, G.C. Verschoor, *J. Chem. Soc. Dalton Trans.*, (1984), 1349.
13. R.B. King, *Inorg. Chem.*, 1963, **2**, 641.
14. R. Eisenberg, J.A. Ibers, *J. Am. Chem. Soc.*, 1965, **87**, 3776.
15. R. Eisenberg, J.A. Ibers, *Inorg. Chem.*, 1966, **5**, 411.
16. C.G. Pierpont, R. Eisenberg, *J. Chem. Soc. A*, 1971, 2285.
17. J.F.R. de Villiers, J.C.A. Boeyens, *Acta. Crystallogr., Section B*, 1971, **28**, 2335.

18. J.A. Bertrand, J.A. Kelly, E.G. Vassian, *J. Amer. Chem. Soc.*, 1969, **91**, 2394.

19. E.B. Fleischer, A.E. Gabela, P. Tasker, *Inorg. Chem.*, 1972, **92**, 6365.

20. E.B. Fleischer, A.E. Gabela, P. Tasker, D.R. Swift, *Inorg. Chem.*, 1970, **11**, 2775.

21. J.C. Bailar, Jr., *J. Inorg. Nucl. Chem.,* 1965, **8**, 165.

22. R.B. King, *J. Organomet. Chem.*, 2001, **623**, 95.

23. A.K. Brisdon, Inorganic Spectroscopic Methods (oxford chemistry primer), published in 1998, pp.60.

24. L.F. Szczepura, L.M. Witham, K.J. Takeuchi, *Coord. Chem. Rev.*, 1998, **174**, 5.

25. J.P. Wibaut, G.L.C. La Bastide, *Rec. Trav. Chim.*, 1933, **52**, 493.

26. W.R. McWhinnie, G.C. Kulasingam, J.C. Draper, *J. Chem. Soc.*, 1966, **A**, 1199.

27. S. Kaizaki, J.I. Legg, *Inorg. Chim. Acta*, 1994, **218**, 179.

28. K.K. Mosny, R.H. Crabtree, *Inorg. Chim. Acta*, 1996, **247**, 93.

29. W.R. McWhinnie, R.C. Poller, M. Thevarasa, *J. Chem. Soc.* **A**, 1967, 1671.

30. G.C. Kulasingam , W.R. McWhinnie, *J. Chem. Soc.* **A**, 1967, 1253.

31. G.C. Kulasingam , W.R. McWhinnie, *J. Chem. Soc.* **A**, 1968, 254.

32. P.L. Dedert, J.S. Thompson, J.A. Ibers, T.J. Marks, *Inorg. Chem.*, 1982, **21**, 969.

33. D. Boys, C. Escobar, W. Zamudio, *Acta. Crystallogr.* **C 48**, 1992, 1118.

34. J.P. Wibaut, A.P. De Jonge, G.P. Van Der Voort, P.Ph.H.L Otto, *Rec. Trav. Chim.*, 1951, **70**, 1054.

35. C. Osuch, R. Levine, *J. Am. Chem. Soc.*, 1956, **78**, 1723.

36. D.L. White, J.W. Faller, *Inorg. Chem.*, 1982, **21**, 3119.

37. T. Astley, P.J. Ellis, H.C. Freeman, M.A. Ifitchman, F.R. Keene, E.R.T. Tiekink, *J. Chem. Soc., Dalton Trans.*, 1995, 595.

38. E.S. Zvargulis, I.E. Buys, T.W. Hambley, *Polyhedron*, 1995, **14**, 2267.

39. R.K. Boggess, S.J. Boberg, *J. Inorg. Nucl. Chem.*, 1980, **42**, 21.

40. R.K. Boggess, A.H. Lamson, S. York, *Polyhedron*, 1991, **10**, 2791.

41. D.J. Szalda, F.R. Keene, *Inorg. Chem.*, 1986, **25**, 2795.

42. A.J. Canty, L.A. Titcombe, B.W. Skelton, A.H. White, *J. Chem. Soc., Dalton Trans.*, 1988, 35.

43. R.A. Brown, J. Huguet, *Can. J. Chem., Dalton Trans.*, 1980, **58**, 889.

44. G. Cote, *J. Chem. Res. (Synop)*, 1983, 143.

45. M. Kodera, H. Shimakoshi, M. Nishimura, H. Okawa, S. Iilima, K. Kano, *Inorg. Chem.*, 1996, **35**, 4967.

46. P.L. Dedert, T. Sorrell, T.J. Marks, J.A. Ibers, *Inorg. Chem.*, 1982, **21**, 3506.

47. J.W. Faller, Y. Ma, *J. Am. Chem. Soc.*, 1991, **113**, 1579.

48. J.W. Faller, L.L. Gundersen, *Tetrahedron Lett.*, 1993, 2275.

49. V. Levacher, H. Adolfsson, C. Moberg, *Acta Chem. Scand.*, 1996, **50**, 454.

50. R. Clavreul, B. Bloch, *Makromol Chem.*, 1987, **47**, 118.

51. D.M. Shin, I.S. Lee, Y.-A. Lee, Y.K. Chung, *Inorg. Chem.*, 2003, **42**, 2977.

52. S. Trofimenko, *J. Am. Chem. Soc.*, 1967, **89**, 3170.

53. S. Trofimenko, *Chem. Rev.*, 1972, **72**, 497.

54. T. Ruman, Z. Ciunik, E. Szklanny, S. Wolowiec, *Polyhedron*, 2002, **21**, 2743.

55. M. Lukasiewicz, Z. Ciunik, T. Ruman, M. Skora, S. Wolowiec, *Polyhedron*, 2001, **20**, 237.

56. T. Ruman, M. Lukasiewicz, Z. Ciunik, S. Wolowiec, *Polyhedron*, 2001, **20**, 2551.

57. C. Janiak, H. Hemling, *J. Chem. Soc., Dalton Trans.*, 1994, 2947.

58. E. Craven, E. Mutlu, D. Lundberg, S. Temizdemir, S. Dechert, H. Brombacher, C. Janiak, *Polyhedron*, 2002, **21**, 553.

59. C. Janiak, S. Temizdemir, C. Rohr, *Z. Anorg. Allg. Chem.*, 2000, **626**, 1265.

60. C. Janiak, S. Temizdemir, S. Dechert, *Inorg. Chem. Commun.*, 2000, **3**, 271.

61. A.L. Rheingold, B.S. Haggerty, G.P.A. Yap, S. Trofimenko, *Inorg. Chem.*, 1997, **36**, 5097.

62. S. Trofimenko, *J. Am. Chem. Soc.*, 1970, **92**, 5118.

63. P.K. Byers, A.J. Canty, R.T. Honetman, *J. Organomet. Chem.*, 1990, **385**, 417.

64. D.L. Reger, *Comments Inorg. Chem.*, 1999, **21**, 1.

65. L.J. Charbonniere, R. Ziessel, *Tetrahedron Lett.*, 2003, **44**, 6305.

66. F. Mani, *Inorg. Nucl. Chem. Lett.*, 1979, **15**, 297.

67. A.K. Ghosh, P. Mathivanan, J. Cappiello, *Tetrahedron Asymm.*, 1998, **9**, 1.

68. T.N. Sorrell, F.C. Pigge, P.S. White, *Inorg. Chim. Acta*, 1993, **210**, 87.

69. K. Kawasaki, S. Tsumura, T. Katsuki, *Synlett*, 1995, 1245.

70. T.H. Chuang, J.M. Fang, C. Bolm, *Synth. Commun.*, 2000, **30**, 1627.

71. S.G. Kim, K.H. Ahn, *Chem. Eur. J.*, 2000, **6**, 3399.

72. S.G. Kim, K.H. Ahn, *Tetrahedron Lett.*, 2001, **42**, 4175.

73. S.G. Kim, K.H. Kim, J. Jung, S.K. Shin,K.H. Ahn, *J. Am. Chem. Soc.*, 2002, **124**, 591.

74. J. Zhou, Y. Tang, *Chem. Soc. Rev.*, 2005, **34**, 664.

75. C. Dro, S. Bellemin-Laponnaz, R. Welter, L.H. Gade, *Angew. Chem.*, 2004, **116**, 4579.

76. J.P. Collman, M. Zhong, W. Zhong, Miao, *Org. Lett.*, 1999, **1**, 949.

77. M. Kujime, H. Fujii, *Tetrahedron Lett.*, 2005, **46**, 2809.

78. T.N. Sorrell, A.S. Borovik, *J. Am. Chem. Soc.*, 1987, **109**, 4255.

79. A.G. Blackman, *Polyhedron*, 2005, **24**, 1.

80. G. Anderegg, F. Wenk, *Helv. Chim. Acta*, 1967, **50**, 2330.

81. A. Hazell, J. McGinley, H. Toftlund, *J. Chem. Soc. Dalton Trans.*, 1999, 1271.

82. D.M. Corsi, N.M. Murthy, V.G. Young Jr., K.D. Karlin, *Inorg. Chem.*, 1999, **38**, 848.

83. I.W.C.E. Arends, K.U. Ingold, D.D.M. Wayner, *J. Am. Chem. Soc.*, 1995, **117**, 4710.

84. N. Wei, N.M. Murthy, Q. Chen, J. Zubieta, K.D. Karlin, *Inorg. Chem.*, 1994, **33**, 1953.

85. N. Wei, N.M. Murthy, K.D. Karlin, *Inorg. Chem.*, 1994, **33**, 6093.

86. L. Stratford, *Ph.D. Thesis*, 2003, Chapter 5, 140.

87. F. Mani, G. Scapacci, *Inorg. Chim. Acta*, 1980, **38**, 151.

88. W.L. Driessen, *Recl. Trav. Chim. Pays-Bas*, 1982, **101**, 441.

89. W.L. Driessen, W.G.R. Wiesmaijer, M. Schipper-Zablotskaja, R.A.G. De Graaff, J. Reedijk, *Inorg. Chim. Acta*, 1989, **162**, 233.

90. W.L. Driessen, R.A.G. De Graaff, W.G.R. Wiesmaijer, *Acta Crystallogr.* **Sect. C**, 1988, **43**, 2319.

91. K.J. Oberhausen, R.J. O'Brien, J.F. Richardson, R.M. Buchanan, *Inorg. Chim. Acta*, 1990, **173**, 145.

92. R.M. Buchanan, S. Chen, J.F. Richardson, M. Bressan, L. Forti, A. Morvillo, R.H. Fish, *Inorg. Chem.*, 1994, **33**, 3208.

93. Y.-H. Chiu, J.W. Canary, *Inorg. Chem.*, 2003, **42**, 5107.

94. L.K. Thompson, B.S. Ramaswamy, E.A. Seymour, *Can. J. Chem.*, 1977, **55**, 878.

95. T. Sakurai, H. Oi, A. Nakahara, *Inorg. Chim. Acta*, 1984, **92**, 131.

96. X. Zhang, J.-L. Wang, F.-M. Miao, *Huaxue Yanjiu Yu Yingyong*, 2000, **12**, 503.

97. T. Brandsch, F.A. Schell, K. Weis, M. Ruf, B. Mueller, H. Vahrenkamp, *Chem. Ber.*, 1997, **130**, 283.

98. E. Quiroz-Castro, S. Bernes, N. Barba-Behems, R. Tapia-Benavides, R. Contreras, H. Noth, *Polyhedron*, 2000, **19**, 1479.

99. R. Wietzke, M. Mazzanti, J.-M. Latour, J. Pcaut, *Jacques. Chem. Commun.*, 1999, 209.

100. G.A. McLachlan, G.D. Fallon, R.L. Martin, L. Spiccia, *Inorg. Chem.*, 1995, **34**, 254.

101. M. Murali, M. Palaniandavar, T. Pandiyan, *Inorg. Chim. Acta.*, 1994, **224**, 19.

102. F.A. Chavez, M.M. Olmstead, P.K. Mascharak, *Inorg. Chem.*, 1996, **35**, 1410.

103. Y. Sugiura, T. Takita, H. Umezawa, "Bleomycin antibiotics: metal complexes and their biological action", in: H. Siegel (Ed.), "Metal Ions in Biological systems", vol. 19, Marcel Dekker, New York, 1985, pp. 81-108

104. S.J. Brown, D.W. Stephen, P.K. Mascharak, *J. Am. Chem. Soc.*, 1988, **110**, 1996.

105. L. Huang, J.C. Quada Jr, J.W. Lown, *Curr. Med. Chem.*, 1995, **2**, 543.

106. Y. Ishikawa, Y. Morishita, T. Yamamoto, H. Kurosaki, M. Goto, H. Matsuo, M. Sugiyama, *Chem. Lett.*, 1998, 39.

107. A.T Phillip, A.T. Casey, C.R. Thompson, *Aust. J. Chem.*, 1970, **23**, 491.

108. B.J. Hathaway, Copper, in: Comprehensive Coordination Chemistry, vol. 5, Pergamon Press, Oxford, 1987, pp. 533-774.

109. W.O.Gillum, R.A.D.Wentworth, R.F.Childers, *Inorg. Chem.*, 1970, **9** 1829.

110. E. Larsen, G.N. La Mar, B.E. Wagner, J.E. Parks, R.H. Holm, *Inorg. Chem.*, 1972, **11**, 2652.

111. D.H. Busch, *Rec. Chem. Progr.*, 1964, **25**, 107.

112. F. Lions, K.V. Martin, *J. Am. Chem. Soc.*, 1957, **79**, 1572.

113. L.J. Wilson, N.J. Rose, *J. Amer. Chem. Soc.*, 1968, **90**, 6041.

Chapter Two

The Synthesis of Bis(pyrid-2-yl)ketone and Tris(pyrid-2-yl)methanol Derivatives

2.1 Introduction

Although the tris(pyrid-2-yl)methanol ligand was first reported almost fifty years ago,[1] work relating to the synthesis of tri-substituted derivatives is rare,[2,3] a rather surprising finding considering their potential application and the commercial availability of many dipyridyl-based ligands. This can at least, in part, be attributed to the complexity of the pyridyllithium chemistry[4,5] used to prepare the ligand as shown in Scheme 2.1. As a consequence of this, it was decided to investigate the reasoning behind it. In this Chapter the development of tpmOH framework will be investigated to synthesise a series of ester and acid tripodal derivatives, but firstly the background literature on similar tripodal ligands and their uses will be discussed briefly.

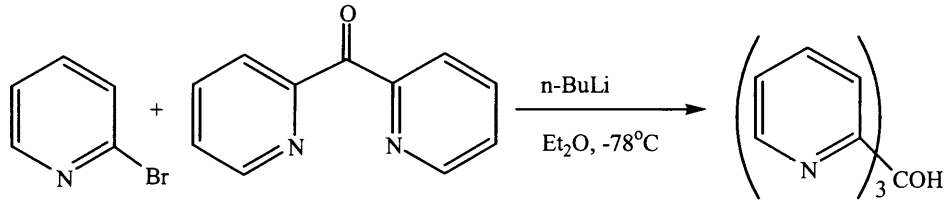

Scheme 2.1 Synthesis of tris(pyridy-2-yl)methanol.[4,5]

2.1.1 Heptadentate tripodal ligands N_4O_3

Recent investigations by Mazzanti *et al.* have reported the gadolinium complex of the new heptadentate tripodal ligand tpaa (H_3tpaa = α,α',α"nitrilotri(6-methyl-1-pyridinecarboxylicacid)) containing three pyridinecarboxylato arms connected to a

nitrogen atom (Scheme 2.2).[6,7] The Gd(tpaa) complex results in a decrease in the thermodynamic stability with respect to the complexes of macrocyclic heptadentate ligands (such as dtpa, dota etc.), but the relaxtivity was found to be remarkably higher than those of the currently clinically used contrast agents based on complexes of octacoordinate ligands, such as $[Gd(dtpa)(H_2O)]^{2-}$ and $[Gd(dota)(H_2O)]^{-}$.

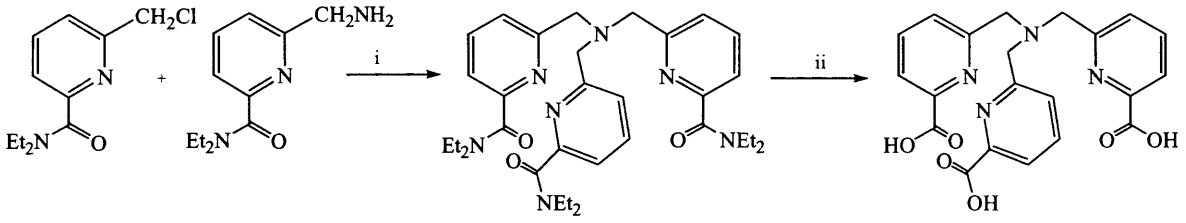

Scheme 2.2 Synthesis of H_3tpaa = α,α',α"nitrilotri(6-methyl-1-pyridinecarboxylic acid). (i)K_2CO_3, CH_3CN, reflux. (ii) EtOH/NaOH.[6,7]

2.1.2 Synthetic routes to tris(6-carboxypyrid-2-yl)methanol

Previously, various groups have synthesised derivatives of tris(6-carboxypyrid-2-yl)methanol, using several different approaches. Similar to Takalo's strategy,[8] Adolfsson *et al.* reported the synthesis of ligands **V-VII** via the tris(pyrid-2-yl N-oxide)methanol intermediate (Scheme 2.3).[9] She envisaged these chiral tripodal C_3-symmetric pyridine ligands to be promising candidates for the synthesis of catalytically active transition metal complexes.

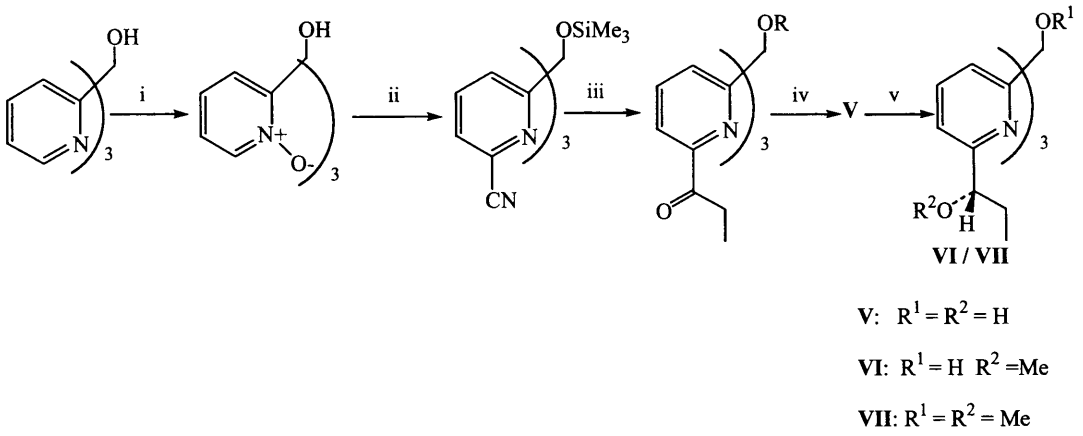

Scheme 2.3 The synthesis of Ligands **V-VII**. (i) *m*-chloroperbenzoic acid, (ii) *N,N*-dimethylcarbamoyl chloride, trimethylsilyl cyanide, (iii) EtMgBr, H_2O (iv) (-)-Ipc_2BCl, 2,2'-iminodiethanol, (v) NaH, MeI.[9]

Another approach was investigated by the group of Gibb *et al.* (Scheme 2.4) via the tris(6-carbinolpyrid-2-yl)methanol precursor. Four distinct tris(pyrid-2-yl)methanol derivatives were synthesised via lithiated intermediates.[10]

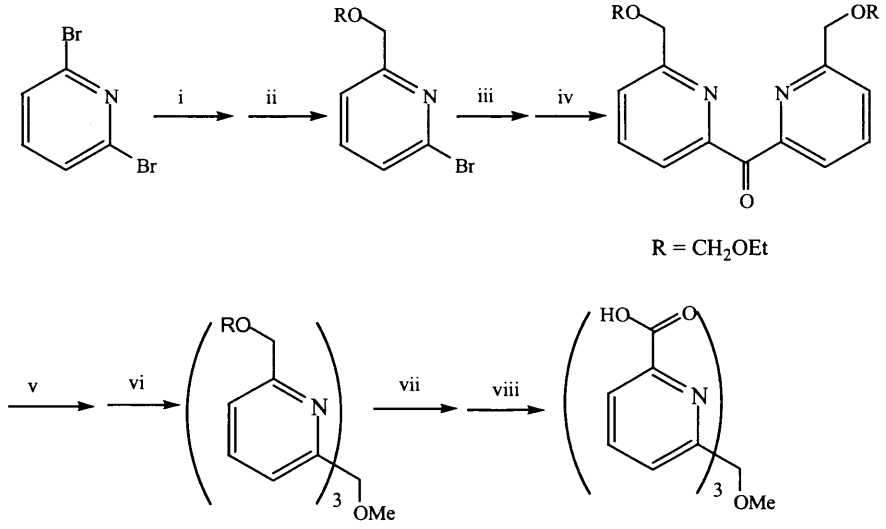

Scheme 2.4 Synthesis of tris(2-(picolinic acid)methanol methyl ether. (i) *n*-BuLi, DMF, H_3O^+. (ii) $NaBH_4$. (iii) $EtOCH_2Cl$, DIPEA. (iv) *n*-BuLi, $(EtO)_2CO$. (v) lithiate derived from X + *n*-BuLi. (vi) NaH, MeI. (vii) $MeOH/H_3O^+$. (viii) $KMnO_4$.[10]

Similarly, Gibb also synthesised a series of tris(glycine) derivatives using 2-bromo-5-methyl pyridine as the starting material (see Scheme 2.5).[11] Further work on this tridentate ligand, has led to the development of successful carbonic anhydrase mimics and catalysts.

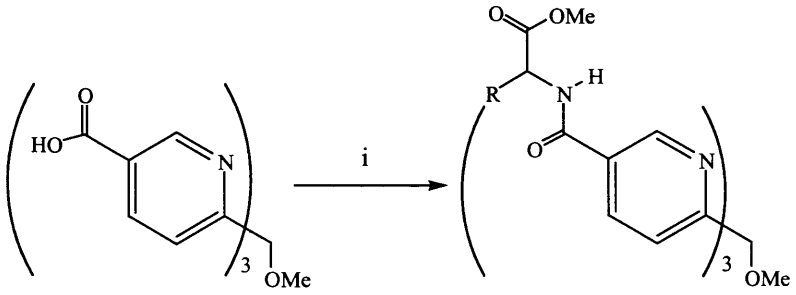

R = H, CH_2OH, CH_2Ph

Scheme 2.5 Synthesis of tris-glycine, tris-serine, and tris-phenylanaline. (i) HBTU, Et_3N, DMF, respective amino acid methyl esters.[11]

Recent investigations by Peng *et al.* utilised tris(6-bromopyrid-2-yl)methanol as the intermediate in the synthesis of the tris(6-sodiumcarboxypyrid-2-yl)methanol derivative (see Scheme 2.6). This ligand was coordinated to gadolinium for possible use as MRI contrast agents.[12]

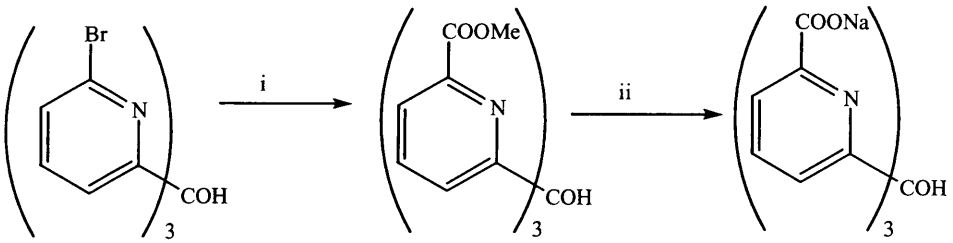

Scheme 2.6 Synthesis of of tris(6-sodiumcarboxypyrid-2-yl)methanol. (i) $Pd(TPP)_4$, Et_3N, MeOH, Toluene, CO(500psi), 100°C (ii) NaOH(3.4 eq.), H_2O/MeOH.[12]

2.2 Aims of the current research

The chemistry of tris(pyrid-2-yl)methanol (tpmOH) has been fairly well investigated. Coordination chemistry of this symmetric, facially capping tri-nitrogen donor ligand has not been extensively explored since its original synthesis fifty years ago.[1-3] The stepwise synthesis of tpmOH allows for countless substitutions to this ligand template, which is not always the case for other ligand templates. Other facially capping, tri-nitrogen ligands, while readily prepared, are often difficult to modify and purify. By exploiting the synthetic versatility in the preparation of tpmOH, a family of ligands (L^{1-8}) will be generated, that consists of mono, bis and tris picolinic acid / 6-methylcarboxypyrid-2-yl units as shown in Figure 2.1.

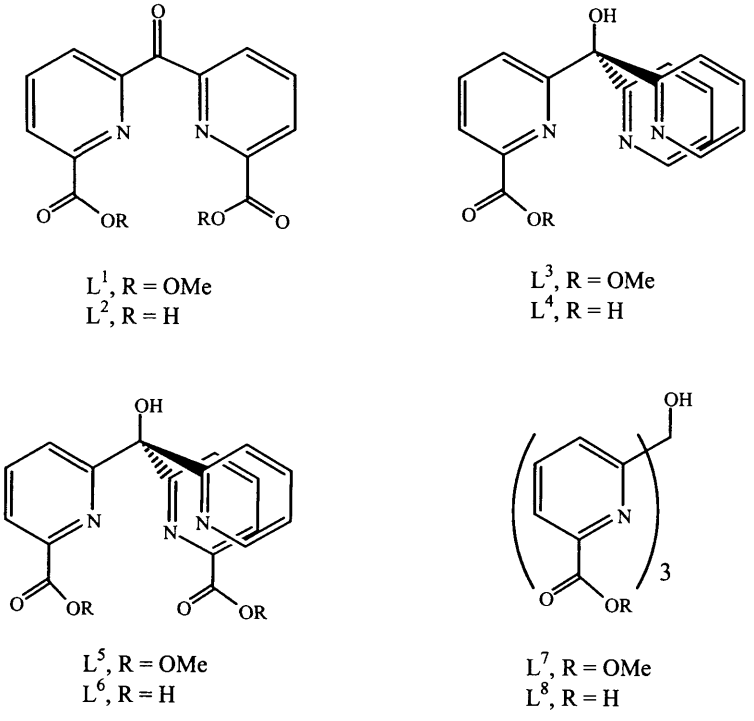

L^1, R = OMe
L^2, R = H

L^3, R = OMe
L^4, R = H

L^5, R = OMe
L^6, R = H

L^7, R = OMe
L^8, R = H

Figure 2.1 Examples of the desired mono, bis and tris(6-carboxy / methylesterpyrid-2-yl) derivatives.

2.3 Results and discussion

2.3.1 Route A – Attempted synthesis of mono, bis and tris(pyrid-2-yl N-oxide)methanol derivatives via selective oxidative methods.

Route A is illustrated in Scheme 2.7, it proposes the syntheses of compounds **3a-c** via the selective oxidation of the pyridyl nitrogen[13] in order to synthesise the respective mono, bis and tris(pyrid-2-yl N-oxide)methanol derivatives.

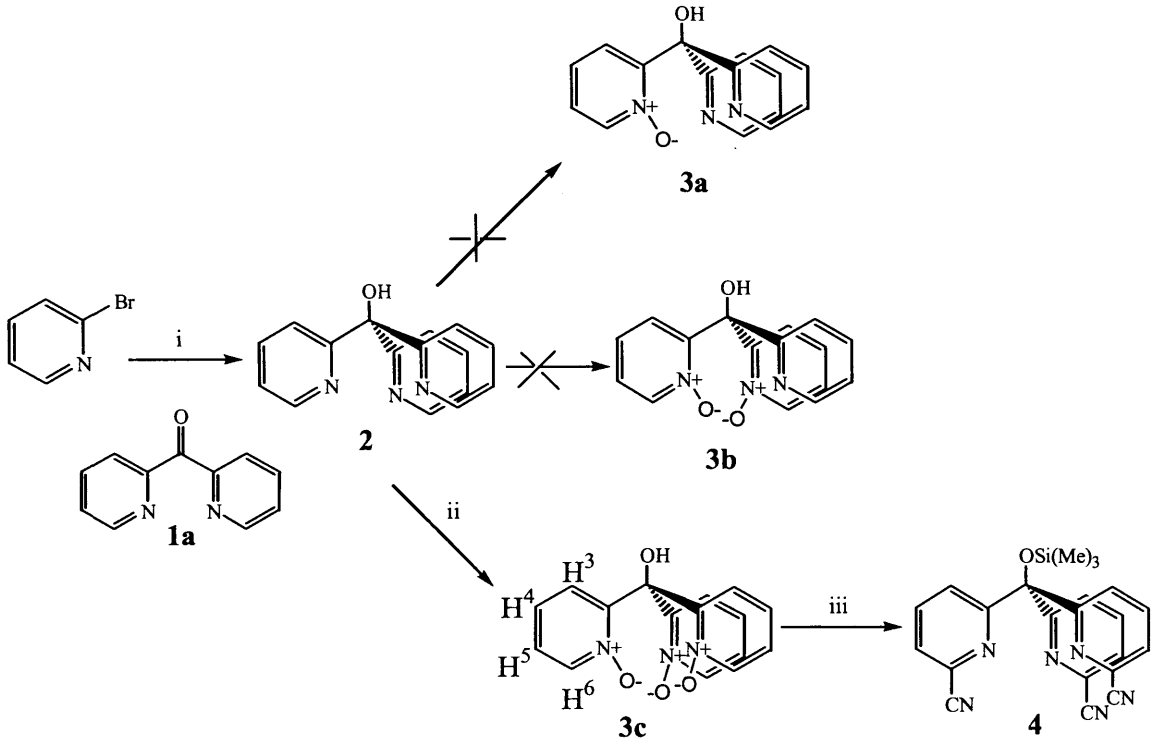

Scheme 2.7 Route A Attempted synthesis of mono, bis and tris(pyrid-2-yl N-oxide)methanol **3a-c**. Step i) *n*-BuLi, Et_2O, -78°C. ii) H_2O_2, glacial acetic acid, reflux. iii) Benzoyl chloride, trimethylsilyl cyanide (TriMSCN), DCM.

There are numerous methods available in the literature for the preparation of N-oxides in heterocyclic chemistry.[14] The oxidation of pyridine to its N-oxide is usually perceived as a straightforward chemical transformation and is most often accomplished

using a peracid, such as peracetic acid, meta-chloroperbenzoic acid (mcpba) or magnesium monoperphalate.[15] By use of methods that can be generalised into selective and non-selective oxidation methods, various N-oxide chelates can be selectively synthesised. Previously the use of large, sterically hindered oxidising agents such as mcpba has allowed the selective oxidation of oligopyridines. Thus, by simply altering the stoichiometry of the oxidant (one, two or three equivalences of mcpba) one might expect the respective mono, bis and tris(pyrid-2-yl-N-oxide)methanol intermediates to be generated **3a-c**. The mono and bis oxide derivatives **3a**, **3b** could not be synthesised cleanly; mixtures were observed in their ^{1}H NMR spectra. Attempts to purify and separate the mixtures as instructed by Takalo's procedures and further column chromatography proved to be ineffective as the resulting yields were very low and still impure.[13] Only the tris(pyrid-2-yl-N-oxide)methanol precursor, **3c** could be synthesised by a non-selective oxidation method. Previously, the group of Case synthesised the terpyridine tris-oxide via the generation of peroxyacetic acid *in situ* by the addition of excess H_2O_2 (30% vol.) to glacial acetic acid.[16-18] After refluxing the mixture for 18 hours the terpy tris-oxide was obtained with simple purification and high yields. Similarly **3c** was synthesised, glacial acetic acid and hydrogen peroxide were refluxed together with tris(pyrid-2-yl)methanol (tpmOH), **2** for 63 hours, the synthesis of **2** is adapted from the method used by Gibb *et. al.*[10] The removal of excess of the oxidation reagent by high vacuum evaporation yielded a yellow sticky solid that was purified by the addition of excess acetone. The precipitate was filtered and dried to give pure tris(pyrid-2-yl-N-oxide)methanol, **3c** (92%). This was characterised by ^{1}H NMR spectroscopy, the data for compounds **2** and **3c** are illustrated in Table 2.1. A decrease in chemical shift of the aromatic protons suggests that they become

more shielded upon oxidation. This behaviour is characteristic of the introduction of N-oxide group (s).[19-21] It is also important to note the number of peaks in their spectra, 4 major peaks are observed for compounds **2** and **3c** suggesting the three pyridyl rings are equivalent in both cases.

	H^3	H^4	H^5	H^6
2	7.74 d, 3H	7.68, t, 3H	7.27, dd, 3H	8.50, d, 3H
3c	7.47, d, 3H	7.35, dd, 3H	7.25, dd, 3H	8.20, d, 3H
4	7.79, m, 3H	7.79, m, 3H	7.55,d, 3H	—

Table 2.1 Chemical shifts for proton resonances of compounds **2**, **3c** and **4** ($CDCl_3$) in *ppm*.

The IR spectrum of **3c** confirms the presence of the characteristic $\nu_{N\text{-}O}$ band seen at 1249cm^{-1}.[17] The EI mass spectrum also supported its successful synthesis, a mass to charge ratio of 334.1, $[\mathbf{3c}+Na]^+$ was obtained.

Further investigations to construct an alternative route for the synthesis of the bis(pyrid-2-yl N-oxide)-mono(pyrid-2-yl)methanol precursor, **3b** via the oxidation of bis (2-pyridyl)ketone are discussed later in Section 2.4. Meanwhile, the subsequent step (see Scheme 2.7 (iii)) was followed to synthesise the intermediate tris(6-cyanopyrid-2-yl)methoxy(trimethylsilane), **4**. The cyanation step was adapted from previous reports seen for the synthesis of similar ligands.[13,14] Tris(pyrid-2-yl-N-oxide)methanol, **3c** was treated with a ten-fold excess of trimethylsilanecyanide (TriMSCN) in the presence of a four-fold excess of benzoyl chloride in dichloromethane (DCM) and stirred for 14 hours at ambient temperature. The crude product of tris(6-cyanopyrid-2-yl)methoxy(trimethylsilane) **4** was purified by column chromatography on silica gel and eluted with MeOH / DCM (0.1:9.9). From the fractions a pale pink solid and also a white

solid was obtained in poor yields (20 and 9% respectively). ^{1}H NMR analysis of the pale pink solid confirmed the successful preparation of the desired precursor, tris(6-cyanopyrid-2-yl)methoxy(trimethylsilane) **4** and the white solid to be benzoic acid, a side product of the reaction with benzoyl chloride the formation of which is shown in Scheme 2.8. The success of this reaction was confirmed by the IR data; the $\nu_{N\text{-}O}$ band is absent however a ν_{CN} band appears at 2238 cm^{-1} and can be assigned to nitrile functional group of the ligand. Table 2.1 compares the ^{1}H NMR spectrum of **4** with **3c**, the aromatic proton $\mathbf{H^6}$ has been substituted by the cyano group as expected. Only two peaks are now observed in the aromatic region, one at 7.55 *ppm* with an integration of three protons and the other at 7.79 *ppm* equivalent to six protons. This shift to higher frequencies is caused by the replacement of $\mathbf{H^6}$ by an electron withdrawing group such as CN^- that takes more electron density from the pyridyl ring than the $\mathbf{H^6}$ and the N-oxide in compound **3c**. A strong peak equivalent to twelve protons is also observed around 0 *ppm*, this is where the tetramethylsilane (TMS) standard normally appears. This peak confirms the likely substitution of the tertiary alcoholic proton by a trimethylsilane group from the reagent, TriMSCN used in the reaction. Previously Moberg and Adolfsson[9] have also reported this ligand while using a similar method however they could only characterise it using spectroscopic analyses. Not only were the spectroscopic data for compound **4** very similar to that published but also a crystal structure was obtained and is depicted in Figure 2.2. Table 2.2 displays its selected bond lengths and angles. The carbon bridgehead has an average C(4)-C (of each adjacent pyridine) bond distance of 1.536 Å and a C(4)-O(1) bond length of 1.402 Å these values are similar to tpmOH and are therefore typical.[25,26]

The EI mass spectrum displayed an ion at m/z = 411 [M+TriMS] also confirming its existence.

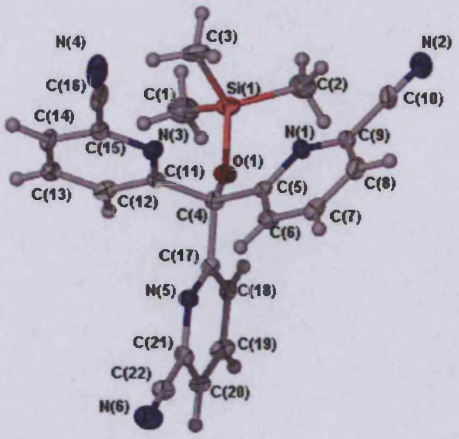

Figure 2.2 Crystal structure of tris(6-cyanopyrid-2-yl)methoxy(trimethylsilane) **4**.

Table 2.2 Bond distance (Å) and angles (°) for **4**.

C(4)-O(1)	1.402(4)	C(15)-C(16)	1.451(6)
C(4)-C(11)	1.530(5)	C(16)-N(4)	1.151(5)
C(4)-C(17)	1.537(5)	C(21)-C(22)	1.445(5)
C(4)-C(5)	1.542(5)	C(22)-N(6)	1.138(4)
C(9)-C(10)	1.460(6)	O(1)-Si(1)	1.663(2)
C(10)-N(2)	1.140(5)		
C(4)-O(1)-Si(1)	136.0(2)	N(4)-C(16)-C(15)	177.9(4)
N(2)-C(10)-C(9)	177.9(5)	N(6)-C(22)-C(21)	178.0(4)

The precursor, tris(6-cyanopyrid-2-yl)methoxy(trimethylsilane) **4** was hydrolysed with a basic aqueous NaOH solution in ethylene glycol and refluxed at ~200°C for 2.5 hours. The resulting product was precipitated by neutralisation with dilute HCl to obtain a grey solid, tris(6-carboxypyrid-2-yl)methanol **5** (L^8, 30%). The ^{1}H NMR spectrum of this compound was performed in DMSO-d_6, the absence of the TriMS peak at ~0 *ppm* was indicative of the recovery of the tertiary alcohol. The IR spectrum verified the loss of the

nitrile band and the introduction of a ν_{CO} stretch at ~1710 cm^{-1}, typical of carboxylic acid groups. The extra broad ν_{OH} peak seen at ~3366 cm^{-1} suggests the absence of the TriMS group and hence the recovery of the tertiary alcohol. The mass spectrum is consistent with the above data, it confirms the presence of the expected parent ion coordinated to a Na^+ ion $[M+Na]^+$. A plausible mechanism for the successful synthesis of **5** is illustrated in Scheme 2.8 (the mechanism for the synthesis of **4** is taken from a journal by Fife[22]).

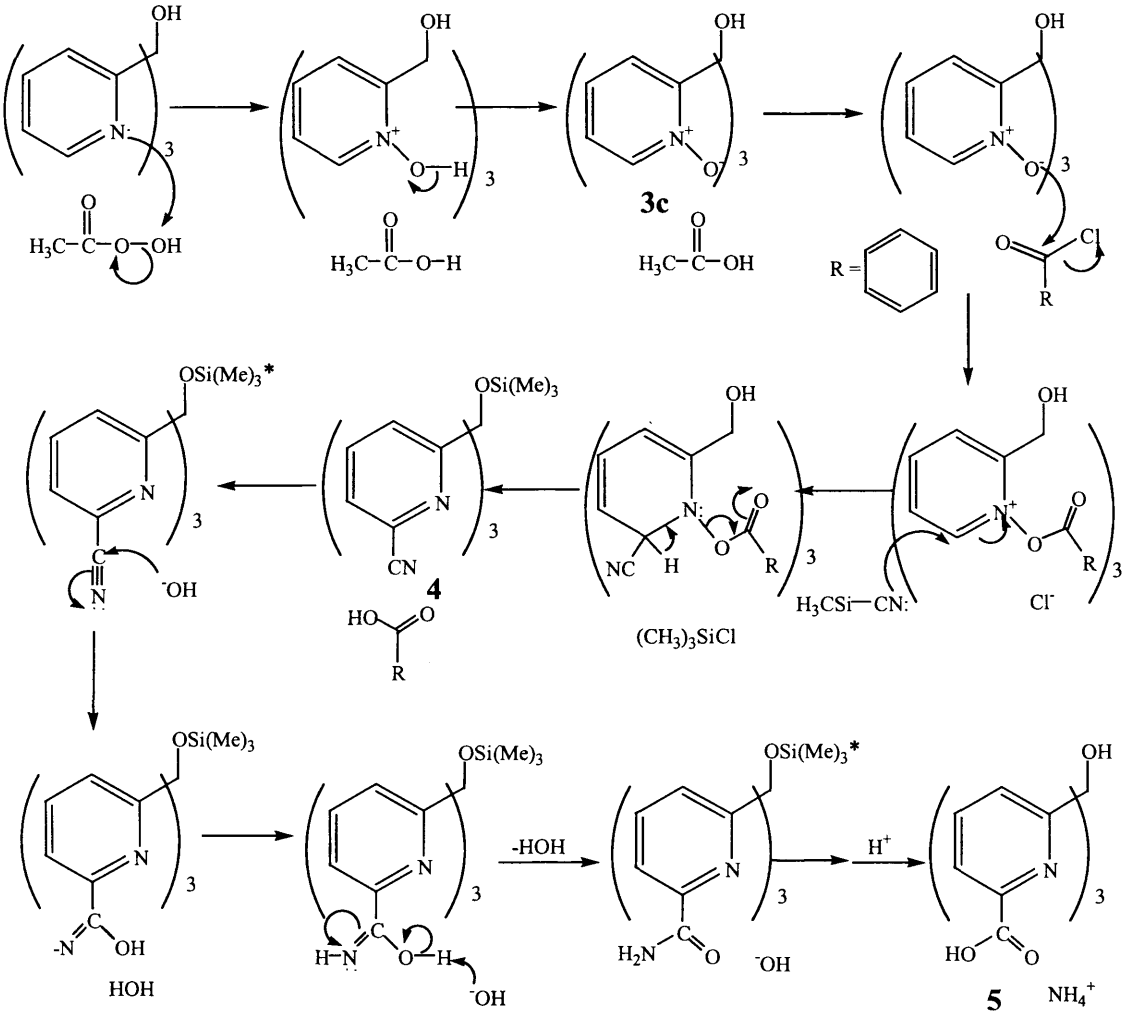

Scheme 2.8 stepwise mechanisms for the synthesis of the final ligand, tris(6-carboxypyrid-2-yl)methanol **5** (L^8). * It is uncertain where the TriMS group cleaves, it can either occur during the base hydrolysis stage or later during acid hydrolysis, the latter being more likely and is reflected in the scheme.

Overall, this route proved to be unfavourable as the desired ligand L^8 could not be synthesised in reasonable yield. Consequently, another prospective route was proposed, route B, one with less synthetic steps and could also permit synthesis of the desired unsymmetrical mono and bis(6-carboxypyrid-2-yl)methanol derivatives.

2.3.2 Route B - Attempted synthesis of mono, bis and tris(6-cyanopyrid-2-yl)methanol precursors via a copper cyanide route.

The cyanation of aromatic halides with copper(I) cyanide is a common procedure that has been used for many years. Pearse *et al.* synthesised 2,6-dicyanopyridine from 2,6-dibrompyridine and Cu(I)CN.[23] Later, a review by Ellis *et al.* summarised a series of aromatic halides undergoing cyanation with a range of cyanide salts (e.g. CuCN, NaCN).[24] All the reactions were carried out at extreme temperatures so the solvents used had high boiling points, e.g., quinoline, pyridine and dimethylformamide (DMF). It was decided to adapt this procedure to synthesise a series of desired cyanide precursors, in particular the mono and bis(6-cyanopyrid-2-yl)methanol (**7a** and **7b**) in order to develop the respective desirable ligands, L^1 and L^2 that could not be attained using route A.

Firstly, 2-bromo-6-cyanopyridine, **6** was prepared (Figure 2.3) by simply refluxing one molar equivalent of Cu(I)CN with 2,6-dibromopyridine in dry DMF. The crude product obtained was chromatographed on silica gel to yield a white crystalline solid (31%). The spectroscopic analyses suggested the successful preparation of compound **6**, its ^{1}H NMR spectrum displayed just one peak in the aromatic region at 7.60 *ppm*. A ν_{CN} band at 2227 cm^{-1} was seen in the IR spectrum indicating the presence of the cyano group.

However, it was the electrospray mass spectrum (ESMS) that confirmed its existence, the isotopes (m/z) 181.9 [$M^{79}Br^-$], 183.9 [$M^{81}Br$] were detected.

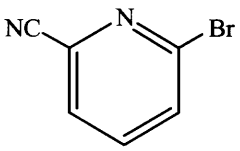

Figure 2.3 molecular structure of 2-bromo-6-cyanopyridine, **6**.

A plausible SN_2 mechanism for the synthesis of **6** is proposed in Scheme 2.9. This is simply an adaptation of the mechanism proposed in the review by Ellis *et. al.*[24]

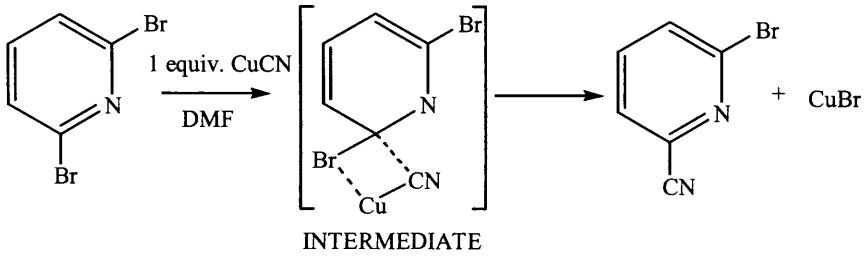

Scheme 2.9 Mechanism for the synthesis of 2-bromo-6-cyanopyridine, **6**.

The successful synthesis of this precursor, **6** offered the opportunity to investigate a series of possible routes to the cyano precursors, **7a-c**. The attempted syntheses are illustrated in Scheme 2.10.

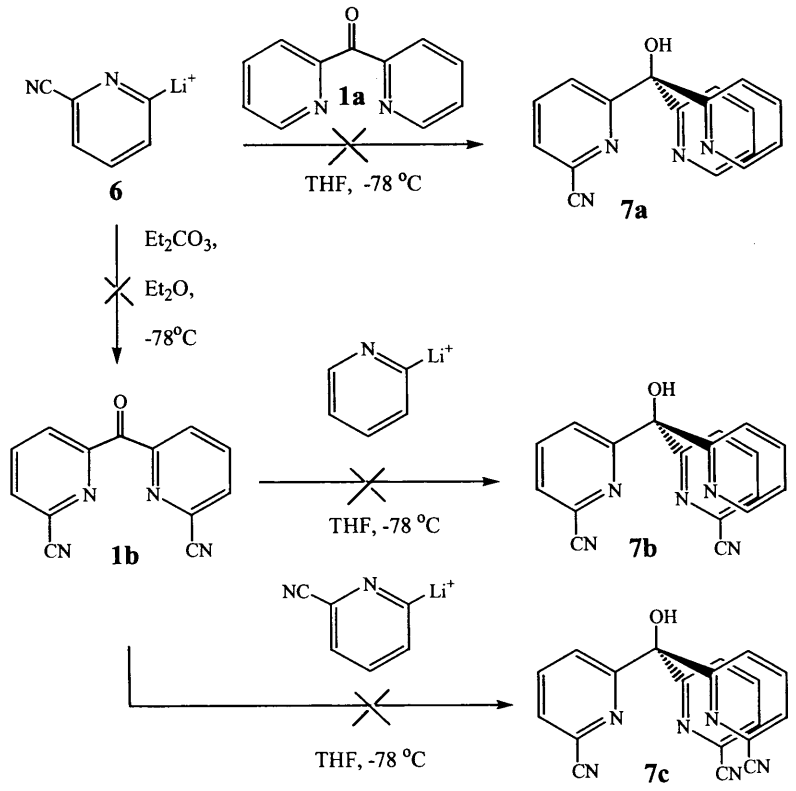

Scheme 2.10 Attempted synthesis of mono, bis and tris(6-cyanopyrid-2-yl)methanol **7a-c**.

The reactions attempted with this precursor (**6**) proved to be extremely problematic, ^{1}H NMR analysis of the reaction mixture of **7a** indicated peaks largely due to the starting materials, bis(2-pyridyl)ketone, **1a** and 2-bromo-6-cyanopyridine, **6**. Comparison of the IR spectra of compounds **1a** and **6** with the crude mixture of **7a** also indicated the presence of un-reacted starting material. The ν_{CO} band corresponding to the ketone is seen at 1681 cm^{-1} (one would expect the loss of this band upon the formation of a tertiary alcohol). The EI mass spectrum of this compound also confirmed the presence of the starting materials, **1a** and **6**. This problem was also seen while synthesising bis(2-cyanopyrid-6-yl)ketone **1b.** These unsuccessful reactions were supported by the ^{1}H NMR spectrum; peaks obtained in the aromatic region were very similar to the starting material, **6**. As a result of this, further reactions with this precursor were stopped. Its lack of

reactivity was probably due to the instability of the lithiated intermediate species formed upon the addition of n-butyl lithium (1.6M *n*-BuLi in hexane). The lithiated species may be reacting with itself (as shown in Figure 2.4) and as a consequence preventing the reaction proceeding.

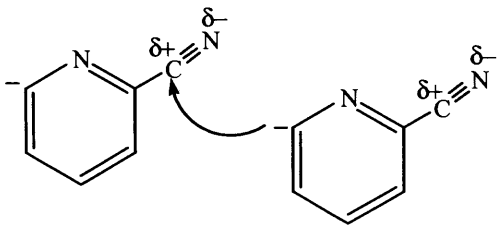

Figure 2.4 Lithiated intermediate.

Thus, an alternative approach to the synthesis of these desired cyano precursors **7a-c** and **1b** was initiated, one that did not involve the lithiation of bromo derivatives in the presence of cyano groups. Scheme 2.11 presents a series of reactions with mono, bis and tris(6-bromopyrid-2-yl)methanol derivatives, **8a-c** and Cu(I)CN (one, two or three molar equivalents respectively) in dry DMF to synthesise the respective cyano derivatives **7a-c**. Firstly, the mono, bis and tris bromo derivatives **8a-c** were prepared (shown in Scheme 2.11) by adapting the method used widely in previous literature for the synthesis of tris(6-bromopyrid-2-yl)methanol ligand.[10,12] The relevant bromopyridine derivative was suspended in an ether solution and cooled to –78 °C, to this one molar equivalent of *n*-BuLi was added. After five minutes of stirring, the relevant pyridyl ketone derivative solution was added to the lithiated intermediate and reacted for a further two hours at this temperature. The resulting reaction mixture was warmed to 0°C, quenched with dilute 10 % HCl solution and then basified with 10 % K_2CO_3 solution. The aqueous phase was washed with chloroform and the organic layers were combined, dried and evaporated

under a reduced pressure. The oily mono(6-bromopyrid-2-yl)-bis(pyrid-2-yl)methanol (**8a**) and bis(6-bromopyrid-2-yl)-mono(pyrid-2-yl)methanol (**8b**) derivatives obtained required further purification by column chromatography (DCM / MeOH 9.5: 0.5). They were isolated in good yields (86% and 55% respectively). The tris(6-bromopyrid-2-yl)methanol derivative, **8c** only required re-crystallisation with cold methanol. The white solid was isolated in high yield (93%). These novel mono and bis bromo tripodal derivatives were characterised by using the following spectroscopic instrumentation, ^{1}H and ^{13}C NMR, infrared (IR) and EIMS. There was not much difference in their IR spectra as all three derivatives contain the same functional groups. In their ^{1}H NMR spectra, aromatic peaks between 7.10 – 8.45 *ppm* were observed at virtually the same chemical shifts in all three derivatives but with varying integration values that were dependent on the presence of mono, bis or tris(6-bromopyrid-2-yl) unit (s). The two unsymmetrical novel bromo derivatives **8a** and **8b** gave accurate masses (342.0237 and 419.9342 respectively) for the ion $[\mathbf{8a} / \mathbf{8b}+H]^{+}$.

The cyanation of these bromo derivatives were performed in DMF at high temperatures in the presence of Cu(I)CN (see experimental for full procedure). The crude products of **7a**, **7b** and **7c** were chromatographed in turn on silica gel and eluted with DCM / MeOH (95:5) as mixtures were observed in their spectroscopic data possibly due to mixtures of all three cyano derivatives. The fractions obtained from the column were still impure as indicated by the ^{1}H NMR spectra and TLC (thin layer chromatography). Attempts to further purify the fractions were unsuccessful. Further investigations are required to explain the reactivity of this synthetic route. The reactions were therefore not continued in the intended direction (Scheme 2.11 step iii) hence, an alternative route for

the synthesis of these desired ligands L^3-L^8 was to be investigated. A cleaner route that did not require the use of potentially hazardous reagents such as Cu(I)CN in DMF or Me_3SiCN.

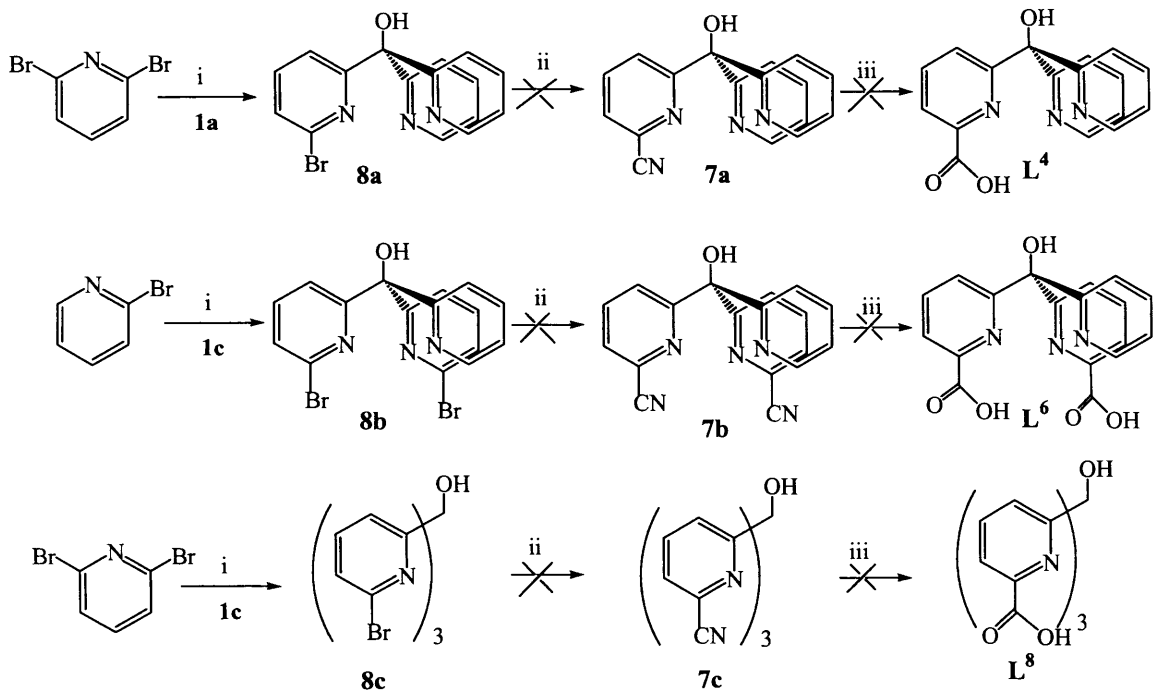

Scheme 2.11 Route B Attempted synthesis of mono, bis and tris(6-carboxypyrid-2-yl)methanol, L^4, L^6 and L^8. i)Et_2O, *n*-BuLi, **1a** / **1c**, -78 °C ii) Cu(I)CN, DMF, stir at 120°C iii) NaOH, ethylene glycol, reflux.

2.3.3 Route C - Synthesis of mono, bis and tris(6-sodiumcarboxypyrid-2-yl)methanol via Pd catalysed carbonylation reactions.

It has been observed that Peng *et al.* synthesised the tris(6-sodiumcarboxypyrid-2-yl)methanol ligand (78%) via the tris(6-methylcarboxypyrid-2-yl)methanol intermediate.[12] The yield obtained was encouragingly better than route **A** and its publication instigated the development of route C which is shown in Scheme 2.12.

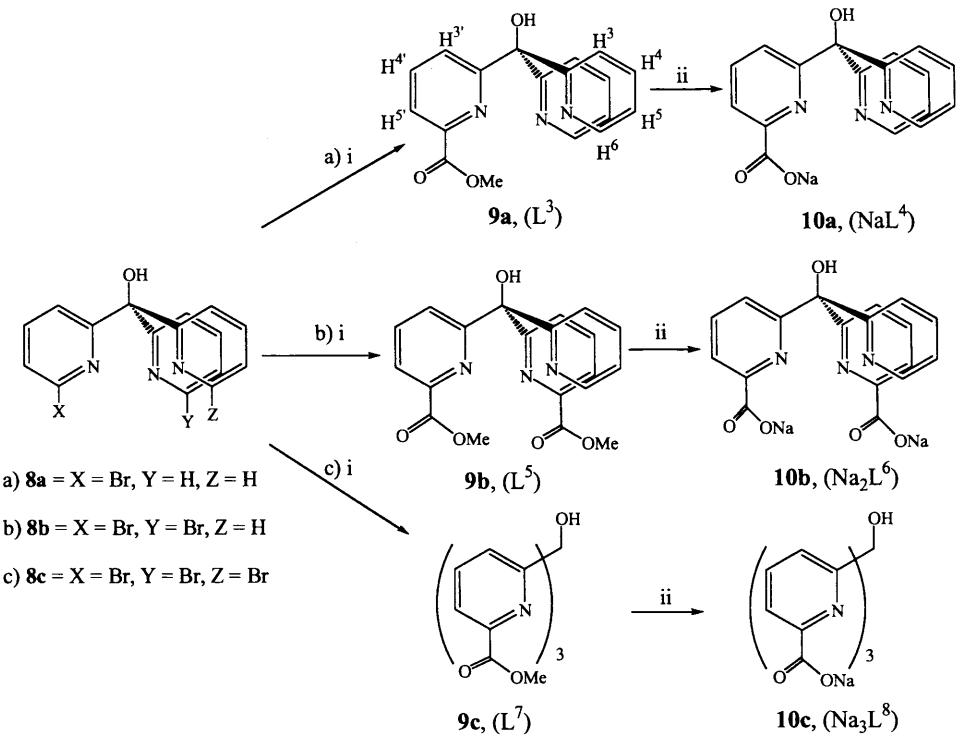

Scheme 2.12 Route C Synthesis of mono, bis and tris(6-methylcarboxypyrid-2-yl) / (6-sodiumcarboxypyrid-2-yl)methanol, L^{3-8} Key: i) $Pd(PPh_3)_4$, CO, NEt_3, MeOH, toluene, 33 bar and 100°C ii) NaOH, H_2O, toluene, reflux.

Again, the mono, bis and tris(6-bromopyrid-2-yl)methanol tripodal derivatives, **8a-c** were readily prepared (Scheme 2.11) in good yields. In turn, these ligands were suspended in toluene to which a 10 molar excess of methanol and triethylamine was added. The reaction mixtures in the presence of a palladium catalyst, $Pd(PPh_3)_4$ (5% w/w of bromo derivative) were subjected to high pressures (33 bar) of carbon monoxide gas at high temperatures (100°C) in a stainless steel Parr reactor and reacted for 72 hours. Carbonylation of all three bromo tripodal derivatives proved to be successful. The mono(6-methylcarboxypyrid-2-yl)bis(pyrid-2-yl)methanol, **9a** (L^3) and tris(6-methylcarboxypyrid-2-yl)methanol, **9c** (L^7) intermediates were purified by simply washing with cold methanol to give beige solids (52% and 60% respectively). The bis(6-

methylcarboxypyrid-2-yl)mono(pyrid-2-yl)methanol, **9b** (L^5) required further purification, the crude product was chromatographed on silica gel and eluted with DCM / MeOH (95:5) to give an orange / brown oil (45%). These ligands were fully characterised by spectroscopic analyses; clear ^1H NMR spectra were obtained for all three (6-methylcarboxypyrid-2-yl)methanol derivatives **9a**, **9b** and **9c** (see Table 2.3). Comparison of their spectra helped assign each proton in the aromatic region. It is noticed that the protons in the aromatic region for all three ligands appear at roughly the same chemical shifts as expected, the only difference being the integration values for each peak, like the bromo derivatives it too is dependant on the presence of one, two or three (6-methylcarboxypyrid-2-yl) group (s).

	Chemical shift (δ) in *ppm* ($CDCl_3$)						
9a (L^3)	3.90 s, 3H	7.10 t, 2H	7.25 s, 1H	7.60- 7.65 d, dd, 4H	7.76 t, 1H	7.98-8.01 d, 2H	8.45 d, 2H
9b (L^5)	3.82 s, 6H	7.10 t, 1H	7.35 s, 1H	7.60-7.65 m, 2H	7.75 t, 2H	7.95-8.05 d, 4H	8.45 d, 1H
9c (L^7)	3.89 s, 9H	—	—	—	7.71 t, 3H	7.85-7.99 d, 6H	—
$\mathbf{H^x}$	$-OCH_3$	$\mathbf{H^4}$	-OH	$\mathbf{H^3}$, $\mathbf{H^5}$	$\mathbf{H^{4'}}$	$\mathbf{H^{3'}}$, $\mathbf{H^{5'}}$	$\mathbf{H^6}$

Table 2.3 Comparison of chemical shifts in the ^1H NMR spectra's of ligands **9a**, **9b** and **9c**.

The IR spectra support the introduction of the methylcarboxy groups upon carbonylation, a strong ν_{CO} band was observed around 1735 cm^{-1} typical of ester functional groups. Their molecular structures were later supported by accurate mass measurements using ESMS, m/z = 322.1186 $[\mathbf{9a}+H]^+$, 380.1241 $[\mathbf{9b}+H]^+$ and 438.1321 $[\mathbf{9c}+H]^+$.

A plausible mechanism for the synthesis of tris(6-methylcarboxypyrid-2-yl)methanol is illustrated in Scheme 2.13, it is derived from the renowned Heck reaction typically involving the coupling of a halogen atom with an olefin in the presence of a Pd(0) catalyst.[25] This mechanism is applicable to all bromo pyridyl derivatives in this Chapter.

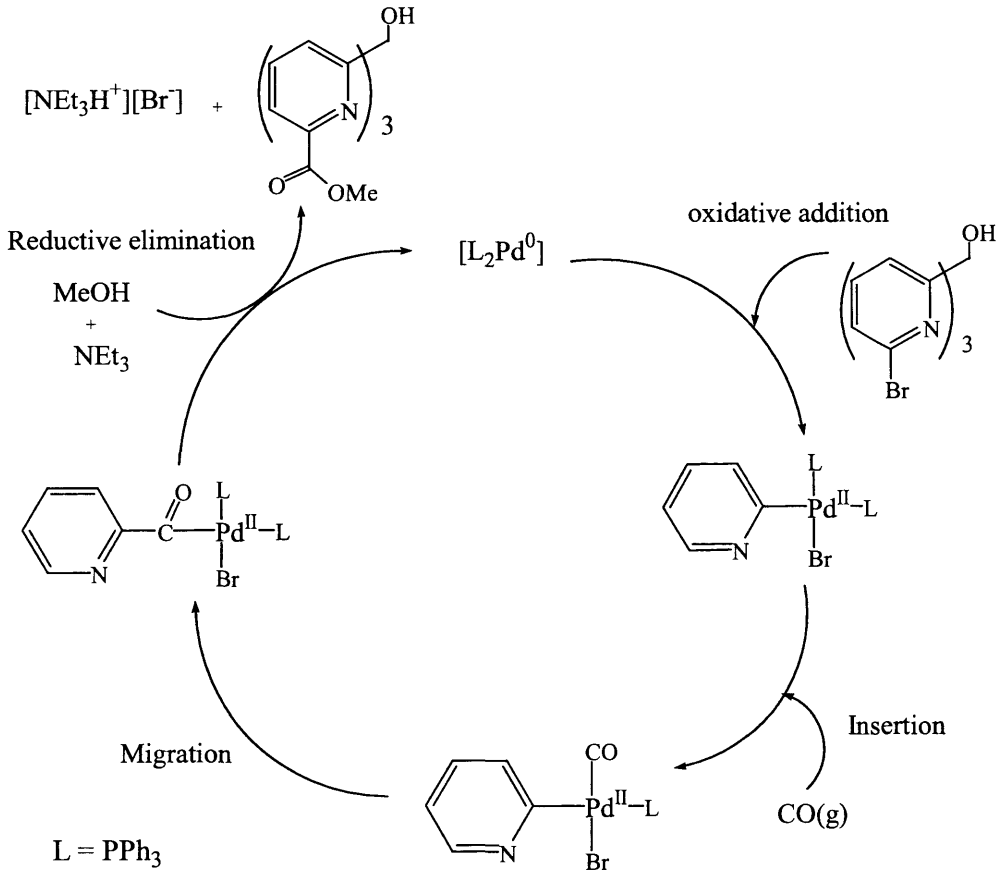

Scheme 2.13 A possible mechanism for the synthesis of tris(6-methylcarboxypyrid-2-yl)methanol **9c**.

These ester derivatives, **9a-c** were finally de-esterified (Scheme 2.12, step ii) by base hydrolysis, the ligands in turn were refluxed with aqueous NaOH solution in toluene for one hour. Upon cooling, the two layers formed were separated, the aqueous phase was treated with activated carbon for 10 minutes at 100°C, cooled and filtered to yield white

solids of the respective mono, bis and tris(6-sodiumcarboxypyrid-2-yl)methanol derivatives, **10a-c** ($Na_xL^{4,6,8}$, 68-75%). The mechanism of the base hydrolysis is illustrated in Scheme 2.14.

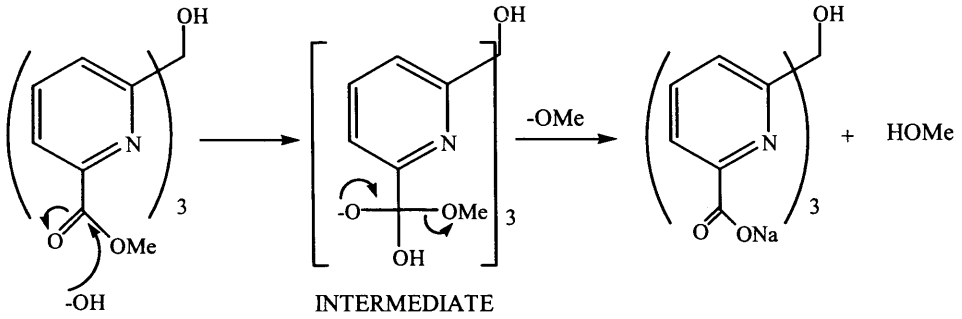

Scheme 2.14 Mechanism for the synthesis of tris(6-sodiumcarboxypyrid-2-yl)methanol derivatives (Na_3L^8).

Again the following spectroscopic investigations indicated the successful synthesis of the desired ligands **10a-c**. Table 2.4 illustrates their ^1H NMR data. Again, it is noticed the protons in the aromatic region for all three ligands appear at roughly the same chemical shifts as expected, the only difference is the integration values for each peak. Again, this variance is dependent on the presence of one, two or three sodiumcarboxylate (s) at the periphery of the pyridine ring (s).

	Chemical shift (δ) in *ppm* (D_2O)				
10a (NaL^4)	7.45, t, 2H	7.52, m, 4H	7.58, t, 1H	7.85-7.95, m, 2H	8.48, d, 2H
10b (Na_2L^6)	7.40, t, 1H	7.56, m, 2H	7.61, t, 2H	7.90-7.98, m, 4H	8.48, d, 1H
10c (Na_3L^8)	__	__	7.63, t, 3H	7.85-7.90, d, 6H	__
$\mathbf{H^x}$	$\mathbf{H^4}$	$\mathbf{H^3}$, $\mathbf{H^5}$	$\mathbf{H^{4'}}$	$\mathbf{H^{3'}}$, $\mathbf{H^{5'}}$	$\mathbf{H^6}$

Table 2.4 Comparison of chemical shifts in the ^1H NMR spectra's of ligands **10a**, **10b** and **10c**.

The IR data for the above ligands were compared to that of the methylcarboxy derivatives. A noticeable shift (to lower wave numbers, ~ 100 cm^{-1}) in ν_{CO} band was observed and can be attributed to the formation of sodium carboxylate groups. The ES mass spectra for all three ligands shows peaks for the following ions; m/z = 330 [**10a**+H]$^+$, 352 [**10a**+Na]$^+$, 414 [**10b**+Na]$^+$ and 396 [**10c**-3Na + 4H]$^+$

2.4 Bis(pyrid-2-yl)ketone derivatives

These widely used starting materials, bis(2-bromopyrid-6-yl)ketone **1c** and bis(2-pyridyl)ketone **1a** have not received much attention since they were synthesised. So far, these ligands have only been used as starting materials to synthesise tripodal derivatives discussed earlier in this Chapter.[9-12] Thus, in conjunction with the investigations into the initial development of ligands L[3-8] it was also decided to take this opportunity to broaden the research of these bis(pyrid-6-yl)ketone precursors. Routes A, B and C were similarly applied to this system to develop a series of novel bis(pyrid-6-yl)ketone derivatives.

Initially, the synthesis of bis(pyrid-6-yl N-oxide)ketone **11** was a much desired ligand in constructing an alternative route for the synthesis of bis(pyrid-2-yl N-oxide) mono(pyrid-2-yl)methanol, **3b** (Scheme 2.15).

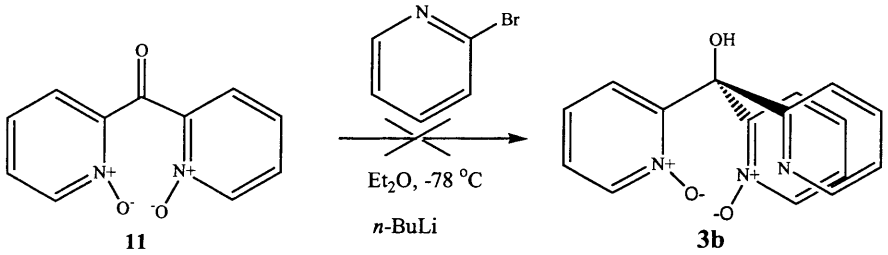

Scheme 2.15 Desired synthesis of bis(pyrid-2-yl N-oxide) mono(pyrid-2-yl)methanol **3b**.

2.4.1 **Route A** – Preparation of bis(6-carboxypyrid-2-yl)1,3-dioxolane, **15** via pyridine-N-oxide.

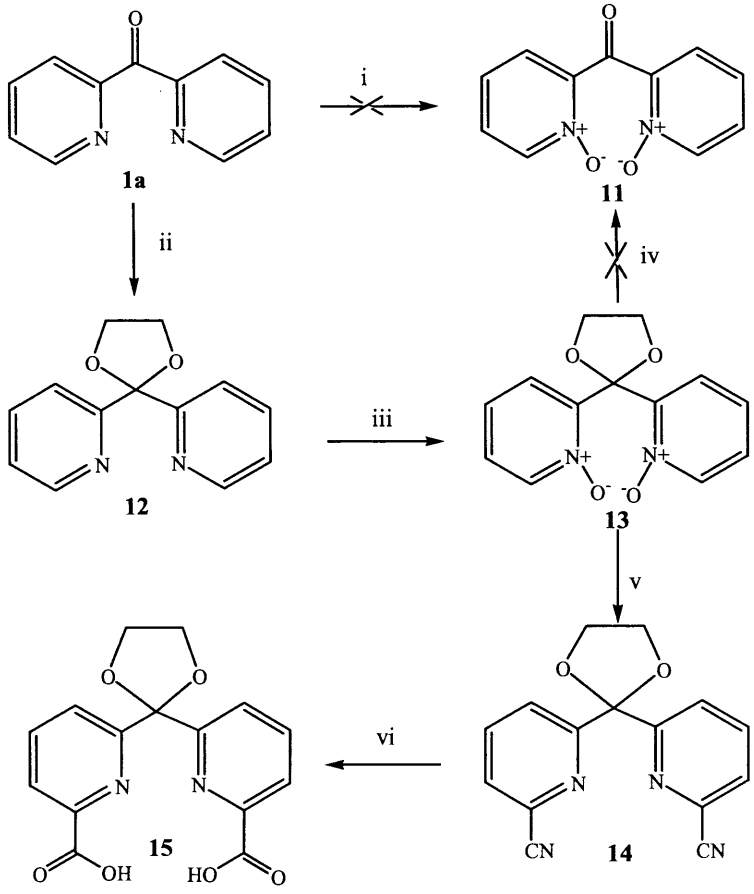

Scheme 2.16 Synthetic steps for the synthesis of bis(6-carboxypyrid-2-yl)1,3-dioxolane **15**. Key: i) glacial acetic acid, H_2O_2 ii) ethylene glycol, toluene, conc.H_2SO_4, reflux for 3 days iii) glacial acetic acid, H_2O_2 iv) 6M HCl, MeOH, reflux for 72hrs v) Me3SiCN, benzolyl chloride, DCM vi) NaOH, toluene, reflux.

Attempts to oxidise bis(2-pyridyl)ketone, **1a** (Scheme 2.16 step i) with glacial acetic acid and H_2O_2 was not a straightforward procedure. A mixture of compounds was observed in the ^1H NMR spectrum, possibly containing both mono and bis(pyrid-6-yl N-oxide)ketone derivatives, which proved difficult to separate using column chromatography. The reaction was therefore repeated with two equivalence of mcpba,

mixtures of un-reacted starting materials were observed in the spectroscopic data. It was assumed that the carbonyl group was inhibiting this reaction and as a result of this problem the carbonyl group was protected. A cyclic ketal-protecting group was integrated and the intermediate, bis(pyrid-2-yl)1,3-dioxolane, **12** (76%) was formed (see step (ii) in Scheme 2.16). This technique was adapted from reports published by Newkome *et al.*[26] Bis(2-pyridyl)ketone, **1a** and ethylene glycol was refluxed in toluene using a Dean-Stark apparatus in the presence of an acid catalyst (conc. H_2SO_4) for three days. The mixture was concentrated and purified by washing with water and then chloroform. The organic layer was evaporated under a reduced pressure to give the protected compound, **12** in good yield (76%). Crystals of this ligand was grown by the slow diffusion of diethyl ether into acetonitrile solution of **12**. X-ray diffraction studies confirmed the expected structure illustrated in Figure 2.5. Table 2.5 reveals its selected bond lengths and angles, which were typical.

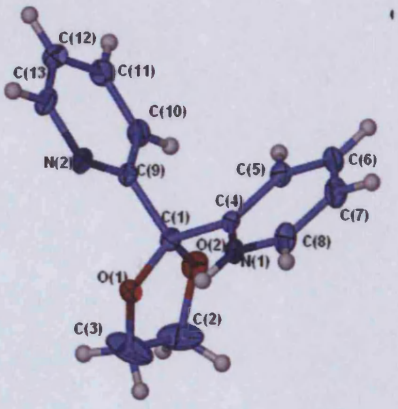

Figure 2.5 Crystal structure of bis(pyrid-2-yl)1,3-dioxolane, **12**.

Table 2.5 Bond distance (Å) and angles (°) for **12**.

C(1)-O(2)	1.410(3)	O(2)-C(1)-O(1)	108.1(2)
C(1)-O(1)	1.415(3)	O(2)-C(1)-C(4)	109.6(2)
C(1)-C(4)	1.520(4)	O(1)-C(1)-C(4)	109.1(2)
C(1)-C(9)	1.530(4)	O(2)-C(1)-C(9)	110.3(2)
C(4)-N(1)	1.337(3)	O(1)-C(1)-C(9)	110.8(2)
C(9)-N(2)	1.341(4)	N(1)-C(4)-C(1)	118.5(2)
		N(2)-C(9)-C(1)	114.9(2)

Spectroscopic data confirmed that the oxidation (Scheme 2.16 (iii)) of **12** was now successful. Table 2.6 compares the ^{1}H NMR spectra of the oxide derivative **13** with **12**, a typical shift in the aromatic region is observed. There is a clear decrease in chemical shift for protons H^5 and H^6 that lie closest to the N-oxide group, protons H^3 and H^4 experience only a slight increase in chemical shift. The expected N-oxide band is seen in the IR spectrum at 1248 cm^{-1}. The spectroscopic data obtained is consistent with the mass spectrum and confirms the presence of the parent ion m/z = 261 [**13**+H]. Numerous attempts were made to de-protect (Scheme 2.16 iv)[26] the bis(pyrid-6-yl N-oxide)1,3-dioxolane **13** in order to recover the ketone by refluxing with methanol in strong acidic conditions (6M HCl and 12M HCl respectively).[26] The ketal group was monitored by ^{1}H NMR experiments, the presence of the ketal peak at ~ 4.20 *ppm* in all the spectra obtained proved the de-protection was unusually unsuccessful. There are a number of other methods[27] that could have been used to cleave the 1,3-dioxolane, the following in particular may have been successful; heating the **13** with pyridinium tosylate (PPTS) in acetone and water,[28] or heating with 80% AcOH at 65 °C for 5 minutes.[29] Regardless of the problems experienced, it was decided to pursue in the subsequent directions (Scheme 2.16 steps v, vi). Bis(6-cyanopyrid-2-yl)1,3-dioxolane **14** was synthesised (Scheme 2.16 step v) using the same synthetic conditions as seen for the preparation of tris(6-cynopyrid-

2-yl)trimethylsilane precursor, **4**. The crude product of **14** was chromatographed on silica gel and eluted with DCM / MeOH (95:5) to give a beige solid (37%). The ^{1}H NMR spectrum of this compound displayed three peaks in the aromatic region integrating to two protons each, suggesting that the protons on both pyridyl rings are equivalent. Table 2.6 shows proton $\mathbf{H^6}$ is absent indicating its substitution by a cyano group. The electronegativity of this group is suggested by the shift of the aromatic peaks to higher frequencies. The IR spectrum confirms that the electronegative group is a cyano group. The mass spectrum also supported this by giving the expected parent ion $[M+H]^+$. Finally the cyano derivative **14** is hydrolysed (Scheme 2.16 step vi) with aqueous NaOH in toluene to give the final ligand bis(6-carboxypyrid-2-yl)1,3-dioxolane **15** (48%). The structure of this compound was again deduced by analyses of its ^{1}H NMR, IR and ESMS data. The IR spectra, produced a ν_{CO} band at ~1728 cm^{-1} corresponding to carboxylic acid groups. Another indication of a successful reaction was the disappearance of the ν_{CN} band at 2237 cm^{-1}.

Ligand (Solvent)	Chemical shift (δ) in *ppm*				
	Ketal	**H^3**	**H^4**	**H^5**	**H^6**
1a ($CDCl_3$)	—	8.04,d	7.43,dd	7.84,dd	8.70,d
12 ($CDCl_3$)	4.14	7.80,d	7.70,t	7.11,dd	8.50,d
13 ($CDCl_3$)	4.25	7.92,d	7.20,dd	7.40,dd	8.18,d
14 ($CDCl_3$)	4.15	7.61,d	7.89,t	8.05,d	—
15 (DMSO-d_6)	4.00	8.23,d	8.37,dd	8.48,d	—

Table 2.6 Comparison of ^{1}H NMR spectra's of ligands, **1a**, **12**, **13**, **14**, and **15**.

The successful synthesis of the bis(2-carboxypyrid-6-yl)ketone was still a challenge in this investigation as route A failed to do so, route B was adapted accordingly.

2.4.2 Route B – Preparation of bis(2-carboxypyrid-6-yl)ketone, **17** via copper cyanide route.

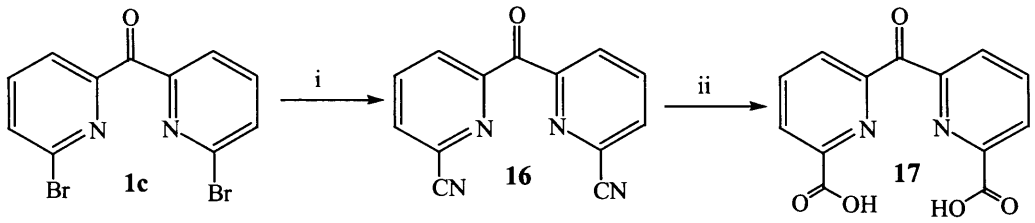

Scheme 2.17 Synthesis of the bis(2-carboxypyrid-6-yl)ketone **17** (L^2). (i) CuCN, DMF, 110°C (ii) NaOH, H_2O, Toluene.

Cyanation of bis(2-bromopyrid-6-yl)ketone, **1c** with Cu(I)CN (Scheme 2.17, (i)) in DMF was successful. The crude product of **16** was chromatographed on silica gel and again eluted with DCM / MeOH (95:5) to yield a beige / brown solid (24%). The ^{1}H NMR spectrum of this compound was compared with bis(2-cyanopyrid-6-yl)1,3-dioxolane **14** to discover that the peaks around the aromatic region were the same indicating the successful preparation of bis(2-cyanopyrid-6-yl)ketone, **16**. The expected nitrile band was seen in the IR spectrum at 2222 cm^{-1} and the parent ion was detected in the mass spectrum. These analyses confirmed the synthesis of compound **16**. The last step involved the hydrolysis of **16** (Scheme 2.17, ii), this was preformed in the same manner as seen in route A (Scheme 2.16, vi) to synthesise bis(2-carboxypyrid-6-yl)ketone, **17** (L^2, 59%). The absence of the ν_{CN} peak and the presence of a ν_{CO} band at 1699 cm^{-1} in the IR spectrum indicate a successful reaction. Comparison of its ^{1}H NMR spectrum with its analogous compound **15** also proved a successful reaction.

2.4.3 Route C – Preparation of bis(2-sodiumcarboxypyrid-6-yl)ketone, **19** via a palladium catalysed carbonylation.

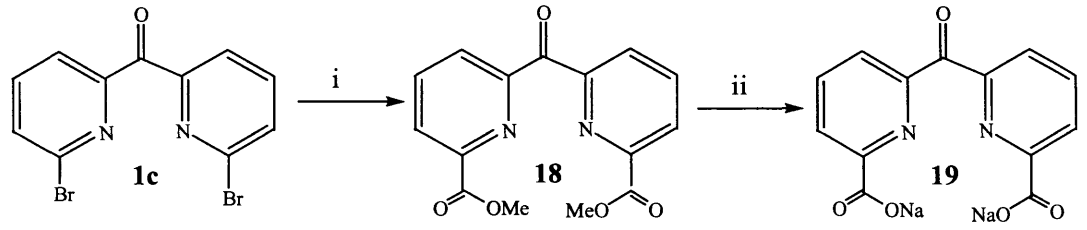

Scheme 2.18 Synthesis of bis(2-methylcarboxypyrid-6-yl)ketone, **18** (L^1) and bis(2-sodiumcarboxypyrid-6-yl)ketone, **19** (Na_2L^2). Key: i) $Pd(PPh_3)_4$, CO, NEt_3, MeOH, toluene, 33 bar and 100°C ii) NaOH, H_2O, toluene, reflux.

However, it was route C (illustrated in Scheme 2.18) that proved to be the simplest and highest yielding. The intermediate, bis(2-methylcarboxypyrid-6-yl)ketone, **18** (L^1) was synthesised with relative ease in comparison to the other two routes. The product was recrystallised from methanol and a beige solid was obtained (65%). The expected ν_{CO} bands corresponding to the ester groups (1745 cm^{-1}) and the ketone (1717 cm^{-1}) was seen in the IR along with the expected parent ion $[M+H]^+$ in the mass spectrum. This intermediate allowed the synthesis to pursue in the subsequent directions. Compound **18** was de-esterified (Scheme 2.18 step ii) in the same way as seen for compounds **9a-c** to give bis(2-sodiumcarboxypyrid-6-yl)ketone **19** (Na_2L^2, 88%). Again the expected ν_{CO} bands were observed in the IR spectrum, one at 1662 cm^{-1} for the ketone and one at 1622 cm^{-1} for the sodium carboxylates. The parent ion $[M-Na]^-$ was also detected in the mass spectrum. The ^1H NMR data of the ligands **1c**, **18** and **19** were compared to help assign each peak to each proton, their data is presented in Table 2.7. The two pyridyl rings are equivalent in all three compounds as only three major peaks are present in the aromatic region.

Ligand (Solvent)	Chemical shift (δ) in *ppm*			
	-OMe	H^3	H^4	H^5
1c ($CDCl_3$)	—	7.70, d, 2H	7.76, t, 2H	8.09, d, 2H
18 (L^1, $CDCl_3$)	3.95, s, 6H	8.25, d, 2H	8.00, t, 2H	8.35, d, 2H
19 (Na_2L^2, DMSO-d_6)	—	8.58, d, 2H	8.75, t, 2H	8.80, d, 2H
(D_2O)	—	7.80, d, 2H	7.63, t, 2H	7.85, d, 2H

Table 2.7 Comparison of ^{1}H NMR spectra of ligands, **1c**, **18** and **19**.

2.5 Conclusions and suggestions for further research

Overall, route A proved to be unsuccessful as all four desired acid derivatives could not be synthesised. Selective oxidations of the pyridyl nitrogen atoms were unattained with mcpba. Although the intermediate, tris(pyrid-2-yl-N-oxide)methanol **3c** (92%) was easily obtained using a non-selective method. Pursuing in the proposed direction produced the cyano intermediate, tris(6-cyanopyrid-2-yl)methoxy(trimethylsilane) **4** and its base hydrolysis product gave the desired ligand, tris(6-carboxypyrid-2-yl)methanol **5** (L^8, 30%). Route A was also used for the attempted synthesis of bis(pyrid-2-yl N-oxide)ketone **11** precursor in a view to synthesise the desired unsymmetrical tripod, bis(pyrid-2-yl N-oxide)mono(pyrid-2-yl)methanol, **3b**. This also proved to be unsuccessful as **11** could not be prepared even via the protection route that involved the synthesis of bis(pyrid-2-yl N-oxide)1,3-dioxolane, **13**. The ketone could not be recovered even in strong acidic conditions. Regardless of the problems experienced, it was decided to pursue in the subsequent directions to synthesise the novel ligands, bis(6-cyanopyrid-2-yl)1,3-dioxolane, **14** and bis(6-carboxypyrid-2-yl)1,3-dioxolane, **15** respectively.

However, an alternative route for the development of mono, bis and tris(6-carboxypyrid-2-yl)methanol derivatives (L^4, L^6 and L^8) was investigated. Route B involved the cyanation of mono, bis and tris(6-bromopyrid-2-yl)methanol derivatives, **8a-c** with Cu(I)CN. The problems that were encountered were obtaining pure samples of the respective mono, bis and tris(6-cyanopyrid-2-yl) derivatives **7a-c** again limiting the chances of synthesising the desirable ligands. Nevertheless, in the process of this investigation some useful novel compounds were synthesised, mono, bis and tris(6-bromo pyrid-2-yl)methanol intermediates **8a-c**. These compounds could also be used in route C for the successful preparation of the desired ligands (sodium salts) mono, bis and tris (6-sodiumcarboxypyrid-2-yl)methanol derivatives. The chemistry of bis(2-bromopyrid-6-yl)ketone, **1c** was studied and the cyanation of **1c** with Cu(I)CN was successful but gave low yielding bis(2-cyanopyrid-6-yl)ketone, **16** (24%). Hydrolysis of this intermediate **16** resulted in the synthesis of bis(2-carboxypyrid-6-yl)ketone, **17** in reasonable yield (59%).

Finally, route C was adapted from previous work carried out by Peng *et al.* He published the synthesis of tris(6-sodiumcarboxypyrid-2-yl)methanol via a tris(6-methylcarboxypyrid-2-yl)methanol intermediate. This procedure was adapted to develop unsymmetrical derivatives via the carbonylation of the mono and bis (6-bromopyrid-2-yl)methanol derivatives, **8a** and **8b**. These reactions proved to be successful in that the following novel intermediates were synthesised, mono and bis(6-methylcarboxypyrid-2-yl)methanol **9a** (L^3, 45%) and **9b** (L^5, 60%). These ligands were de-esterified like its analogous tris(6-methylcarboxypyrid-2-yl) methanol derivative to produce the desired sodium salts, mono and bis(6-sodiumcarboxypyrid-2-yl)methanol **10a** and **10b** (NaL^4 and Na_2L^6) in good yields (68-75%). This route was also employed to synthesise bis(2-

methylcarboxypyrid-6-yl)ketone **18** (L^1), it involved the carbonylation of bis(2-bromopyrid-6-yl)ketone **1c**, which in turn led to the preparation of the desired bis(2-sodiumcarboxypyrid-6-yl)ketone **19** (Na_2L^2), a simpler and higher yielding approach to that used in route B.

Route C proved to be very successful as it produced some useful novel ligands. It may prove interesting to synthesise similar amide derivatives. This may be achieved by replacing the methanol reagent at the carbonylation step by an amine group (e.g. such as a tertiary amine, triethylamine).

2.6 Experimental

2.6.1 Instrumentation

NMR spectra were recorded on a Bruker DPX 400 spectrometer at 400 (^{1}H) and 100.7 MHz (^{13}C), respectively, and the spectra were referenced to the residual solvent peak. Coupling constants, *J*, are in Hertz. Infrared absorptions were recorded on a Perkin-Elmer 1600 series FTIR spectrometer in KBr or a Jasco FT / IR-660 Plus. The national mass spectrometry service centre at the University of Wales, Swansea sponsored by EPSRC performed Mass spectrometry. See Chapter 3 for X-ray diffraction instrumentation.

2.6.2 Synthesis of tris(pyrid-2-yl)methanol derivatives

Preparation of bis(pyrid-2-yl)ketone derivatives [10]

A common method was employed for the preparation bis(pyrid-6-yl)ketone derivatives. The required bromopyridine derivative (typically 21mmol) was suspended in dry diethyl ether (*ca.* 150ml) and cooled to –78 °C. A solution of n-butyl lithium (n-BuLi) in hexanes

(23mmol, of a 1.6M solution) was added drop wise to the stirring solution. After a period of 5mins, a solution of diethyl carbonate (9.5mmol in 20ml of diethyl ether) was slowly transferred *via* a cannula to the orange lithiated solution. After stirring for a further 2 hours at -78°C the reaction was allowed to warm to 0 °C and quenched with 10% HCl until acidic. The resulting mixture was then basified with 10% aqueous K_2CO_3 and the crude product was partitioned between $CHCl_3$ and water. The aqueous layer was washed twice with $CHCl_3$ (60ml) and the organic layers combined and dried with anhydrous $MgSO_4$ (s). After filtration, the organic solvent was evaporated under a reduced pressure.

Preparation of bis(pyrid-2-yl)ketone **1a**

For the preparation of **1a**, 2-bromopyridine was used as the starting material. A dark brown oil was produced and did not require further purification (90%). ^{1}H NMR ($CDCl_3$); δ 7.43 (dd, 2H, J = 7.8, 1.6 Hz, H^5); 7.84 (dd, 2H, J = 7.8, 1.6Hz, H^4); 8.04 (d, 2H, J = 7.8Hz, H^6); 8.70 (d, 2H, J = 7.8Hz, H^3); IR KBr/cm^{-1}: ν = 3926s, 2840s, 1681s, 1585w, 1463m, 1356m, 1303m, 997w, 936m, 745m; EIMS (m/z): 184 [M].

Attempted synthesis of bis(2-cyanopyrid-6-yl)ketone **1b**

2-Bromo,6-cyanopyridine **6** was the starting material for the preparation of **1b**. A dark orange oil was obtained as a result of the work up (86%). Characterisations of the compound proved the synthesis of **1b** was unsuccessful.

Spectroscopic data for bis(2-bromopyrid-6-yl)ketone[10,12] **1c**

For the preparation of **1c**, 2,6-dibromopyridine was used as the starting material. A white solid was obtained after recrystallisation with hot methanol (92%). ^{1}H NMR ($CDCl_3$) δ 7.70 (d, 2H, J = 7.9 Hz, H^5), 7.76 (t, 2H, J = 8.0 Hz, H^4), 8.09 (d, 2H, J = 7.9 Hz, H^3); ^{13}C NMR ($CDCl_3$) δ 124, 131, 139, 141, 154, 190 (C=O); IR KBr/cm^{-1}: ν =1681s, 1559s, 1460m, 1322s, 1239m, 1095w;EIMS (m/z): 341 [M+H$^+$]

Preparation of tris(pyrid-2-yl)methanol **2**

2-Bromopyridine (6.3mmol) was dissolved in diethyl ether (45ml). With vigorous stirring the temperature was lowered to -78°C and n-BuLi (6.3mmol, of a 1.6M solution) was added drop wise. After stirring for 5mins, a solution of bis(2-pyridyl)ketone **1a** (6.3mmol in 10ml THF) was slowly transferred via a cannula to the lithiated intermediate. The product was isolated in the same manner as seen above for compounds **1a-c**. The dark brown crude solid was recrystallised from petroleum ether 60-80 to give a beige solid (83%). ^{1}H NMR ($CDCl_3$); δ 7.20 (s, 1H, O*H*), 7.27 (dd, 3H, J = 8.0, 5.1 Hz, H^5), 7.68 (t, 3H, J = 8.1 Hz, H^4), 7.74 (d, 3H, J = 8.1 Hz, H^3), 8.50 (d, 3H, J = 5.1 Hz, H^6); IR KBr/cm^{-1}: ν = 3470m, 3040m, 2995w, 1580s, 1458s, 1340m, 1232m, 1186m, 1158w, 1105s, 1041m, 985m, 920m, 768w, 730m; MS (m/z): 262 [M-H]$^+$.

Preparation tris(pyrid-2-yl N-oxide)methanol **3c**

Tris(pyrid-2-yl)methanol, **2** (0.95mol) was refluxed with glacial acetic acid (2.5ml) and three molar equivalence of H_2O_2 (30 aq. wt / %) for 63h. The solvent was evaporated carefully using a pre-trap to leave a yellow sticky solid. This was purified by washing

with acetone to give a pale yellow solid (92%). ^{1}H NMR ($CDCl_3$); δ 7.25 (dd, 3H, J = 6.5, 5.9, 6.5 Hz, H^5); 7.35 (dd, 3H, J = 6.3 Hz, H^4); 7.47 (d, 3H, J = 6.4 Hz, H^3); 8.20 (d, 3H, J = 6.5 Hz, H^6); IR KBr/cm^{-1}: ν = 3470w, 3040m, 2995w, 1580s, 1458s, 1340m, 1249s, 1186w, 1158m, 1105m, 1041m, 985w, 920w, 768m, 730m; EIMS (m/z): 334.1[M+Na$^+$]

Preparation of tris(6-cyanopyrid-2-yl)methoxy(trimethylsilane) **4**

Me_3SiCN (0.051mol.) was added slowly to a solution of tris(pyrid-2-yl N-oxide)methanol, **3c** (5.1mmol.) in DCM (55ml). After a period of 5 minutes, benzoyl chloride (0.02mol.) was added and stirred overnight. The reaction mixture was concentrated to half the volume very carefully using a pre-trap. To this 10% K_2CO_3 solution (50ml) was added and the layers were separated. The organic layer was collected and carefully evaporated to give a solid when immersed in a cold solvent. The brown liquid was decanted from the flask and the solid was left to dry under vacuum. The crude product was chromatographed on silica gel and eluted with DCM / MeOH (99:1). The removal of the solvent under a reduced pressure gave the desired light pink product (20%). ^{1}H NMR ($CDCl_3$); δ 0.01 (s, 9H, CH_3) 7.55 (d, 3H, J = 7.8 Hz, H^5), 7.79 (m, 6H, H^3, H^4); ^{13}C NMR ($CDCl_3$) δ 116 (RCN), 126, 128, 131, 137, 148, 163; IR KBr/cm^{-1}: ν = 2238s, 1582s, 1442s, 1261s, 1145m, 1084w, 900s, 786w; EI MS (m/z): 411[M+TriMS].

Preparation of tris(6-carboxypyrid-2-yl)methanol **5** (L^8)

tris(6-cyanopyrid-2-yl)methoxy(trimethylsilane), **4** (0.372mmol) and solid NaOH (1.48mmol) were suspended in ethylene glycol (10ml) and refluxed for 2.5hrs at 220°C during which ammonia was evolved. The resulting solution was cooled and water (10ml)

was added and extracted with ether-toluene (2 x 10ml). The aqueous layer was collected and concentrated to half the volume. To this stirring solution, 5M HCl (4-5drops) was added until it reached pH 4.5. A fine grey precipitate was observed and could only be filtered through a filter cannula. The grey solid was dried under a reduced pressure for two hours (30%). ^{1}H NMR (D_2O): 7.63 (dd, 3H, J = 7.6, 2.0 Hz, H^4), 7.80 (m, 6H, H^3, H^5); ^{13}C NMR (D_2O): 80(C-OH), 123, 128, 133, 152, 161, 173; IR KBr/cm^{-1}: ν = 3366mb, 1710m, 1653m, 1581m, 1261s, 1192w, 1081w, 804m; FAB MS (m/z): 418 [M+Na$^+$]

Preparation of 2-bromo-6-cyanopyridine **6**

A mixture of 2,6-dibromopyridine (0.03mol), copper(I) cyanide (0.03mol) and dry DMF (40ml) were gently heated to 100°C and stirred overnight under an argon atmosphere. The reaction mixture was cooled and poured into a beaker containing water (*ca.* 50ml). The mixture was made slightly alkaline with dilute aqueous ammonia solution and carefully decanted into a separating funnel in small portions for washing with DCM (5 x 50ml). The organic layers were combined, dried with $MgSO_4$, filtered and the solvent evaporated. The crude product was chromatographed on silica gel and eluted with hexane / DCM (75:25). A white crystalline solid was obtained (31%). ^{1}H NMR ($CDCl_3$) δ 7.60-7.65 (m, 3H, H^3, H^3 + H^5); ^{13}C NMR ($CDCl_3$): 119(RCN), 125, 135, 141, 145, 152; IR KBr/cm^{-1}: ν = 2227m, 1568s, 1430s, 1261m, 982m, 806s; ESMS (m/z): 181.9 [M^{79}Br$^-$], 183.9 [M^{81}Br]

Attempted preparation of mono (6-cyanopyrid-2-yl)methanol **7a**

2-Bromo-6-cyanopyridine **6** (4.6mmol) dissolved in diethyl ether (46ml) was stirred vigorously and cooled to -78°C to which a solution of n-BuLi in hexanes (4.6mmol of a

1.6M solution) was added dropwise. After stirring for 5mins, a solution of bis(2-pyridyl) ketone **1a** (4.2mmol, in 14ml THF) was slowly transferred *via* a cannula to the lithiated solution. The product was isolated in the same manner as seen above for compounds **1a-c**. A dark brown oil was obtained (86%). Attempts were made to purify the crude by column chromatograph on silica gel with DCM / MeOH (95:5).

Attempted preparation of mono, bis and tris(6-cyanopyrid-2-yl)methanol **7a-c**

A common method was applied for the cyanation of the bromo tripodal derivative **8a-c**.[24] For the preparation of **7a**, mono(2-pyridyl-6-bromo)bis(2-pyridyl)methanol (**8a** 1.3mmol), Cu (I) CN (2.91mmol) and dry DMF (7ml) were gently heated to 120°C and left to stir overnight. The solution was left to cool to room temperature and dilute aqueous ammonia solution (~40ml) was added to the reaction flask. A dark purple solution was formed and washed with DCM (5 x 30ml). The organic layers were combined and dried over $MgSO_4$. The solvent was evaporated under a reduced pressure to leave a dark brown crude product (45%). The crude product was chromatographed on silica gel and eluted with DCM / MeOH (95:5).

Preparation of mono, bis, tris(6-bromopyrid-2-yl)methanol derivatives **8a**, **8b**, **8c**

A general method was adapted for the preparation of these bromo derivatives.[10,12] For example, for the preparation of **8a**, 2,6-dibromopyridine (4.6mmol) was dissolved in diethyl ether (46ml). With vigorous stirring, the temperature was lowered to -78°C to which one molar equivalent of n-BuLi (4.6mmol of a 1.6M solution in hexane) was added drop wise. After stirring for 5mins, a solution of bis(2-pyridyl)ketone **1a** (4.2mmol, in

14ml THF) was slowly transferred to the lithiate. The product was isolated in the same manner as described for compounds **1a-c**.

Spectroscopic data for mono(6-bromopyrid-2-yl) bis(pyrid-2-yl)methanol **8a**

A dark brown oily crude product was obtained, this was chromatographed on silica gel and eluted with DCM / MeOH (95:5) to give a pale yellow solid (42%). ^{1}H NMR ($CDCl_3$): 6.90 (s, 1H, O*H*), 7.10 (d, 1H, J = 7.9 Hz, $H^{5'}$(Br)), 7.25 (dd, 2H, J = 6.4, 1.7 Hz, H^5), 7.45 (d, 1H, J = 7.4 Hz, $H^{3'}$(Br)), 7.60-7.70 (m, 5H, H^3, H^4, $H^{4'}$(Br)), 8.45 (d, 2H, J = 6.4 Hz, H^6). ^{13}C NMR ($CDCl_3$): 79 (C-OH), 121, 122, 123, 126, 136, 138, 139, 147, 161, 164; IR KBr/cm^{-1}: ν = 3407m, 1595s, 1563m, 1428s, 1410m, 1171m, 1141m, 996s, 804m, 755w, 704m; accurate EIMS (m/z): 342.0237 $[M+H]^+$.

Spectroscopic data for bis(6-bromopyrid-2-yl) mono(pyrid-2-yl)methanol **8b**

A dark brown oily crude product was obtained which crystallised upon cooling. The crystals were washed with diethyl ether to give an off-white solid (45%). This was not always the case as sometimes the crude product had to be chromatographed on silica gel and eluted with DCM / MeOH (95:5) to give a white solid (55%). ^{1}H NMR ($CDCl_3$) δ: 6.70 (s, 1H, OH), 7.15 (dd, 1H, J = 6.5, 1.9 Hz, H^5), 7.30 (d, 2H, J = 7.9 Hz, $H^{5'}$), 7.45 (d, 2H, J = 7.2 Hz, $H^{3'}$), 7.65-7.70 (m, 4H, H^3, H^4, $H^{4'}$), 8.45 (d, 1H, J = 6.5 Hz, H^6). ^{13}C NMR ($CDCl_3$) δ: 79 (C-OH), 121, 122, 123, 126, 136, 138, 139, 147, 160, 163; IR KBr/cm^{-1}: ν = 3411m, 1587s, 1562s, 1434m, 1413m, 1166s, 1140m, 989m, 807s, 761m, 712w; accurate EIMS (m/z): 419.9342 $[M+H]^+$.

Spectroscopic data for tris(6-bromopyrid-2-yl)methanol **8c**

A light brown solid was obtained and recrystallised from cold MeOH to yield a beige solid (93%). ^{1}H NMR ($CDCl_3$) δ 6.80 (s, 1H, OH), 7.39 (d, 3H, J = 7.6 Hz, $H^{5'}$), 7.56 (t, 3H, J = 7.7 Hz, $H^{4'}$), 7.69 (d, 3H, J = 7.7 Hz, $H^{3'}$); ^{13}C NMR ($CDCl_3$) δ 80 (C-OH), 122, 127, 139, 140, 163; IR KBr/cm^{-1}: ν = 3406m, 1591s, 1566s, 1436m, 1412s, 1168s, 1143m, 993m, 808w, 759m, 709w; ES MS (m/z): 422 [M-Br^{-}].

Preparation of mono, bis and tris(6-methylcarboxypyrid-2-yl)methanol derivatives[12] **9a, 9b, 9c** ($L^{3,5,7}$)

A common method[12] was used for the carbonylation of bromo pyridyl derivatives **8a-c**. Under argon the relevant bromo tripodal methanol derivative, for example for the synthesis of mono(6-methylcarboxypyrid-2-yl)methanol **9a**, bromo derivative **8a** (2.49mmol) was dissolved in toluene (50ml) to which 10 molar equivalence of triethylamine (0.025mol), methanol (0.026mol) and a palladium catalyst, $Pd(PPh_3)_4$ (0.124mmol, 5% w/w of **8a**) was added. This solution was transferred to a 300 ml stainless steel Parr reactor and was purged with nitrogen (x 3) followed by three purges with CO (g). Finally the reactor was pressurised to 33 bar. The CO (g) cylinder was pressurised to 2 atm. And the autoclave was programmed to heat up to 100 °C and stirred at 500 RPM and left to react for 72 hours. After allowing the reactor to cool to room temperature, the system was depressurised and purged with nitrogen. The solution was filtered to remove the salts that were produced; the filtrate was evaporated to yield the crude product. The crude product was recrystallised with cold MeOH.

Spectroscopic data for mono(6-methylcarboxypyrid-2-yl)bis(pyrid-2-yl)methanol **9a** (L^3)

An orange/brown solid (crude product) was washed with cold MeOH to obtain an off-white solid (52%). ^{1}H NMR ($CDCl_3$): δ 3.90 (s, 3H, C*H*$_3$), 7.10 (t, 2H, *J* = 7.2 Hz, H^4) 7.25 (s, 1H, O*H*), 7.60 (d, 2H, *J* = 7.2 Hz, H^3) 7.65 (dd, 2H, *J* = 7.8, 7.2 Hz, H^5), 7.76 (t, 1H, *J* = 7.9 Hz, $H^{4'}$(OOMe)), 7.98-8.01 (d, 2H, *J* = 7.9 Hz, $H^{5'}$, $H^{3'}$), 8.45 (d, 2H, *J* = 7.8 Hz, H^6). ^{13}C NMR ($CDCl_3$): 50 (CH_3), 80 (C-OH), 121, 122, 123, 126, 136, 138, 149, 151, 161, 164; IR KBr/cm^{-1}: ν = 3257sb, 1732s, 1684w, 1588m, 1435s, 1323m, 1267m, 1148m, 994w; accurate ES+MS (m/z): 322.1186 $[M+H]^+$.

Spectroscopic data for bis(6-methylcarboxypyrid-2-yl) mono(pyrid-2-yl)methanol **9b** (L^5)

An orange/brown oily liquid was obtained (45%). ^{1}H NMR ($CDCl_3$): 3.82 (s, 6H, OC*H*$_3$), 7.10 (t, 1H, *J* = 7.8 Hz, H^4), 7.35 (s, 1H, O*H*), 7.60-7.65 (m, 2H, $H^{3,}$ H^5), 7.75 (t, 2H, *J* = 7.6 Hz, $H^{4'}$). 7.95 (d, 2H, *J* = 7.6 Hz, $H^{3'}$), 8.05 (d, 2H, *J* = 7.6 Hz, $H^{5'}$), 8.45 (d, 1H, *J* = 8.0 Hz, H^6); ^{13}C NMR ($CDCl_3$): 50, 80, 121, 122, 123, 126, 135, 138, 149, 151, 161, 164; IR KBr/cm^{-1}: ν = 3257m, 1745s, 1684m, 1585s, 1435s, 1321w, 1134w, 1019w, 954m; accurate ESMS (m/z): 380.1241 $[M+H]^+$

Spectroscopic data for tris(6-methylcarboxypyrid-2-yl)methanol **9c** (L^7)

The filtrate was evaporated to yield orange oil. The crude product was recrystallised from cold methanol, a beige solid was obtained (60%). ^{1}H NMR ($CDCl_3$) δ 3.89 (s, 9H, OC*H*$_3$), 7.71 (t, 3H, *J* = 7.8 Hz, $H^{4'}$), 7.85 (d, 3H, *J* = 7.8 Hz, $H^{3'}$), 7.99 (d, 3H, *J* = 7.9 Hz, $H^{5'}$), ^{13}C NMR ($CDCl_3$) δ 53, 81, 124, 127, 137, 146, 162, 166; IR KBr/cm^{-1}: ν = 3299mb,

2945s, 2676w, 1730s, 1586s, 1436s, 1315m, 1141m, 994m, 824w; accurate ESMS (m/z): 438.1321 $[M+H]^+$.

Preparation of mono, bis and tris(6-sodiumcarboxypyrid-2-yl)methanol[12] **10a-c**

A common method was used for the ester hydrolysis of methylcarboxy pyridyl derivatives **9a-c**.[12] For example, mono(6-methylcarboxypyrid-2-yl)bis(pyrid-2-yl)methanol, **9a** (0.163g, 0.506mmol) was dissolved in toluene (10ml). NaOH (50% in water, 0.16g, 4mmol) diluted with water (8ml) was added upon which a precipitate was formed. The mixture was refluxed for 1hr., upon cooling to room temperature, the solution phased into two layers. The bottom layer was collected, treated with activated carbon (0.1g) for 10mins at 100°C, and then filtered. The filtrate was evaporated to yield the product.

Spectroscopic data for mono(6-sodiumcarboxypyrid-2-yl)bis(pyrid-2-yl)methanol **10a** (NaL^4)

A pale yellow solid was obtained (70%). ^{1}H NMR (D_2O): 7.45 (t, 2H, J = 6.9 Hz, H^4), 7.52 (m, 4H, H^3, H^5), 7.58 (t, 1H, J = 6.4 Hz, $H^{4'}$), 7.85-7.95 (m, 2H, $H^{3'}$, $H^{5'}$), 8.48 (d, 2H, J = 6.9 Hz, H^6); ^{13}C NMR (D_2O): 83, 121, 122, 123, 126, 136, 138, 149, 152, 161, 166, 173; IR KBr/cm^{-1}: ν = 3388mb, 1630s, 1595s, 1428w, 1381m, 1262m, 1071w, 995m; ESMS (m/z): 330 $[M+H]^+$ and 352 $[M+Na]^+$

Spectroscopic data for bis(6-sodiumcarboxypyrid-2-yl)mono(pyrid-2-yl)methanol **10b** (Na_2L^6)

a pale yellow solid was obtained (68%). ^{1}H NMR (D_2O): 7.40 (t, 1H, J = 6.8 Hz, H^4), 7.56 (m, 2H, H^3, H^5), 7.61 (t, 2H, J = 6.6 Hz, $H^{4'}$), 7.90-7.98 (m, 4H, $H^{3'}$, $H^{5'}$), 8.48 (d, 1H, J = 6.7 Hz, H^6); ^{13}C NMR (D_2O): 83, 122, 123, 126, 136, 139, 148, 152, 161, 166, 173; IR KBr/cm^{-1}: ν = 3428sb, 1649s, 1559m, 1387s, 1262m, 1000m; ESMS(m/z): 414 $[M+Na]^+$.

Spectroscopic data for tris(6-sodiumcarboxypyrid-2-yl)methanol **10c** (Na_3L^8)

A white solid was obtained (75%). ^{1}H NMR (D_2O): 7.63 (t, 3H, J = 6.6 Hz, $H^{4'}$), 7.85-7.90 (d, 6H, J = 6.5 Hz, $H^{3'}$, $H^{5'}$); ^{13}C NMR (D_2O): 82, 123, 123, 152, 161, 166, 173; IR KBr/cm^{-1}: ν = 3411mb, 1652s, 1595m, 1565m, 1455s, 1387m, 1284m, 1077w; ESMS (m/z): 396 [M-3Na + 4H].

2.6.3 Bis(pyrid-2-yl)ketone derivatives

Attempted synthesis of bis(pyrid-2-yl N-oxide)ketone **11**

Bis(2-pyridyl)ketone **1a** (0.25g), glacial acetic acid (5ml) and H_2O_2 (5ml) was added to a round-bottomed flask and refluxed for 63 hrs. The yellow oily substance was evaporated until all the acetic acid was no longer observed in the NMR spectrum. Acetic acid was removed by adding a little Na_2CO_3 to the solution of DCM to yield a white solid (57%).

Attempted synthesis of bis(pyrid-2-yl N-oxide)ketone **11**

2 molar equivalence mcpba was added to a mixture of the ketone **1a** (1 mole) and DCM (8ml). After stirring overnight the mixture was evaporated under vacuum to yield a beige solid (43%).

Attempted synthesis of bis(pyrid-2-yl N-oxide)ketone **11**

A solution of bis(pyrid-6-yl N-oxide)1,3-dioxolane, **13** (0.55mmol), aqueous HCl (18ml, 6M) and MeOH (18ml) was refluxed for 72hrs. The solution was left to cool and then evaporated to dryness to yield a yellow solid (49%).

Preparation of bis(pyrid-2-yl)1,3-dioxolane[26] ***12***

A mixture of bis(2-pyridyl)ketone, **1a** (5.4mmol), ethylene glycol (0.054mol) and conc. H_2SO_4(2 drops) in toluene(33ml) was refluxed gently for 3 days. Water was removed by means of a Dean-Stark apparatus. The cooled mixture was concentrated and extracted with water and $CHCl_3$ (4 x 25ml). The combined organic phases were dried over $MgSO_4$ and evaporated to dryness to give a brown solid (76%). ^{1}H NMR ($CDCl_3$); δ 4.14 (s, ketal, 4H), 7.11 (dd, 2H, J = 6.9, 5.8 Hz, H^5), 7.70 (t, 2H, J = 5.8 Hz, H^4), 7.80 (d, 2H, J = 5.8 Hz, H^3), 8.50 (d, 2H, J = 6.9 Hz, H^6); ^{13}C NMR ($CDCl_3$): 70, 121, 123, 136, 149, 159; IR KBr/cm^{-1}: ν = 3470w, 3040m, 2995w, 1680m, 1454s, 1341m, 1259m, 1252s, 1186s, 1160m, 1115s, 1031s, 985w, 920w, 768m, 730m; EIMS m/z: 228 [M].

Preparation of bis(pyrid-2-yl N-oxide)1,3-dioxolane ***13***

Bis(pyrid-6-yl)1,3-dioxolane, **12** (4.1mmol), glacial acetic acid (9.4ml) and H_2O_2 (9.4ml) were refluxed together for 24 hours. The mixture was evaporated under a reduced pressure using a pre-trap. To extract the solid, the mixture was washed with acetone to yield a pale yellow precipitate which was collected and dried (38%). ^{1}H NMR ($CDCl_3$); δ 4.25 (s, ketal, 4H), 7.20 (dd, 2H, J = 7.2, 1.5 Hz, H^4), 7.40 (dd, 2H, J = 7.2, 1.2 Hz, H^5), 7.92 (d, 2H, J = 7.5 Hz, H^3), 8.18 (d, 2H, J = 7.5 Hz, H^6); ^{13}C NMR ($CDCl_3$): 70, 121, 123, 136, 148, 152, 159; IR KBr/cm^{-1}: ν = 2965m, 1430s, 1308w, 1248s, 1212s, 1190m, 1098s, 1018mb, 951m, 802s; ESMS m/z: 261 [M^++H].

Preparation of bis(6-cyanopyrid-2-yl)1,3-dioxolane **14**

Under nitrogen Me_3SiCN (15.5mmol, 2.07ml) was added to a solution of bis(pyrid-6-yl N-oxide)1,3-dioxolane, **13** (1.55mmol) in DCM (20ml). After 5mins of stirring, benzoyl chloride (6mmol) was added over 2 minutes. The mixture was stirred at room temperature for 24 hours and then washed with 10% K_2CO_3 solution (3 x 50ml). The organic layer was dried and evaporated. The crude product was chromatographed on silica gel and eluted with DCM / MeOH (95:05). The removal of solvent under a reduced pressure gave the desired product as a beige solid (37%). ^{1}H NMR ($CDCl_3$); δ 4.15 (s, ketal, 4H), 7.61 (d, 2H, J = 8.0 Hz, H^3), 7.89 (t, 2H, J = 8.0 Hz, H^4), 8.05 (d, 2H, J = 8.1 Hz, H^5); ^{13}C NMR ($CDCl_3$): 70, 120 (RCN), 127, 134, 138, 152, 160; IR KBr/cm^{-1}: ν = 2237m, 1582s, 1447s, 1261s, 1193w, 1122m, 1010m, 950m; CIMS m/z; 279 [M+H].

Preparation of bis(6-carboxypyrid-2-yl)1,3-dioxolane **15**

Bis(2-cyanopyrid-6-yl)1,3-dioxolane **14** (0.372mmol.) and solid NaOH (1.48mmol) were suspended in ethylene glycol (10ml) and refluxed for 2.5hrs at 220 °C. Ammonia was evolved upon heating the mixture to reflux. The solution was cooled and water (10ml) was added and extracted with a 50:50 mixture of ether and toluene (2 x 10ml). The aqueous layer was concentrated to half the volume. To this stirring solution, 5M HCl (4-5 drops) was added until it reached pH 4.5. A grey precipitate was obtained and could only be filtered through fine filter paper using a filter cannula. The grey solid was dried under a vacuum (30%). ^{1}H NMR (d_6-DMSO); δ 4.00 (s, ketal, 4H), 8.23 (d, 2H, J = 7.7 Hz, H^3), 8.37 (dd, 2H, J = 7.6, 5.0 Hz, H^4), 8.48 (d, 2H, J = 5.4 Hz, H^5); ^{13}C NMR ($CDCl_3$): 70, 122, 126, 138, 148, 159, 172; IR KBr/cm^{-1}: ν = 1763w, 1728s, 1589w, 1395m, 1282s, 1085sb, 948w, 803s; EIMS m/z: 360 $[M-2H+2Na]^+$.

Preparation of bis(2-cyanopyrid-6-yl)ketone **16**

Bis(2-bromopyrid-6-yl)ketone **1c** (2.93mmol) was dissolved in dry DMF (15ml). To this solution was added Cu(I)CN (6.59mmol) and the reaction was stirred overnight at 120 °C under argon. The solution was allowed to cool to room temperature and to this was added dilute aqueous ammonia solution (50ml). The dark purple mixture was extracted several times with DCM (30ml x 6) to obtain a dark purple organic phase that was dried ($MgSO_4$), filtered and evaporated under a reduced pressure (using a pre-trap for safety). The crude product was chromatographed on silica gel and eluted with DCM/MeOH (95:5) to yield a beige/brown solid (24%). ^{1}H NMR ($CDCl_3$): δ 7.51 (d, 2H, J = 8.0 Hz, H^3); 7.80 (t, 2H, J = 7.9 Hz, H^4); 8.00 (d, 2H, J = 8.0 Hz, H^5); ^{13}C NMR ($CDCl_3$): δ 120 (RCN),

133, 139, 148, 159, 166, 195 (C=O); IR KBr/cm^{-1}: ν = 3926s, 2840s, 2222m, 1681s, 1585w, 1463m, 1356m, 1303m, 997w, 936m, 745m; ESMS (m/z): 235 [M+H$^+$].

Preparation of bis(2-carboxypyrid-6-yl)ketone **17** (L^2)

Bis(2-cyanopyrid-6-yl)ketone, **16** (0.85mmol) and solid NaOH (2.55mmol) were suspended in ethylene glycol (5ml) and refluxed for 2.5 hrs at 220 °C. Ammonia was evolved upon heating the mixture to reflux. The solution was cooled and water (10ml) was added and extracted with a 50:50 mixture of ether and toluene (2 x 10ml). The aqueous layer was concentrated to half the volume. To this stirring solution, 5M HCl (4-5drops) was added until it reached pH 4.5. A grey precipitate was seen and could only be filtered through fine filter paper using a filter cannula. The grey solid was dried under a reduced pressure (59%). ^{1}H NMR (d_6-DMSO): δ 8.60 (d, 2H, J = 7.9 Hz, H^3); 8.79 (t, 2H, J = 8.0 Hz, H^4); 8.85 (d, 2H, J = 7.9 Hz, H^5); ^{13}C NMR ($CDCl_3$): δ 124, 129, 139, 148, 159, 175 (COOH), 195 (C=O); IR KBr/cm^{-1}: ν = 3411mb, 1699s, 1595m, 1565m, 1455s, 1387m, 1284m, 1077w; ESMS (m/z): 294 [M-H+Na$^+$].

Preparation of bis(2-methylcarboxypyrid-6-yl)ketone **18** (L^1)

The same reaction conditions was used here as described above for the preparation of **9a-c** except the following quantities of starting materials were used; bis(2-brompyrid-6-yl)ketone, **1c** (1.612mmol), $Pd(PPh_4)_3$ (2% w/w of **1c**, 3.65x10^{-5}mol), triethylamine (0.016mol) and methanol (0.034mol) dissolved in toluene (50ml). Upon evaporation of the filtrate an orange / brown solid was obtained which was washed with cold MeOH to obtain a white solid (55%). ^{1}H NMR ($CDCl_3$): 3.95 (s, 6H, CH_3), 8.00 (t, 2H, J = 7.9 Hz,

H^4), 8.25 (d, 2H, J=7.8 Hz, H^3), 8.35 (d, 2H, J = 7.8 Hz, H^5). ^{13}C NMR ($CDCl_3$): 52, 122, 123, 137, 147, 153, 165 ($COOCH_3$), 197; IR KBr/cm^{-1}: ν = 1745s, 1717s, 1683m, 1575m, 1455w, 1436m, 1322s, 1235s, 1134m, 992w; ESMS (m/z): 301 $[M+H]^+$

Preparation of bis(2-sodiumcarboxypyrid-6-yl)ketone **19** (Na_2L^2)

Bis(2-methylcarboxypyrid-6-yl)ketone **18** (0.506mmol) was hydrolysed the same way as compounds **9a-c**. The filtrate was evaporated to yield a white solid (85%). ^1H NMR (D_2O): 7.63(t, 3H, J = 4.5 Hz, $H^{4'}$), 7.8-7.85 (d, 6H, J = 4.7 Hz, $H^{3'}$, $H^{5'}$); ^1H NMR (d^6-DMSO): δ 8.58 (d, 2H, J = 7.6 Hz, H^3); 8.75 (t, 2H, J = 7.7 Hz, H^4); 8.80 (d, 2H, J = 7.5 Hz, H^5); ^{13}C NMR (d^6-DMSO): 123, 125, 147, 152, 161, 173, 199; IR KBr/cm^{-1}: ν = 3411mb, 1662s, 1622s, 1595m, 1565m, 1455s, 1387m, 1284m, 1077w; accurate ES- MS (m/z): 293.0185 [M-Na]

2.7 References

1. J.P. Wibaut, A.P. De Jonge, H.G.P. Van Der Voort, P.H.L. Otto, *Rec. Trav. Chim. Pays-Bas.*, 1951, **70**, 1054.
2. H. Adolfsson, K. Warnmark, C. Moberg, *Chem. Commun.*, 1992, 1054.
3. M.J. Hannon, P.C. Mayers, P.C. Taylor, *Teterahedron Lett.*, 1998, **39**, 8509.
4. M.A. Paterson, J.R. Mitchell, *J. Org. Chem.*, 1997, **62**, 8237.
5. Y.G. Gu, E.K. Bayburt, *Teterahedron Lett.*, 1996, **37**, 2565.
6. V.M. Mukkala, J. Kankare, *Helv. Chim. Acta*, 1992, **75**, 1578.
7. Y. Bretonniere, M. Mazzanti, J. Pecaut, F.A. Dunand, A.E. Merbach, *Inorg. Chem.*, 2001, **40**, 6737.

8. H. Takalo, J. Kankare, V.M. Mukkala, M. Helenius, I. Hemmila, *Helv. Chim. Acta*, 1993, **76**, 1361.

9. H. Adolfsson, K. Warnmark, C. Moberg, *J. Chem. Soc. Chem. Commun.*, 1992, 1054.

10. X. Li, C.L.D. Gibb, M.E. Kuebel, B.C. Gibb, *Tetrahedron*, 2001, **57**, 1175.

11. J. Gong, B.C. Gibb, *Org. Lett.*, 2004, **6**, 1353.

12. W.J. Peng, D.A. Aguilar, 1999, *US Patent No. 5*,861,140.

13. V.M. Mukkala, C. Sund, M. Kwaiatkowski, P. Pasanen, M. Hogberg, J. Kankare, H. Takalo, *Helv. Chim. Acta*, 1992, **75**, 1621.

14. "Heterocyclic N-oxides" by A. Albini, S. Pietra, Published 1991, P 31.

15. P. Broughham, M.S. Cooper, D.A. Cummerson, H. Heaney, N. Thompson, *Synthesis*, 1987, 1015.

16. F.H. Case, *J. Org. Chem.*, 1962, **27**, 640.

17. C. Coperet, H. Adolfsson, V.T.A. Khuong, A.K. Yudin, K.B. Sharpless, *Tetrahedron Lett.*, 1998, **39**, 761.

18. M. Ramakrishan Prasad, G. Kamalakar, G. Madhavi, S.J. Kulkarni, K.V. Raghavan, *J. Chem. Soc. Chem. Commun.*, 2000, **17**, 1577.

19. A.R. Katrizky, J.M. Lagowski, *Chemistry Of Heterocyclic N-oxides.,* Academic Press., 1971.

20. R.P. Thummel, Y. Jahng, *J. Org. Chem.*, 1985, **50**, 19.

21. G.V. Kireev, O.S. Otroshchenko, V.B. Leont'ev, Y.V. Kurbatov, O.S. Sadikov, *Tashk. Gos. Uzb. Khim. Zh.*, 1978, **3**, 57.

22. W.K. Fife, *J. Org. Chem.*, 1983, **48**, 1375.

23. G.A. Pearse, J. Wisowaty, *J. Heterocycl. Chem.*, 1973, **10**, 647.

24. G.P. Ellis, T.M. Romney-Alexander, *Chem. Rev.*, 1987, **87**, 779.

25. G. Battistuzzi, S. Cacchi, G. Fabrizi, *Org. Lett.,* 2003, **5**, 777.

26. G.R. Newkome, H.C.R. Taylor, F.R. Fronczek, T.J.Delord, *J. Org. Chem.*, 1984, **49**, 2961.

27. "Greene's protective groups in organic synthesis" (4th Ed.) by P.G.M. Wuts and T.W. Greene, Published 2006, Chapter 4 – Protection of carbonyls.

28. H. Hagiwara, H. Uda, *J. Chem. Soc.*, Chem. Commun., 1987, 1351.

29. J.H. Babler, N.C. Malek, M.J. Coghlan, *J. Org. Chem.*, 1978, **43**, 1821.

Chapter Three

Transition Metal Complexes of Ligands L^1 – Na_3L^8

3.1 Introduction

There is much interest in new multidentate ligands that may be useful in the synthesis of stable complexes. Some such complexes have found application in research areas such as the formation of metallo-enzyme mimics,[1-3] catalysis,[4-6] as well as contrast agents[7,8] and luminescent labels.[9,10] Tripodal polydentate N-donor ligands based on tris-pyrazolyl species,[11] tren,[12,13] triaminocyclohexane,[14,15] tris(2-pyridylmethyl) amine[16] and trispyridylmethane systems[17-20] are some of the most well known tripodal ligands and their derivatives widely used. In contrast, the carboxylic acid derivative, tris(6-carboxypyrid-2-yl)methanol (TCPM) has been studied to a much lesser degree as a ligand. Previously, the ligand has been associated with MRI contrast agents,[21] possible carbonic anhydrase mimic[22,23] and potential catalysts.[24] Characterisations of these complexes has not been fully accomplished. Prior to this investigation there has been no evidence of any crystallographic data, although other spectroscopic analyses (elemental analysis and mass spectrometry) have been used to determine the structural formula. Figure 3.1 illustrates the structure of [Gd(TCPM)] proposed by Peng *et al.*[21]

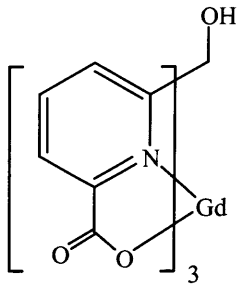

Figure 3.1 Structure of [Gd(TCPM)].

3.2 Aims of the current research

The unknown chemistries of the novel ligands synthesised in Chapter 2 (L^{1-8}, shown in Figure 3.2) gives the opportunity to explore their coordinative properties with some first row transition metal ions. Another attraction is the changes that may be observed when the steric and electronic demands of d^6, d^8, d^9 and d^{10} metal centres (e.g. Fe^{II}, Ni^{II}, Cu^{II} and Zn^{II}) are imposed upon these ligands. The structural and electronic properties of complexes with 1:1 ligand to metal stoichiometries will be described.

In addition, electrochemical (cyclic voltammetries) investigations will be performed on the Cu, Ni and Fe complexes to observe and compare their oxidation and reduction chemistries. The following spectroscopic methods will be used to help determine the structure of the compounds: ultra-violet/visible and infra-red spectroscopy, mass spectrometry, and ^1H NMR spectroscopy for the zinc complexes.

3.3 Results and Discussion

3.3.1 Complexation to divalent copper, nickel, zinc and iron

The polydentate ligands synthesised in Chapter 2 is illustrated in Figure 3.2 and were complexed to divalent Cu, Ni, Zn and Fe (Scheme 3.1).

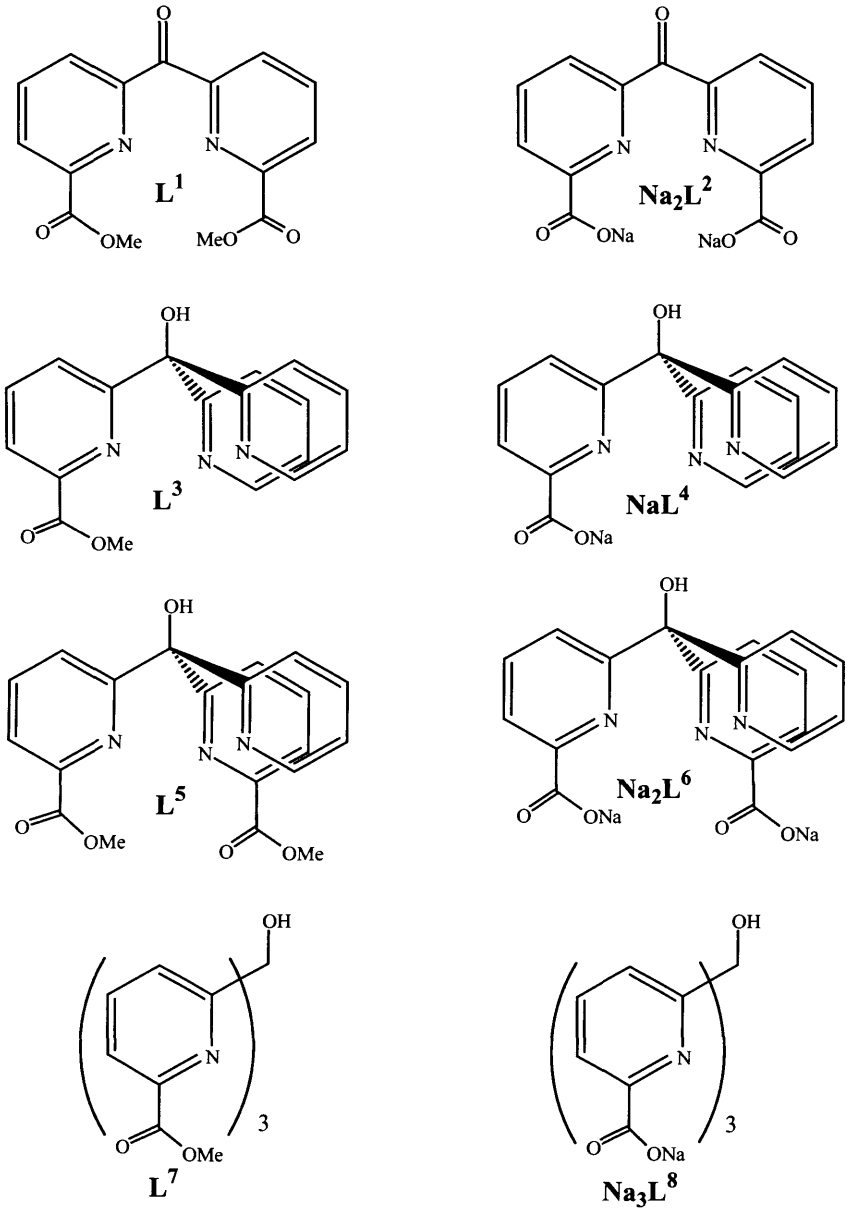

Figure 3.2 Labelling of ligands synthesised in Chapter 2.

$$L^X + M(ClO_4)_2 \xrightarrow{MeOH/H_2O} [M(L^X)_Y][ClO_4]_Z$$

M = Cu, Ni, Zn, Fe

Scheme 3.1 Preparation of metal complexes.

In all cases, complexations were carried out using a 1:1 ratio of metal to ligand. Both reagents were dissolved in the minimum amount of solvent in order to maximise the amount of precipitation of product. Typically the solvents used were methanol to dissolve the ligand and water to dissolve the metal perchlorate salt. The methanolic solutions were warmed to ensure that the ligand was fully dissolved and the minimum amount of solvent was used. The yield of product obtained from these reactions was moderate, with yields between 49 – 80% observed. The precipitate was then crystallised, typically by vapour diffusion of diethyl ether into a solution of complex.

3.3.2 $[M(L^2)]$

$$L^X + M(ClO_4)_2 \xrightarrow{MeOH/H_2O} [M(L^2)(H_2O)_y]$$

$L^X = L^1$, Na_2/H_2L^2, y = 1 or 2

Scheme 3.2 Synthesis of $[M(L^2)(H_2O)_y]$.

Scheme 3.2 suggests that both ligands, L^1 or Na_2/H_2L^2 can be used to synthesise complexes of type $[M(L^2)(H_2O)_y]$. It is not uncommon to see ester hydrolysis in protic solvents (e.g. MeOH / EtOH) prior to coordination.[25] Precipitates were obtained for $[Zn(L^2)(H_2O)_y]$ (55%) and $[Fe(L^2)(H_2O)_y]$ (49%). Crystallisation gave blue and grey /

purple coloured crystalline solids for $[Cu(L^2)(H_2O)]$ and $[Ni(L^2)(H_2O)_2]$ complexes of 32 and 45% yield respectively.

Comparison of the IR spectra with ligands L^1 and Na_2L^2 as well as its M(II) complexes are listed in Table 3.1 together with assignments for most of the major peaks. The IR spectrum of L^1 shows two strong carbonyl bands at 1745 and 1717 cm^{-1}. The former value is assigned to the methyl ester groups and the latter to the bridging ketone moiety. Similarly, Na_2L^2 also displays two carbonyl bands but at significantly lower wave numbers 1662 cm^{-1} (assigned to the ketone) and 1622 cm^{-1} (typical of sodium carboxylate salts). Comparison of the ν_{CO} show that the stretching frequency of the metal complexes is intermediate of the two free ligands, the absorption bands for the ketone are seen in the region of 1663 –1687 cm^{-1} and for the carboxylate coordination to the metal ions are seen at lower wave numbers, 1649- 1654 cm^{-1}. A likely explanation for this shift in frequency is the greater electron resonance experienced. Coordination to a metal ion causes the bonding to become more ionic and single bond in character. The frequency of the pyridyl ketone is also affected by this carboxylate coordination because of their close proximity.

	IR, wavenumber (cm^{-1})		
	O-H	**C=O**	**C=N (py)**
L^1	—	1745s, 1717s	1576s
Na_2L^2	—	1662s, 1622s	1580s
$[Cu(L^2)(H_2O)]$	3450mb	1672s, 1650s	1617m
$[Ni(L^2)(H_2O)_2]$	3420sb	1663s, 1652s	1627m
$[Zn(L^2)(H_2O)_y]$	3426mb	1684s, 1649s	1625m
$[Fe(L^2)(H_2O)_y]$	3427mb	1687s, 1654s	1590m

Table 3.1 IR assignment of L^1, Na_2L^2 and complexes $[M(L^2)(H_2O)_y]$.

The band located at ~1580 cm^{-1} is assigned to the $\nu_{C=N}$ stretching vibration of the pyridyl nitrogen. Pyridyl coordination is indicated by a 14-51 cm^{-1} shift to higher wave numbers in all the complexes.[26] In addition the broad O-H stretch present in all the complexes suggests the possible coordination to water molecule(s).

The following ions were observed in the electrospray mass spectra (ESMS), the copper and nickel complexes gave accurate masses of 333.9645 $[Cu(L^2)+H]^+$ and 345.9730 $[Ni(L^2)+H_2O]^+$. The latter mass suggests the coordination to a water molecule, which is also supported by the IR data. The $[Zn(L^2)]$ complex gives a mass peak at 335 indicating the presence of the parent ion $[Zn(L^2)+H]^+$ and the $[Fe(L^2)(H_2O)_y]^+$ compound produces a mass peak at 369 for the following possible ion $[Fe(L^2)(H_2O)+Na]^+$. The mass spectra also confirm the absence of methyl ester groups.

A ^1H NMR spectrum was obtained for the zinc complex. Table 3.2 compares the data with the free ligands.**ffdainfdf** The protons shift to slightly lower frequencies suggesting that they become more shielded upon complexation. Only three peaks are seen in the spectrum suggesting that the two picolinate rings are equivalent. It is also noted the singlet assigned to the methyl protons in L^1 is absent in the $[Zn(L^2)(H_2O)_y]$ complex and is therefore consistent with the IR data.

	^1H NMR (DMSO-d_6) *ppm*			
	-OCH_3	**$H^{3'}$**	**$H^{4'}$**	**$H^{5'}$**
L^1	3.88	8.79	8.60	8.85
Na_2L^2	__	8.75	8.58	8.80
$[Zn(L^2)(H_2O)_y]$	__	8.45	8.45	8.55

Table 3.2 Comparison of ^1H NMR spectra for **L^1**, **Na_2L^2** and **$[Zn(L^2)(H_2O)_y]$**.

3.3.2.1 Electronic spectra

The UV-vis spectrum of $[Cu(L^2)(H_2O)]$ exhibits a broad asymmetric peak at 621 nm (16.1 x 10^3 cm^{-1}). This is in agreement with CuN_2O_3 chromophore. For example, the Cu(II) square pyramidal complex characterised by van Koningsbruggen *et al.*,[27] $[Cu(spa)(H_2O)(NO_3)]_2$ (where, spa = N^3-Salicycloylpyridine-2-carboxamidrazonato) exhibits an asymmetric band centred around 649 nm. The absorption at 621 nm has an extinction coefficient of 43 $M^{-1}cm^{-1}$ and is typical of spin allowed, Laporte forbidden transitions.

The $[Ni(L^2)(H_2O)_2]$ complex exhibits only two d-d transitions in the spectrum, typically three bands are expected for an octahedral Ni(II) (d^8, high spin) complex however, it is not uncommon to see only two as the third band can be obscured by charge transfer bands or π-π^* transitions in some systems.[28] Assuming octahedral symmetry, the following bands are assigned; the $^3A_{2g} \rightarrow {}^3T_{2g}$ band (υ_1) that lies at the lowest energy transition is seen at 838 nm (13 $M^{-1}cm^{-1}$), the υ_2 band $^3A_{2g} \rightarrow {}^3T_{1g}(F)$ is observed at 564 nm (5 $M^{-1}.cm^{-1}$) and the υ_3 band, $^3A_{2g} \rightarrow {}^3T_{1g}(P)$ that lies at the highest energy transition is most likely obscured by a very intense metal to ligand charge transfer (MLCT) band seen at 380 nm (3597 $M^{-1}.cm^{-1}$). This high extinction coefficient (ε) value suggests that this transition is a charge transfer band (typically have ε = 1000 - 50,000 $M^{-1}cm^{-1}$ and is symmetry allowed). The lowest energy transition provides the energy of Δ, therefore Δ = 11,933 cm^{-1}. The ratio of the first two absorptions may be used to find the value of Δ/B from the applicable Tanabe-Sugano diagram (d^8, Ni^{2+}, discussed in Chapter 1), which in turn determines the B value for the complex (641 cm^{-1}). These values are similar to the octahedral Ni(II) complexes discussed in Chapter 1, where $[Ni((py)_3tren)]^{2+}$ and

$[Ni(P(py)_3)_2)]^{2+}$ display Δ values of 12,550 cm^{-1} and 12600 cm^{-1}, and B values of 710 cm^{-1} and 690 cm^{-1} respectively.[29,30]

Inserting the Δ and B values into Equation 3.1[28] predicts that the third band should occur at 27,634 cm^{-1} (362 nm):

$$\frac{1}{2}\left[15 + 3\Delta + (225B^2 - 18B\Delta + \Delta^2)^{1/2}\right]$$

Equation 3.1 Formula for predicting the value of the third band.[28]

The Racah parameter B (defined in Chapter 1) relates to the free ion and can be used to calculate the Nephelauxetic ratio. The delocalisation is called the nephelauxetic effect, and the nephelauxetic ratio β is defined as follows:[31]

$$\beta = \frac{B\ (complex)}{B\ (free\ ion)}$$

Equation 3.2 Nephelauxetic parameter, β is equal to the ratio of B for a complex and that for the free ion.

The typical free ion value for a Ni^{2+} ion is 1082 cm^{-1}, from this; a β value of 0.592 is calculated suggesting a reasonable degree of delocalisation of the electron density i.e. the bonding between the metal and ligand is reasonably covalent and more so in comparison to $[Ni((py)_3tren)]^{2+}$ (β = 0.66) and $[Ni(P(py)_3)_2)]^{2+}$ (β = 0.64).[29,30] From these values we may assume the complex is of octahedral symmetry and that electronically the ligand has similar field strength and hence a similar delocalisation to $[Ni((py)_3tren)]^{2+}$ and $[Ni(P(py)_3)_2)]^{2+}$.

The UV-vis spectrum of the $[Fe(L^2)(H_2O)_y]$ complex surprisingly did not give any d-d transitions in the expected region. One would expect the tetradentate ligand to either

produce a square planar geometry with Fe(II) or a pseudo octahedral geometry, $[Fe(L^2)(H_2O)_2]$ by coordinating to an additional two water ligands. The latter being more likely, one would expect the following in the electronic spectrum, one transition if high spin or two strong transitions and one weak transition if low spin. Previous reports have shown typical octahedral Fe(II) complexes to produce d-d transitions at ~ 19,200 cm^{-1} with a shoulder at about 20,300 cm^{-1} in their spectrum.[29] The lack of d-d transitions in the spectrum may also be a result of change in oxidation state of the metal centre, Fe(III), d^5, high spin complexes do not show d-d transitions as they are forbidden by all selection rules. For these reasons you would expect to see a very weakly coloured complex, however, this was not the case. A dark red solution is observed and is probably caused by the intense metal to ligand charge transfer (MLCT is formally allowed by the all selection rules) band observed at 28,090 cm^{-1} (356 nm, 2560 $M^{-1}cm^{-1}$) and is typical of Fe(II) complexes.[32]

3.3.2.2 Crystallographic data

Slow evaporation of an aqueous solution of $[M(L^2)(H_2O)_y]$ yielded dark blue single crystals of $[Cu(L^2)(H_2O)].H_2O$ (32%). The molecular structure is depicted in Figure 3.3 whereas relevant bond lengths and angles information is listed in Table 3.3.

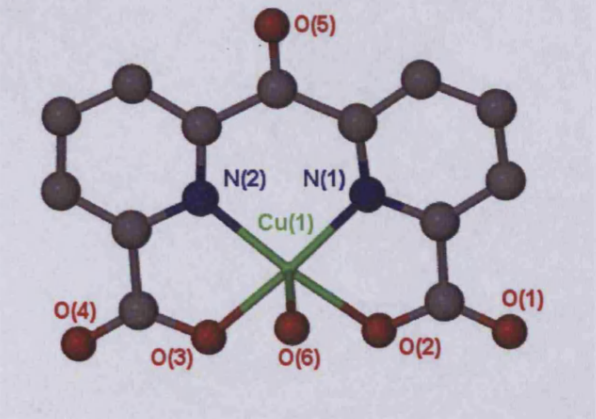

Figure 3.3 Molecular structure of $[Cu^{II}(L^2)(H_2O)].H_2O$. Hydrogen atoms and solvent molecules are omitted for clarity.

Table 3.3 Bond distance (Å) and angles (°) for $[Cu^{II}(L^2)(H_2O)].H_2O$.

Cu(1)-N(1)	1.958(3)	Cu(1)-O(2)	1.968(2)
Cu(1)-N(2)	1.966(3)	Cu(1)-O(6)	2.272(2)
Cu(1)-O(3)	1.940(2)		
O(3)-Cu(1)-N(1)	172.50(10)	N(2)-Cu(1)-O(6)	98.74(9)
N(2)-Cu(1)-O(2)	168.83(10)	O(2)-Cu(1)-O(6)	92.28(9)
O(3)-Cu(1)-N(2)	84.37(10)	O(3)-Cu(1)-O(6)	95.13(8)
N(1)-Cu(1)-O(2)	83.98(10)	N(1)-Cu(1)-O(6)	92.32(9)
N(1)-Cu(1)-N(2)	93.71(10)	O(3)-Cu(1)-O(2)	96.52(9)

The compound crystallised in the monoclinic P $2_{1/n}$ space group. The Cu(II) ion may at first be considered as having a square pyramidal ligand field. The basal plane of the square pyramid is formed by the four L^2 ligand donor atoms (N1, N2, O1, O2) while a water molecule occupies the apical position of the pyramid. This type of coordination is not uncommon for planar tetradentate ligands[33] and the bond lengths observed are similar to those seen in other bis-picolinic acid complexes[34,35] (Cu-O 1.960(2) and 1.935(2); Cu-N 1.951(2) and 1.953(3)) while the Cu-N/O bond lengths observed for the copper(II) complex of 6,6'-bisphenolate-2,2'-bipyridine[36] (Cu-O 1.891(5) and 1.900(5); Cu-N 1.983(6) and 1.957(7)) and for the copper N,N'-bis(3,5-di-tert-butyl-2-hydroxyphenyl)-

1,2-phenylenediamine complex[37] (Cu-O 1.918(2) and 1.942(2); Cu-N 1.954(2) and 1.922(2)) have similar Cu-N bond lengths, but the phenolic Cu-O bonds are significantly shorter. Conversely, the copper(II) complex of bis(pyridine methoxy ether) again has similar Cu-N bond lengths (Cu-N 1.960(7) and 1.944(6)) but significantly longer Cu-ether bond lengths (Cu-O 2.006(4) and 1.987(5)).[33]

As explained in Chapter 1, the degree of trigonal bipyramidal or square pyramidal character can be measured for five coordinate systems by calculating the τ value.[38] This is illustrated in Figure 3.4 for the $[Cu^{II}(L^2)(H_2O)].H_2O$ complex;

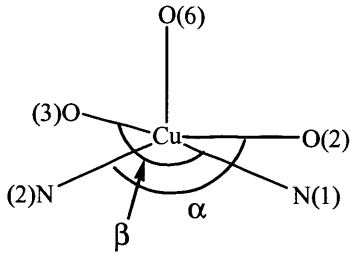

Figure 3.4 τ labelling of $[Cu^{II}(L^2)(H_2O)].H_2O$.

To calculate τ, α is assigned as N(2)-Cu(1)-O(2) (168.83(10)°) and β as O(3)-Cu(1)-N(1) (172.50(10)°).

$$\tau = (\beta - \alpha) / 60 = (172.5 - 168.83) / 60 = 0.061.$$

This illustrates that the solid-state geometry of this complex is closer to a regular square based pyramid with only 6.1% trigonal bipyramidal character and is consistent with the UV-vis data.

Closer inspection of the crystal lattice shows that while the monomer is a five co-ordinate square based pyramid, the complex dimerises in the solid state to form the six coordinate species shown in Figure 3.5. The driving force for this dimerisation is not entirely clear as, while it at first appears the dimerisation is due to the bridging nature of

one of the carboxylate donors, it should be noted that the bridging Cu-O bond is very long (3.052 Å) and there may well be significant π- π interactions between the two planar faces of the interacting monomers. While there is a previous example of the dimerisation of a planar CuN_2O_2 units,[35] in this case the bridging interaction is significantly shorter (Cu-O 2.512(6)Å) and the planarity of the ligand is actually disrupted in order that a shorter Cu-O interaction is made. Given the nature of the bonding in the dimer, it would seem reasonable to assume that the complex exists as a monomer in solution.

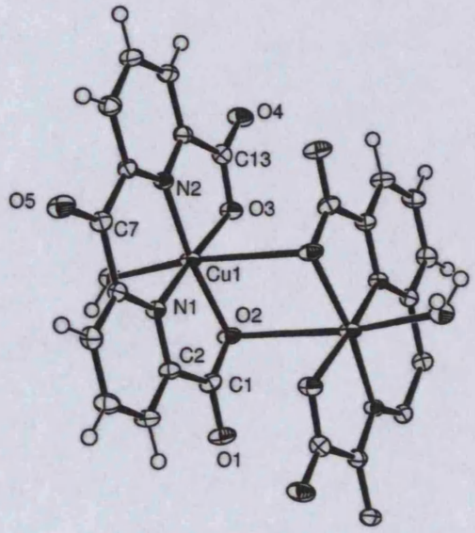

Figure 3.5 Dimerisation of $[Cu(L^1)(H_2O)]\cdot H_2O$ via long intermolecular Cu-O interactions. Solvent molecules are omitted for clarity and thermal ellipsoids are set at 50%.

$[Ni(L^2)(H_2O)_2]$

Suitable purple/grey coloured crystals were grown for the $[Ni(L^2)(H_2O)_2]$ complex (45%). X-ray diffraction gave the structure shown in Figure 3.6. Table 3.4 lists the selected bond lengths and angles relating to the structure.

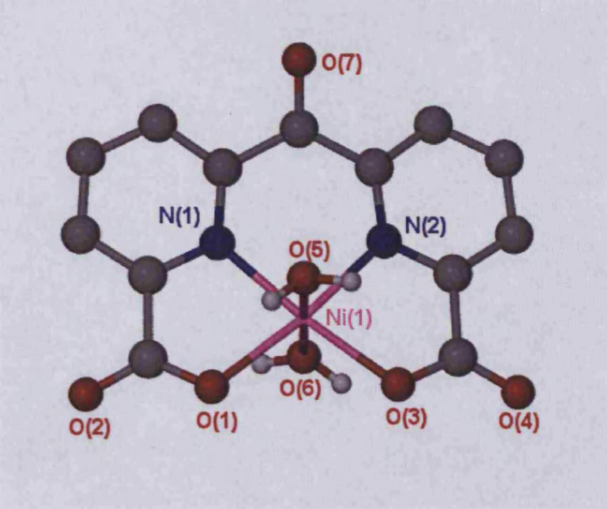

Figure 3.6 Molecular structure of [Ni (L^2)(H_2O)$_2$]. Hydrogen atoms are omitted for clarity.

Table 3.4 Bond distance (Å) and angles (°) for [Ni (L^2)(H_2O)$_2$].

N(1)-Ni(1)	2.0341(16)	Ni(1)-O(3)	2.0506(13)
N(2)-Ni(1)	2.0290(16)	Ni(1)-O(6)	2.0641(16)
Ni(1)-O(1)	2.0418(14)	Ni(1)-O(5)	2.0850(15)
N(2)-Ni(1)-N(1)	92.04(6)	O(1)-Ni(1)-O(6)	88.23(6)
N(2)-Ni(1)-O(1)	172.25(6)	O(3)-Ni(1)-O(6)	86.38(6)
N(1)-Ni(1)-O(1)	81.04(6)	N(2)-Ni(1)-O(5)	91.27(6)
N(2)-Ni(1)-O(3)	81.20(6)	N(1)-Ni(1)-O(5)	89.52(6)
N(1)-Ni(1)-O(3)	172.78(6)	O(1)-Ni(1)-O(5)	92.16(6)
O(1)-Ni(1)-O(3)	105.54(5)	O(3)-Ni(1)-O(5)	93.14(6)
N(2)-Ni(1)-O(6)	88.38(6)	O(6)-Ni(1)-O(5)	179.44(6)
N(1)-Ni(1)-O(6)	90.92(6)		

Like its analogous Cu(II) complex it too crystallised in the monoclinic P $2_{1/a}$ space group. The solid-state structure of [Ni(L^2)(H_2O)$_2$] consists of a neutral six-coordinate mononuclear molecule. The Ni(II) centre coordinates in a $N_2O_2O'_2$ fashion where N is the pyridyl nitrogen atoms and O is the carboxylate oxygen atoms which make up the basal positions. The remaining two O' atoms are from each bonding water molecule and are in the apical positions forming a pseudo-octahedral coordination geometry. Typically for an octahedral complex one would expect twelve L-M-L 90° angles and three 180° angles. Here we see slight deviations from a regular octahedron, the deviations from 90° and a

180° occur due to the sterics of the ligand, the nitrogen donors cannot spread out far enough as they are restricted by the bridgehead carbon atom however, the oxygen atoms are not and are therefore better positioned to give the desired angles.

The equatorial nitrogen donor atoms about the Ni(II) centre are slightly shorter in comparison to similar Ni(II) octahedral complexes reported previously, some of which are listed in Table 3.5. The following complexes, trans-diaqua-bis(picolinato-N,O)-nickel(II) dehydrate (**1**) and bis(methanol)-bis(2-pyridylcarboxylato)-nickel (**2**) have average equatorial Ni-N bond lengths of 2.089(4) Å and 2.040(3.5) Å.[39,40] They are longer because unlike the picolinic units in $[Ni(L^2)(H_2O)_2]$ they are not bridged together by a carbon atom, hence, the nitrogen donors are able to spread out and produce longer bond lengths. This also explains why the equatorial Ni-O bond lengths are typical. Despite these differences, the bond lengths are typical of carbon bridged picolinic units, the pseudo-octahedral $[Ni(L^6+H)(MeOH)(EtOH)]^+$ complex discussed later in this Chapter has very similar bond lengths.

Compound	Geometry	Chromophore	Average Ni-L bond length (Å)		
			Ni-O ax	Ni-O eq.	Ni-N eq.
1[39]	Pseu. Oh.	$CuN_2O_2O'_2$	2.115(6)	2.052(4.5)	2.089(4)
2[40]	Pseu. Oh.	$CuN_2O_2O'_2$	2.126(6)	2.029(5)	2.040(3.5)
$[Ni(L^2)(H_2O)_2]$	Pseu. Oh.	$CuN_2O_2O'_2$	2.075(15.5)	2.046(13.5)	2.032(16)
$[Ni(L^6+H)]^+$	Pseu. Oh.	$CuN_2O_2O'O''$	2.072(5)	2.055(4.5)	2.020(5.5)

Table 3.5 Comparison of pseudo octahedral Ni(II) complexes. **1** = trans-diaqua-bis(picolinato-N,O)-nickel(II), **2** = bis(methanol)-bis(2-pyridylcarboxylato)-nickel. Ax = axial, eq. = equatorial.

3.3.2.3 Electrochemistry

Cyclic voltammetry (CV) measurements were performed on compounds $[Cu(L^2)(H_2O)]$, $[Ni(L^2)(H_2O)_2]$ and $[Fe(L^2)(H_2O)_y]$ in an attempt to analyse the stability of various oxidation states of the respective metal complexes. These analyses were performed in a 0.1M Bu_4NPF_6 acetonitrile solution, using ferrocene (Fc/Fc^+) as an internal reference standard. The cyclic voltammograms for complexes $[Cu(L^2)(H_2O)]$ and $[Ni(L^2)(H_2O)_2]$ are shown in Figures 3.7 and 3.8. The electrochemical scan for $[Cu(L^2)(H_2O)]$ exhibits a reversible reduction process at -0.999 V vs Fc/Fc^+. 'Reversible' is taken to mean that the anodic and the cathodic peak currents are equal, and the peak to peak separation is 70-80 mV at a scan rate of 200 mV s^{-1}. This redox potential is 75 mV and is most likely due to the pyridyl ligand bonded to the Cu(II). This complex can be compared to a similar complex, $[Cu(PA)_2]^{2+}$ (PA = picolinic acid) where a quasi-reversible one electron Cu^{II}/Cu^{I} process is seen at + 0.239 V vs Fc/Fc^+ and one irreversible reduction processes is seen at –0.806 V vs Fc/Fc^+ and is due to the PA ligand bonded to the Cu(II).[41] The $[Ni(L^2)(H_2O)_2]$ and $[Fe(L^2)(H_2O)_y]$ complexes also produce irreversible reduction processes at -1.015 and –0.448 V vs Fc/Fc^+ respectively. The former value can be assigned to the reductions of the ligand ((py → py^-) and the latter to either the Fe^{III}/Fe^{II}.[42]

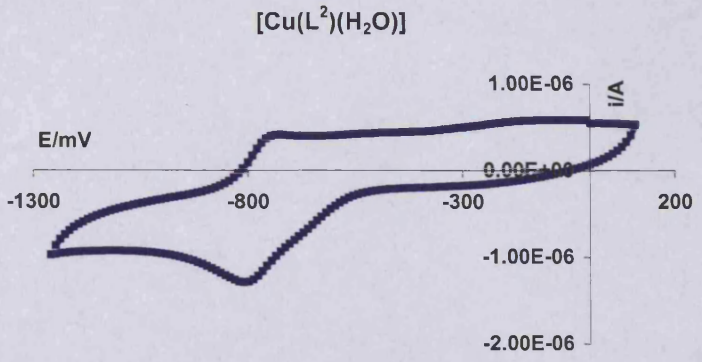

Figure 3.7 CV of complex $[Cu(L^2)(H_2O)]$ in CH_3CN + 0.1M Bu_4NPF_6 at 20 °C vs.Fc/Fc^+.

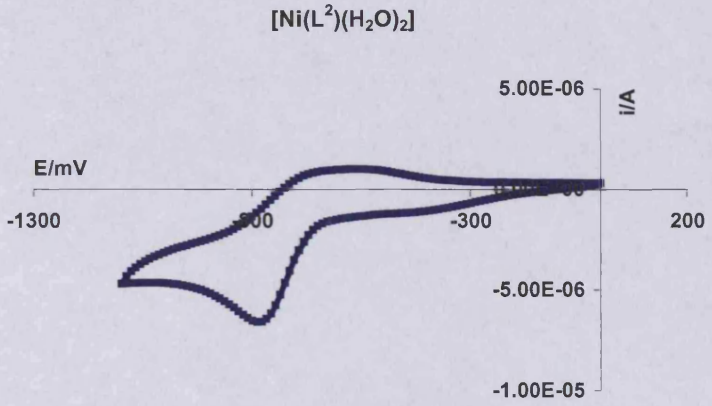

Figure 3.8 Cyclic Voltammogram of complex $[Ni(L^2)(H_2O)_2]$ in CH_3CN + 0.1M Bu_4NPF_6 at 20 °C vs.Fc/Fc^+ reference standard.

3.3.3 $[M(L^4)][ClO_4]$

Complexes of type $[M(L^4)][ClO_4]$ were synthesised in the same manner as for complexes of type $[M(L^2)]$. Precipitates were obtained in reasonable yields (49 - 70%). Again the IR spectra of the ligands L^3 and NaL^4 as well as its complexes with M(II) are listed in Table 3.6 along with assignments for most of the major peaks. Both ligands display strong broad $\nu_{O\text{-}H}$ absorption bands at ~3300 cm^{-1} due to the bridgehead methanol

group. It is noted that these ν_{O-H} bands shift to higher frequencies (~100 cm^{-1}) upon coordination but not in $[Fe(L^3\text{-}H)_2][ClO_4]$ complex, where the band is absent suggesting coordination via the methanol bridgehead.

Metal coordination to the carboxylate is indicated by the shift in ν_{CO} band and is seen in-between the ν_{CO} bands of the two ligands. Coordination to the pyridyl nitrogen is also indicated by a small shift to higher wave numbers in all complexes. It is also important to note that the characteristic ν_{Cl-O} band due to the ClO_4^- counter-ion is present in all the complexes.

	IR, wave number (cm^{-1})			
	O-H	**C=O**	**C=N(py)**	**Cl-O**
L^3	3257shb	1732s	1588s	—
NaL^4	3356sb	1624s	1592s	—
$[Cu(L^4)]_4[ClO_4]_2$	3422sb	1634s	1597s	1089s
$[Ni(L^4)(H_2O)_2][ClO_4]$	3470sb	1639s	1596s	1091s
$[Zn(L^4)][ClO_4]$	3469mb	1636s	1599s	1090s
$[Fe(L^3\text{-}H)_2]_2[ClO_4]_2$	—	1719s	1593s	1093s
$[Fe(L^4)][ClO_4]$	3435mb	1652s	1596m	1087s

Table 3.6 Comparison of IR data for the free ligands and their metal complexes.

The expected ions were observed in the electrospray mass spectra (ESMS) for all the complexes. A MALDI accurate mass spectrum was obtained for $[Cu(L^4)]_4[ClO_4]_2$, a mass peak of 836.983 was observed suggesting that the tetramer had fragmented to give the following ion $[(CuL^4)_2+ClO_4]^+$. The $[Ni(L^4)][ClO_4]$ complex displays two peaks in the spectrum, one for the parent ion without the perchlorate counterion, 364.1 $[Ni(L^4)+H]^+$ and one at 396 $[Ni(L^4)(H_2O)_2]$ for the complex with two additional water ligands. These

analyses reveal a 1:1 ligand to metal complex whereby the nickel centre may take two possible geometries; square planar or octahedral. ESMS of $[Zn(L^4)][ClO_4]$ illustrated mass peaks for the parent ion $[Zn(L^4)]^+$ at 370 revealing a 1:1 metal to ligand complex. An accurate mass spectrum of $[Fe(L^3\text{-}H)_2]_2[ClO_4]_2$ produced a mass peak of 696.1414, supporting a 2:1 ligand to metal complex, explaining the difference observed in the IR spectrum. However, the iron complex $[Fe(L^4)][ClO_4]$ gave a 1:1 metal to ligand complex consisting of the parent ion $[Fe(L^4)+H]^+$.

Table 3.7 compares the ^1H NMR data for $[Zn(L^4)][ClO_4]$ in DMSO-d_6 with the free ligands.**ffdainfdf** The protons shift to slightly higher frequencies suggesting that they become more deshielded upon complexation. Here only two of the pyridyl rings are equivalent and the methyl protons are absent in the zinc complex confirming ester hydrolysis upon complexation of L^3.

	^1H NMR (DMSO-d_6) *ppm*							
	-OCH_3	$H^{3'}$	$H^{4'}$	$H^{5'}$	H^3	H^4	H^5	H^6
L^3	3.88	8.23	8.48	8.37	7.75	8.05	7.40	8.65
NaL^4	—	8.33	8.55	8.43	7.84	8.12	7.48	8.70
$[Zn(L^4)][ClO_4]$	—	8.55	8.63	8.55	7.82	8.09	7.46	8.71

Table 3.7 Comparison of ^1H NMR spectra for **L^3**, **NaL^4** and **$[Zn(L^4)][ClO_4]$**.

3.3.3.1 Electronic spectra

The UV-vis spectrum of $[Cu(L^4)]_4[ClO_4]_2$ exhibits a broad asymmetric peak at 696 nm (ε = 85 $M^{-1}cm^{-1}$) with a shoulder much further to the right of it at 972 nm (ε = 46 $M^{-1}cm^{-1}$) as shown in Figure 3.9, the extinction coefficient values obtained are typical of spin allowed, Laporte forbidden transitions (d-d). This pattern suggests the presence of two

different geometries within the complex or a very large distortion of the Cu coordination geometry. The former conclusion can also be supported by the X-ray crystallography data and is also consistent with previous data reported for dinuclear metal geometries within a complex. For example, the electronic spectrum of $[Cu_2(\mu\text{-}O_2CCH_2CH_3)_2(\mu\text{-}OH)(dpyam)_2](ClO_4)$ (τ = 0.22 and 0.43) exhibits a broad asymmetric band centred at ~ 781 nm with a high energy shoulder at ~ 680 nm.[43] However this pattern is characteristic of distorted square pyramidal copper(II) complexes but the transitions are normally seen at higher energies, typically 600 nm (~220 $M^{-1}cm^{-1}$) and 850 nm (~30 $M^{-1}cm^{-1}$).[44]

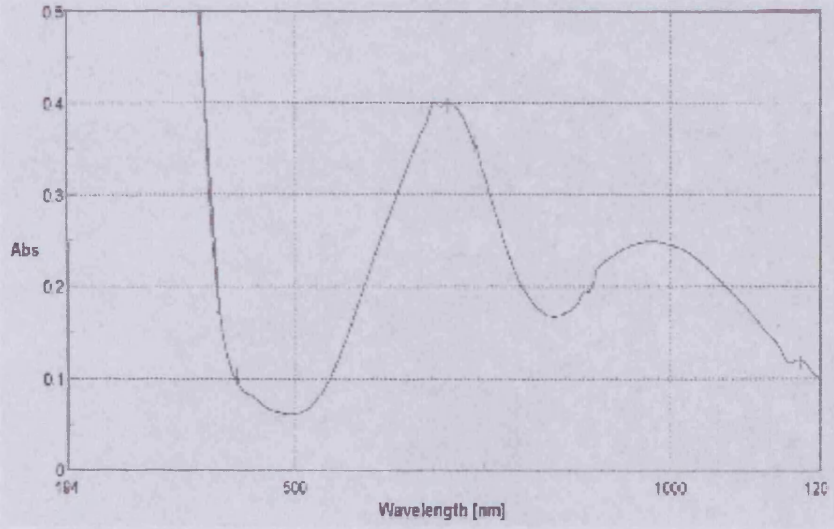

Figure 3.9. UV-vis spectrum of $[Cu(L^4)]_4[ClO_4]_2$ in CH_3CN.

The $[Ni(L^4)][ClO_4]$ complex exhibits only two peaks in the spectrum that may be assigned to d-d transitions. Assuming the complex is of octahedral symmetry, the following energies are assigned: ν_1 band ($^3A_{2g} \rightarrow {}^3T_{2g}$), 12,300 cm^{-1} (10 $M^{-1}cm^{-1}$) and the ν_2 band ($^3A_{2g} \rightarrow {}^3T_{1g}(F)$); 19,120 cm^{-1} (6 $M^{-1}cm^{-1}$). Intense absorptions caused by the charge transfer band ($\pi \rightarrow \pi^*$) (37,736 cm^{-1}, ε = 5394 $M^{-1}cm^{-1}$) obscure the ν_3 band $^3A_{2g} \rightarrow {}^3T_{1g}(P)$. Inserting the following values, Δ = 12,300 cm^{-1} and B = 811 cm^{-1} into Equation

3.1 predicts the third band should have the following energy transition, 30,007 cm^{-1} (333 nm). The nephelauxetic parameter, β is 0.750 and has some degree of delocalisation but not as much as $[Ni^{II}(L^2)(H_2O)_2]$ discussed earlier. However, previous reports on near octahedral $[Ni(pic)_3tach]^{2+}$ complex (where, $(pic)_3tach$ = N,N',N"-tris(2-picolyl)-*cis*,*cis*-1,3,5-triaminocyclohexane)[71] has Δ = 12,500 cm^{-1} and B = 855 cm^{-1} (β = 0.790), this striking similarity in parameters suggest that electronically this ligand has similar field strength as L^4 and therefore cause similar delocalisation.

The UV-vis spectrum of the $[Fe(L^3\text{-}H)_2]_2[ClO_4]_2$ complex is shown in Figure 3.10, it exhibits a band at 23,585 cm^{-1} (424 nm, ε = 4451 $M^{-1}cm^{-1}$) with a shoulder at about 26,882 cm^{-1} (372 nm, ε = 3236 $M^{-1}cm^{-1}$). The absence of d-d transitions is characteristic of Fe(III) d^5, high spin complexes as d-d transitions are forbidden by all three selection rules.[45] The former band can be assigned to a LMCT (L→ Fe^{III}) band and the latter is intra-ligand in nature. These bands are formally allowed and give rise to the intensely coloured solution.

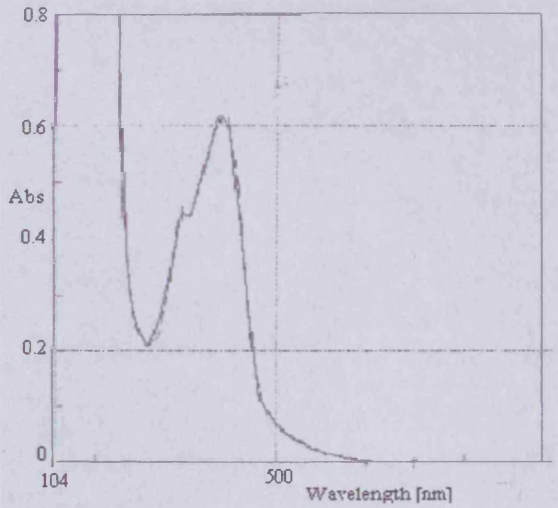

Figure 3.10 UV-vis spectrum of $[Fe(L^3\text{-}H)_2]_2[ClO_4]_2$ in CH_3CN.

3.3.3.2 Crystallographic data

Diffusion of diethyl ether into a methanolic solution of $[(CuL^4)]_4[ClO_4]_2$ gave blue single crystalline solid (52%). The structure obtained by X-ray diffraction is illustrated in Figures 3.8 and 3.9 whereas the relevant bond lengths and angles are listed in Table 3.8.

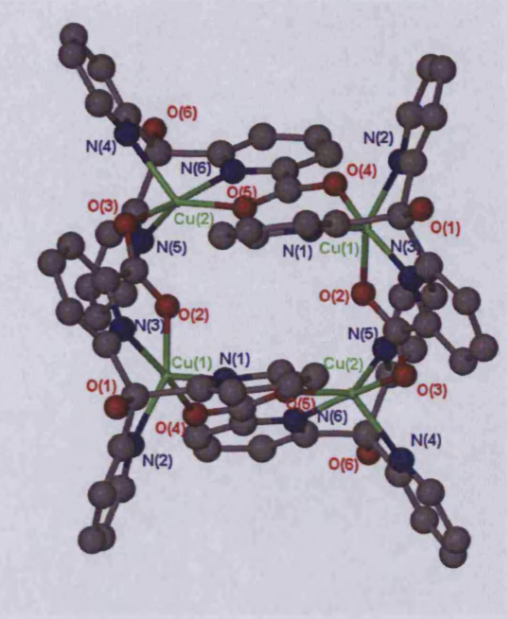

Figure 3.11 Crystal structure of $[(CuL^4)]_4[ClO_4]_2$. Hydrogen atoms omitted for clarity.

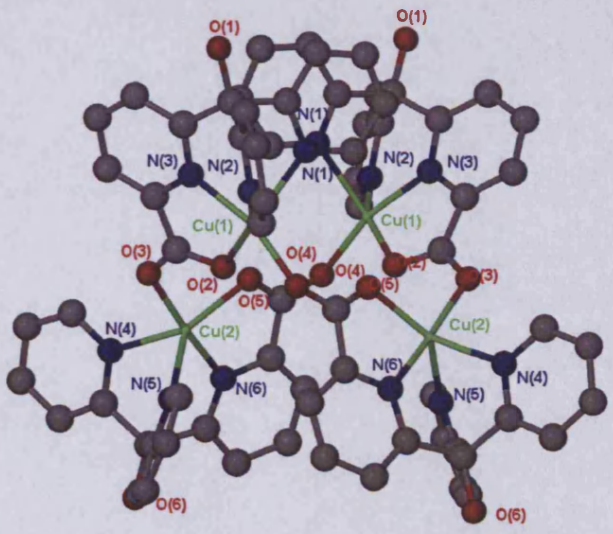

Figure 3.12 A closer look at the coordination sites of $[(CuL^4)]_4[ClO_4]_2$. Hydrogen atoms omitted for clarity.

Table 3.8 Bond distance (Å) and angles (°) for $[(CuL^4)]_4[ClO_4]_2$.

N(1)-Cu(1)	2.234(8)	N(4)-Cu(2)	2.110(7)
N(2)-Cu(1)	2.034(7)	N(5)-Cu(2)	2.102(7)
N(3)-Cu(1)	1.961(7)	N(6)-Cu(2)	1.957(7)
O(2)-Cu(1)	1.989(6)	O(3)-Cu(2)	1.925(6)
O(4)-Cu(1)	1.916(6)	O(5)-Cu(2)	2.012(6)
O(4)-Cu(1)-N(3)	164.6(3)	O(3)-Cu(2)-N(6)	171.7(3)
O(4)-Cu(1)-O(2)	89.3(3)	O(3)-Cu(2)-O(5)	93.4(3)
N(3)-Cu(1)-O(2)	81.0(3)	N(6)-Cu(2)-O(5)	81.2(3)
O(4)-Cu(1)-N(2)	93.2(3)	O(3)-Cu(2)-N(5)	100.9(3)
N(3)-Cu(1)-N(2)	90.8(3)	N(6)-Cu(2)-N(5)	87.2(3)
O(2)-Cu(1)-N(2)	155.8(3)	O(5)-Cu(2)-N(5)	139.4(3)
O(4)-Cu(1)-N(1)	112.3(3)	O(3)-Cu(2)-N(4)	92.6(3)
N(3)-Cu(1)-N(1)	82.9(3)	N(6)-Cu(2)-N(4)	86.4(3)
O(2)-Cu(1)-N(1)	116.6(3)	O(5)-Cu(2)-N(4)	130.9(3)
N(2)-Cu(1)-N(1)	84.5(3)	N(5)-Cu(2)-N(4)	86.6(3)

The compound crystallised in the monoclinic C 2/c space group. The structure consists of a cyclic tetramer, four five coordinate copper(II) centres are linked via bridging carboxylate groups of the neighbouring ligand. The metals have an 'open butterfly-like' arrangement, resulting in a C_2 axis of symmetry. The unit consists of two types of copper centres. The coordination environment around Cu(1) can be best described as distorted square pyramidal, it has a CuN_3O_2 chromophore with a τ value of 0.147 ($\tau = (\beta - \alpha) / 60 = (164.6 - 155.8) / 60 = 0.15$). The four shorter bonds in the basal plane involve two pyridyl nitrogen atoms (Cu-N 2.034(7) and 1.961(7) Å), an oxygen atom from the ligands carboxylate group (Cu-O(2) 1.989(6) Å) and an oxygen atom from the bridging carboxylate group of the second ligand (Cu-O(4) 1.916(6) Å). The pyridyl nitrogen completes the fifth coordination site (Cu-N 2.234(8) Å). The bond lengths obtained are consistent with distorted square pyramidal geometry.[43] The Cu(1)-N(3) bond length (1.961(7) Å) is considerably shorter than the other two Cu-N distances, this effect may be due to the bidentate coordination with the picolinic ring. It is also interesting to

note the M-L bond lengths and angles around the Cu(1) centre is very similar to that seen in $[Cu^{II}(L^2)(H_2O)]$ complex discussed earlier in this Chapter confirming a typical distorted square pyramidal environment.

The geometry around Cu(2) is intermediate of a trigonal bipyramid and a square pyramid it is distorted via a Berry-Twist process[46] and has a τ value of 0.54 ($\tau = (\beta - \alpha) / 60 = (171.7 - 139.4) / 60 = 0.54$). The basal plane comprises of two nitrogen atoms from the L^4 ligand (Cu-N 2.102(7) and 1.957(7) Å), an oxygen atom from the ligands carboxylate group (Cu-O(5) 2.012(6) Å) and an oxygen atom from the bridging carboxylate group of the second L^4 ligand (Cu-O(3) 1.925(6) Å). The fifth apical coordination site is occupied by a pyridyl nitrogen atom that lies furthest away and has a Cu(2)-N(4) distance of 2.110(7) Å).

Tetranuclear Cu(II) complexes with similar tetradentate ligands have not been reported. However, the unusual tetramer, $[(CuL^4)]_4[ClO_4]_2$ can be compared with similar dinuclear bridging copper(II) complexes consisting of both distorted square pyramidal and intermediate geometries, their bond lengths are listed in Table 3.9. The copper(II) environments of $[(CuL^4)]_4[ClO_4]_2$ (τ = 0.15 and 0.54) are similar to the following dinuclear structures, compounds **1** (τ = 0.11 and 0.43),[47] **2** (τ = 0.14 and 0.47)[48] and **3** (τ = 0.22 and 0.43).[49] The apical Cu-O distances in these compounds are between 2.10-2.30 Å and are similar to the apical Cu-N distance observed in $[(CuL^4)]_4[ClO_4]_2$. The equatorial Cu-N and Cu-O bond lengths in the tetrameric complex also have similar values to compounds **1**, **2** and **3**.

Compound	Geometry	τ	Chromophor	Cu-L bond length (Å)		
				Axial	Equat. Cu-O	Equat. Cu-N
1[45]	Dist. Spy.	0.11	CuN_2O_3	2.140	1.927-2.029	2.005-2.011
	Intermed.	0.43	CuN_2O_3	2.190	1.928-2.012	1.990-2.015
2[46]	Dist. Spy.	0.14	CuN_2O_2O'	2.238	1.939-1.977	2.001-2.019
	Intermed.	0.47	CuN_2O_3	1.930	1.974-2.169	1.992-2.033
3[47]	Dist. Spy.	0.22	CuN_2O_2O'	2.318	1.931-1.959	1.985-2.018
	Intermed.	0.43	CuN_2O_3	2.236	1.942-2.065	1.986-2.010
$[(CuL^4)]_4[ClO_4]_2$	Dist. Spy.	0.15	CuN_2O_2N'	2.234(8)	1.916(6)-1.989(6)	1.961(7)-2.034(7)
	Intermed.	0.54	CuN_3O_2	2.110(7)	1.925(6)-2.012(7)	1.957(7)-2.102(6)
$[Cu^{II}(L^2)(H_2O)]$	Dist. Spy.	0.06	CuN_2O_2O'	2.272(2)	1.940(2)-1.968(2)	1.958(3)-1.966(3)

Table 3.9. Comparison of dinuclear copper(II) complexes.**1** = $[Cu_2(\mu\text{-}OH)(\mu\text{-}O_2CH)_2(bipy)_2](BF_4)$, **2** = $[Cu_2(\mu\text{-}O_2CCH_3)_3(bipy)_2](ClO_4)$, **3** = $[Cu_2(\mu\text{-}O_2CCH_2CH_3)_2(\mu\text{-}OH)(dpyam)_2](ClO_4)$.

$[Fe(L^3\text{-}H)_2][ClO_4]$

Dark red crystals were isolated for $[Fe(L^3\text{-}H)_2][ClO_4]$ (20%). X-ray diffraction studies indicated a 2:1 ligand to metal complex explaining the low yield obtained. Therefore, the complexation was repeated using this time a 2:1 ratio of ligand to metal. Dark red single crystals were again isolated but with a higher yield (65%). The molecular structure is depicted in Figure 3.13. The relevant bond lengths and angles are listed in Table 3.10.

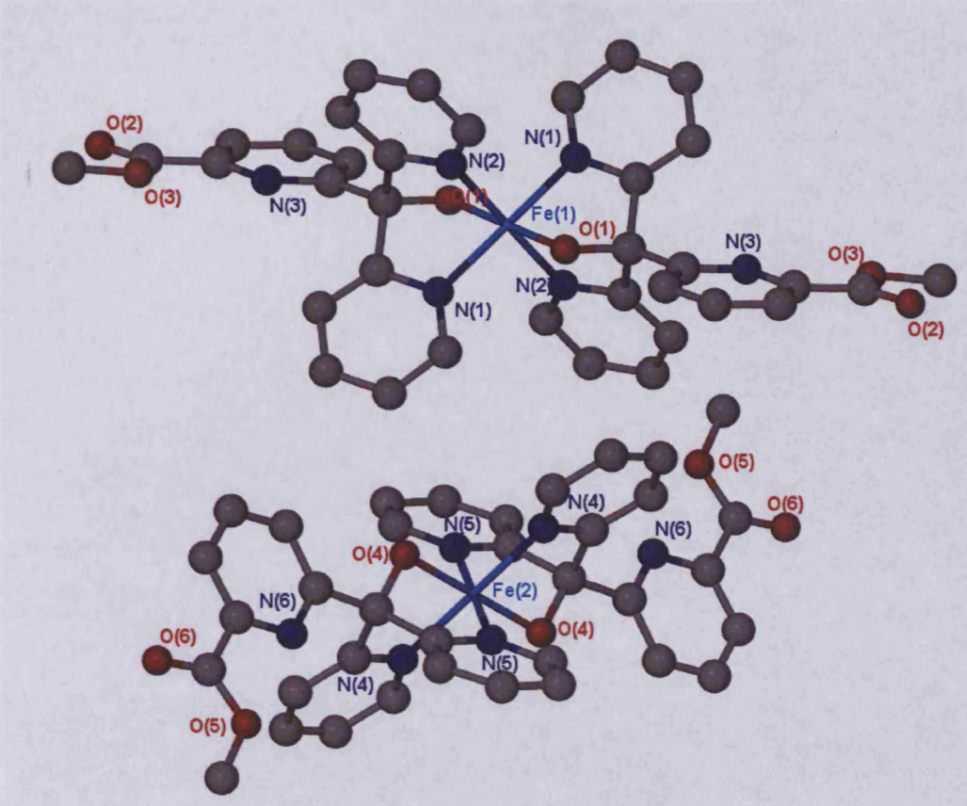

Figure 3.13 Crystal structure of $[Fe(L^3\text{-}H)_2]_2[ClO_4]_2$. Hydrogen atoms omitted for clarity.

Table 3.10 Bond distance (Å) and angles (°) for Fe(1) centre only .

N(1)-Fe(1)	1.954(4)	Fe(1)-O(1)#1	1.854(4)
N(2)-Fe(1)	1.955(5)	Fe(1)-N(1)#1	1.954(4)
O(1)-Fe(1)	1.854(4)	Fe(1)-N(2)#1	1.955(5)
O(1)-Fe(1)-O(1)#1	180.00(10)	N(1)-Fe(1)-N(2)	87.65(19)
O(1)-Fe(1)-N(1)	82.11(18)	N(1)#1-Fe(1)-N(2)	92.35(19)
O(1)#1-Fe(1)-N(1)	97.89(18)	O(1)-Fe(1)-N(2)#1	96.80(18)
O(1)-Fe(1)-N(1)#1	97.89(18)	O(1)#1-Fe(1)-N(2)#1	83.20(18)
O(1)#1-Fe(1)-N(1)#1	82.11(18)	N(1)-Fe(1)-N(2)#1	92.35(19)
N(1)-Fe(1)-N(1)#1	180.000(1)	N(1)#1-Fe(1)-N(2)#1	87.65(19)
O(1)-Fe(1)-N(2)	83.20(18)	N(2)-Fe(1)-N(2)#1	180.000(1)
O(1)#1-Fe(1)-N(2)	96.80(18)		

The compound crystallised in the triclinic P –1 space group and consists of two crystallographically symmetrical independent molecules in the unit cell. The two molecules show only slight differences in bond lengths and angles, thus, all data are given

for Fe(1) ion. Immediately it is noticed that each iron centre is sandwiched between two ligands forming a pseudo-octahedral geometry. It also contains one perchlorate counter-ion suggesting the iron centre has been reduced to the +III oxidation state. Another important factor to note is that unlike the copper and the nickel complexes seen so far in this Chapter, but consistent with the spectroscopic data, the ester group is present in this complex and hangs pendant and far away from the coordination cavity. The observation of the ester group is a little surprising but might be explained by the fact that the formed complex has no vacant co-ordination sites for solvent water to bond. This would mean that the metal centre could not now act as an acid, which is required for the hydrolysis of the ester. This also implies that either the starting material, $[Fe(H_2O)_6]^{2+}$, is not acidic enough to hydrolyse the ester group or the ligand co-ordinates to the metal at a faster rate than hydrolysis occurs. Despite this assumption, another explanation may simply be that this mode of co-ordination is preferred due to the steric hindrance caused by the presence of this bulky ester group making it a less favourable coordination site.

Here we observe the first symmetrical bis tridentate, $(N,N',O^-)_2$ coordination mode with L^3-H. Previous reports[32] have only shown the following coordination modes with iron(II), the symmetrical $[Fe(N, N', N''\text{-tpmOH})_2]^{2+}$ and the unsymmetrical $[Fe(N, N', N''\text{-tpmOH})(N, N', O\text{-tpmOH})]^{2+}$ complexes. Other examples of unsymmetrical coordination modes are shown in Figure 3.14, $(N,N',N'')(N,N',O/O^-)$ and are seen with cobalt(III) and ruthenium(II) ions.[50,51]

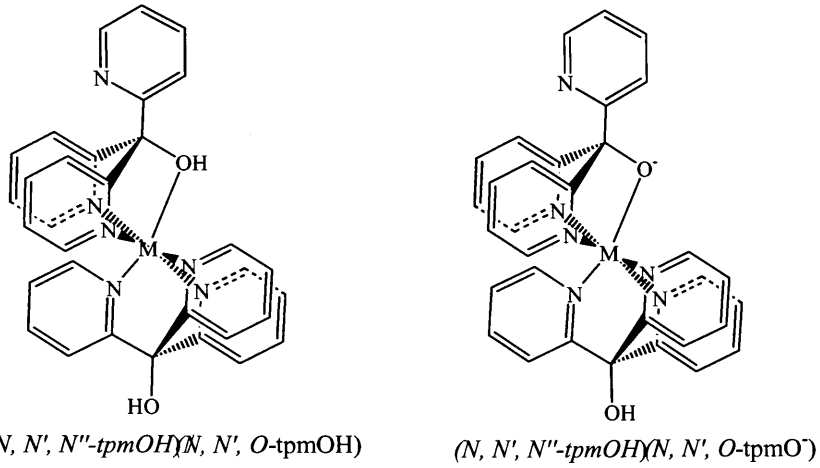

Figure 3.14 Examples of unsymmetrical coordination modes seen in previous literature.[48,49]

Close inspection of the donor-metal-donor bond angles strongly indicates octahedral symmetry (typically, twelve L-M-L 90° angles and three 180° angles) but we see some deviations (~7°) from 90° for the L-M-L angles. The smaller (<<90°) and the bigger angles (>>90°) are associated with the N-M-O angles. The nitrogen and the oxygen atoms are very close to the carbon bridgehead of the tripod, where the steric of the ligand causes the O(1) atom to lie closer to the N(2) atom. This in turn restricts the donors from spreading out far enough to give 90° angles, but also explains why angles >>90° are also seen. The N-M-N angles are better positioned to give the desired angles.

The $[Fe^{III}(L^3\text{-}H)_2]_2[ClO_4]_2$ complex has an average Fe-N bond length of 1.955(5) Å which is significantly shorter than typical Fe-N bond distances seen in similar Fe(II) complexes. For example, in [Fe(PY5)(MeOH)], (where PY5 = 2,6-(bis-(bis-2-pyridyl)-methoxymethane) pyridine has the coordination mode (N,N',N'',N''')), Fe-N bond lengths range between 2.097-2.217 Å.[52,53] The average Fe-O bond length is only 1.861(4) Å and is considerably shorter in comparison to the ruthenium complex (same group as iron) where the coordination mode is similar, (N,N',N'')(N,N',O/O$^-$) the Ru-O bond

length is 2.079 Å.[54] Two possible explanations for this may be that the oxygen atom lies directly above and below the iron centre whereas the oxygen atom in the ruthenium complex lies further away due to the unsymmetrical coordination mode (see Figure 3.14, right diagram) and secondly, the ruthenium atom is bigger than iron and therefore can form longer bonds.

3.3.3.3 Electrochemistry

Cyclic voltammetry (CV) measurements were performed on compounds $[Cu(L^4)]_4[ClO_4]_2$, $[Ni(L^4)][ClO_4]$, $[Fe(L^3)_2][ClO_4]$ and $[Fe(L^4)][ClO_4]$. These analyses were again performed in acetonitrile with 0.1M concentration of Bu_4NPF_6 electrolyte. Ferrocence was used at the end of the analysis as an internal reference compound. With this ligand only the Fe complex, $[Fe(L^3\text{-}H)_2][ClO_4]$ gave a cyclic voltammogram with clear redox features (see Figure 3.15). A quasi-reversible oxidation at +0.732 V (64 mV) vs Fc/Fc^+ and a quasi-reversible reduction at -0.208 V (86 mV) vs Fc/Fc^+ was observed. The wave at +0.732 V can be attributed to the one-electron $[Fe^{II}L^{3\text{-}H}]^{3+}/[Fe^{III}L^{3\text{-}H}]^{4+}$ oxidation process in the complex and the wave at -0.208 V may be due to the one-electron Fe^{III}/Fe^{II} reduction process.[45] Its half way potential is close to that found for the regular $[Fe(bipy)_3]^{2+}$ complex ($E_{1/2}$ = 0.76 V vs Fc/Fc^+) suggesting similar stability of oxidation states.[55]

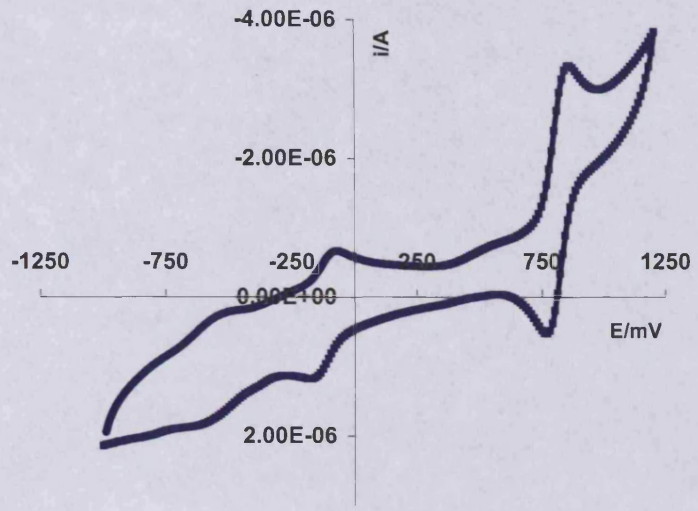

Figure 3.15 Cyclic Voltammogram of complex $[Fe(L^3\text{-}H)_2][ClO_4]$ in CH_3CN + 0.1M Bu_4NPF_6 at 20 °C vs.Fc/Fc^+.

3.3.4 $[M(L^6)]$

Complexations of ligands L^5 and Na_2L^6 with M(II) ion again formed precipitates which were collected in reasonable yields (44 - 75%). Single crystals could only be grown for the nickel and zinc complexes via the re-crystallisation technique mentioned above. Table 3.11 compares the IR data of the free ligands L^5 and Na_2L^6 and its M(II) complexes. Both ligands, L^5 and Na_2L^6 have very similar stretching frequencies to L^3 and NaL^4 respectively. The strong broad $\nu_{O\text{-}H}$ band is seen at ~3300 cm^{-1} and can similarly be assigned to the tertiary alcohol group of the ligand or solvent molecules (H_2O or CH_3OH) that may be formally bound, however, this band shifts to higher frequencies (~100 cm^{-1}) upon coordination in all the complexes. The ligands also display the characteristic carbonyl bands at the expected stretching frequencies. Metal coordination is again indicated by similar shift in frequency (intermediate of the two ligands) of the ν_{CO} and ν_{CN}

bands. Importantly the IR data also confirms the presence of the $\nu_{Cl\text{-}O}$ band due to the perchlorate counter-ion in the nickel complex $[Ni(L^6+H)]^+$.

	IR, wave number (cm^{-1})			
	O-H	**C=O**	**C=N(py)**	**Cl-O**
L^5	3257mb	1745s	1585s	—
Na_2L^6	3428sb	1649s	1580s	—
$[Cu(L^6)(H_2O)]$	3432mb	1647s	1595s	—
$[Ni(L^6+H)]^+$	3397sb	1636s	1590s	1090s
$[Zn(L^6)]$	3398sb	1668s	1595s	—
$[Fe(L^6)(H_2O)]$	3340mb	1652s	1591s	—

Table 3.11 Comparison of IR data complexes of type $[M(L^6)]$, with ligands L^5 and Na_2L^6.

Accurate masses were obtained for the copper complex $[Cu(L^6)]$, 430.033 for the parent ion $[Cu(L^6)(H_2O)+H]^+$ and the nickel complex, 408.0125 for the $[Ni(L^6)+H]^+$ ion, both indicating a 1:1 ligand to metal ratio. The $[Zn(L^6)]$ and $[Fe(L^6)(H_2O)]$ complexes gave spectra suggestive of monomeric species $[M(L^6)+H]^+$ in solution with mass peaks of 413 and 405 respectively.

A ^1H NMR spectrum was obtained for the zinc complex in DMSO-d_6, Table 3.12 compares the spectra of the free ligands and the dimeric $[Zn(L^6)]_2$ complex. Again the spectrum is consistent with the parent ligand, in terms of numbers of signals and their multiplicity. The shift of the peaks move towards higher ppm suggesting that the protons become more deshielded upon complexation. It is also noticed, the methyl protons are absent in the $[Zn(L^6)]$ complex, once again supporting ester hydrolysis upon complexation and is consistent with the IR data obtained earlier. From the number of signals it can be said that the two picolinic rings are equivalent.

	^{1}H NMR (DMSO-d_6) *ppm*							
	-OCH_3	$H^{3'}$	$H^{4'}$	$H^{5'}$	H^3	H^4	H^5	H^6
L^5	3.88	8.23	8.48	8.37	7.75	8.05	7.40	8.65
Na_2L^6	—	8.20	8.45	8.36	7.70	8.00	7.20	8.60
$[Zn(L^6)]_2$	—	8.35	8.55	8.46	7.85	8.10	7.50	8.72

Table 3.12 Comparison of ^{1}H NMR spectra for L^5, $L^6$and $[Zn(L^6)]_2$.

3.3.4.1 Electronic spectra

The electronic spectrum of $[Cu(L^6)(H_2O)]$ shows a broad symmetrical peak at 632 nm (ε = 47 $M^{-1}cm^{-1}$). We know from the results obtained from the above Cu(II) complexes that asymmetric bands or two bands are typically seen in five coordinate complexes. We can also eliminate square-planar geometry as they typically give rise to broad transitions between 500 – 588 nm.[44] Therefore the expected geometry about the metal centre is likely to be octahedral and the band seen can be assigned to $^2Eg \rightarrow {}^2T_{2g}$ transition (electron transition from the $d_{xz,yz}$ orbital to the d_{x2-y2} orbital).

Pseudo-octahedral $[Ni(L^6+H)(MeOH)(EtOH)]$ complex only exhibits two d-d transitions. The bands observed were at the following wavelengths, 823 nm and 524 nm with extinction coefficient values of 12 and 10 $M^{-1}cm^{-1}$ respectively. The lowest energy transition is equal to Δ = 12,150 cm^{-1} and B = 863 cm^{-1}. The third band should be seen at 30,319 cm^{-1} (360 nm) but is again obscured by the intense broad ligand ($\pi \rightarrow \pi^*$) absorption band seen at 272 nm (2179 $M^{-1}cm^{-1}$). The nephelauxetic parameter, β, is 0.798 and indicates some degree of covalency in the bonding between the metal and the ligand. These values are similar to the $[Ni(L^4)](ClO_4)$ and $[Ni(pic)_3tach]^{2+}$ complexes discussed

earlier suggesting the ligands have similar field strengths and hence cause similar covalency.

The UV-vis spectrum of the $[Fe(L^6)(H_2O)]$ complex again do not show d-d transitions in the visible region of the spectrum. However, a broad intense charge transfer band is seen around 466 nm (5651 $M^{-1}cm^{-1}$), which is probably due to the $Fe^{II} \rightarrow L$ transition, it is formally allowed and gives rise to the intensely coloured solution.

3.3.4.2 Crystallographic data

$[Ni(L^6+H)(MeOH)(EtOH)]_2[ClO_4]_2$

Purple crystals were isolated (40%) by the slow diffusion of ether into an ethanolic solution of the complex. Figure 3.16 illustrates the solid-state structure obtained by X-ray crystallography. Table 3.13 lists the relevant bond lengths and angles.

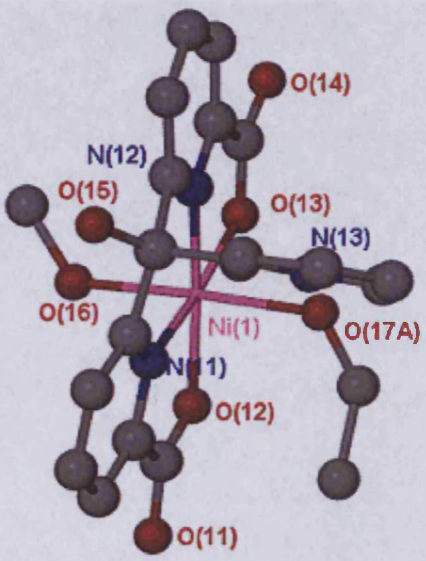

Figure 3.16 Crystal structure for Ni(1) centre in $[Ni(L^6+H)(MeOH)(EtOH)]_2[ClO_4]_2$. The pendant pyridine is protonated but the hydrogen atoms and Ni(2) molecule are omitted for clarity.

Table 3.13 Bond distance (Å) and angles (°) for $[Ni(L^6+H)(MeOH)(EtOH)]_2[ClO_4]_2$.

N(11)-Ni(1)	2.021(6)	N(21)-Ni(2)	2.016(6)
N(12)-Ni(1)	2.020(5)	N(22)-Ni(2)	2.023(5)
Ni(1)-O(12)	2.035(4)	Ni(2)-O(22)	2.031(5)
Ni(1)-O(13)	2.074(5)	Ni(2)-O(23)	2.059(5)
Ni(1)-O(16)	2.097(5)	Ni(2)-O(26)	2.085(6)
O(17A)-Ni(1)	2.079(5)	O(27A)-Ni(2)	2.064(6)
N(12)-Ni(1)-N(11)	92.5(2)	N(21)-Ni(2)-N(22)	92.6(2)
N(12)-Ni(1)-O(12)	174.4(2)	N(21)-Ni(2)-O(22)	82.1(2)
N(11)-Ni(1)-O(12)	82.0(2)	N(22)-Ni(2)-O(22)	174.0(2)
N(12)-Ni(1)-O(13)	81.7(2)	N(21)-Ni(2)-O(23)	173.7(2)
N(11)-Ni(1)-O(13)	174.1(2)	N(22)-Ni(2)-O(23)	81.7(2)
O(12)-Ni(1)-O(13)	103.81(18)	O(22)-Ni(2)-O(23)	103.57(19)
N(12)-Ni(1)-O(17A)	88.9(2)	N(21)-Ni(2)-O(27A)	91.3(2)
N(11)-Ni(1)-O(17A)	90.7(2)	N(22)-Ni(2)-O(27A)	90.4(2)
O(12)-Ni(1)-O(17A)	92.0(2)	O(22)-Ni(2)-O(27A)	92.3(2)
O(13)-Ni(1)-O(17A)	90.2(2)	O(23)-Ni(2)-O(27A)	91.2(2)
N(12)-Ni(1)-O(16)	96.1(2)	N(21)-Ni(2)-O(26)	89.6(3)
N(11)-Ni(1)-O(16)	91.8(2)	N(22)-Ni(2)-O(26)	91.3(2)
O(12)-Ni(1)-O(16)	83.3(2)	O(22)-Ni(2)-O(26)	86.0(2)
O(13)-Ni(1)-O(16)	87.8(2)	O(23)-Ni(2)-O(26)	88.0(2)
O(17A)-Ni(1)-O(16)	174.3(2)	O(27A)-Ni(2)-O(26)	178.0(2)

The complex crystallised in the triclinic P −1 space group. There are two crystallographically symmetrical independent molecules in the unit cell of $[Ni(L^6+H)(MeOH)(EtOH)]_2[ClO_4]_2$. The two molecules show only slight differences in bond lengths and angles, thus, only data for Ni(1) ion will be discussed. L^6 coordinates in a tetradentate fashion, the two picolinate rings occupy the equatorial plane whereas the oxygen atoms from the solvent molecules, methanol and ethanol coordinate in the axial positions to form a pseudo-octahedral geometry. Unusually, the pyridyl ring is protonated and is not involved in the coordination; it hangs pendant and away from the coordination cavity producing a sterically favourable environment for the nickel centre. Its coordination geometry is almost identical to the $[Ni^{II}(L^2)(H_2O)_2]$ complex characterised earlier in this Chapter and the L-M-L bond angles deviate from a regular octahedron for the same reasons.

The complex has average Ni-N, Ni-O (COO^-) and Ni-O (OEt /OMe) bond lengths of 2.020(5.5) Å, 2.055(5) Å and 2.072(5.5) Å respectively. These are almost identical with the bond lengths seen in $[Ni^{II}(L^2)(H_2O)_2]$ and therefore can be regarded typical of pseudo-octahedral complexes of $N_2O_2O_2$' chromophore .

$[Zn(L^6)]_2$

Transparent single crystals were isolated for the zinc(II) compound, $[Zn(L^6)]_2$ (58%). Similar to the Ni(II) complex, it too crystallised in the triclinic P –1 space group. X-ray crystallography reveals the dimeric species depicted in Figure 3.17 whereas the relevant bond lengths and angles are listed in Table 3.14.

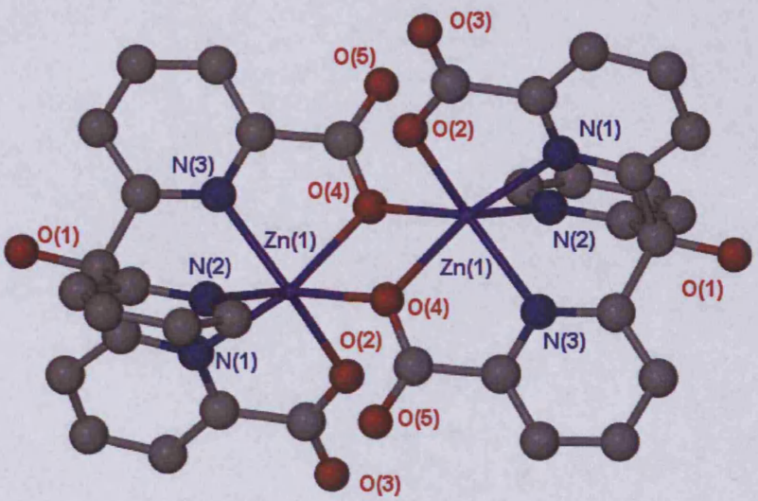

Figure 3.17 Crystal structure of $[Zn(L^6)]_2$. Hydrogen atoms omitted for clarity.

Table 3.14 Bond distance (Å) and angles (°) for $[Zn(L^6)]_2$.

N(1)-Zn(1)	2.143(4)	O(2)-Zn(1)	2.107(4)
N(2)-Zn(1)	2.182(4)	Zn(1)-O(4)	2.168(3)
N(3)-Zn(1)	2.138(4)	Zn(1)-O(4)#1	2.096(3)
O(4)#1-Zn(1)-O(2)	83.90(17)	O(2)-Zn(1)-O(4)	88.81(16)
O(4)#1-Zn(1)-N(3)	131.12(14)	N(3)-Zn(1)-O(4)	74.85(13)
O(2)-Zn(1)-N(3)	132.58(15)	N(1)-Zn(1)-O(4)	130.60(13)
O(4)#1-Zn(1)-N(1)	145.80(14)	O(4)#1-Zn(1)-N(2)	93.35(14)
O(2)-Zn(1)-N(1)	75.75(17)	O(2)-Zn(1)-N(2)	132.12(16)
N(3)-Zn(1)-N(1)	81.96(14)	N(3)-Zn(1)-N(2)	83.19(14)
O(4)#1-Zn(1)-O(4)	75.07(14)	N(1)-Zn(1)-N(2)	80.90(14)
O(2)-Zn(1)-O(4)	88.81(16)	O(4)-Zn(1)-N(2)	136.65(15)

An interesting symmetrical dimeric species is formed where, L^6 now coordinates to the zinc centres in a pentadentate fashion, the sixth coordination site is occupied by a bridging carboxylate oxygen donor atom from the second ligand. It is important to notice that both metal centres have a trigonal prismatic geometry. Each metal centre has an N_3O_3 donor set, with three N donors forming one triangular face and three oxygen donors forming the other. In this complex, ϕ (the twist angle between the two triangular faces; see Figure 3.19, a)[56] is ~ 0°, with the dihedral angle between the pyridine ring and the carbonyl of each bidentate donor arm being C2-N1-Zn1-O2, 0.2°, C13-N3-Zn1-O4, 3.6° and C7-N2-Zn1-O4', 10.7°, this results in C_3 symmetry along the O(1)-C(18) axis. These angles suggest that the geometry about the Zn(II) ion is a distorted trigonal prism, the ORTEP diagram of the molecule with the atomic numbering is shown in Figure 3.18.

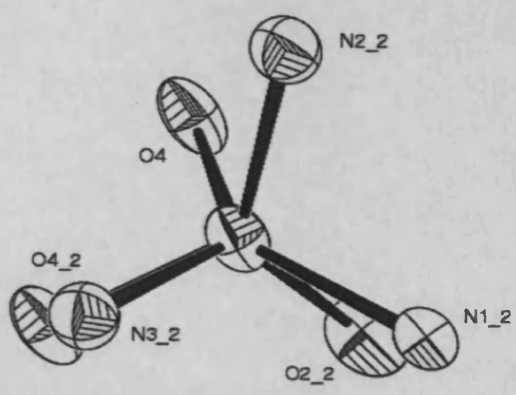

Figure 3.18 ORTEP diagram of the distorted trigonal prismatic $[Zn(L^6)]_2$ complex.

In addition, close inspection of the donor-metal-donor bond angles, also support the complex to be distorted trigonal prismatic. That is, for an octahedral complex one would expect twelve L-M-L 90° angles and three 180° angles.

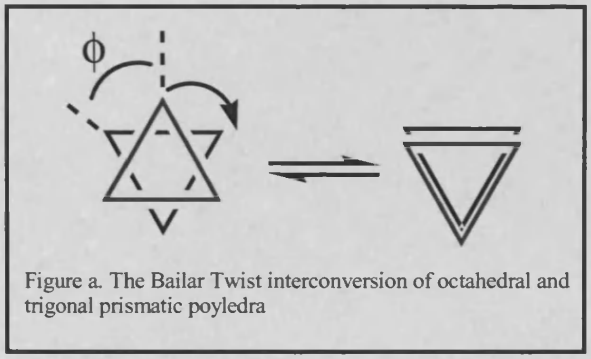

Figure a. The Bailar Twist interconversion of octahedral and trigonal prismatic poyledra

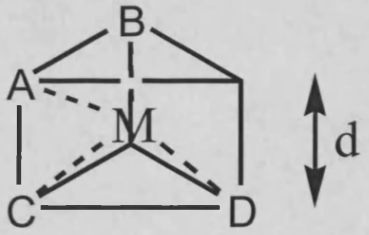

Figure b. Bond angles associated with trigonal prismatic metal centres

Figure 3.19 Bailar Twist Interconversion of octahedral and trigonal prismatic polyhedra.[56]

However, applying the Bailar twist[56] to this polyhedron results in a trigonal prism that has six 90° angles (A-M-B, three for each triangular face), three 70.5° angles (A-M-C) and six 131.7° angles (A-M-D). (Figure 3.19, b; however note these angles are based on a Bailar twist so that the distance between the two triangular faces, d, is retained with respect to the octahedron. If, however, d is lengthened, then A-M-B becomes more acute, while A-

M-C and A-M-D becomes more obtuse). For the observed structure, the six angles associated with the triangular faces (A-M-B) are 83.60(14), 80.90(14), 81.96(14), 88.81(16), 93.35(14) and 83.90(17). The three angles associated with the donors along the edge of a square face, (A-M-C) is 75.75(17), 75.07(14) and 74.85(13), where as the six angles associated with donors in opposite corners of the square face of the trigonal prism (A-M-D) are 131.12(14), 132.58(15), 130.60(13), 132.12(16), 136.65(15) and 145.80(14). While the angles are obviously indicative of trigonal prismatic, the deviation from 90° for the A-M-B angles are readily explained. The smaller A-M-B angles (<<90°) are associated with the N-M-N angles. These nitrogen donors are close to the bridgehead carbon of the tripod, where the sterics of the ligand will not allow the N donors to spread out far enough to give 90° angles, whereas the O-M-O angles are better positioned to give the desired angle. Such behaviour has also been observed by Ward *et al.* [57] for the Co(II) complex of the tris(2-pyridyl) pyrazolylborate ligand, where the three pyrazolyl rings are also directly bonded to a central linker atom (in this case boron).

The average Zn-N and the Zn-O bond lengths are similar, 2.154(4) and 2.124(3) Å. These bond lengths are typical of TP Zn(II) complexes, for example the TP $[Zn(C_{20}H_{18}N_2O_6)]\cdot CH_3OH$ complex characterised by Wang *et al.*[58] has the average bond lengths: Zn-N, 2.075 Å and Zn-O, 2.16 Å. It is noticed, these values are also very similar to the TP Fe(II) triester complex, $[Fe(L^7)][ClO_4]_2$ discussed later in this Chapter (see Figure 3.20) and is probably due to identical donor sets, N_3O_3 which has a strong affinity for this type of geometry.

3.3.4.3 Electrochemistry

CV measurements were performed on compounds $[Cu(L^6)]$, $[Ni(L^6+H)(MeOH)(EtOH)]_2[ClO_4]_2$ and $[Fe(L^6)]$. The $[Cu(L^6)]$ complex produced an irreversible oxidation processes at +1.079 V and may be assigned to either the $Cu^{II} \rightarrow Cu^{I}$ reduction or $ClO_4^- \rightarrow ClO_3^-$ reduction, the latter is more likely as the value is closest to where it is typically seen, +0.801 V vs Fc/Fc^+[28] whereas, $Cu^{II} \rightarrow Cu^{I}$ redox typically occurs at much higher oxidation potentials. For example, $[Cu^{II}(PA)^-_3]$ (PA = picolinic acid) has two reversible processes, one at +2.14 V vs Fc/Fc^+ corresponding to the ΔE for the $Cu^{II}(PA)_3^- + e^- \rightarrow Cu^{I}(PA) + 2PA^-$ reduction in the complex and one at –0.356 V vs Fc/Fc^+ and is characteristic of Cu^{II}/Cu^{I} reduction.[42] The $[Ni(L^6+H)(MeOH)(EtOH)]_2[ClO_4]_2$ complex produced an irreversible reduction process at –0.598 V vs Fc/Fc^+ and may be assigned to the Ni^{II}/Ni^{I} couple, similar electrochemical behaviour has been reported for $[Ni(6\text{-}Ph_2TPA)(CH_3CN)(CH_3OH)](ClO_4)_2$ where a quasi-reversible Ni^{II}/Ni^{I} couple is seen at –0.637 V vs Fc/Fc^+.[59]

3.3.5 $[Fe(L^7)][ClO_4]_2$ / $Na[M(L^8)]$

Complexations with L^7 / Na_3L^8 and M(II) were carried out in the same manner as described above, the yield of product obtained was reasonable (56-80%). Infrared spectra for the transition metal complexes are given in Table 3.15, again the expected carbonyl stretching frequencies for the coordinated carboxylate groups are present. Comparison of ν_{CO} bands to those of the free ligand and the sodium salt, show that the stretching frequency of the metal complexes is again intermediate of the two, typically they range between 1650 – 1668 cm^{-1}. However there is an exception to this, the carbonyl stretch

observed in $[Fe(L^7)][ClO_4]_2$ occurs at a higher frequency (1696 cm^{-1}) and is most likely caused by metal coordination to the ester carbonyl suggesting that ester hydrolysis does not occur upon complexation and is probably due to the weak acidity of the Fe^{2+} ion. Pyridyl coordination is suggested in all the complexes but only $[Fe(L^7)][ClO_4]_2$ contains the $\nu_{Cl\text{-}O}$ bands due to the per-chlorate counter-ion.

	IR, wavenumber (cm^{-1})			
	O-H	**C=O**	**C=N(py)**	**Cl-O**
L^7	3299sb	1728s	1586s	__
Na_3L^8	3411sb	1636s	1586s	__
$Na[Cu(L^8)]$	3333mb	1650s	1595s	__
$Na[Ni(L^8)]$	3348mb	1652s	1590s	__
$Na[Zn(L^8)]$	3425mb	1647s	1586m	__
$[Fe(L^7)][ClO_4]_2$	3434mb	1696s	1590m	1090s
$Na[Fe(L^8)]$	3444mb	1668s	1592m	__

Table 3.15 Correlation of IR spectra of **L^7** / **Na_3L^8** and its complexes **$[M(L^7)]$** / **$Na[M(L^8)]$**.

The IR data supports the mass spectra obtained for all metal complexes. The Cu complex contains the parent ion $[Cu(L^8)+2Na]^+$ and the Ni, Zn and Fe complexes have the parent ion, $[M(L^8)+Na]^+$ in their spectrum. An accurate mass for $[Fe(L^7)][ClO_4]_2$ (m/z 591.7551) confirms the presence of all three ester groups and a ClO_4^- counter-ion.

The ^1H NMR data of the zinc complex and the free ligand are compared in Table 3.16. The data obtained is consistent with the parent ligand spectrum, in terms of numbers of signals and their multiplicity suggesting that all three rings are equivalent. The shift of the peaks moved slightly but this time to higher ppm becoming more shielded upon co-ordination.

	^{1}H NMR (DMSO-d_6) *ppm*		
	$H^{3'}$	$H^{4'}$	$H^{5'}$
Na_3L^8	8.23	8.48	8.37
$Na[Zn(L^8)]$	8.00	8.37	8.25

Table 3.16 Comparison of ^{1}H NMR spectra for Na_3L^8 and $Na[Zn(L^8)]$.

3.3.5.1 Electronic spectra

The UV-vis spectrum of $Na[Cu(L^8)]$ exhibits an asymmetric broad peak at 626 nm with a shoulder to right at 795 nm. Their extinction coefficients are 91 and 71 $M^{-1}cm^{-1}$ respectively. The small shoulder observed indicates a slight distortion from a regular octahedron, which is expected of hexadentate ligands.[29]

The UV-vis spectrum of $Na[Ni(L^8)]$ complex exhibits again only two d-d transitions in the spectrum. Again assuming octahedral symmetry, the ν_1 band ($^3A_{2g} \rightarrow {}^3T_{2g}$) is seen at 11,416 cm^{-1} (36 $M^{-1}cm^{-1}$) and the ν_2 band ($^3A_{2g} \rightarrow {}^3T_{1g}(F)$) is seen at 18,587 cm^{-1} (48 $M^{-1}cm^{-1}$). The ν_3 band, $^3A_{2g} \rightarrow {}^3T_{1g}(P)$ that lies at the highest energy is probably hidden under the intense ligand peak ($\pi \rightarrow \pi^*$) seen at 38,462 cm^{-1}. From these values we know that Δ = 11,416 cm^{-1} and B = 1044 cm^{-1}, close to the free ion value (1082 cm^{-1}).[35] An unusually high β value is calculated 0.965 for an octahedral complex. Remarkably high values are usually obtained when geometries such as TP or intermediate of TP and TAP are assumed octahedral. Previously, Wentworth *et al.* reported[29] $[Ni(py)_3tach]^{2+}$ to have unusually high values when assumed octahedral symmetry, Δ = 12,100 cm^{-1} and B = 980 cm^{-1}. One would expect a ligand of this nature to adopt a trigonal prismatic geometry like its analogous $[Fe^{II}(L^7)][ClO_4]_2$ complex and therefore would explain the unusually

high values obtained. The intensity of the bands is also higher than the other Ni(II) complexes, this is also suggestive of near TP symmetry.

The electronic absorption spectrum of $[Fe^{II}(L^7)][ClO_4]_2$ (d^6) exhibits a broad peak at 448 nm (114 $dm^3.mol^{-1}.cm^{-1}$) implying a lower symmetry or vibronic coupling. Clearly this band is not characteristic of octahedral systems. Octahedral complexes such as $Fe(bipy)_3^{2+}$ and $Fe(\alpha\text{-diimine})_3^{2+}$ typically possess a band at ~ 521 nm, with a shoulder at ~ 493 nm. This difference in spectra may be a result of the trigonal prismatic geometry. Similarly, the UV-vis spectrum of $Na[Fe(L^8)]$ complex also gave no d-d transitions but a broad peak at 440 nm (223 $M^{-1}cm^{-1}$) like its analogous $[FeL^7][ClO_4]_2$ complex suggests the formation of a similar trigonal prismatic geometry.

3.3.5.2 Crystallographic data

Dark red / orange crystals were isolated (47%) by the slow diffusion of diethyl ether into a methanolic solution of $[Fe(L^7)][ClO_4]_2$. X-Ray crystallography revealed the crystal structure in Figure 3.20. Table 3.17 lists the selected bond lengths and angles.

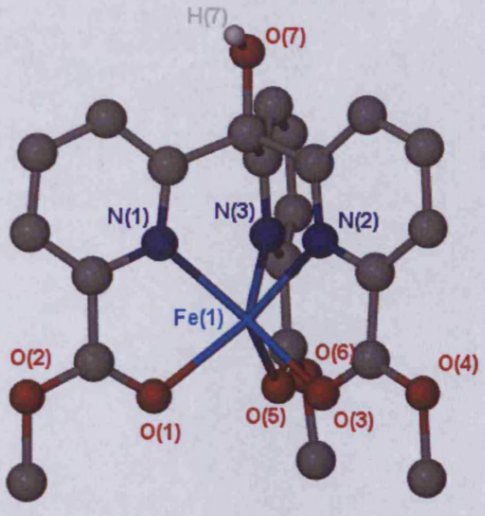

Figure 3.20 Crystal structure of $[Fe(L^7)][ClO_4]_2$. Hydrogen atoms omitted for clarity.

Table 3.17 Bond distance (Å) and angles (°) for $[Fe(L^7)][ClO_4]_2$.

N(1)-Fe(1)	2.114(4)	O(1)-Fe(1)	2.154(3)
N(2)-Fe(1)	2.157(4)	O(3)-Fe(1)	2.147(3)
N(3)-Fe(1)	2.135(4)	O(5)-Fe(1)	2.154(3)
N(1)-Fe(1)-N(3)	83.60(14)	O(3)-Fe(1)-O(1)	86.57(11)
N(1)-Fe(1)-O(3)	128.98(13)	O(5)-Fe(1)-O(1)	94.80(12)
N(3)-Fe(1)-O(3)	134.59(12)	N(1)-Fe(1)-N(2)	81.82(13)
N(1)-Fe(1)-O(5)	138.71(13)	N(3)-Fe(1)-N(2)	80.74(14)
N(3)-Fe(1)-O(5)	75.76(13)	O(3)-Fe(1)-N(2)	75.20(13)
O(3)-Fe(1)-O(5)	89.61(12)	O(5)-Fe(1)-N(2)	128.09(12)
N(1)-Fe(1)-O(1)	76.20(12)	O(1)-Fe(1)-N(2)	132.20(13)
N(3)-Fe(1)-O(1)	136.56(12)		

Like compounds $[Cu(L^2)(H_2O)]$ and $[Ni(L^2)(H_2O)_2]$ this also crystallised in the monoclinic P $2_{1/n}$ space group. Two important features of this structure are immediately obvious. Firstly, unlike the other complexes seen in this Chapter, but consistent with the spectroscopic data, all three ester groups are present and coordinate to the iron centre through each of the carbonyl oxygen atoms. The other three coordination sites are occupied by each of the pyridyl nitrogen atoms to form a six-coordinate complex. In fact, the co-ordination of picolinic esters to iron centres is rare, with few examples listed in the Cambridge crystallographic database (CCDC).[60,61] The observation of this ester complex is a little surprising although it has been seen in $[Fe(L^3\text{-}H)_2][ClO_4]$ described earlier in this Chapter, there the ester was not involved in coordination. The same explanation for the presence of the esters may also be applied here.

The second factor of note is that the complex has a trigonal prismatic geometry. It is very similar to the dimeric $[Zn(L^6)]_2$ complex discussed earlier except here we see a monomeric species. It also has an N_3O_3 donor set, with the three N donors forming one triangular face and the three oxygen donors forming the other. In this complex, ϕ (the twist angle between the two triangular faces) is ~ 0°, with the dihedral angle between the

pyridine ring and the carbonyl of each bidentate donor arm being O1-C7-C6-N1 3.6°, O3-C14-C13-N2 0.3° and O5-C21-C20-N3 0.2°, this results in C_3 symmetry along the O(7)-C(1) axis (see Figure 3.21).

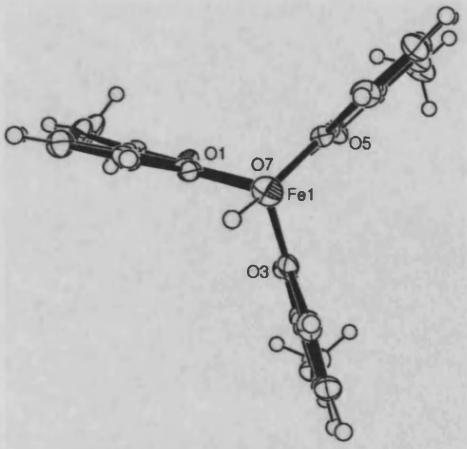

Figure 3.21 ORTEP view along the O(7)-C(1) axis for $[Fe(L^7)][ClO_4]_2$.

The donor-metal-donor bond angles show the complex to be trigonal prismatic. For the observed structure, the six angles associated with the triangular faces (A-M-B) are 83.60(14), 81.82(13), 80.74(14), 86.57(11), 94.80(12) and 89.61(12). The three angles associated with the donors along the edge of a square face, (A-M-C) are 75.76(13), 76.20(12) and 75.20(13), and the six angles associated with donors in opposite corners of the square face of the trigonal prism (A-M-D) are 128.98(13), 134.59(12), 138.71(13), 136.56(12), 128.09(12) and 132.20(13). While the angles are obviously indicative of trigonal prismatic, slight deviations from 90˚ occur for the same reasons as explained for the $[Zn(L^6)]_2$ complex.

Comparison of the metal donor bond lengths to similar complexes with N_3O_3 donor sets shows that the Fe-N bond lengths (average 2.135 Å) and the Fe-O bond lengths (average 2.151 Å) are typical for iron(II) complexes. For example, the picolinic acid

complex of Fe(II)[62] has average Fe-N bond lengths of 2.165 Å and average Fe-O bond lengths of 2.130 Å. It should be noted that the analogous Fe(III) complex[63] is readily distinguishable as the Fe-O bonds are notably shorter (1.948-1.972 Å), despite the similar Fe-N bond lengths (2. 126-2.150 Å).

There are numerous examples of trigonal prismatic complexes in the literature,[64-67] most of which are associated with rigid ligands predisposed to the geometry and / or metal centres which has no steric chemical preference (Zn^{2+}, d^{10} or Mn^{2+} d^5)[68,69] or metals which in some situations have a slight preference for trigonal prismatic geometry (e.g. Co^{2+} , d^7).[70] The rigid nature of this ligand means that if a monomeric species is to be formed then it would be trigonal prismatic or a severe distortion of the ligand from typically expected bond angles would be required to give an octahedral complex. An alternative would be the formation of tetranuclear octahedral complexes as has been observed for the related tris(2-pyridinepyrazolyl) borate ligand.[56] In such a case, each ligand would reside on the face of a tetrahedron donating one bidentate ligand to each metal of the triangle. This results in the formation of four octahedral metal centres in a tetrahedral array. As mentioned earlier, Ward *et al.*[57] observed the tetramer formation for Mn^{2+} and Zn^{2+}, but the trigonal prismatic monomer for Co^{2+}. While the rigidity of the ligand is an important factor in the formation of trigonal prismatic complexes (for example Wentworth[29,71] has clearly shown that the rotational barrier in the C=N bond in tris(pyridine-2-carboxyaldimino) cyclohexane is responsible for the isolation of trigonal complexes), rigid ligands are still capable of forming multinuclear octahedral complexes so long as the steric energies associated with it are favourable with respect to the ligand field stabilisation energies which result from the structure, i.e. the formation of an

octahedral complex could occur so long as the extra ligand field stabilisation energy from octahedral geometry (versus trigonal prismatic) outweighs any steric repulsion which might result from the structures. It is clear that for this ligand, even the large ligand field stabilisation energy associated with low spin octahedral d^6 does not allow the formation of an octahedral complex.

3.3.5.3 Electrochemistry

Cyclic voltammetry (CV) measurements were performed on the above Cu, Ni and Fe compounds. The $Na[Cu(L^8)]$ complex did not give any redox activity unlike its analogous complex $[Cu^{II}(PA)^-_3]$ (PA = picolinic acid) where, two reversible processes are seen, one at +2.14 V vs Fc/Fc^+ corresponding to the ΔE for the $Cu^{II}(PA)_3^- + e^- \rightarrow Cu^I(PA) + 2PA^-$ reduction in the complex and one at –0.356 V vs Fc/Fc^+ characteristic of Cu^{II}/Cu^I reduction.[42] The $Na[Ni(L^8)]$ complex produced one irreversible free ligand based reduction process at -1.613 V vs Fc/Fc^+ and the $[Fe(L^7)][ClO_4]_2$ complex gave two reversible oxidation processes, the cyclic voltammogram of which is illustrated in Figure 3.22 (+0.412 V, 75 mV and +0.861 V, 74 mV vs Fc/Fc^+). There may be two possible explanations for the reversible nature of this complex; one may be that there are two different iron complexes present, $[FeL^7]^{2+}$ and $Na[FeL^8]^+$, the latter complex may have formed as a result of ester hydrolysis in the presence of a protic solvent. Both would give rise to a reversible one electron Fe^{II}/Fe^{III} oxidation but at different potentials, the wave at +0.861 V being more stable than the other complex which is likely to be $[FeL^7]^{2+}$. Another possible explanation may be oxidations in the $[FeL^7]^{2+}$ complex, the first wave seen at +0.412 V may be due to the reversible one electron Fe^{II}/Fe^{III} oxidation in the free

ion and the second wave at +0.861 V is likely to be a reversible one electron $[Fe^{II}L^7]^{3+}/[Fe^{III}L^7]^{4+}$ oxidation in the complex.[55] Alternatively, the wave at +0.861 V could also be caused by the reduction of $ClO_4^- \rightarrow ClO_3^-$ as we know this typically occurs at +0.801 V vs Fc/Fc^{+}[28]

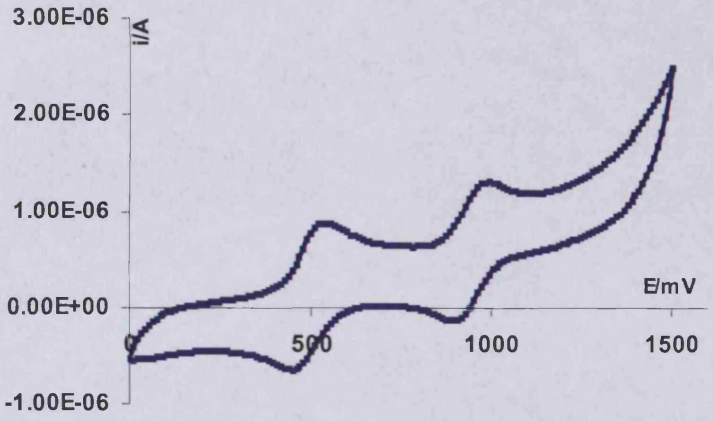

Figure 3.22 Cyclic Voltammogram of complex $[Fe(L^7)][ClO_4]_2$ in CH_3CN + 0.1M Bu_4NPF_6 at 20 °C vs.Fc/Fc^+ reference standard.

3.4 Conclusions and suggestions for further research

The transition metal complexes synthesised in this Chapter have been accomplished in reasonable yields and with high purity for some as a series of crystal structures were obtained. The structures confirmed the hydrolysis of the ester groups upon complexation but was not the case in all the complexes, the crystal structures of $[Fe(L^3\text{-}H)_2]_2[ClO_4]$ and $[Fe(L^7)][ClO_4]_2$ complexes showed the presence of the ester groups.

The Cu(II) ion prefers five coordinate geometries, with Na_2L^2, a square based pyramidal geometry is preferred to trigonal bipyramidal. However with NaL^4 an unusual tetrameric compound is formed, $[(Cu^{II}L^4)]_4[ClO_4]_4$ containing two different Cu(II) centres, one preferring a square based pyramidal geometry and the other prefers a

geometry intermediate of square based pyramid and trigonal bipyramidal. The presence of these two geometries is supported by the UV-vis spectrum as two distinctive absorption peaks are seen at 696 nm and 972 nm, this pattern is also seen in the spectrum of $[(Cu^{II}L^{8})]$ but may be a result of Jahn-Teller distortion. The remaining UV-vis spectra for $[(Cu^{II}L^{6})]$ and $[(CuL^{7})]$ complexes suggest octahedral symmetry.

X-Ray crystallography for Ni(II) ions show pseudo-octahedral geometries with Na_2L^2 and Na_2L^6. In both cases, it is noticed that solvent molecules occupy the apical coordination sites located above and below the square plane. One would expect the two complexes to have similar UV-vis spectra but this was clearly not the case. Table 3.18 compares all the UV-vis data obtained for the Ni(II) complexes.

Ni complex	ν (nm) / ε ($M^{-1}cm^{-1}$)	Δ (cm^{-1})	B (cm^{-1})	β
$[Ni(L^2)(H_2O)_2]$	838(13), 564(5)	11 933	641	0.590
$[Ni(L^4)]$	813(10), 523(6)	12 300	836	0.773
$[Ni(L^6+H)]^+$	823(12), 524(10)	12 150	863	0.790
$Na[Ni(L^8)]$	876(36), 538(48)	11 416	1037	0.958

Table 3.18 UV-vis spectra for Nickel complexes in CH_3CN.

UV-vis spectrum of pseudo-octahedral $[Ni(L^2)(H_2O)_2]$ complex produce Racah B value of 638 cm^{-1} and has the highest amount of delocalisation in the complex ($\beta = 0.590$) and may be a result of the carbonyl brigehead. One would expect the pseudo-octahedral $[Ni(L^6+H)]^+$ complex to have similar values to $[Ni(L^2)(H_2O)_2]$ however, a high Racah B value of 863 cm^{-1} is obtained and is similar to complex $[Ni(L^4)]$ ($B = 836$ cm^{-1}) implying that electronically the ligands have similar field strengths and therefore cause similar covalency in the complex. $Na[Ni(L^8)]$ has a remarkably high B value and can be attributed

to the severe distortion from a regular octahedron. This is typical of near TP geometry when assumed it is of octahedral symmetry. One would expect this nickel complex to have TP symmetry like it analogous $[FeL^7][ClO_4]_2$ complex. TP geometry is also seen in the dimeric $[Zn(L^6)]_2$ complex, both of which have been characterised by X-ray crystallography. The dihedral angles between the pyridine ring and the carbonyl of each bidentate donor arm show that the zinc complex distorts slightly from a regular trigonal prism than the iron complex.

For all Zn complexes, the ^1H NMR spectra obtained are consistent with the parent ligand spectrum, in terms of numbers of signals and their multiplicity. The shift of the peaks however, did change slightly upon co-ordination and in general of shift of ~0.15 ppm to higher ppm was observed. From these observations it is clear that the ligands are bound to the metal in such as way as to not lower the symmetry of the ligand when co-ordinated or that if it is unsymmetrically bound to the zinc, it is fluxional on a timescale greater than that of the NMR experiment and a symmetrical average signal is observed. On considering the solid state structures displayed by these ligands, 1:1 complexes for L^2 and L^8 and the observed 2:2 complex for L^6 would all be consistent with the observed NMR spectra, however, it seems most unlikely that anything like the tetrameric structure observed for copper (II) with L^4 should be observed for the zinc analogue.

The IR spectra for the complexes gave characteristic carbonyl stretching frequencies for the co-ordinated carboxylate groups and in the case of L^2, for the bridging ketone moiety. Comparison of ν_{CO} bands to those of the free ligand and the sodium salt, show that the stretching frequency of the transition metal complexes is intermediate of the two. In addition, the ketone group in L^2 is also affected to a large extent by the

deprotonation of the free ligand. In addition to these changes in ν_{CO} , the presence or absence of $\nu_{Cl\text{-}O}$ due to the ClO_4^- counterion is helpful in determining the structure of the products. L^2 and L^6, which both have two carboxylate groups react with divalent transition metals to yield complexes with no perchlorate stretches in the IR. One exception to this is the nickel complex of L^6. In comparison, L^4, with only one carboxylate group, yields complexes; all with a ClO_4^- counterion, while the trianionic L^8 reacts with metal ions to yield species with no perchlorate present. All these observations are consistent with elemental analyses and crystallographic studies.

We can also conclude that these complexes prefer to be in the +II oxidation state although one exception is seen in the $[Fe(L^3\text{-}H)_2]_2[ClO_4]_2$ complex where the oxidation state is +III. The cyclic voltammograms obtained show typical ligand (py→py-) based reduction in some of the complexes. The potentials at which this commonly occurs is in the range of -1.015 V to –1.613 V depending very much on the ligand involved.

Future work may be concentrated on obtaining crystallography data for the transition metal complexes that were unattained in this Chapter. Preparation of lanthanide complexes with the above ligands may also prove to be of great interest as previous work by Peng *et al.* on sodium tris(2-carboxy-6-pyridyl) methanol and its lanthanide complexes was successful. Further investigations of these may involve luminescence spectroscopy, relaxtivity measurements of the gadolinium complexes and X-ray crystallography.

3.5 Experimental

3.5.1 Instrumentation

The ^{1}H and ^{13}C NMR experiments were recorded on a Bruker DPX 400 spectrometer.

The electronic spectra were recorded on a Perkin-Elmer λ800 spectrophotometer under a normal atmosphere at 298 K in CH_3CN, CH_3OH or DMF with λ_{max} in nm and ε in $M^{-1}cm^{-1}$.

The infrared absorptions were recorded on a Perkin-Elmer 1600 series FTIR spectrometer in KBr or a Jasco FT / IR-660 Plus.

The national mass spectrometry service centre at Swansea University sponsored by EPSRC performed Mass spectrometry and the University of Nottingham performed elemental analyses.

Electrochemical experiments were conducted using an Autolab PGSTAT12 and a conventional three-electrode cell (A pyrolytic carbon working electrode, platinum wire auxiliary electrode and silver pseudoreference electrode). Dry acetonitrile with 0.1 M *n*-Bu_4NPF_6 supporting electrolyte was used as solvent for all the complexes. Ferrocene was used as an internal reference standard. Prior to the experiments nitrogen gas was bubbled through the solution to create an inert atmosphere. All measurements were made at 25°C. The potential of the regular ferrocene/ferricinium (Fc/Fc^{+}) redox couple used as an internal standard was 0.07 V under our experimental conditions (scan rate of 200 mV s^{-1}).

Single-crystal intensity measurements were collected at room temperature with Siemens four-circle diffractometer or a Rigaku AFCS Diffractometer, using Mo Kα radiation with graphite monochromator and ω/2θ-scans. Lattice parameters for the complexes were obtained using least-squares refinement of the angles of 24 reflections with $22<2\theta<26°$.

The structure was solved by direct methods using SHELXS-97 and refined with all data by full-matrix least-squares on F^2 using SHELXL-97. All non-hydrogen atoms were refined anisotropically. Hydrogen atoms were fixed in idealised positions with a riding model or refined isotropically.

3.5.1.1 A general procedure for the synthesis of transition metal complexes

The ligand (1 equivalent, typically 0.1 mmol) was dissolved in the minimum amount of methanol (typically 3ml). To this stirring solution was added dropwise, a solution of $M(ClO_4)_2$ salt (1 equivalent) in distilled water (typically ~2ml). The precipitate formed at varying rates, depending upon the ligand used. This precipitate was collected and dried in air (yield: 49-80%). Recrystallisation of the compounds typically involved the diffusion of ether into methanol at temperatures below 10°C.

N.B. $M(ClO_4)_2 = Cu(ClO_4)_2$, $Ni(ClO_4)_2$, $Zn(ClO_4)_2$, $Fe(ClO_4)_2$.

3.5.2 *Spectroscopic data for* $[M(L^2)]$

$[Cu^{II}(L^2)(H_2O)].H_2O$

Blue crystalline solid was obtained (32%). IR (KBr disc, cm^{-1}), ν = 3450mb, 1672s, 1650s, 1617m, 1595m, 1367s, 1285m; ESMS (m/z): 333.9; accurate ESMS: 333.9645 $[Cu(L^2)+H]^+$; UV-vis (DMF): λmax (nm), ε (M^{-1} cm^{-1}) 290 (4126), 621 (43) (Found: C, 47.47; H, 2.95; N, 7.14%. $C_{13}H_{10}CuN_2O_7$ requires C, 42.23; H, 2.73; N, 7.58%)

$[Ni^{II}(L^2)(H_2O)_2]$

Purple / grey crystals obtained (45%). IR (KBr disc, cm^{-1}), ν = 3420sb, 1663s, 1652s, 1627m, 1586m, 1382s, 1320m, 1259w; ESMS (m/z): accurate mass = 345.9730

$[Ni(L^2)(H_2O)]^+$; UV/Vis (CH_3CN): λmax (nm), ε (M^{-1} cm^{-1}): 380 (3597), 564 (5), 838 (13). (Found C, 42.44; H, 2.62; N, 7.51. $C_{13}H_6NiN_2O_5.2H_2O$ requires C, 42.79; H, 2.76; N, 7.68%).

$[Zn^{II}(L^2)(H_2O)_y]$

White precipitate was collected (55%). ^1H NMR (400MHz DMSO-d_6): 8.45 (m, 4H, $H^{3'}$, $H^{4'}$), 8.55 (d, 2H, J = 8.0 Hz, $H^{5'}$); IR (KBr disc, cm^{-1}), ν = 3426mb, 1684s, 1649s, 1625m, 1434w, 1393s; ESMS (m/z): 335 $[Zn(L^2)+H]^+$

$[Fe^{II}(L^2)(H_2O)_y]$

Bright orange / red precipitate was collected (49%). IR (KBr disc, cm^{-1}), ν = 3427mb, 1687s, 1654s, 1590m, 1376s, 1332m, 1264w, 1086m; ESMS (m/z): 369 $[Fe(L^2)(H_2O)_2+Na]^+$; UV-vis (CH_3CN): λmax (nm), ε (M^{-1} cm^{-1}): LMCT 356 nm (2560).

3.5.3 *Spectroscopic data for* $[Fe(L^3\text{-}H)][ClO_4]_2$ / $[M(L^4)][ClO_4]$

$[(Cu^{II}L^4)]_2[ClO_4]_2 \cdot 1.5H_2O$

Blue single crystals were isolated (52%). IR (KBr disc, cm^{-1}), ν = 3422sb, 1634s, 1597s, 1461m, 1401m, 1371s, 1289m, 1089s; ESMS 369 $[Cu(L^4)]^+$; MALDI MS: 837 $[\{Cu(L^4)\}_2+ClO_4]$; accurate MALDI MS (m/z): 836.98088 $[(CuL^4)_2+ClO_4]$, calculated 836.98289; UV-vis (CH_3CN): λmax (nm), ε (M^{-1} cm^{-1}) 262 (4475), 696 (85), 972 (46). (Found C, 42.38; H, 2.61; N, 8.78%. $C_{34}H_{27}N_6O_{15.5}Cu_2Cl_2$ requires C, 42.29; H, 2.82; N, 8.70%).

$[Ni^{II}(L^4)][ClO_4]$

A dark purple precipitate was formed (49%); IR (KBr disc, cm^{-1}), ν = 3470sbr, 1639s, 1596s, 1392s, 1281m, 1091s; ESMS (m/z): 364.1 $[Ni(L^4)+H]^+$ and 396 $[Ni(L^4)(H_2O)_2]$; UV-vis (CH_3CN): λmax (nm), ε (M^{-1} cm^{-1}) 265 (5394), 523 (6), 813 (10).

$[Zn^{II}(L^4)][ClO_4]$

White precipitate collected (62%). ^1H NMR (400MHz, DMSO-d_6): 7.46 (dd 2H, J = 8.5, 4.0 Hz, H^5), 7.82 (d, 2H, J = 7.8 Hz, H^3), 8.09 (dd, 2H, J = 7.8, 4.2 Hz, H^4), 8.55 (m, 2H, $H^{5'}$, $H^{3'}$), 8.63 (t, 1H, J = 7.2 Hz, $H^{4'}$), 8.71 (d, 1H, J = 8.0 Hz, H^6); IR (KBr disc, cm^{-1}), ν = 3469mb, 1636s, 1599s, 1463w, 1397s, 1282m, 1090s; ESMS (m/z): 370 $[Zn(L^4)]^+$

$[Fe^{III}(L^3\text{-}H)_2]_2[ClO_4]_2$

Dark red crystals were grown (33%). IR (KBr disc, cm^{-1}), ν = 1719s, 1593s, 1458m, 1329w, 1265s, 1093s; accurate ESMS (m/z): 696.1414 $[Fe(L^3)_2]^+$; UV-vis (CH_3CN): λmax (nm), ε (M^{-1} cm^{-1}) λmax (nm), ε (M^{-1} cm^{-1}) 372 (3236), 424 (4451). (Found C, 53.70; H, 3.54; N, 10.21 $C_{36}H_{28}ClFeN_6O_{10}$ requires C, 54.26; H, 3.67; N, 10.55)

$[Fe^{II}(L^4)][ClO_4]$

Red precipitate was obtained (70%); IR (KBr disc, cm^{-1}), ν = 3435mb, 1652s, 1596m, 1463w, 1372s, 1279m, 1087s; accurate ESMS (m/z): 363 $[Fe(L^4)+H]^+$; UV-vis (CH_3CN): λmax (nm), ε (M^{-1} cm^{-1}) 250 (11564), 372 (2453).

3.5.4 *Spectroscopic data for* [M(L^6)]

[$Cu^{II}(L^6)(H_2O)$]

Blue precipitate was obtained (54%). IR (KBr disc, cm^{-1}), ν = 3432mb, 1670m, 1647s, 1595s, 1570m, 1463m, 1383s, 1079w; ESMS (m/z): 413 [Cu(L^6)+H] (100%), accurate ESMS = 430.033 $[Cu(L^6)(H_2O)]^+$; UV-vis (MeOH): λmax (nm), ε (M^{-1} cm^{-1}) 632 (47).

[$Ni^{II}(L^6$+H)(MeOH)(EtOH)][ClO_4]

A purple / grey precipitate was obtained (69%). IR (KBr disc, cm^{-1}), ν = 3397sb, 1636s, 1590s, 1457m, 1383s, 1263w, 1090s; accurate ESMS (m/z): 408.0125 $[Ni(L^6)+H]^+$; UV/Vis (MeOH): λmax (nm), ε (M^{-1} cm^{-1}) 260 (39,00), 524 (10), 823 (12). (Found C, 43.23; H, 3.52; N, 6.95 $C_{21}H_{22}ClNiN_3O_{11}$ requires C, 43.00; H, 3.78; N, 7.16).

[$Zn^{II}(L^6)_2$]

A white precipitate was collected (75%). ^{1}H NMR (400MHz, DMSO-d_6): 7.50 (dd, 1H, *J* = 7.8, 6.1 Hz, H^5), 7.85 (d, 1H, *J* = 7.8 Hz, H^3), 8.10 (t, 1H, *J* = 7.8 Hz, H^4) 8.35 (d, 2H, *J* = 7.5 Hz, $H^{3'}$), 8.46 (d, 2H, *J* = 7.6 Hz, $H^{5'}$) 8.55 (t, 2H, *J* = 7.6 Hz, $H^{4'}$) 8.72 (d, 1H, *J* = 6.5 Hz, H^6); IR (KBr disc, cm^{-1}), ν = 3398sb, 1668s, 1595s, 1569s, 1457m, 1382s, 1350s, 1078w; MS (m/z): 413 $[Zn(L^6)+H]^+$ (25%), 370 [Zn(L^6)+H-CO_2] (100%). (Found C, 50.28; H, 2.92; N, 9.86. $C_{36}H_{22}N_6O_{10}Zn_2$ requires C, 49.96; H, 3.03; N, 9.71%).

[$Fe^{II}(L^6)(H_2O)$]

Dark red precipitate was formed (44%). IR (KBr disc, cm^{-1}), ν = 3340mb, 1652s, 1591s, 1399s, 1278m, 1088m; ESMS (m/z): 405 $[Fe(L^6)+H]^+$; UV-vis (CH_3CN): λmax (nm), ε (M^{-1} cm^{-1}) 466 (5651).

3.5.5 *Spectroscopic data for* $[Fe(L^7)][ClO_4]_2$ / $Na[M(L^8)]$

$Na[Cu^{II}(L^8)]$

A blue precipitate was collected (60%). IR (KBr disc, cm^{-1}), ν = 3333mb, 1650s, 1595s, 1484 m, 1392s, 1305 w, 1079w; ESMS (m/z): 501.2 $[Cu(L^8)+2Na]^+$; UV-vis (MeOH): λmax (nm), ε (M^{-1} cm^{-1}) 270 (13396), 626 (91), 795 (71).

$Na[Ni^{II}(L^8)]$

A green precipitate was collected (52%). IR (KBr disc, cm^{-1}), ν = 3348mb, 1652s, 1590m, 1564w, 1455m, 1386s, 1214w, 1075m, 703w; ESMS (m/z): 474.3 $[Ni(L^8)+Na]^+$; UV-vis (MeOH): λmax (nm), ε (M^{-1} cm^{-1}); 283 (2232), 538 (48), 876 (36).

$Na[Zn^{II}(L^8)]$

Again a white precipitate was formed (75%). ^1H NMR (400MHz, DMSO-d_6): 8.00 (d, 3H, J = 7.7Hz, $H^{3'}$) 8.25 (d, 3H, J = 7.5 Hz, $H^{5'}$), 8.37 (t, 3H, J = 7.5 Hz, $H^{4'}$); IR (KBr disc, cm^{-1}), ν = 3425mb, 1647s, 1586m, 1570s, 1458s, 1393s, 1287w, 1160w, 1073w; ESMS (m/z): 480.41 $[Zn(L^8)+Na]^+$.

$[Fe^{II}(L^7)][ClO_4]_2$

An orange precipitate was obtained (59%). IR (KBr disc, cm^{-1}), ν = 3434mb, 1696s, 1590m, 1458w, 1361s, 1286m, 1090s; ESMS (m/z): 591.7551 $[Fe(L^7)+ClO_4]^+$; UV-vis (MeOH): λmax (nm), ε (M^{-1} cm^{-1}) 448 (114). (Found C, 37.91; H, 3.44; N, 5.32. $C_{22}H_{19}Cl_2FeN_3O_{15}$ requires C, 38.12; H, 3.60; N, 5.56).

$Na[Fe^{II}(L^8)]$

A red precipitate was collected (69%). IR (KBr disc, cm^{-1}), ν = 3444mb, 1668s, 1605m, 1592s, 1458m, 1387s, 1268m 1152m, 1062w; ESMS (m/z): 471 $[Fe(L^8)+Na]^+$; UV-vis (MeOH): λmax (nm), ε (M^{-1} cm^{-1}) 440 (223).

3.6 References

1. J.P. Collman, M. Rapta, M. Bröring, L. Raptova, R. Schwenninger, B. Boitrel, L. Fu, M.L. Her, *J. Am. Chem. Soc.*, 1999, **121**, 1387.
2. M. Wall, B. Linkletter, D. Williams, A.-M. Lebuis, R.C. Hynes, J. Chin, *J. Am. Chem. Soc.*, 1999, **121**, 4710.
3. M. Kodera, K. Katayama, Y. Tachi, K. Kano, S. Hirota, S. Fujinami, M. Suzuki, *J. Am. Chem. Soc.*, 1999, **121**, 11006.
4. J. Zhou, Y. Tang, *Org. Biomol. Chem.*, 2004, **2**, 429.
5. S-G, Kim, H.R. Seong, J. Kim, K.H. Ahn, *Tetrahedron Lett.*, 2004, **45**, 6835.
6. T.G. Gant, A.I. Meyers, *Tetrahedron*, 1994, **50**, 2297.
7. W-J. Peng, D.E. Relchert, *U.S. Patent No. 5,869,026*, 1999.
8. *U.S. Patent No. 5,405,601*, 1999 discloses functionalised tripodal ligands for imaging applications.
9. F. Bodar-Houillon, A. Marsura, *Tetrahedron Lett.*, 1995, **36**, 865.
10. W-K. Wong, H. Liang, J. Guo, W-Y. Wong, W-K. Lo, K-F. Li, K-W. Cheah, Z. Zhou, W-T. Wong, *Eur. J. Inorg. Chem.*, 2004, 829.
11. S. Trofimenko, *Chem. Rev.*, 1993, **93**, 945.
12. A.J. Blake, D.M.J. Doble, W.-S. Li, M. Schröder, *J. Chem. Soc. Dalton Trans.*, 1997, 3655.
13. S.J. Archibald, A.J. Blake, S. Parsons, M. Schröder, R.E.P. Winpenny, *J. Chem. Soc. Dalton Trans.*, 1997, 173.
14. K Hegetschweiler, B. Morgenstern, J. Zubieta, P.J. Hagrman, N. Lima, R. Sessoli, F. Totti, *Angew. Chem., Int. Ed.*, 2004, **43**, 3436.

15. N. Ye, G. Park, A.M. Pryzborowska, P.E. Sloan, T. Clifford, C.B. Bauer, G.A. Broker, R.D. Rogers, R. Ma, S.V. Torti, M.W.Brechbiel, R.P. Planalp, *J. Chem. Soc. Dalton Trans.*, 2004, 1304.

16. S. Bellemin-Laponnaz, L.H. Gade, *Chem. Comm.*, 2002, 1286.

17. I.M. Wasser, C.F. Martens, C.N. Verani, E. Rentschler, H. Huang, P. Moeenne-Loccoz, L.N. Zakharov, A.L. Rheingold, K.D. Karlin, *Inorg. Chem.*, 2004, **43**, 651.

18. J.B. Mandel, C. Maricondi, B.E. Douglas, *Inorg. Chem.*, 1988, **27**, 2990.

19. L. Karmazin, M. Mazzanti, J. Pecaut, *Inorg. Chem.*, 2003, **42**,5900.

20. A. Hazell, J. McGinley, H. Toftlund, *J. Chem. Soc. Dalton Trans.*, 1999,1271.

21. W.-J. Peng, D.A. Aguilar, *US Patent 5*, 861, 140.

22. X. Li, C.L.D. Gibb, M.E. Kuebel, B.C. Gibb, *Tetrahedron*, 2001, **57**, 1175.

23. M.J. Hannon, P.C. Mayers, P.C. Taylor, *Tetrahedron Letters,* 1998, **39**, 8509.

24. H. Adolfsson, K. Wärnmark, C. Moberg, *J. Chem. Soc. Chem. Comm.*, 1992, 1054.

25. P. Sykes, *A guidebook to mechanism in organic chemistry*, published in 1974 (4th edition), pp. 234-236.

26. G.G. Mohamed, N.E.A. El-Gamel, *Spectrochemica Acta Part A*, 2005, **61**,1089.

27. P.J. van Koningsbruggen, J.G. Haasnoot, R.A.G. de Graaff, J. Reedijk, *Inorg. Chim. Acta.*, 1995, **234**, 87

28. S.F.A. Kettle, "Physical Inorganic Chemistry, A Coordination Chemistry Approach", New edition (April 13, 2000), p.161.

29. W.O.Gillum, R.A.D.Wentworth, R.F.Childers, *Inorg. Chem.*, 1970, **9** 1829

30. E. Larsen, G.N. La Mar, B.E. Wagner, J.E. Parks, R.H. Holm, *Inorg. Chem.,* 1972, **11**, 2652.

31. A.K. Brisdon, "*Inorganic Spectroscopic Methods*", *Ox. Chem. Primer*, Published 1998, P.66.

32. R.K. Boggess, A.H. Lamson, S. York, *Polyhedron*, 1991, **10**, 2791

33. H-L. Kwong, L-S. Cheng, W-S. Lee, W-L. Wong, W-T. Wong, *Eur. J. Inorg. Chem.*, 2000, 1997.

34. A. Takenaka, H. Utsumi, T. Yamamoto, A. Furusaki, I. Nitta, *J. Chem. Soc. Jpn, Pure Chem.*, 1970, **91** 928.

35. P. Segl'a, M. Jamnicky, M. Koman, J. Sima, T. Glowiak, *Polyhedron*, 1998, **17,** 4535.

36. S. Midollini, A. Orlandini, A. Vacca, *Inorg. Chem. Commun.*, 2004, **7**, 1113.

37. D.E. Nikles, M.J. Powers, F.L. Urbach, *Inorg. Chem.*, 1983, **2**, 3210.

38. A.W. Addison, T.N. Rao, J. Reedijk, J. van Rijn, G.C. Verschoor, *J. Chem. Soc. Dalton Trans.*, (1984), 1349.

39. A. Takenaka, H. Utsumi, N. Ishihara, A. Furusaki, I. Nitta, *J. Chem. Soc. Jpn, Pure Chem.*, 1970, **91** 921.

40. S. Parsons, X. Tan, R. Winpenny, P.Wood, *Private Commun.*, 2004.

41. A.L. Portela, M.L. Teijelo, G.I. Lacconi, *Electrochemica Acta.*, 2005

42. D.T. Swayer, *Inorg. Chim. Acta.*, 1994, **226**, 99.

43. S. Youngme, G.A. van Albada, O. Roubeau, C. Pakawatchai, N. Chaichit, J. Reedijk, *Inorg. Chimi. Acta.*, 2003, **342**, 48.

44. E.V. Rybak-Akimova, A.Y. Nazarenko, L. Chen, P.W. Krieger, A.H. Herrera, V.V. Tarasov, P.D. Robinson, *Inorg. Chim. Acta,* 2001, **324**, 1.

45. S.V. Kryatov, S. Taktak, I.V. Korendovych, E.V. Rybak-Akimova, *Inorg. Chem.*, 2005, **44**, 85.

46. S. Berry, *J. Chem. Phys.*, 1960, **32**, 933.

47. G. Christou, S.P. Perlepes, E. Libby, K. Folting, J.C. Huffman, R.J. webb, D.N. Henrickson, *Inorg. Chem.* 1990, **29**, 3657.

48. T. Tokii, M. Nagamatsu, H. Hamada, M. Nakashima, *Chem. Lett.*, 1992, 1091.

49. S. Youngme, C. Chailuecha, G.A. van Albada, C. Pakawatchai, N. Chaichit, J. Reedijk, *Inorg. Chim. Acta.*, 2005, **358**, 1068.

50. F.R. Keene, D.J. Szalda, T.A. Wilson, *Inorg. Chem.*, 1987, **26**, 2211.

51. F.R. Keene, D.J. Szalda, *Inorg. Chem.*, 1986, **25**, 2795.

52. C.R. Goldsmith, R.T. Jonas, A.P. Cole, T.D.P. Stack, *Inorg. Chem.*, 2002, **41**, 4642.

53. R.J.M.K. Gebbink, R.T. Jonas, C.R. Goldsmith, T.D.P. Stack, *Inorg. Chem.*, 2002, **41**, 4633.

54. D. Onggo, F. Martak Ismunandar, B.M. Yamin, S.W. Ng, *Acta. Crystallogr., Sect E*, 2006, **62**, m1112.

55. A. Ion, J.C. Moutet, E. Saint-Aman, G. Royal, S. Tingry, J. Pecaut, S. Menage, R. Ziessel, *Inorg. Chem.*, 2001, **40**, 3632.

56. J.C. Bailar, Jr., *J. Inorg. Nucl. Chem.*, 1958, **8**, 165.

57. R.L. Paul, A.J. Amoroso, P.L. Jones, S.M. Couchman, Z.R. Reeves, L.H. Rees, J.C. Jeffery, J.A. McCleverty and M.D.Ward, *J. Chem. Soc., Dalton Trans.*, 1999, 1563.

58. J. Wang, D.-S. Zhu, K.-Z. Shao, L. Xu, *Acta Cryst.*, 2006, E**62**, m1884-m1886.

59. M.M. Makowska-Grzyska, E. Szajna, C. Shipley, A.M. Arif, M.H. Mitchell, J.A. Halfen, L.M. Berreau, *Inorg. Chem.*, 2003, **42**, 7472.

60. J.J. Kodanko, D. Xu, D.Song, S.J Lippard, *J. Am. Chem. Soc.,* 2005, **127**, 16004

61. R. March,W. Clegg, R.A. Coxall, L. Cucurull-Sánchez, L. Lezama, T. Rojo, P. González-Duarte, *Inorg. Chim. Acta.,* 2003, **353**, 129.

62. D. Onggo, F. Martak Ismunandar, B.M. Yamin, S.W. Ng, *Acta Crystallogr., Sect E,* 2006, **62**, m1112.

63. S. Kiani, A. Tapper, R. J. Staples, P. Stavropoulos, *J. Am. Chem. Soc.*, 2000, **122**, 7503.

64. E. Larsen, G.N. La Mar, B.E. Wagner, J.E. Parks, R.H. Holm, *Inorg. Chem.*, 1972, **11**, 2652

65. K.N. Raymond, T.J. McMurray, T.M. Garrett, *Pure & Appl. Chem.*, 1988, **60**, 545

66. D. Funkemeier, R. Mattes, *J. Chem. Soc., Dalton Trans.*, 1993, 1313

67. T.B. Karpishin, T.D.P. Stack, K.N. Raymond, *J. Am. Chem. Soc.*, 1993, **115**, 182.

68. G. Park, A.M. Przyborowska, N. Ye, N.M. Tsoupas, C.B. Bauer, G.A. Broker, R.D. Rogers, M.W. Brechbiel, R.P. Planalp, *Dalton Trans.*, 2003, 318;

69. A.A. Belal, P. Chaudhuri, I. Fallis, L.J. Farrugia, R. Hartung, N.M. Macdonald, B. Nuber, R.D. Peacock, J. Weiss, K. Wieghardt, *Inorg. Chem.*, 1991, **30**, 4397.

70. H. Al-Sagher, I. Fallis, L. J. Farrugia, R.D. Peacock, *Chem. Comm.,* 1993, 1499.

71. R.A.D. Wentworth, *Inorg. Chem.,* 1971, **10**, 2615.

Chapter Four

The synthesis of bis(2,2'-bipyrid-6-yl)ketone and tris(2,2'-bipyrid-6-yl)methanol derivatives

4.1 Introduction

Bipyridines are aromatic nitrogen heterocycles that form complexes with most transition metals.[1-3] This class of compounds contains six possible regioisomers, the most common of which is the bidentate chelate, 2,2'-bipyridine illustrated in Figure 4.1. Bipyridine ligands interact with metals via both σ-donating nitrogen atoms and π-accepting molecular orbitals.[4]

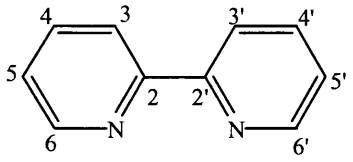

Figure 4.1 Molecular structure of 2,2'-bipyridine.[4]

Bipyridines[5] and symmetrically substituted derivatives[6,7] have traditionally been synthesised by a number of different routes, including the Ullmann reaction, which involves homo-coupling of a halopyridine in the presence of M^0 where M = copper or nickel. The process most often used for large-scale industrial manufacturing of bipy is Raney nickel coupling of simple pyridines.[8,9] While this Ni^0 catalyst can also be used with methyl pyridines (picolines) to form dimethyl-substituted bipyridines, the process is limited to simple, symmetric derivatives. More complex unsymmetrical derivatives have

been generated by reaction of pyridinium salts with α, β-unsaturated ketones followed by treatment with ammonium acetate to effect cyclisation of the second ring.[10]

Many functionalised bipy ligands can be synthesised from the appropriate alkyl precursors, which are most efficiently constructed using one of the coupling strategies. Simply joining appropriately functionalised pyridine halves via cross-coupling methods has generated countless derivatives. Some examples are given in Schemes 4.1 and 4.2.[11,12]

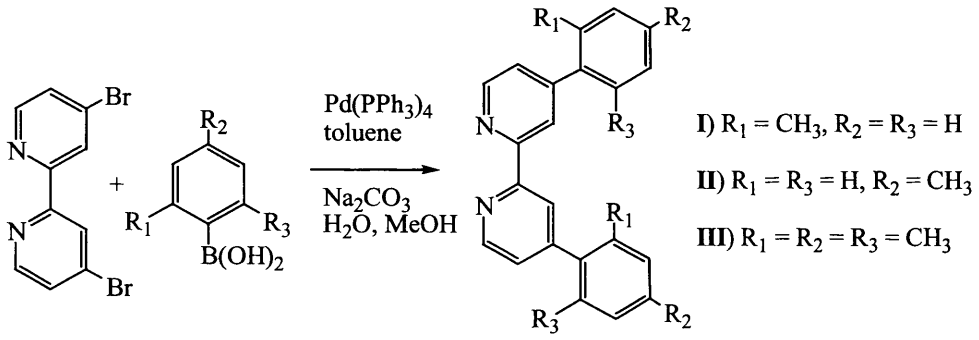

Scheme 4.1 Synthesis of 4,4'-di*o*-tolyl- (**I**), 4,4'-di*p*-tolyl- (**II**) and 4,4'-dimesityl-bipy (**III**) via a Suzuki coupling method.[11]

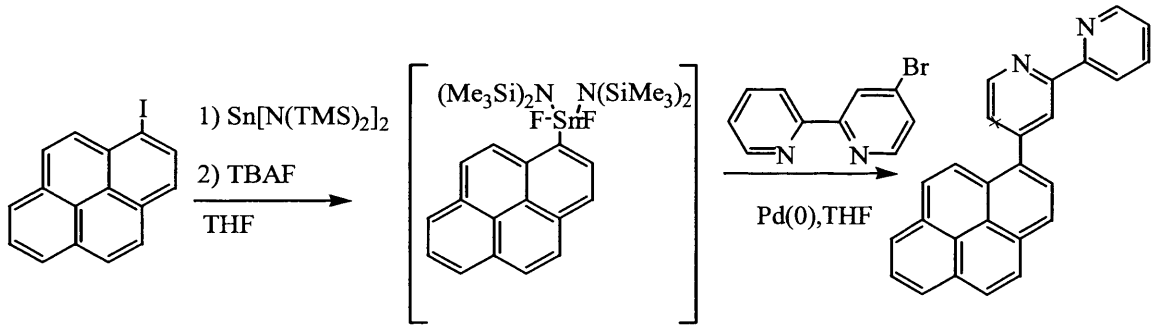

Scheme 4.2 Synthesis of pyrenyl-bipy.[12]

Bipyridines have been functionalised with a variety of macrocycles[13] including crown diethyl ethers,[14] porphyrins,[15] calixarenes[16] and cyclodextrin groups, as well as many others. There are other examples where bipy units are integrals to the macrocyclic

ring. These structures may have additional bipy groups[17] or other heteroatomic donors. They may be bound either at two positions on one bipy ring,[13] or contain two connected bipy ligands[18] and are capable of binding one or two or more metals.[19,20] One example of these macrocycles is comprised of two 4,4'-pyridinium units bound to two 2,2'-bipyridyl units. When synthesised in the presence of macrocyclic polydiethyl ethers, "intertwined" catenanes are formed (Figure 4.2, **V**).[21]

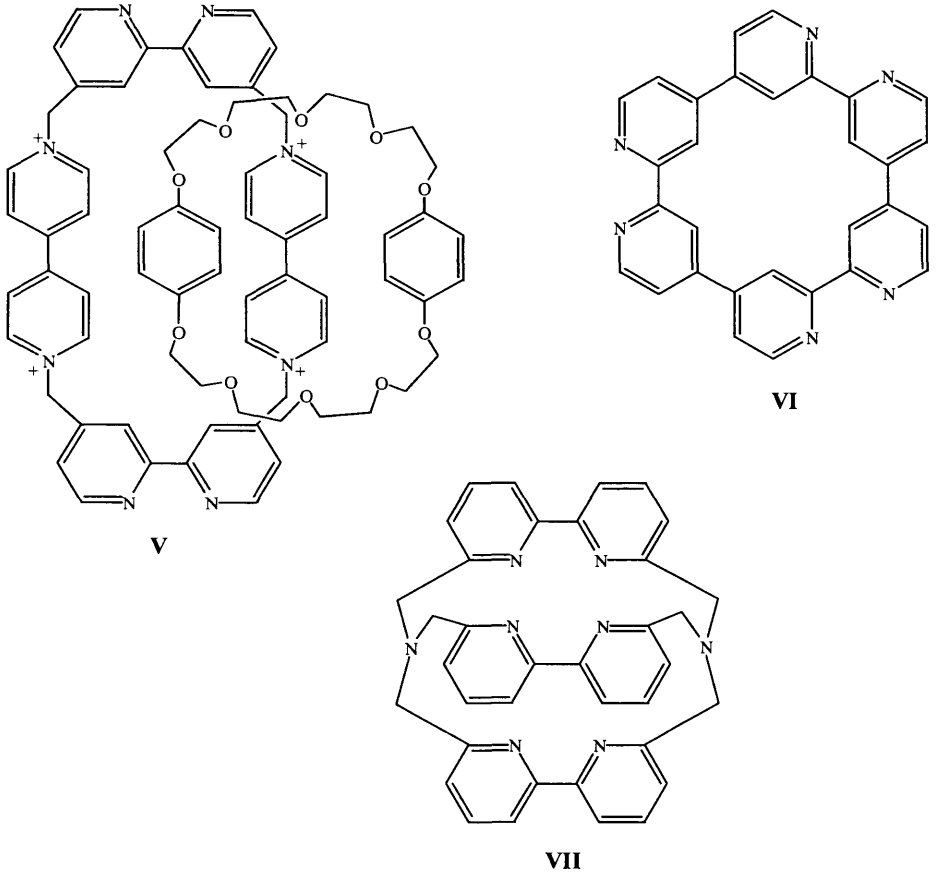

Figure 4.2 Molecular structures of **VI**, **VII** and **VII**.[21]

Cyclo-sexipyridines are another class of macrocycle and have been prepared with the nitrogen atoms directed either outwards,[22] (Figure 4.2, **VI**) or to the centre of the molecule

(endosexipyridine).[23] Cryptates can also be comprised of bipyridine ligands such as compound **VII** shown in Figure 4.2.[24]

4.1.1 Multidenate chelates

Bipyridines have been functionalised with additional coordinating groups to form numerous multidentate structures. Among these systems are bipyridines with additional pyridyl or bipyridyl[17] groups (terpyridine and higher oligopyridines), oxygen chelates (**VIII**),[25] sulphur groups (**IX**),[26] as well as cyclic (**X**) and higher order amines (**XI**) shown in Figure 4.3.[27]

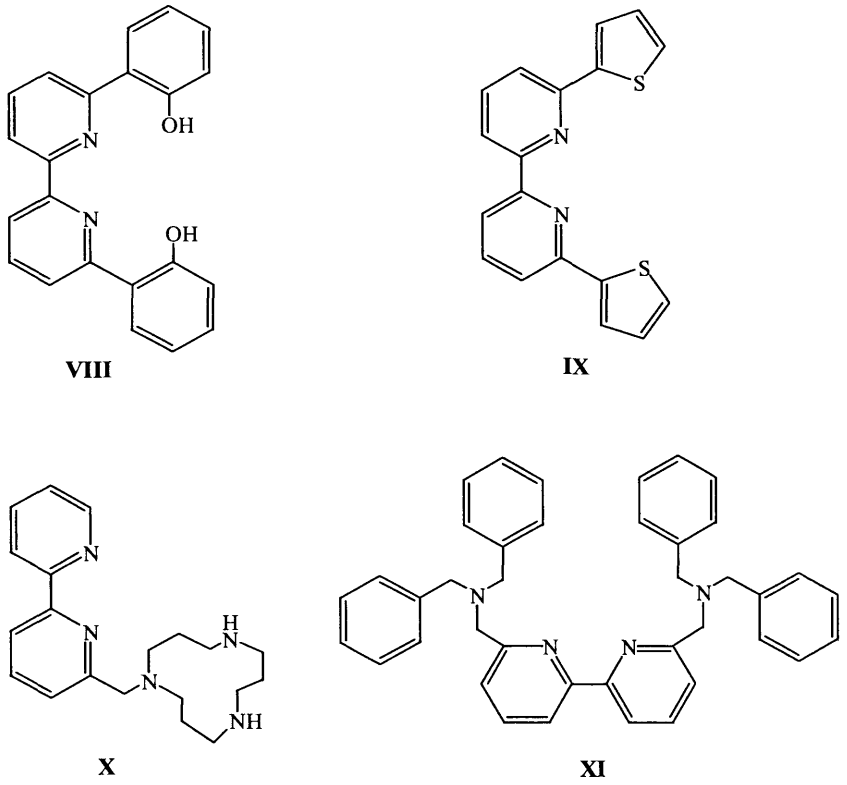

Figure 4.3 Examples of multidentate chelates containing bipyridines.[25-27]

4.2 Aims of the current research

Previous work by Leize *et al.* reported the synthesis of bis(2,2'-bipyrid-6-yl) ketone,[28] via a coupling reaction between bis(2-bromopyrid-6-yl)ketone and 2-tributylstannylpyridine in the presence of a palladium catalyst (Scheme 4.3).

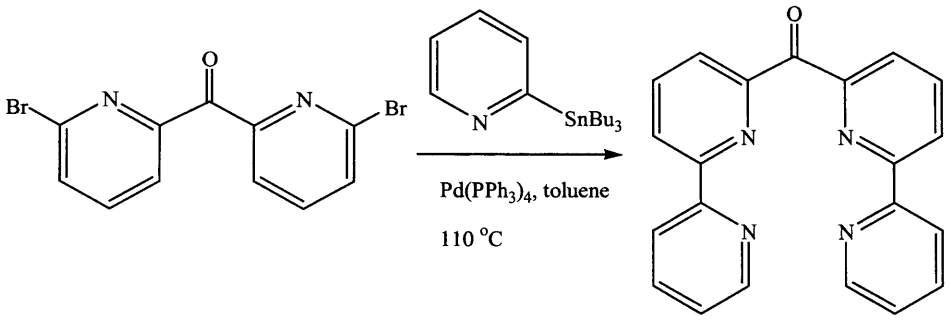

Scheme 4.3 Synthesis of bis(2,2'-bipyrid-6'-yl)ketone.[28]

This reaction initiated ideas to develop mixed pyridyl and bipyridyl tripodal donor ligands bridged by a tertiary alcohol group, similar to that seen in Chapter 2. Syntheses of the respective mono, bis and tris (2,2'-bipyrid-6-yl) methanol derivatives will be attempted. This may be accomplished by coupling 2-tributylstanylpyridine to the bromo pyridyl tripod ligands synthesised in Chapter 2 [see Experimental Section, Chapter 2 for preparation of compounds **8a-c**].

4.3 Results and discussion

4.3.1 Synthesis of bis(2,2'-bipyrid-6-yl)ketone, 22 (L^9)

Bis(2,2'-bipyrid-6-yl)ketone, **22** has recently been prepared by the group of Leize[28] (see Scheme 4.4), they complexed it to copper(II) in different solvents to produce a mixture of coordination polymers. Their synthetic procedure was followed to synthesise 2-tributylstannylpyridine, **21** (96%) and subsequently compound **22** (L^9) in reasonable yields (77%). The crude product of bis(2,2'-bipyrid-6-yl)ketone was purified by column chromatography using silica gel, the crude was eluted with a acetone / hexane mixture (2:5). This compound gave possible routes for the preparation of asymmetric bipy tripods, **23a**, **23b** and **23c** is shown in Scheme 4.4.

Bis(2,2'-bipyrid-6-yl)(6-bromopyrid-2-yl) methanol **23a** was synthesised by mono-lithiating 2,6-dibromopyridine in diethyl diethyl ether solution at –78 °C. To this orange solution one equivalent of bis(2,2'-bipyrid-6-yl)ketone **22** solution was added and further reacted for two hours at the same temperature. Once the reaction mixture was warmed to 0 °C it was quenched with 10% HCl and basified by 10% K_2CO_3 solution.

The ^1H NMR spectrum of this compound was difficult to interpret even after numerous attempts to purify the crude product of **23a** by column chromatography. The IR spectrum however demonstrated the loss of the ν_{CO} band at 1686 cm^{-1} corresponding to the ketone and the appearance of a broad ν_{OH} band of medium intensity at 3315 cm^{-1} indicating the loss of the pyridyl ketone **22** and the formation of a tertiary alcohol group. The ES+ mass spectrum of this compound confirmed the presence of the parent ion, $[M+H]^+$ (m/z = 496.2) suggesting the reaction was successful.

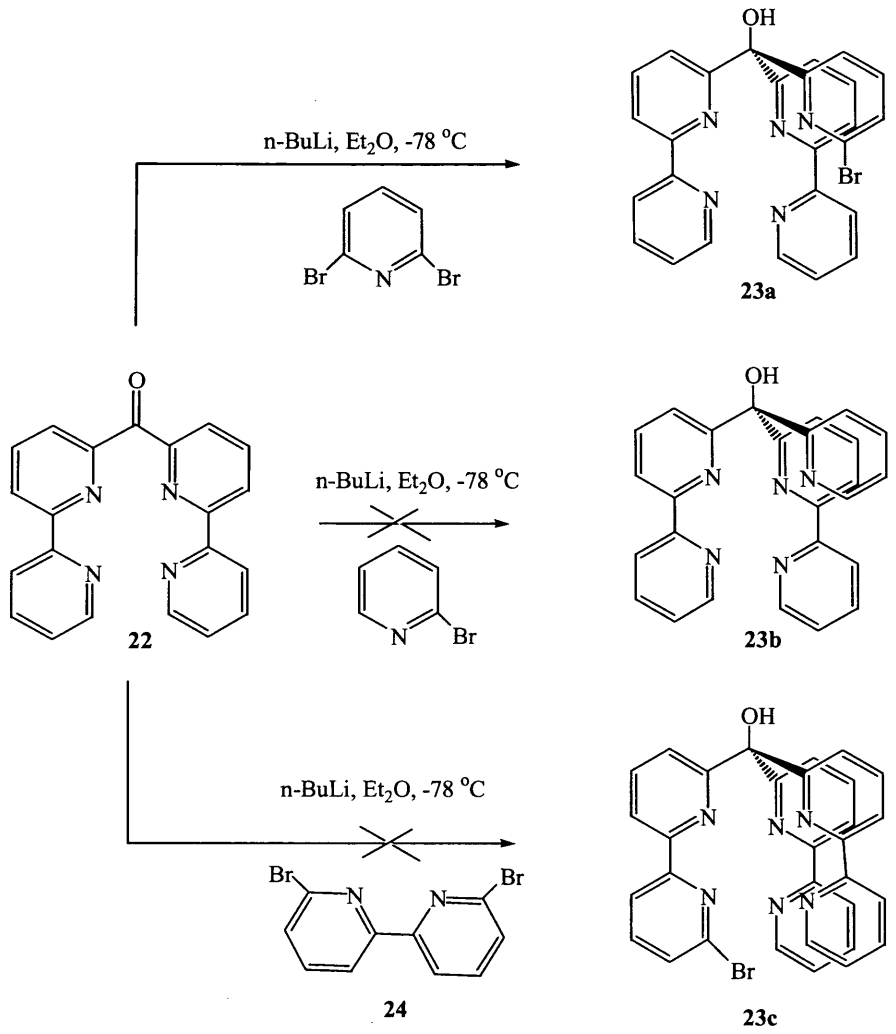

Scheme 4.4 Possible synthetic routes to asymmetric bipy tripods, **23a-c**.

Parallel to this, preparations of bis(2,2'-bipyrid-6-yl)(pyrid-2-yl)methanol, **23b** and bis(2,2'-bipyrid-6-yl)(6'-bromo-2,2'-bipyrid-6-yl)methanol, **23c** were also being investigated. These were attempted by following the same Experimental conditions as described above for ligand **23a**, instead the starting materials, 2-bromopyridine and 6,6'-dibromo-2,2'-bipyridine **24** was used and were mono-lithiated respectively. Attempts to purify the crude product of **23b** and **23c** by column chromatography (DCM / MeOH, 95:5) were also unsuccessful as indicated by their ^{1}H NMR spectra. Mixtures were

observed in the aromatic region between 7.20 – 8.60 *ppm*, the integrals could not be easily be distinguished due the product being impure however, the protons associated with the starting material **22** were detected in their spectra. Recrystallisation of crude material with methanol also proved to be unsuccessful. The IR and mass spectra also confirmed the presence of the starting material **22**, the characteristic ν_{CO} band at 1682 cm^{-1} (ketone) was present in the crude compounds. Thus the synthesis of **23b** and **23c** proved to be unsuccessful. Further work is required to explain the lack of reactivity.

4.3.2 The syntheses of mono, bis and tris(2,2'-bipyrid-6-yl)methanol derivatives ($L^{10\text{-}12}$)

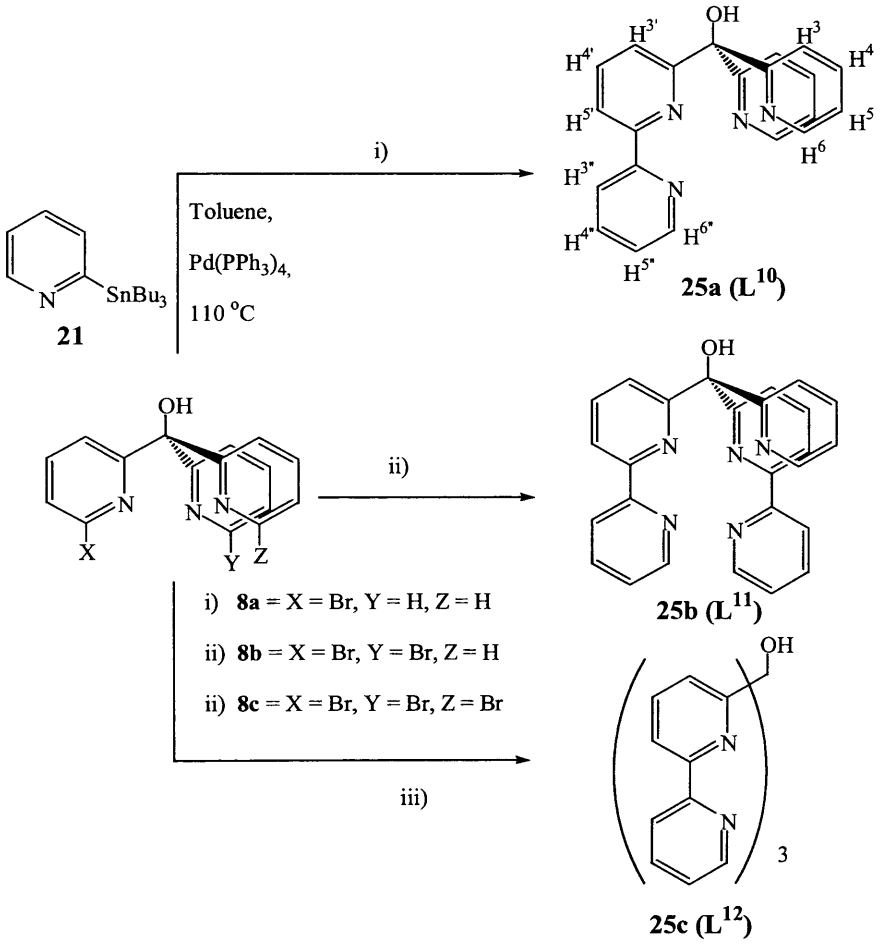

Scheme 4.5 Preparation of ligands **25a-c** ($L^{10\text{-}12}$).

An alternative route for the preparation of these bipy tripodal derivatives was investigated. Scheme 4.5 illustrates a series of synthetic routes for the preparation of ligands **25a-c**. The bromo derivatives, **8a-c** synthesised in Chapter 2 were again readily prepared here in reasonable yields. In turn, the respective bromo derivative was suspended in toluene and treated with an excess of 2-tributylstannylpyridine, **21** in the presence of the palladium catalyst ($Pd(PPh_3)_4$). After 24 hours at 110 °C the respective bipy derivatives were generated (**25a-c**). These were formed via a Stille coupling reaction, the mechanism of which is illustrated in Scheme 4.6. The crude products of (2,2'-bipyrid-6-yl)bis(pyrid-2-yl)methanol (**25a)** and bis(2,2'-bipyrid-6-yl)(pyrid-2-yl)methanol (**25b)** were purified by flash chromatography on silica gel. Initially the column was flushed with DCM / MeOH (99:1) to extract the excess starting material (**21)** and finally with MeOH (100%) to obtain the desired compounds, a white solid of **25a** was isolated (55%) and a light brown solid for **25b** (60%). The crude product of **25c** was acidified and extracted with DCM to remove unwanted starting material **21** and other impurities. The aqueous layer was then basified and extracted with DCM. Removal of the solvent under a vacuum gave the purified product, tris(2,2'-bipyrid-6-yl)methanol **25c** as a yellow solid (42%). These novel ligands were characterised using the following spectroscopic instrumentation; firstly, their ^1H NMR spectra were compared to their starting materials **8a-c**. It was noticed that the peaks in the aromatic region shifts to slightly higher frequencies, this is probably due to the replacement of the bromide group(s) by another pyridyl ring(s), an inductive effect is experienced by the protons being adjacent to a ring current. Comparisons of ^1H NMR spectra for ligands **25a-c** are displayed in Table 4.1; the bipyridyl protons can easily be distinguished from the pyridyl protons. Little could be

determined from the IR spectra as only the expected $\nu_{C\text{-}C/N}$ aromatic stretches belonging to the pyridyl rings and ν_{OH} broad band at 3300 cm^{-1} characteristic of tertiary alcohol groups were observed. The ES+ mass spectra were the most informative method for identifying these particular ligands, calculated accurate masses were obtained for **25a** and **25b**; m/z = 341.1964 and 418.2209 for the parent ion $[M+H]^+$. Accurate mass could not be obtained for **25c,** however the following mass to charge ratio was observed at 495.2 $[M+H]^+$ confirming its formation.

Ligand	Chemical shift (δ) in *ppm*										
($CDCl_3$)	H^3	H^4	H^5	H^6	$H^{3'}$	$H^{4'}$	$H^{5'}$	$H^{3''}$	$H^{4''}$	$H^{5''}$	$H^{6''}$
25a (L^{10})	7.70	7.70	7.20	8.48	7.70	7.70	7.12	8.10	8.28	7.70	8.60
25b (L^{11})	7.75	7.75	7.20	8.48	7.75	7.75	7.12	8.10	8.28	7.60	8.58
25c (L^{12})	—	—	—	—	7.82	7.82	7.15	8.12	8.30	7.60	8.59

Table 4.1 Comparison of ^1H NMR spectra of ligands, **25a-c**.

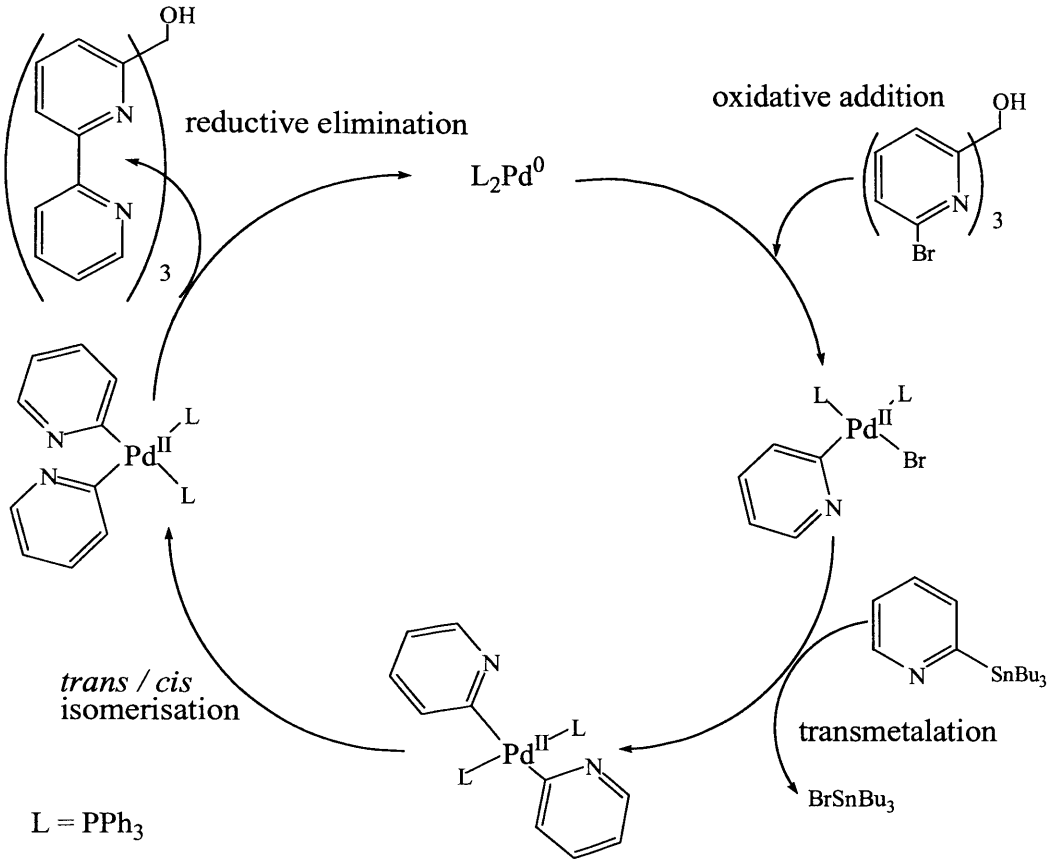

Scheme 4.6 Mechanism for a typical Stille coupling with tris(6-bromopyrid-2-yl)methanol and 2-tributylstannylpyridine.

4.3.3 Synthesis of (2,2'-bipyrid-6-yl)tetra(pyrid-2-yl)dimethanol derivatives

Previously, Rillema *et al.* developed an efficient route for the synthesis of 6,6'-dibromo-2,2'-bipyridine, **24**.[29] This method was utilised here to synthesise compound, **24** in good yield. The procedure involved the monolithiation of 2,6-dibromopyridine with *n*-BuLi in diethyl diethyl ether at –80 °C. After half an hour the solution was allowed to warm to –65 °C in order for complete solvation and then cooled to –90 °C prior to the addition of 0.5 molar equivalent of CuBr. After a further half hour of vigorous stirring at this temperature the mixture was warmed to – 70 °C and bubbled with a stream of dry

compressed air for 1 hour. Once the oxidation step was complete the solution was warmed to –20 °C. Water was added to the red solution to give a brown precipitate which was collected and washed with hexane / acetone (50:50) to yield a brown solid (72%). The spectroscopic data obtained could be compared with that published by Rillema[29] and confirms the successful synthesis of compound **24**. Thus, the synthetic routes shown in Scheme 4.7 were attempted in order to develop further desirable bipy derivatives (ligands **26-28**).

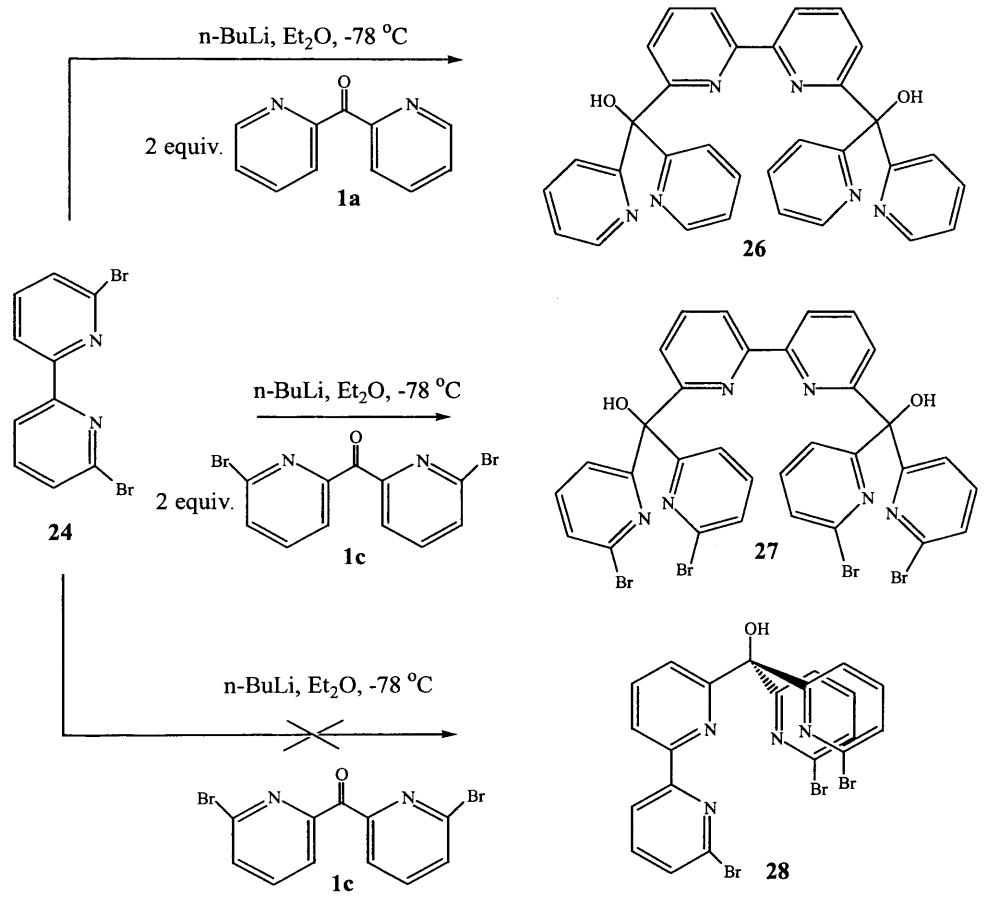

Scheme 4.7 Synthetic routes to **26** and **27**.

The same reaction conditions as for the synthesis of compound **23** was used; two molar equivalents of bis(2-pyridyl)ketone (**1a**) in THF solution was added to the dilithiate of compound **24** (in THF) to give the desired reaction product, (2,2'-bipyrid-6-yl) tetra(pyrid-2-yl)dimethanol, **26**. The IR spectrum confirmed the absence of the ν_{CO} band eliminating the presence of the ketone starting material. Also a broad ν_{OH} band at 3377 cm^{-1} indicates the presence of the tertiary alcohol group that is formed. ESMS data displayed a mass peak at 507, suggesting the fragmentation of the parent ion, $[M\text{-}OH_2]$.

In addition to this, the derivative (2,2'-bipyrid-6-yl)tetra(6-bromopyrid-2-yl)dimethanol, **27** was similarly synthesised. This was also prepared in the same manner as described above for ligand **26** except the precursor, bis(2-bromopyrid-6-yl) ketone (**1c**) was added to the dilithiate of **24**. Comparison of spectroscopic data for compounds **26** and **27** demonstrated close similarities as expected. No ν_{CO} peaks were observed in the IR spectrum once again indicating a successful reaction. The ESMS data gave mass peaks for the fragmentations of the parent ion, the main fragment being $[M\text{-}OH]^+$ for the loss of the tertiary alcohol group. The data obtained from the ^1H NMR spectra is illustrated in Table 4.2, it shows the four pyridyl rings are equivalent in both compounds and can easily be distinguished from the bipyridyl unit.

Ligand	Chemical shift (δ) in *ppm*							
($CDCl_3$)	-OH	$H^{3'}$	$H^{4'}$	$H^{5'}$	H^3	H^4	H^5	H^6
26	6.45	7.70	7.70	7.45	7.12	8.32	8.10	8.48
27	—	7.70	7.70	7.45	7.10	8.30	8.05	—

Table 4.2 Comparison of ^1H NMR spectra of ligands, **26** and **27**.

Attempts were also made to synthesise (6'-bromo-2,2'-bipyrid-6-yl)bis(6-bromopyrid-2-yl)methanol, **28** by reacting one equivalent of bis(2-bromopyrid-6-yl)ketone **1c** to the mono-lithiate of **24**. It was clear from the spectroscopic analyses that this reaction was unsuccessful; the data obtained were the same as for compound **27** suggesting its formation. A possible explanation for this may be the inability for compound **24** to selectively lithiate.

4.4 Conclusions and suggestions for further research

The successful synthesis of bis(2,2'-bipyrid-6-yl)ketone **22** initiated further investigations into the development of a series of novel 2,2'-bipy tripodal derivatives. Initially the syntheses of ligands **23a-c** were attempted via lithiated intermediates. Using this route only compound **23a**, bis(2,2'-bipyrid-6-yl)(6-bromopyrid-2-yl) methanol could be synthesised and was characterised by various spectroscopic analyses. The other two derivatives (**23b** and **23c**) required further investigations to explain their unsuccessful reactions. Consequently, an alternative route for the synthesis of mono, bis and tris bipy tripods was developed. This involved the Stille coupling of 2-tributylstannylpyridine (**21**) with the respective bromo tripod derivatives **13a-c** to give the desired mono, bis and tris(bipy) methanol derivatives, **25a-c** in good yields. Further studies involved the preparation of (mono(bipy) bis(pyrid-2-yl) methanol)$_2$ ligands **26** and **27** through the dilithiation of 6,6'-dibromo-2,2'-bipyridine, **24** and the subsequent addition of the relevant pyridyl ketone (**2c** and **2a** respectively). It was evident from their spectroscopic analyses that these reactions were successful. The (6-bromo-2,2'-bipyridine) bis(pyrid-2-yl) methanol **28** was prepared by the mono-lithiating compound **24** but proved to be

unsuccessful. Spectroscopic data showed that ligand **27** was synthesised instead, restricting compound **24** to dilithiation.

The successful preparation of these bipy tripodal derivatives provides the opportunity to explore their coordination chemistries with transition metals. It may also prove interesting to synthesise the bromo bipy tripodal derivatives and apply the chemistry from Chapter 2 to such systems, examples of such routes are shown in Schemes 4.9 and 4.10.

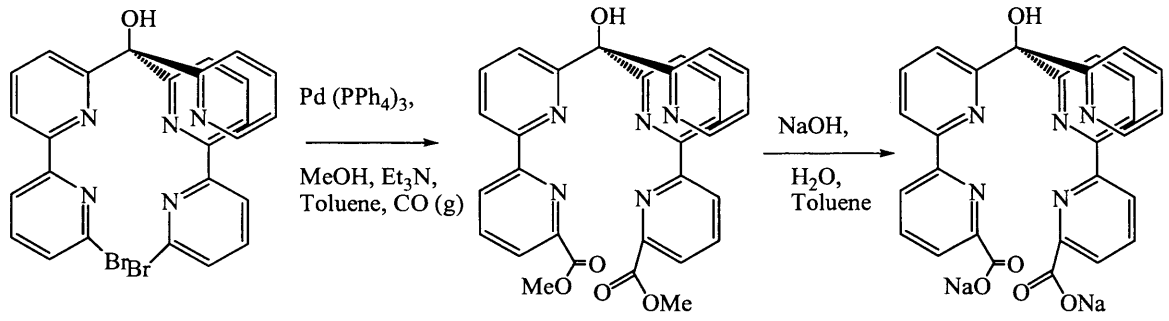

Scheme 4.9 A possible synthetic route to bis(bipy acid)-mono(pyridyl) methanol derivative.

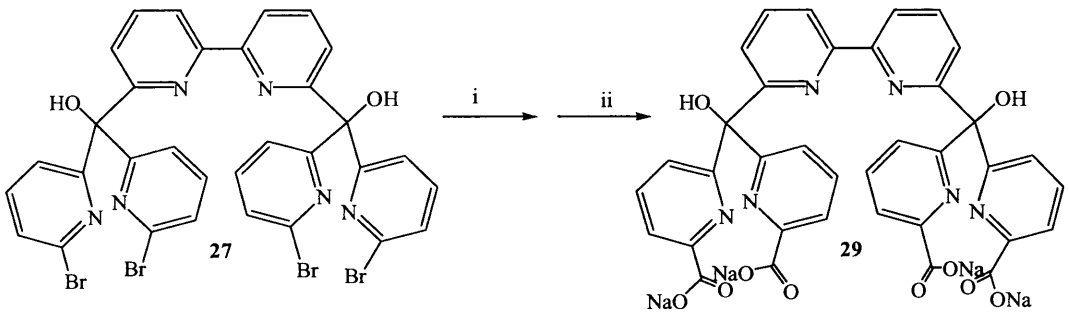

Scheme 4.10 A possible synthetic route to [mono(bipy)-bis(pyridyl acid) methanol]$_2$ derivative. Key: i) MeOH, N_3Et, toluene, $Pd(TPP)_4$, $CO_{(g)}$, 100°C ii) NaOH, toluene, reflux.

4.5 Experimental

4.5.1 Instrumentation

NMR spectra were recorded on a Bruker DPX 400 spectrometer at 400 (^{1}H) and 100.7 MHz (^{13}C), respectively, and the spectra were referenced to the residual solvent peak. Coupling constants, *J*, are in Hertz. Infrared absorptions were recorded on a Perkin-Elmer 1600 series FTIR spectrometer in KBr or a Jasco FT / IR-660 Plus. The national mass spectrometry service centre at the University of Wales, Swansea sponsored by EPSRC performed Mass spectrometry.

4.5.2 Synthesis of bis (2,2'-bipyrid-6-yl) ketone (L^9)

Preparation of 2-Tributylstannylpyridine,[28] **21**

A 1.6M solution of *n*-butyl lithium in hexane (39.2 ml, 0.062mol) was slowly added to a solution of 2-bromopyridine (6 ml, 0.062mol) in THF (120ml) cooled to –78 °C under argon. After 30 min, Bu_3SnCl (16.8 ml, 0.062mol) was added to give a dark solution, which was stirred at –78 °C for a further one hour. The solution was allowed to warm to room temperature and a saturated aqueous solution of NH_4Cl (60ml) was added. The aqueous phase was extracted with diethyl ether (3 x 100ml) and dried with Na_2SO_4 (s). The solution was filtered and solvent was removed under pressure to give the crude product, a yellow oil (22.1g, 96%). ^{1}H NMR ($CDCl_3$); δ 0.85 (t, 9H, J = 7.3 Hz, CH_3), 1.70-1.05 (m, 18H, CH_2), 7.10 (dd, 1H, J = 6.9, 1.7 Hz, H^4), 7.39 (d, 1H, J = 7.4 Hz, H^3), 7.48 (dd, 1H, J = 7.4, 1.8 Hz, H^5), 8.73 (d, 1H, J = 4.8, Hz, H^6); IR KBr/cm^{-1}: ν = 1686s, 1581s, 1430m, 1320s, 1258m, 1097m, 992s, 752m, 667m; ESMS: *m/z* (%) 367.1.

Preparation of bis(2,2'-bipyrid-6-yl)ketone,[28] **22** (L^9)

Toluene (20ml) was added to **21** (2.15g, 5.48mmol), bis(6-bromo-2-pyridyl) ketone (chapt. 2, **2a**, 0.50g, 1.46mmol) and tetrakis(triphenlphosphane) palladium catalyst ($Pd(PPh_3)_4$) (0.34g, 20% w/w). The resulting mixture was stirred at 110 °C under argon for 24 hours. The solution was cooled and toluene was evaporated. The residue was chromatographed on silica gel and eluted with acetone / hexane (20:50). The pale yellow solid was washed with hexane to afford a white solid (77%). ^{1}H NMR ($CDCl_3$); δ 7.30 (dd, 2H, J = 7.5, 4.8 Hz, $H^{5''}$), 7.65 (dd, 2H, J = 7.7, 4.8 Hz, $H^{4''}$), 8.04 (t, 2H, J = 7.7 Hz, $H^{5'}$), 8.16 (dd, 2H, J = 7.6, 1.3 Hz, $H^{4'}$), 8.29 (d, 2H, J = 7.8 Hz, $H^{6''}$), 8.62 (d, 2H, J = 7.6 Hz, $H^{3'}$), 8.68 (dd, 2H, J = 7.8, 1.3 Hz, $H^{3''}$). ^{13}C NMR ($CDCl_3$): δ 121, 123, 124, 125, 136, 137, 144, 149, 154, 193; IR KBr/cm^{-1}: ν = 1686s, 1581s, 1430m, 1320s, 1258m, 1097m, 992s, 752m, 667m. FAB-MS: *m/z* (%) 339.1 (100) [M + 1], 155 (7) [M-183 (bipy)].

Synthesis of bis(2,2'-bipyrid-6-yl)(6-bromopyrid-2-yl)methanol **23a**

Under argon, dry diethyl diethyl ether (50ml) was added to 2,6-dibromopyridine (1.33 mmol). The solution was cooled to –78 °C using a dry ice and acetone bath. To this slurry, n-butyl lithium (1.33 mmol) was added slowly. After 5 minutes, a solution of **22** (1.33 mmol) in THF (30ml) was transferred to the reaction flask. The mixture was allowed to react at this temperature for a further 2 hours. The reaction was allowed to warm up to 0°C, then quenched with 10% HCl until acidic. The resulting mixture was basified with 10% aqueous K_2CO_3 and the crude product was partitioned between $CHCl_3$ and water. The aqueous layer was washed twice with $CHCl_3$ (60 ml) and the organic layers were

combined and dried with anhydrous $MgSO_4$. The resulting brown solution was evaporated under a reduced pressure. The crude product was chromatographed on silica gel and eluted with DCM / MeOH (95:5) to give a brown oily product (56%). ^1H NMR ($CDCl_3$); δ 7.10 – 7.40 (m, 7H), 7.50-8.00 (m, 10H); IR KBr/cm^{-1}: ν =3315m, 1580s, 1571s, 1452m, 1429s, 1395m, 1270w, 1068m, 991m, 774s, 739m; ESMS: *m/z*; 496.2 $[M+H]^+$.

Preparation of 6,6'-dibromo-2,2'-bipyridine,[29] **24**

Under argon, dry diethyl diethyl ether (100ml) was added to 2,6-dibromopyridine (0.042mol). The resulting solution was cooled to –80 °C, to which n-butyl lithium (0.042mol) was slowly added over an hour. The orange suspension was allowed to stir at –80 °C for another ½ hour and then allowed to warm to –65 °C to allow complete solvation of the suspension. The solution was again cooled to –90 °C and CuBr (0.021mol) was added at once with vigorous stirring. The yellow suspension was held at –85 °C for ½ hour and then warmed to –70 °C and stirred for a further ½ hr. Dry compressed air was bubbled through the reaction suspension for 1 hr. The reaction temperature did not exceed –60 °C during the oxidation step. The reaction was warmed to –20 °C and H_2O (~30ml) was added. A red coloured solution became brown and allowed to stir at room temp. The brown solid was filtered and the filtrate was concentrated to half its volume, the remaining solid left in the filtrate was filtered. The crude solid was washed with hexane / acetone (50:50) to yield a brown solid (72%). ^1H NMR ($CDCl_3$); δ 7.50(d, 2H, J = 7.8 Hz, H^5), 7.67 (t, 2H, J = 7.8 Hz, H^4), 8.38 (d, 2H, J = 7.5 Hz, H^3); ^{13}C NMR ($CDCl_3$): δ 120, 128, 140, 141, 155; IR KBr/cm^{-1}: ν = 3292m, 1583s, 1564s, 1460m, 1425s, 1395m, 1266w, 1060m, 993m, 774s, 738m; EIMS *m/z*; 311.8892.

4.5.3 Synthesis of mono, bis and tris(2,2'-bipyrid-6-yl)methanol derivatives ($L^{10\text{-}12}$)

The Experimental conditions used for the preparation of ligand **22** was used here also:

Preparation of (2,2'-bipyrid-6-yl)bis(pyrid-2-yl) methanol **25a** (L^{10})

The starting material, mono(6-bromopyrid-2-yl) bis(pyrid-2-yl)methanol (for preparation see Chapter 2 compound **8a**, 1.209g, 3.54mmol) was used instead of the di(2-brompyrid-6-yl)ketone. This was mixed to diethyl ether with 2-tributylstannylpyridine **21** (2.86g, 7.08mmol) and $Pd(PPh_3)_4$ (0.82g, 20% w/w) in toluene (40ml). The crude product (0.95g, 75%) was chromatographed on silica gel and eluted firstly with CH_3OH / DCM (1:99) to extract the excess starting material **21** and finally flushed with CH_3OH (100%). Evaporation of CH_3OH fractions yielded a white solid (0.55g, 55%). ^1H NMR ($CDCl_3$); δ 7.12 (dd, 1H, J = 7.6, 3.0 Hz, $H^{5'}$), 7.20 (dd, 2H, J = 7.8, 4.8 Hz, H^5), 7.70 (m, 7H, H^{3+4}, $H^{3'+4'}$, $H^{5''}$), 8.10 (dd, 1H, J = 7.4, 3.2 Hz, $H^{3''}$), 8.28 (dd, 1H, J = 6.9, 5.4 Hz, $H^{4''}$), 8.48 (d, 2H, J = 7.8 Hz, H^6), 8.60 (d, 1H, J = 7.0 Hz, $H^{6''}$). ^{13}C NMR ($CDCl_3$): δ 84, 119, 121, 122, 123, 130, 134, 136, 149, 150, 154, 159, 161 (N.B. three absent carbons). IR KBr/cm^{-1}: ν = 3290m, 1581s, 1565s, 1458m, 1429s, 1394m, 1268w, 1059m, 993m, 774s, 738m. ESMS: *m/z*; 341.1964 $[M+H]^+$

Preparation of bis(2,2'-bipyrid-6-yl)(pyrid-2-yl) methanol **25b** (L^{11})

The following compounds, bis(6-bromopyrid-2-yl)mono(pyrid-2-yl) methanol (for preparation see Chapter 2 compound **8b**, 1g, 2.4mmol), **21** (3.84g, 9.51mmol) and $Pd(PPh_3)_4$ (0.55g, 20% w/w) in toluene (40ml) were reacted in the same manner as seen for compound 22. The crude product obtained (0.90g, 75%) was chromatographed on silica gel and again eluted with MeOH / DCM (1:99) to extract the excess starting

material, **21** and flushed with MeOH (100%) to yield a light brown solid (60%). ^{1}H NMR ($CDCl_3$); δ 7.12(dd, 2H, J = 7.6, 1.6 Hz, $H^{5'}$), 7.20(dd, 1H, J = 7.7, 5.7 Hz, H^{5}), 7.60 (t, 2H, J = 7.7 Hz, $H^{5''}$), 7.75 (m, 6H, H^{3+4}, $H^{3'+4'}$), 8.10 (dd, 2H, J = 7.7, 2.8 Hz, $H^{3''}$), 8.28 (dd, 2H, J = 7.5, 6.0 Hz, $H^{4''}$), 8.48 (d, 1H, J = 7.5 Hz, H^{6}), 8.58 (d, 2H, J = 6.5 Hz, $H^{6''}$); ^{13}C NMR ($CDCl_3$): δ 85, 119, 120, 121, 122, 123, 130, 134, 136, 149, 150, 154, 159, 161 (N.B. three absent carbons); IR KBr/cm^{-1}: ν =3310m, 1583s, 1569s, 1455m, 1431s, 1398m, 1271w, 1064m, 989m, 777s, 741m; ESMS: *m/z* ; 418.2209 $[M+H]^+$

Preparation of tris(2,2'-bipyrid-6-yl)methanol **25c** (L^{12})

Again the same procedure as for the synthesis of ligand **22** was used here, tris(6-bromopyrid-2-yl)methanol (for preparation see Chapter 2 compound **8c**, 1.08g, 2.16mmol), **21** (5.23g, 0.013mol) and $Pd(PPh_3)_4$ (0.46g, 20% w/w) in toluene (40ml) were reacted togdiethyl ether. The crude product obtained from the work up (0.86g, 81%) was acidified with 10% HCl and extracted with DCM (10ml x 2). The aqueous layer was then basified with 10% K_2CO_3 and extracted with DCM (20ml x 2). The organic layer was dried ($MgSO_4$) and evaporated under a reduced pressure. A yellow solid was obtained (0.449g, 42%). ^{1}H NMR ($CDCl_3$); δ 7.15 (dd, 3H, J = 7.8, 4.8 Hz, $H^{5'}$), 7.60 (dd, 3H, J = 7.5, 7.2 Hz, $H^{5''}$), 7.82 (m, 6H, $H^{3'+4'}$), 8.12 (dd, 3H, J = 7.0, 3.1 Hz, $H^{3''}$), 8.30 (t, 3H, J = 7.5 Hz, $H^{4''}$), 8.59 (d, 3H, J =7.2 Hz, $H^{6''}$); ^{13}C NMR ($CDCl_3$): δ 80, 119, 120, 121, 122, 137, 150, 154, 159 (N.B. two absent carbons). IR KBr/cm^{-1}: ν =3322m, 1580s, 1559s, 1453m, 1429s, 1261m, 1147w, 1060w, 991m, 824w, 766s, 678m; ESMS: *m/z*; 495.2 $[M+H]^+$.

4.5.4 Synthesis (2,2'-bipyrid-6-yl)tetra(pyrid-2-yl)dimethanol derivatives

Preparation of **26** *and* **27**

Under argon, 1.6M solution of *n*-butyl lithium in hexane (1.55 mmol) was slowly added to a THF solution of 6,6'-dibromo-2,2'-bipyridine, **24** (0.77 mmol, 50 ml) that had been cooled to –78 °C. After 5 min, bis(2-pyridyl) ketone (**2c**, from Chapter 2, 1.55 mmol N.B. **2a** was used for synthesis of **27**) suspended in THF (20ml) was added to the lithiate and stirred at –78 °C for two hours. The solution was allowed to warm to 0 °C and then quenched with 10% HCl until it became acidic. The resulting mixture was basified with 10% aqueous K_2CO_3 and the crude product was partitioned between DCM and water. The aqueous layer was washed twice with DCM (60 ml) and the organic layers were combined and dried with anhydrous $MgSO_4$. The resulting brown solution was evaporated under a reduced pressure to yield a brown solid (**26** =83%, **27** =75%).

Spectroscopic data for (2,2'-bipyrid-6-yl)tetra(pyrid-2-yl)dimethanol **26**

^{1}H NMR ($CDCl_3$); δ 6.45 (bs, 2H, -O**H**), 7.10 (d, 4H, J = 7.5 Hz, H^3), 7.45 (t, 2H, J = 7.8 Hz, $H^{5'}$), 7.70 (d, 4H, J = 7.7 Hz, $H^{3'+4'}$), 8.05 (t, 4H, J = 7.6 Hz, H^5), 8.30 (dd, 4H, J = 7.7, 6.9 Hz, H^4), 8.48 (d, 4H, J = 7.0 Hz, H^6); ^{13}C NMR ($CDCl_3$): δ 84, 119, 120, 121, 123, 136, 137, 149, 151, 154, 159; IR KBr/cm^{-1}: ν = 3378m, 1685m, 1580s, 1425s, 1400m, 1261s, 1155m, 1123s, 984m, 824w; MS:*m/z*; 507 [M-OH-H$^+$].

Spectroscopic data for (2,2'-bipyrid-6-yl)tetra(6-bromopyrid-2-yl)dimethanol **27**

^{1}H NMR ($CDCl_3$); δ 7.12 (d, 4H, J = 7.3 Hz, H^3), 7.45 (t, 2H, J = 7.7 Hz, $H^{5'}$), 7.7 (m, 4H, $H^{3'+4'}$), 8.10 (t, 4H, J = 7.4, 1,8 Hz, H^5), 8.32 (d, 4H, J = 7.3 Hz H^4); ^{13}C NMR ($CDCl_3$): δ 86, 119, 120, 121, 123, 125, 137, 142, 149, 154, 161; IR KBr/cm^{-1}: ν = 3378m, 1685m, 1580s, 1425s, 1400m, 1261s, 1155m, 1123s, 984m, 824w; MS:*m/z*; 824 [M-OH].

Attempted synthesis of (6'-bromo2,2'-bipyrid-6-yl)bis(6-bromopyrid-2-yl)methanol **28**

The same procedure was used as described above except one equivalent of n-BuLi was added to compound **24**. One equivalent of bis(6-bromo-2-pyridyl) ketone solution was added to this mono-lithiate intermediate and treated in the same manner as above. The brown solid obtained had the same spectroscopic data as compound **27**. The reaction was therefore unsuccessful.

4.6 References

1. T.J. Meyer, *Pure Appl. Chem.* 1986, **58**, 1193.
2. A. Juris, V. Balzani, F. Barigelletti, S. Campagna, P.Belser, A. Von Zelewsky, *Coord. Chem. Rev.* 1988, **84**, 85.
3. E.C. Constable, *Adv. Inorg. Chem.* 1989, **34**, 1.
4. L.F. Lindoy, L.E. Livingstone, *Coord. Chem. Rev.* 1967, **2**, 173.
5. F.H. Burstall, *J. Chem. Soc.* 1938, 1662.
6. F.H. Case, T.J. Kasper, *J. Am. Chem. Soc.* 1956, **78**, 5842.
7. J.A.H. MacBride, P.M. Wright, B.J. Wakefield, *Tetrahedron Lett.* 1981, **22**, 4545.
8. W.H.F. Sasse, *Org. Synth.* 1966, **46**, 5.
9. G.M. Badger, W.H.F. Sasse, *Adv. Heterocycl. Chem.*. 1963, **2**, 179.
10. F. Krohnke, *Synthesis* 1976, 1.
11. N.H. Damrauer, T.R. Boussie, M. Devenney, J.K. McCusker, *J. Am. Chem. Soc.* 1997, **119**, 8253.
12. A.L. Rodriguez, G. Peron, C. Duprat, M. Vallier, E. Fouquet, F. Fages, *Tetrahedron Lett.* 1998, **39**, 1179.
13. A.G.M. Barrett, D. Hamprecht, R.A. James, M. Ohkubo, P.A. Procopiou, M.A. Toledo, A.J.P. White, D.J. Williams, *J. Org. Chem.* 2001, **66**, 2187.
14. O. Kocian, R.J. Mortimer, P.D. Beer, *J. Chem. Soc. Perkin Trans. 1* 1990, 3203.
15. J.-C. Chambron, V. Heitz, J.-P. Sauvage, J.-L. Pierre, D. Zurita, *Tetrahedron Lett.* 1995, **36**, 9321.
16. P. D. Beer, *Chem. Commun.*, 1996, 689

17. C. Kaes, A. Katz, M.W. Hosseini, *Chem. Rev.* 2000, 3553.

18. H. Durr, H. Kilburg, S. Bossmann, *Synthesis* 1990, 773

19. C. Kaes, M.W. Hosseini, A. De Cian, J. Fischer, *Tetrahedron Lett.* 1997, **38**, 3901.

20. C. Kaes, M.W. Hosseini, A. De Cian, J. Fischer, *Tetrahedron Lett.* 1997, **38**, 4389.

21. P.R. Ashton, V. Balzani, A. Credi, O. Kocian, D. Pasini, L. Prodi, N. Spencer, J.F. Stoddart, M.S. Tolley, M. Venturi, A.J.P. White, D.J. Williams, *Chem. Eur. J.* 1998, **4**, 590.

22. T.R. Kelly, Y.-J. Lee, R.J. Mears, *J. Org. Chem.* 1997, **62**, 2774.

23. G.R. Newkome, H.-W. Lee, *J. Am. Chem. Soc.* 1983, **105**, 5956.

24. N. Sabbatini, M. Guardigli, J.-M. Lehn, *Coord. Chem. Rev.* 1993, **123**, 201.

25. M. Albrecht, C. Ridiethyl ether, *Synlett.,* 1995, 309.

26. G. Nocentini, A. Barzi, *Gen. Pharmacol.* 1997, **29**, 701.

27. N.W. Alcock, F. McLaren, P. Moore, G.A. Pike, S.M. Roe, *J. Chem. Soc. Chem. Commun.* 1989, 629.

28. H. Nierengarten, J. Rojo, E. Leize, J.-M. Lehn, A.V. Dorsselaer, *Eur. J. Inorg. Chem.* 2002, 573.

29. J.E. Parks, B.E. Wanger, R.H.J. Holm, *J. Organomet. Chem.* 1973, **56**, 53.

30. F.H. Case, *J. Org. Chem.,* 1966, **31**, 2398.

31. G.R. Newkome, H.C. Taylor, *J. Org. Chem.* 1979, **44**, 1362.

32. N. Furukawa, T. Kawai, *Tetrahedron Lett.,* 1984, **25**, 2549.

33. T. Garber, D.P. Rillema, *Synth. Commun.* 1990, **20**, 1233.

Chapter Five

Transition Metal Complexes of Ligands, L^9 - L^{12}

5.1 Introduction

The bipyridyl (bipy) ligand is one of the most intensively studied class of chelating ligands. Reviews of the coordinating properties of this ligand and its derivatives have been available for the last 40 years.[1-5] The most common coordination species seen is the octahedral cation $[M(bipy)_3]^{n+}$ (Figure 5.1), these are very stable and often kinetically inert (especially with d^3 and d^6 low-spin metal ions). With Fe^{2+}, low-spin species are observed,[4] and with *cis*-octahedral species $[Fe(bipy)_2(NCS)_2]$, high-spin to low-spin transitions may be observed upon cooling.[6]

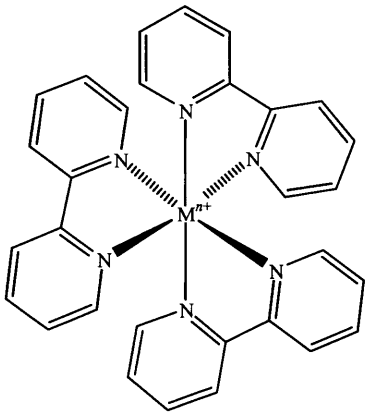

Figure 5.1 Representation of the cation $[M(bipy)_3]^{n+}$.

During recent years, interest in the bipy compounds has been renewed because of their interesting redox and photoredox properties,[7] with particular attention being given to the ruthenium compounds.[8] In the case of Cu^I compounds of this ligand, many systems have been shown to have strong antimicrobial effects.[9]

Apart from the above mentioned interest in *cis*-octahedral species $[M(bipy)_2(anion)_2]$ from the point of view of high-spin to low-spin transitions,[6] this geometry is also of interest for the formation of reactive species, leading to, for example, dinuclear species with catalytic properties, such as the cobalt-peroxo compound shown in Figure 5.2. This compound is active in oxidative phenol coupling.[10] With Cu^{II} the stoichiometry $Cu(bipy)_2X_2$ results in a variety of five-coordinate and distorted six-coordinate structures.[11]

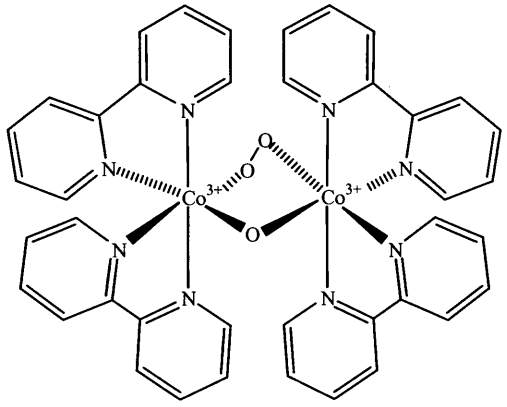

Figure 5.2 Dinuclear Co^{III} species with bipy ligands and with peroxo and hydroxo bridge.[10]

Dinucleating systems with ligands of the bipy type are also known. Provided that the different units of bipy are connected in a suitable way, dinuclear compounds such as **I** shown in Figure 5.3 may be obtained. With certain ligands of sufficient size, however, tetracoordinate mononuclear species **II** may also be formed, an example of which is shown in Figure 5.3.[12]

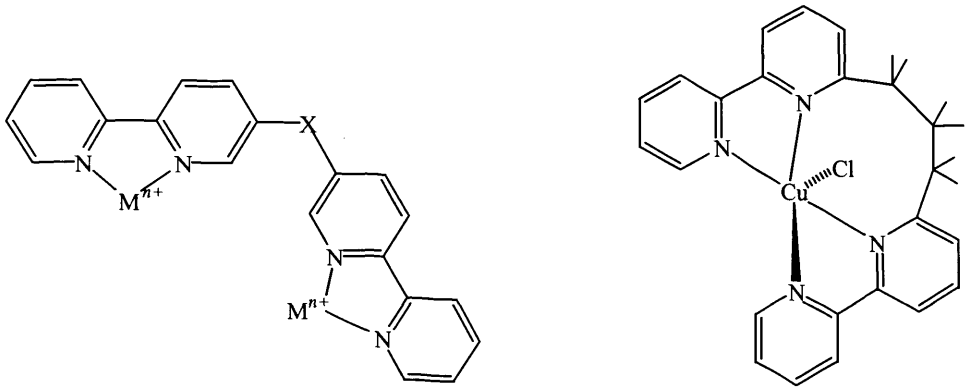

I **II**

Figure 5.3 Structure of a dinuclear bis(bipy) compound (**I**), and of a mononuclear bis(bipy) chelate with a five-coordinate Cu^{II} (**II**).[12]

5.2 Aims of the current research

In this Chapter the coordination chemistries of the bipyridyl derivatives synthesised in Chapter 4 L^9-L^{12} will be investigated. Complexes of these ligands with some first row transition metal ions, Cu, Ni, Zn and Fe will be explored. Another attraction is the changes that may be observed when the steric and electronic demands of d^6, d^8, d^9 and d^{10} metal centres (e.g. Fe^{II}, Ni^{II}, Cu^{II} and Zn^{II}) are imposed upon these ligands. The structural and electronic properties of complexes with a 1:1 ligand to metal stochiometry will be described.

In addition, it was decided to perform electrochemical (cyclic voltammetry) investigations on the complexes to observe their oxidation and reduction abilities and compare them to similar complexes seen in previous literature. Other spectroscopic analyses involve nuclear magnetic resonance, ultra-violet and infrared spectroscopy and mass spectrometry.

5.3 Results and Discussion

5.3.1 Complexation to divalent copper, nickel, zinc and iron

The ligands synthesised in Chapter 4 are shown in Figure 5.4. These were complexed to Cu, Ni, Zn and Fe.

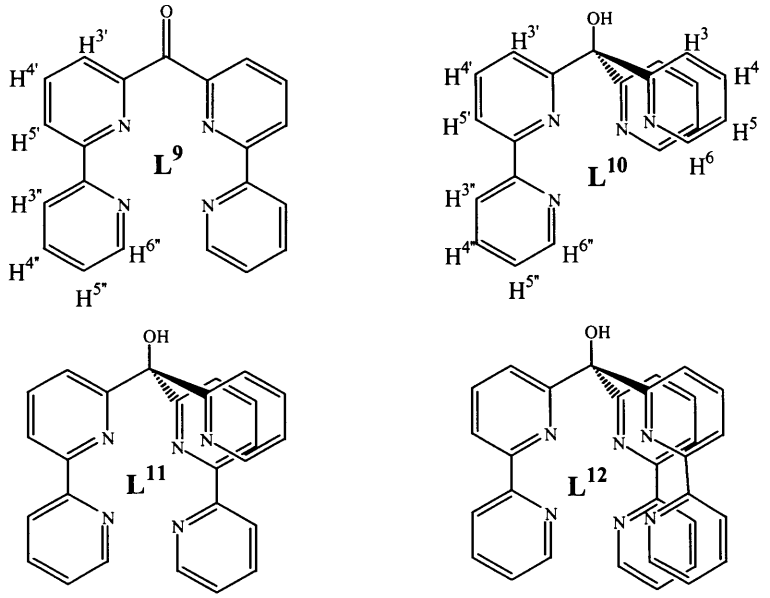

Figure 5.4 Labelling of ligands synthesised in Chapter 4. (L^9 and L^{10} show labelled protons).

The complexes were prepared using the same Experimental conditions as seen in Chapter 3. One molar equivalent of $M(ClO_4)_2$ solution (~1ml of water) was added drop wise to a stirred methanolic ligand (L^X, ~2ml) solution.

$$L^X + M(ClO_4)_2 \xrightarrow{MeOH/H_2O} [M(L^X)_Y][ClO_4]_Z$$

M = Cu, Ni, Zn, Fe

Scheme 5.1 Preparation of metal complexes.

Again, intensely coloured solutions were seen upon complexation. Coloured precipitates were formed upon stirring. The precipitates were filtered, dried and dissolved in hot

methanol and again filtered to obtain clear solutions. These intensely coloured solutions (Cu = blue, Ni = purple /grey, Zn = colourless and Fe = red / orange) were recrystallised by slow diffusion of diethyl ether below 10 °C until crystalline solids were obtained.

5.3.2 $[M(L^9)][ClO_4]_2$

Crystalline solids were isolated for all metal complexes in reasonable yields (47-55%). The IR data for the complexes and the free ligand is illustrated in Table 5.1. Only the copper and nickel complexes gave characteristic carbonyl stretching frequencies for the bridging ketone moiety that shifts only slightly upon complexation in (-8 / +4 cm^{-1}) suggesting no direct coordination. Interestingly this ν_{CO} band is absent in $[Zn(L^9+CH_3)]_2[ClO_4]_2$ and $[Fe(L^9+CH_3)]_2[ClO_4]_2$. However, the pyridyl bands ($\nu_{C=N}$) shift to higher frequencies ~ 1600 cm^{-1} in all the complexes and is suggestive of pyridyl coordination.[13] The ν_{Cl-O} band is present in all the complexes and is due to the ClO_4^- counterion. It is obvious from the IR spectra that the nickel complex contains a solvent molecule in its lattice. This is likely to arise from the coordination to a water molecule, which is later supported by the X-Ray data below.

	IR, wavenumber (cm^{-1})			
	O-H	**C=O**	**C=N (py)**	**Cl-O**
L^9	—	1685s	1581s, 1431s	—
$[Cu(L^9)][ClO_4]_2$	—	1689s	1606s, 1449m	1090s
$[Ni(L^9)(H_2O)_2][ClO_4]_2$	3377sb	1678s	1604s, 1448s	1089s
$[Zn(L^9+OCH_3)]_2[ClO_4]_2$	—	—	1590s, 1447s	1095s
$[Fe(L^9+OCH_3)]_2[ClO_4]_2$	—	—	1596s, 1450s	1097s

Table 5.1 Correlation of IR spectra of L^9 and its complexes.

Accurate masses were obtained for all the complexes. The mass spectrum of $[Cu(L^9)][ClO_4]_2$ and $[Ni(L^9)(H_2O)_2][ClO_4]_2$ give masses of 401.0454 $[Cu(L^9)+H]^+$ and 495.0004 $[Ni(L^9)+ClO_4]^+$ both indicating a 1:1 metal to ligand stoichiometry. Whereas, the zinc and iron complexes give accurate masses of almost double that of Cu and Ni complexes, 968.1741 and 949.0878 respectively confirming the presence of dimeric species with one perchlorate counter-ion, $[(ZnL^9OCH_3)_2+ClO_4]^+$ and $[(FeL^9+OCH_3)_2+ClO_4]^+$

The chemical shifts are very similar to the free ligand perhaps suggesting that it may have de-complexed in solution or that the ligand is bound to the metal in such a way as to not lower the symmetry of the ligand when co-ordinated. Table 5.2 compares the spectra with the free ligand, the presence of a methyl peak (3.24 *ppm*, 3H) in the zinc complex supports the formation of a hemiacetal.

	^{1}H NMR (DMSO-d_6) *ppm*							
	-OCH_3	**$H^{3'}$**	**$H^{4'}$**	**$H^{5'}$**	**$H^{3''}$**	**$H^{4''}$**	**$H^{5''}$**	**$H^{6''}$**
L^9	—	7.50	8.52	7.98	8.52	7.68	7.12	8.60
$[Zn(L^9+OCH_3)]_2[ClO_4]_2$	3.24	7.45	8.51	7.96	8.51	7.66	7.12	8.55

Table 5.2 Comparison of ^{1}H NMR spectra for **L^9** and **$[Zn(L^9+OCH_3)]_2[ClO_4]_2$**.

5.3.2.1 Electronic spectra

The UV-vis spectrum of $[Cu(L^9)][ClO_4]_2$ exhibits an asymmetric broad peak at 612 nm (48 $M^{-1}cm^{-1}$). This value is slightly lower than typical distorted octahedral Cu(II) complexes, for example, $[Cu(pdahx)(ClO_4)_2]$ complex (where pdahx = 1,6-bis(2-pyridyl)-2,5-diazahexane) consists of the same CuN_4O_2 chromophore but exhibits a d-d transition at 599 nm (182 $M^{-1}cm^{-1}$).[14] The lower energy transition (612 nm) can be attributed to the

relatively weak ligand field of bipyridine nitrogens in the chelate-ring system and may be the cause of a red shift in the absorption maxima, as compared to all-amine / pyridine CuN_4 chromophores described by Hathaway *et al.*[15,16] Comparison with the data reported by Urbach and coworkers[17] indicate that the nature of the donor atoms, rather than the chelate ring size sequence plays the major role in the position of the absorption bands in the visible spectra of copper(II) complexes with tetradentate aminopyridine ligands. For example complexes with benzimidazole residues in place of pyridine groups have lower-energy bands in the visible region.[18]

The $[Ni(L^9)(H_2O)_2][ClO_4]_2$ complex exhibits two peaks in the d-d region of the UV-vis spectrum. Assuming the complex is of octahedral symmetry, the bands that lies at the lowest energy, 788 nm (7 $M^{-1}cm^{-1}$) can be assigned to the $^3A_{2g} \rightarrow {}^3T_{2g}$ transition and approximates to Δ_o. The $^3A_{2g} \rightarrow {}^3T_{1g}(F)$ band is seen at 561 nm (9 $M^{-1}cm^{-1}$) and the third $^3A_{2g} \rightarrow {}^3T_{1g}(P)$ band is most likely obscured by the intense metal to ligand charge transfer (MLCT) band seen at 340 nm (13,731 $M^{-1}cm^{-1}$). The equation used in Chapter 3 is used here to predict the position of the third band, it should occur at 358 nm (27,915 cm^{-1}). From this we can determine Δ to be 12,690 cm^{-1} and B of 507 cm^{-1} ($\beta = 0.46$), the B value is much smaller than typical Ni(II) octahedral complexes containing bipy ligands seen in previous literature, for example, the electronic absorption spectrum of the mononuclear distorted octahedral $[Ni(bipy)_2(OAc)]^+$ cation has the same chromophore, but a higher Racah parameter of 820 cm^{-1} and is consistent with octahedral coordination geometries about the Ni(II) ion.[19] Octahedral $[Ni(bipy)_3)][ClO_4]_2$ complex of N_6 chromophore deviates slightly, it has a Δ of 12,800 cm^{-1} and B of 710 cm^{-1}.[20] These differences in B value is a result of the difference in electronic properties of ligands, the electron

withdrawing carbonyl group of the ligand in $[Ni(L^9)(H_2O)_2]$ may well be attributing to the low B value obtained. This low B value is also seen in $[Ni(L^2)(H_2O)_2]$ complex (Δ = 11,933 cm^{-1} and B = 641 cm^{-1}) synthesised in Chapter 3 where the electron withdrawing carbonyl bridgehead group is also present.

The UV-vis spectrum of $[Fe^{II}(L^9{+}OCH_3)]_2[ClO_4]_2$ displays the characteristic MLCT absorption band, typical of iron(II) polypyridine complexes, it also accounts for the intense red colour observed. This peak is seen at 532 nm (ε = 1265 $M^{-1}cm^{-1}$) and is red shifted compared with that of $[Fe(bipy)_2]^{2+}$ and $[Fe(bipy)_3]^{2+}$ (470 nm and 521 nm respectively)[21] and is probably due to the electron withdrawing carbonyl group of the ligand, this behaviour is also observed in similar systems.[22] For example, it is seen in the distorted octahedral complex, $[FeL^X][(ClO_4)_2]$ where, L^X is 1,1-bis(((2,2'-bipy-6-yl) methylamino)carbonyl)ferrocene) the structure of which is shown in Figure 5.12. It consists of the same FeN_4O_2 chromophore but instead exhibits a LMCT band in CH_3CN at a slightly higher wavelength, 460 nm (830 $M^{-1}cm^{-1}$).[21]

5.3.2.2 Crystallographic data

$[Cu(L^9)][ClO_4]_2$

Suitable crystals were grown by the slow diffusion of diethyl ether into a methanolic solution of $[Cu(L^9)][ClO_4]_2$ below 10 °C. Blue single crystals were isolated (30%), the structure of which is illustrated in Figure 5.5. Table 5.3 lists the selected bond lengths and angles.

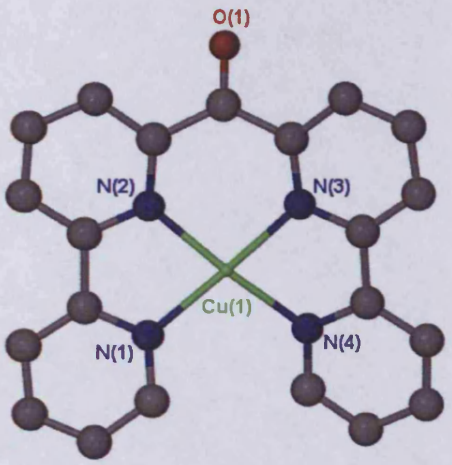

Figure 5.5 Molecular structure of $[Cu(L^9)][ClO_4]_2$. Hydrogen atoms omitted for clarity.

Table 5.3 Bond distance (Å) and angles (°) for $[Cu(L^9)][ClO_4]_2$.

Cu(1)-N(2)	1.964(3)	Cu(1)-N(4)	1.987(3)
Cu(1)-N(3)	1.971(3)	Cu(1)-N(1)	1.995(3)
Cu(1)-O(9)	2.703(3)	Cu(1)-O(5)	2.552(4)
N(2)-Cu(1)-N(3)	95.15(12)	N(2)-Cu(1)-N(1)	82.48(12)
N(2)-Cu(1)-N(4)	169.00(11)	N(3)-Cu(1)-N(1)	165.99(12)
N(3)-Cu(1)-N(4)	82.45(12)	N(4)-Cu(1)-N(1)	102.39(12)

The compound crystallised in the triclinic P –1 space group. The coordination sphere of the Cu(II) ion may at first be considered as having a distorted square planar geometry, however two additional perchlorate anions are weakly coordinated in the apical positions (average Cu-O 2.63 Å) making a Cu(II) coordination number of 4 + 2. The CuN_4 chromophore is almost planar (i.e. no tetrahedral character) and has typical Cu-N bond lengths (average Cu-N 1.979 (3) Å), it is remarkably similar for pyridine and amine nitrogen donors ranging from 1.980 to 1.992 Å.[14] Interestingly, the Cu-N distances seen in the basal plane of the square pyramidal complex $[Cu^{II}(L^2)(H_2O)]$ synthesised in Chapter 3 is closer than those seen in copper complexes containing bipyridine ligands. The bipy units in the following complexes are not restricted by a ketone bridgehead, they can

therefore spread out to achieve their desired positions therefore possessing longer Cu-N bond lengths; $[Cu^{II}(2,2'\text{-bipy})_2(NH_3)][BF_4]$ (ave. Cu-N, 2.031 Å), $[Cu^{II}(2,2'\text{-bipy})_2(Cl)]$-1,1,2,3,3-pentacyanopropenide (ave. Cu-N, 2.023 Å) and $[Cu^{II}(2,2'\text{-bipy})_2][PF_6][BF_4]$ (ave. Cu-N, 1.987 Å).[23-25]

Typically, four *cis* angles around a square planar Cu(II) centre equals 360°.[15] Here the four *cis* angles being N1-Cu1-N4 93.17°, N1-Cu1-N2 80.76°, N3-Cu1-N4 80.76 and N2-Cu1-N3 106.12° add up to 360.81° and strongly supports the square planar theory.

$[Ni(L^9)(H_2O)_2][ClO_4]_2$

The compound gave dark purple / grey single crystals (39%). It crystallised in the orthorhombic P c c n space group, the structure deduced by X-ray diffraction is illustrated in Figure 5.6. Table 5.4 lists the selected bond lengths and angles.

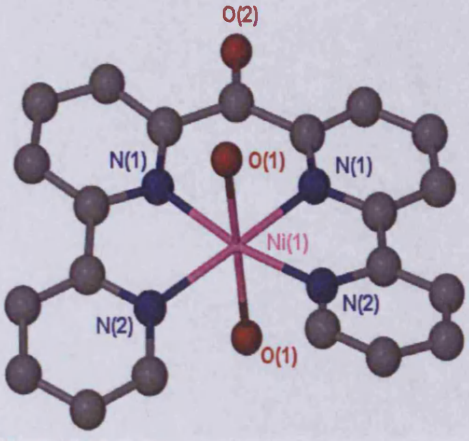

Figure 5.6 Molecular structure of $[Ni(L^9)(H_2O)_2][ClO_4]_2$. Hydrogen atoms omitted for clarity.

Table 5.4 Bond distance (Å) and angles (°) for $[Ni(L^9)(H_2O)_2][ClO_4]_2$.

N(1)-Ni(1)	2.0441(18)	Ni(1)-N(1)#1	2.0441(18)
N(2)-Ni(1)	2.0626(18)	Ni(1)-N(2)#1	2.0626(18)
O(2)-Ni(1)	2.1076(16)	Ni(1)-O(2)#1	2.1076(16)
N(1)-Ni(1)-N(1)#1	93.17(10)	N(2)#1-Ni(1)-O(2)	85.39(7)
N(1)-Ni(1)-N(2)#1	170.67(7)	N(2)-Ni(1)-O(2)	91.93(7)
N(1)#1-Ni(1)-N(2)#1	80.76(7)	N(1)-Ni(1)-O(2)#1	94.95(7)
N(1)-Ni(1)-N(2)	80.76(7)	N(1)#1-Ni(1)-O(2)#1	88.11(7)
N(1)#1-Ni(1)-N(2)	170.67(7)	N(2)#1-Ni(1)-O(2)#1	91.93(7)
N(2)#1-Ni(1)-N(2)	106.11(10)	N(2)-Ni(1)-O(2)#1	85.39(7)
N(1)-Ni(1)-O(2)	88.11(7)	O(2)-Ni(1)-O(2)#1	175.55(9)
N(1)#1-Ni(1)-O(2)	94.95(7)		

The solid-state structure consists of a mononuclear $[Ni^{II}(L^9)(H_2O)_2][ClO_4]_2$ compound. The bipyridyl units in this complex occupy the equatorial plane, and oxygen atoms of the water molecules are in the axial positions forming pseudo-octahedral coordination geometry. The L-M-L bond angles are clearly indicative of octahedral symmetry with twelve angles close to 90° and three close to 180° and, as expected, slight deviations occur due to the sterics of the ligand. [26,27]

The Ni-N bond lengths are almost equivalent with values between 2.0441(18) - 2.0626(18) Å and the longer Ni-O bond lengths average 2.1076 (16) Å, these are typical of similar pseudo-octahedral complexes containing bipy ligands. For example $[Ni^{II}(2,2'\text{-bipy})_2(H_2O)_2][CdBr_4]$ and $[Ni^{II}(2,2'\text{-bipy})_2(H_2O)_2][ClO_4]_2$ produce average Ni-N bond distances of ~2.073 and 2.066 Å respectively[26,27] and average Ni-O bond distances of 2.108 and 2.089 Å.[28,29] This nickel complex also strongly resembles the geometry of $[Ni(L^2)(H_2O)_2]$ reported in Chapter 3. The bond distances around the equatorial plane are similar (2.0290 – 2.0506 Å) however the apical Ni-O bond lengths (also bonding to each water molecules) are slightly shorter (average = 2.0745 Å), this may be a result of the

carboxylate group being not as good a donor as the pyridyl ring, causing the water molecule to be pulled in closer.

$[Zn(L^9{+}OCH_3)]_2[ClO_4]_2$

Transparent single crystals were isolated for the zinc complex (42%). They crystallised in the monoclinic P 2(1)/n space group. X-ray crystallography revealed the structure depicted in Figure 5.7, a dinuclear zinc cluster $[Zn(L^9{+}OCH_3)]_2[ClO_4]_2$. Table 5.5 lists the selected bond lengths and angles.

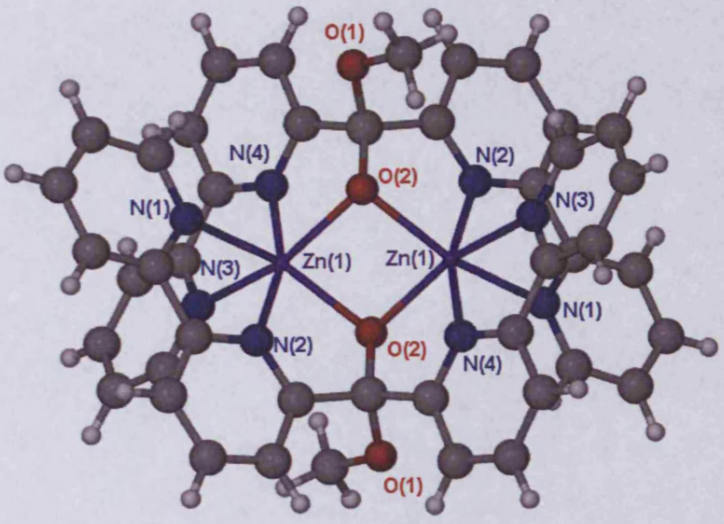

Figure 5.7 Crystal structure of $[Zn(L^9{+}OCH_3)]_2[ClO_4]_2$. Hydrogen atoms omitted for clarity.

Table 5.5 Bond distance (Å) and angles (°) for $[Zn(L^9+OCH_3)]_2[ClO_4]_2$.

N(1)-Zn(1)	2.248(2)	Zn(1)-O(2)	2.0991(19)
N(2)-Zn(1)	2.055(2)	Zn(1)-O(2)#1	2.107(2)
N(3)-Zn(1)	2.286(2)	Zn(1)-Zn(1)#1	3.1241(8)
N(4)-Zn(1)	2.064(2)	O(2)-Zn(1)#1	2.107(2)
N(2)-Zn(1)-N(4)	161.87(9)	O(2)-Zn(1)-N(1)	150.74(8)
N(2)-Zn(1)-O(2)	77.69(8)	O(2)#1-Zn(1)-N(1)	98.19(8)
N(4)-Zn(1)-O(2)	116.64(8)	N(2)-Zn(1)-N(3)	91.90(9)
N(2)-Zn(1)-O(2)#1	115.61(8)	N(4)-Zn(1)-N(3)	74.43(9)
N(4)-Zn(1)-O(2)#1	78.51(8)	O(2)-Zn(1)-N(3)	103.63(8)
O(2)-Zn(1)-O(2)#1	84.07(7)	O(2)#1-Zn(1)-N(3)	152.48(8)
N(2)-Zn(1)-N(1)	75.07(9)	N(1)-Zn(1)-N(3)	87.84(9)
N(4)-Zn(1)-N(1)	92.26(9)		

The formation of the hemiacetal has been extensively reported in previous literature for di-2-pyridyl ketone (dpk) ligands. Studies have shown that water and alcohols (ROH) add to the carbonyl group upon metal coordination of the 2-pyridyl rings producing the *gem*-diol form or the hemiacetal form of the dpk ligand.[30,31] Scheme 5.2 shows how the hemiacetal group is formed in the bis(bipy) ketone ligand, the $^-OCH_3$ ion from the methanol attacks the carbonyl cation. The presence of deprotonated hydroxyl group (L^9+OCH_3) leads to a great coordinative flexibility, due to the well-known ability of the negatively charged oxygen to bridge two or three metal ions.

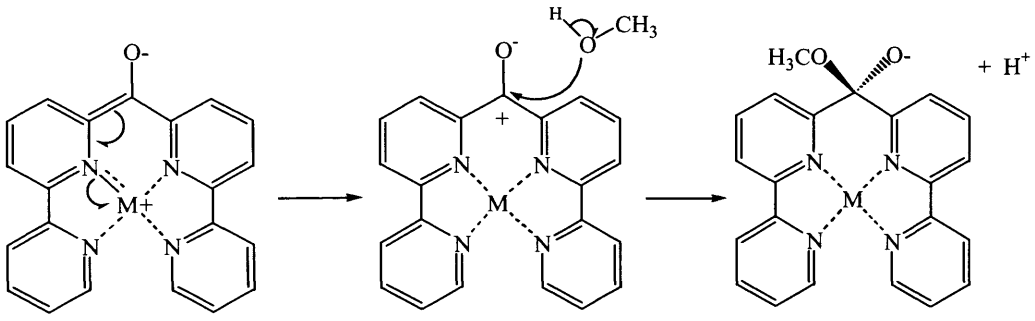

Scheme 5.2 Reaction of methanol with coordinated bis(bipy) ketone.

In this molecule the monoanionic hemiacetal form of the ligand bridges two metal centres through the deprotonated hydroxyl group and the OCH_3 group points away from the metal. The two Zn(II) atoms are doubly bridged by the deprotonated hydroxyl O atoms of the $(bipy)_2C(OMe)O^-$ ligands, while four N atoms from two chelating 2,2'-bipy units complete six coordination at each metal centre. The geometry about the Zn(II) can be described as a heavily distorted octahedron. For the observed structure, there are twelve angles between 74.43(9) and 116.64(8) and three angles between 150.74(8) and 161.87(9). The distortion is caused by the hemiacetal bridgehead which pulls the donor atoms close together and does not let them space out equally as required for O_h symmetry.

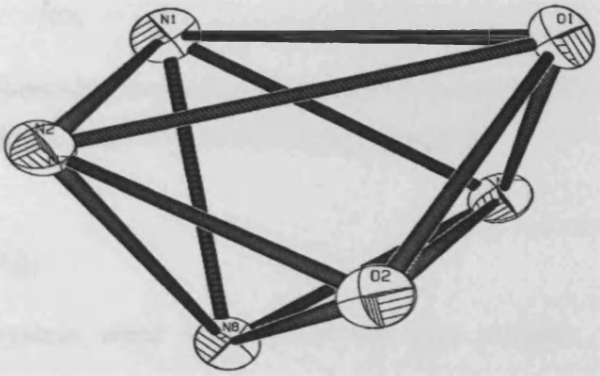

Figure 5.8 Distorted octahedral framework observed around the Zn(1) centre.

The average Zn-N and bridging Zn-O bond lengths are 2.163(2) and 2.103(8) Å respectively. These values are similar to those observed in previous literature for complexes containing bipy ligands, for example the *cis*-bis(2,2'-bipy)-bis(2-chloro-4-nitrophenolato)-Zn(II) compound in Figure 5.9 (left) has the following average bond lengths; Zn-N 2.188 Å and Zn-O 2.052 Å, the latter being slightly shorter.[32] Another similar example is the bridging (nitrito-O,O')- bis(2,2'-bipy)-Zn(II) nitrate complex shown in Figure 5.9 (middle) characterised by Hathaway *et al.*[33] it has average Zn-N and Zn-O bond lengths of 2.101(3) Å and 2.214(5) Å respectively and deviate drastically from

the dimeric species. The $[Zn_2Cl_2\{(py)_2C(OMe)O\}_2]$ reported by Katsoulakou *et al.*[34] has a very similar coordination mode to $[Zn(L^9{+}OCH_3)]_2[ClO_4]_2$ except it has a trigonal bipyramidal geometry and consequently have shorter average Zn-N and Zn-O bond lengths; 2.126(3) and 2.047(4) Å respectively. The bond lengths are also shorter because ligand is smaller.

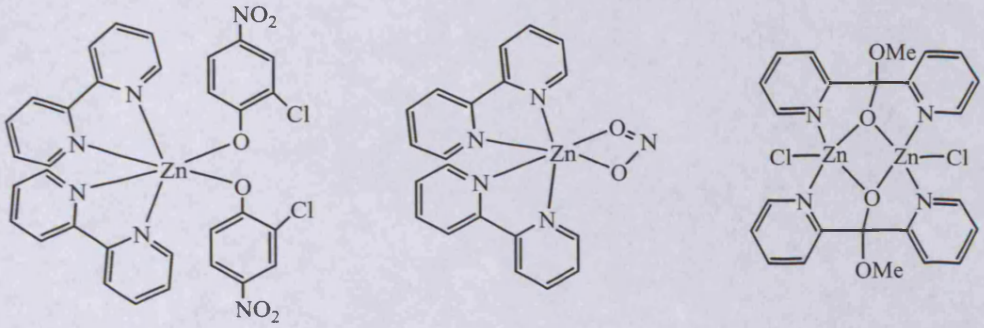

Figure 5.9 *Cis*-bis(2,2'-bipy)-bis(2-chloro-4-nitrophenolato)-Zn(II) (left). (Nitrito-O,O')- bis(2,2'-bipy)-Zn(II) nitrate (middle). $[Zn_2Cl_2\{(py)_2C(OMe)O\}_2]$ (right).

$[Fe(L^9{+}OCH_3)]_2[ClO_4]_2$

Red, single crystals were isolated for the iron complex, it crystallised in the orthorhombic $Pc2_1b$ space group. The X-ray structure obtained is shown in Figure 5.10 .

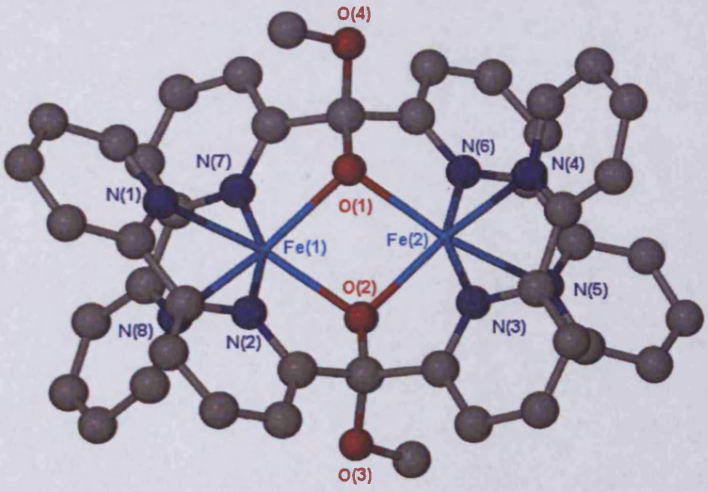

Figure 5.10 Crystal structure of $[Fe(L^9{+}OCH_3)]_2\ [ClO_4]_2$. Hydrogen atoms omitted for clarity.

Table 5.6 Bond distance (Å) and angles (°) for $[Fe(L^9+OCH_3)]_2[ClO_4]_2$.

Fe(1)-O(1)	2.082(3)	Fe(2)-O(2)	2.078(3)
Fe(1)-O(2)	2.085(3)	Fe(2)-N(3)	2.082(4)
Fe(1)-N(2)	2.090(4)	Fe(2)-O(1)	2.087(3)
Fe(1)-N(7)	2.100(4)	Fe(2)-N(6)	2.098(4)
Fe(1)-N(8)	2.216(4)	Fe(2)-N(4)	2.202(4)
Fe(1)-N(1)	2.243(5)	Fe(2)-N(5)	2.269(5)
O(1)-Fe(1)-O(2)	81.35(13)	O(2)-Fe(2)-N(3)	76.02(15)
O(1)-Fe(1)-N(2)	119.26(15)	O(2)-Fe(2)-O(1)	81.38(12)
O(2)-Fe(1)-N(2)	76.28(15)	N(3)-Fe(2)-O(1)	124.01(16)
O(1)-Fe(1)-N(7)	76.01(14)	O(2)-Fe(2)-N(6)	121.23(15)
O(2)-Fe(1)-N(7)	119.39(17)	N(3)-Fe(2)-N(6)	157.23(16)
N(2)-Fe(1)-N(7)	161.00(17)	O(1)-Fe(2)-N(6)	76.04(15)
O(1)-Fe(1)-N(8)	148.26(16)	O(2)-Fe(2)-N(4)	147.54(17)
O(2)-Fe(1)-N(8)	103.52(15)	N(3)-Fe(2)-N(4)	74.40(16)
N(2)-Fe(1)-N(8)	92.12(16)	O(1)-Fe(2)-N(4)	104.51(16)
N(7)-Fe(1)-N(8)	74.40(15)	N(6)-Fe(2)-N(4)	90.94(17)
O(1)-Fe(1)-N(1)	106.63(15)	O(2)-Fe(2)-N(5)	106.71(15)
O(2)-Fe(1)-N(1)	149.42(15)	N(3)-Fe(2)-N(5)	87.55(17)
N(2)-Fe(1)-N(1)	74.14(16)	O(1)-Fe(2)-N(5)	148.33(16)
N(7)-Fe(1)-N(1)	91.14(17)	N(6)-Fe(2)-N(5)	73.69(16)
N(8)-Fe(1)-N(1)	85.23(17)	N(4)-Fe(2)-N(5)	85.15(17)

The dinuclear iron cluster, $[Fe(L^9+OCH_3)]_2[ClO_4]_2$ has similar coordination to its analogous zinc complex $[Zn(L^9+OCH_3)]_2[ClO_4]_2$. The L-M-L bond angles and lengths are also very similar producing a heavily distorted octahedral geometry; the ORTEP diagram of the molecule with the atomic numbering is shown in Figure 5.11.

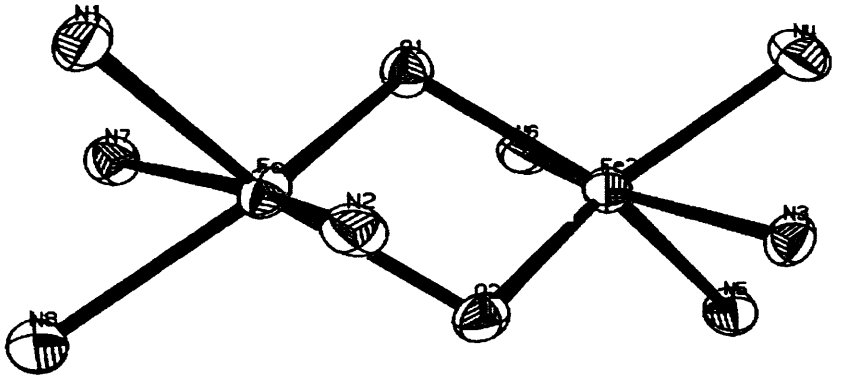

Figure 5.11 ORTEP view of the molecular structure of $[Fe(L^9+OCH_3)]_2[ClO_4]_2$.

The average Fe-N and Fe-O bond lengths are 2.162(4) and 2.083(3) Å, the latter value is shorter than the analogous Zn-O bond length (2.103(8) Å), this is probably due to the smaller zinc radius (ionic radius decreases across a group due to lanthanide contraction). The Fe-N bond length is significantly longer than those seen in octahedral iron(II) bipy complexes, for example, $[Fe(2,2'bipy)_3]^{2+}$ has an average Fe-N bond length of 1.956(6) Å.[35] However, the $[FeL^X][(ClO_4)_2]$ complex shown in Figure 5.12 has similar average bond lengths, Fe-N 2.169 (4) Å and Fe-O 2.115 (4) Å.[27]

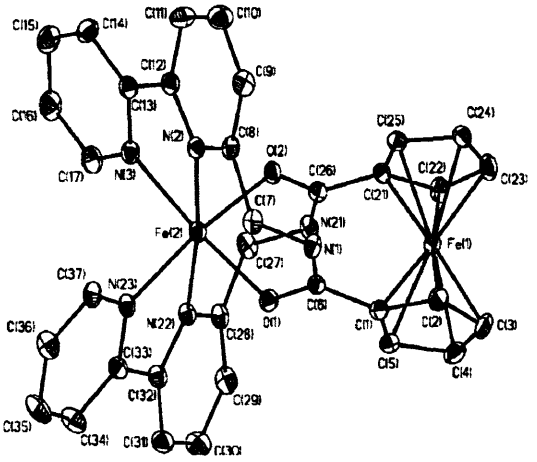

Figure 5.12 Crystal structure of $[FeL^X](ClO_4)_2$.[27]

5.3.2.3 Electrochemistry

Cyclic voltammetry (CV) measurements were performed on the following complexes $[Cu(L^9)][ClO_4]_2$, $[Ni(L^9)(H_2O)_2][ClO_4]_2$ and $[Fe(L^9{+}OCH_3)]_2[ClO_4]_2$ under an argon atmosphere at 20 °C in an attempt to analyse the stability of various oxidation states. These analyses were performed in a 0.1M Bu_4NPF_6 acetonitrile solution, using ferrocene as an internal reference. In all cases a reduction process was observed at a scan rate of 200 mV s^{-1}. A quasi-reversible reduction is seen at -0.358V (64mV) vs Fc/Fc^+ (74mV) for the copper complex, this can be assigned to the $Cu^{II} \rightarrow Cu^{I}$ couple, a similar value is seen for $Cu^{II}(PA)_3^- + e^- \rightarrow Cu^{I}(PA) + 2PA^-$, $E_{1/2} = -0.356$ V vs Fc/Fc^+ suggesting

that the complexes have similar stability.[36] Copper(II) complexes containing bipy ligands for example $[Cu(bipy)_2(OH)]$ produce Cu^{II}/Cu^{I} reduction at +0.144 V and an irreversible ligand centred reduction at –1.06 V vs Fc/Fc^+ due to the bipy ligand bonded to the Cu(II).[37] Only irreversible reductions are seen for the Ni and Fe complexes at -1.415 and –1.586V vs Fc/Fc^+ respectively, these are also due to the bipy ligands bonded to the M(II). Previous reports on iron(II) bipy compounds have typically shown oxidation and reduction processes, for example the $[Fe(bipy)_2MoS_4]$ complex produces an irreversible wave at + 1.28 V vs Fc/Fc^+ and two quasi-reversible waves at –1.01 V and –1.16 V vs Fc/Fc^+, the positive value is assigned to the oxidation of $Fe^{II} \rightarrow Fe^{III}$ couple and negative values are due to the reduction of the bipyridyl ligand bonded to the Fe(II).[37,38]

5.3.3 $[M(L^{10})][ClO_4]_2$

$[M(L^{10})][ClO_4]_2$ type complexes were also obtained in reasonable yields (47-65%). Their IR correlations are illustrated in Table 5.7. Again, similar shifts to complexes of type $[M(L^9)][ClO_4]_2$ were also observed here, pyridyl coordination is suggested by the slight increase in wave number of the pyridyl bands ($\nu_{C=N}$). The broad ν_{O-H} band (assigned to either the tertiary alcohol group of the ligand or solvent in the lattice) shifts to higher wave numbers (between 104 - 157 cm^{-1}) upon complexation. Also the characteristic ν_{Cl-O} band is present in all four complexes suggesting the presence of perchlorate counter-ions.

	IR, wave number (cm^{-1})		
	O-H	**C=N (bipy)**	**Cl-O**
L^{10}	3290mb	1581s, 1429s	—
$[Cu(L^{10})(H_2O)][ClO_4]_2$	3447mb	1589s, 1452m	1087s
$[Ni(L^{10})][ClO_4]_2$	3394mb	1624s, 1450s	1090s
$[Zn(L^{10})][ClO_4]_2$	3399mb	1610s, 1447s	1087s
$[Fe(L^{10})][ClO_4]_2$	3412mb	1604m, 1451m	1088s

Table 5.7 Correlation of IR spectra, L^{10} and complexes $[M(L^{10})][ClO_4]_2$.

All the complexes except $[Zn(L^{10})][ClO_4]_2$ gave mass peaks for the ion $[M(L^{10})+ClO_4]^+$ whereas, the zinc complex produced a mass peak of 335 for the ion $[Zn(L^{10})+H]^+$. However, they all indicate a monomeric species consisting of a 1:1 metal to ligand complex.

Table 5.8 compares the ^1H NMR spectra of the free ligand with the $[Zn(L^{10})][ClO_4]_2$ complex.**ffdainfdf** A small increase in chemical shift is observed upon complexation, protons $H^{6''}$ and H^6 are most affected as they lie adjacent to the coordinating nitrogen atoms. They shift downfield by ~0.09 *ppm* becoming less shielded. It is also noted that the two bipyridyl units are equivalent as their chemical shifts are the same.

	^1H NMR (DMSO-d_6) *ppm*										
	$H^{3'}$	**$H^{4'}$**	**$H^{5'}$**	**$H^{3''}$**	**$H^{4''}$**	**$H^{5''}$**	**$H^{6''}$**	**H^3**	**H^4**	**H^5**	**H^6**
L^{10}	7.49	8.52	7.96	8.50	7.66	7.12	8.59	7.75	8.05	7.40	8.65
$[Zn(L^{10})][ClO_4]_2$	7.51	8.55	7.99	8.55	7.69	7.19	8.67	7.78	8.11	7.47	8.74

Table 5.8 Comparison of ^1H NMR spectra for L^{10} and $[Zn(L^{10})][ClO_4]_2$.

5.3.3.1 Electronic spectra

The UV-vis spectrum of $[Cu(L^{10})(H_2O)][ClO_4]_2.H_2O$ shown if Figure 5.13 exhibits a broad peak at 685 nm with a peak much further to the right of spectrum at 919 nm. This pattern is characteristic of five coordinate complexes. Typically in distorted square-pyramidal Cu(II) complexes the intensity of the higher energy band (ε = ~220 $M^{-1}cm^{-1}$) is significantly higher than the intensity of the lower-energy shoulder (ε = ~30 $M^{-1}cm^{-1}$) and the opposite ratio of intensities is typical for trigonal-bipyramidal complexes.[15,39] From the X-Ray data the latter pattern is expected for this complex however the following intensities are observed, 93 and 73 $M^{-1}cm^{-1}$ suggesting a distorted square-pyramidal geometry in CH_3CN solution. It is also important to note the spectrum is very similar to the tetrameric copper complex, $[Cu(L^4)]_4[ClO_4]_2$ seen in Chapter 3 (696 nm (85 $M^{-1}cm^{-1}$), 972 nm (46 M^{-1} cm^{-1})) where two different geometries are present, this strongly indicates that both geometries could also be present here in solution.

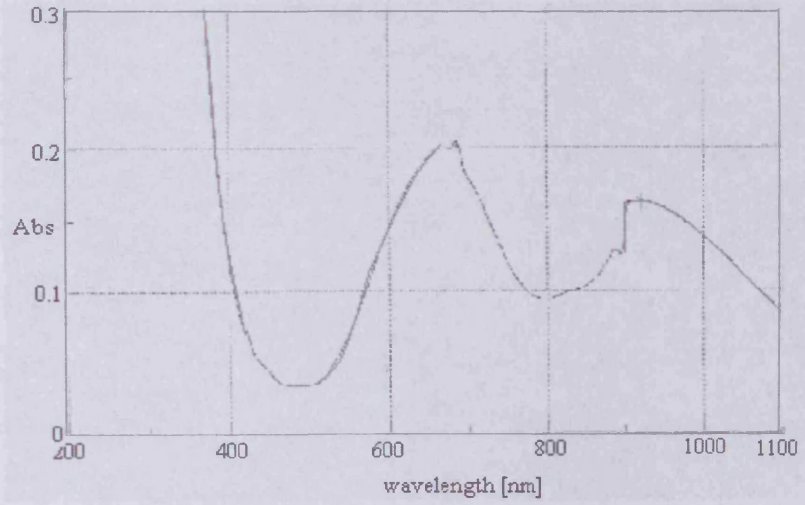

Figure 5.13 UV-vis spectra of $[Cu(L^{10})(H_2O)][ClO_4]_2$ in CH_3CN.

The $[Ni(L^{10})][ClO_4]_2$ exhibits two d-d transitions in the UV-vis spectrum. Assuming the complex is of octahedral symmetry we can assign the band at 900 nm (11 $M^{-1}cm^{-1}$) with a shoulder at 807 nm (8 $M^{-1}cm^{-1}$) to be the $^3A_{2g} \rightarrow {}^3T_{2g}$ transition, the band seen at 504 nm (9 $M^{-1}cm^{-1}$) is typical of the $^3A_{2g} \rightarrow {}^3T_{1g}(F)$ transition, the third $^3A_{2g} \rightarrow {}^3T_{1g}(P)$ band is probably obscured by the MLCT band seen at 309 nm (8412 $M^{-1}cm^{-1}$). This spectrum has a Δ value of 12,392 cm^{-1} and an unusually high Racah B, 976 cm^{-1} (β = 0.91). These values are very similar to the $[Ni(py_3tach)]^{2+}$ spectrum when assumed it is of octahedral symmetry (also discussed in Chapter 3) [20,40], it has an unusually high B and Δ values, 980 cm^{-1} (β = 0.91) and 12,800 cm^{-1} respectively suggesting that electronically the ligands have similar field strengths therefore a similar delocalisation of electrons is experienced, probably indicating that $[Ni(L^{10})][ClO_4]_2$ is not of octahedral but is very distorted from an ideal geometry.

The UV-vis spectrum of $[Fe(L^{10})][ClO_4]_2$ show no clear d-d absorption bands in the visible region of the spectrum. The analysis of the spectrum is somewhat difficult due to a series of shoulders that span from the UV region into the visible part of the spectrum. They are seen at 253 nm (12663 M^{-1} cm^{-1}), 303 nm (8262 $M^{-1}cm^{-1}$), 341 nm (3088 $M^{-1}cm^{-1}$), 371 nm (2007 $M^{-1}cm^{-1}$), 421 nm (860 M^{-1} cm^{-1}) and 569 nm (60 $M^{-1}cm^{-1}$).

5.3.3.2 Crystallographic data

Single blue crystals were isolated for compound $[Cu(L^{10})(H_2O)][ClO_4]_2.H_2O$ (47%). The unit is depicted in Figure 5.14. Selected distances and angles are listed in Table 5.9.

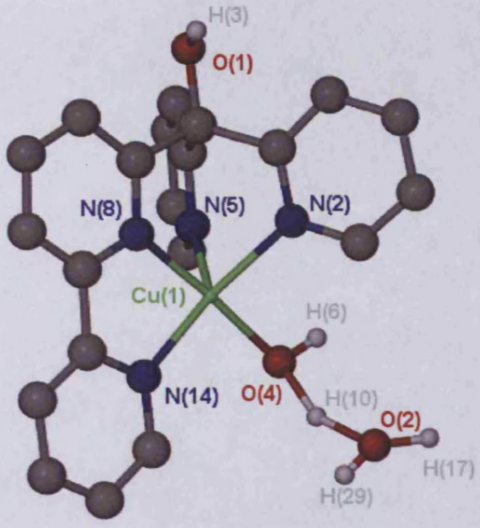

Figure 5.14 Crystal structure of $[Cu(L^{10})(H_2O)][ClO_4]_2.H_2O$.

Table 5.9 Bond distance (Å) and angles (°) for $[Cu(L^{10})(H_2O)][ClO_4]_2.H_2O$.

Cu(1)-N(8)	1.949(5)	Cu(1)-O(4)	1.962(5)
Cu(1)-N(2)	2.065(5)	Cu(1)-N(14)	2.005(6)
Cu(1)-N(5)	2.130(5)		
N(8)-Cu(1)-O(4)	176.9(2)	N(14)-Cu(1)-N(5)	129.5(2)
N(8)-Cu(1)-N(14)	81.6(2)	N(2)-Cu(1)-N(5)	86.0(2)
O(4)-Cu(1)-N(14)	95.4(2)	N(14)-Cu(1)-N(2)	141.9(2)
N(8)-Cu(1)-N(2)	87.7(2)	N(8)-Cu(1)-N(5)	87.33(19)
O(4)-Cu(1)-N(2)	95.3(2)	O(4)-Cu(1)-N(5)	93.8(2)
N(14)-Cu(1)-N(2)	141.9(2)	N(14)-Cu(1)-N(5)	129.5(2)
N(8)-Cu(1)-N(5)	87.33(19)	N(2)-Cu(1)-N(5)	86.0(2)
O(4)-Cu(1)-N(5)	93.8(2)		

The Cu(II) ion has a distorted trigonal bipyramidal (TBP) geometry ($\tau = (\beta - \alpha) / 60 = (129.5 - 87.7) / 60 = 0.70$) of the CuN_4O chromophore, with a nitrogen atom from the bipyridyl unit (Cu(1)-N(14) 2.005(6) Å) and two from the pyridyl nitrogen atoms (Cu(1)-N(5) 2.130(5) and Cu(1)-N(2) 2.065(5) Å) forming the trigonal plane. The axial site is occupied by another nitrogen atom of the bipyridyl unit (Cu(1)-N(8) 1.949(5) Å) and an oxygen atom from a water molecule (Cu(1)-O(4) 1.962(5) Å), these are shorter

than those of the equatorial plane corresponding to the typical environment of the trigonal bipyramidal geometry.[41]

Table 5.10 compares axial and equatorial bond distances with previously reported distorted trigonal bipyramidal (TBP) Cu(II) complexes. It is clear that the axial Cu-O bond length is slightly longer and the axial Cu-N bond length is slightly shorter in $[Cu(L^{10})(H_2O)][ClO_4]_2.H_2O$, again this is probably caused by the carbon bridgehead restricting the nitrogen donors from spreading out. However, the equatorial Cu-N distances are typical of distorted TBP Cu(II) complexes.[42,43] Table 5.10 also compares the bond lengths with $[(CuL^4)]_4[ClO_4]_2$ characterised in Chapter 3. Despite their different geometries the equatorial Cu-N bonds lengths are similar to the distorted TBP complex as the top half of the ligands are the same, however the axial bond lengths are much longer and is simply due to the difference in geometries.

Compound	Geometry	τ	Chromophore	Cu-L bond length (Å)		
				Axial Cu-O	Axial Cu-N	Equat. Cu-N
1[43]	Dist. TBP	0.66	CuN_2O_3	1.927(4)		
2[44]	Dist. TBP	0.72	CuN_2O_2Cl	1.918(2)	1.983(2)	2.031(3)
3[44]	Dist. TBP	0.71	CuN_2O_3	1.934(5)	1.972(4)	2.029(4)
$[Cu(L^{10})(H_2O)]^{2+}$	Dist. TBP	0.70	CuN_4O	1.962(5)	1.949(5)	2.005(6)-2.130(5)
$[(CuL^4)]_4[ClO_4]_2$	Dist. Spy.	0.15	CuN_2O_2N'	2.234(8)Cu-N	___	1.961(7)-2.034(7)
	Intermed.	0.54	CuN_3O_2	2.110(7)Cu-N	___	1.957(7)-2.102(7)

Table 5.10. Comparison of distorted TBP copper(II) complexes. **1** = $[Cu_2(\mu\text{-}O_2CCH_3)_2(\mu\text{-}OCH_3)(bipy)_2](PF_6)$, **2** = $[Cu_2(\mu\text{-}O_2CH)(\mu\text{-}OH)(\mu\text{-}Cl)(dpyam)_2](PF_6)$, **3** = $[Cu_2(\mu\text{-}O_2CH)(\mu\text{-}OH)(dpyam)_2](PF_6)$.

5.3.3.3 Electrochemistry

Cyclic voltammetry measurements were performed on the Cu, Ni and Fe compounds using the same Experimental condition as described above. With this ligand (L^{10}) both copper and nickel complexes gave irreversible reduction processes at -1.448V vs Fc/Fc^+ and can be assigned to the reduction of the bipyridyl ligand bonded to the M(II). The Fe complex, $[Fe(L^{10})][ClO_4]_2$ produced an irreversible oxidation process at + 0.850 V vs Fc/Fc^+, this value is close to that seen for $ClO_4^- \rightarrow ClO_3^-$ reduction which typically occurs at +0.801 V vs Fc/Fc and suggests that is not due to the one electron Fe^{II}/Fe^{III} oxidation in the $[Fe(L^{10})]^{2+}$ complex, it is slightly lower than what is seen for similar complexes. For example, the one electron Fe^{II}/Fe^{III} reversible oxidation in the $[FeL^X]^{2+}$ ion (see Figure 5.12) occurs at a slightly higher $E_{½}$ value, + 0.95 V vs Fc/Fc^+ in CH_3CN[29].

5.3.4 $[M(L^{11})][ClO_4]_2$

Complexes of type $[M(L^{11})][ClO_4]_2$ were obtained in good yields (47-67%). IR correlations of the free ligand and the Cu, Ni, Zn and Fe complexes are illustrated in Table 5.11. Again pyridyl coordination is suggested by the slight increase in wave number of the $\nu_{C=N}$ band. The characteristic ν_{Cl-O} band is also present in all four complexes again suggesting the presence of perchlorate counter-ions.

	IR, wave number (cm^{-1})		
	O-H	C=N	Cl-O
L^{11}	3310mb	1583s, 1431s	—
$[Cu(L^{11})][ClO_4]_2$	3413mb	1594m, 1452m	1085s
$[Ni(L^{11})][ClO_4]_2$	3394mb	1601s, 1450s	1083s
$[Zn(L^{11})][ClO_4]_2$	3395mb	1607s, 1449s	1087s
$[Fe(L^{11})][ClO_4]_2$	3447mb	1603m, 1450m	1090s

Table 5.11 Correlation of IR spectra of L^{11}, and complexes $[M(L^{11})][ClO_4]_2$.

The mass spectra of the metal complexes gave the following masses 580.1, 575.2, 581, and 572 for the ion $[M(L^{11})+ClO_4]^+$ all indicating monomeric species consisting of a 1:1 metal to ligand ratio with a perchlorate counter-ion. This is consistent with the IR data.

Also the ^1H NMR spectrum for the zinc complex is similar to $[Zn(L^{10})][ClO_4]_2$, complex, the only difference being the integration for each peak. Table 5.11 compares the spectra of the free ligand and $[Zn(L^{11})][ClO_4]_2$.**ffdainfdf** It is noted that the two-bipy units are equivalent.

	^1H NMR (DMSO-d_6) *ppm*										
	$H^{3'}$	$H^{4'}$	$H^{5'}$	$H^{3''}$	$H^{4''}$	$H^{5''}$	$H^{6''}$	H^3	H^4	H^5	H^6
L^{11}	7.49	8.52	7.96	8.50	7.66	7.12	8.59	7.75	8.05	7.40	8.65
$[Zn(L^{11})][ClO_4]_2$	7.53	8.56	7.99	8.56	7.70	7.19	8.65	7.79	8.08	7.45	8.72

Table 5.12 Comparison of ^1H NMR spectra for L^{11} and $[Zn(L^{11})][ClO_4]_2$.

5.3.4.1 Electronic spectra

The UV-vis spectrum of $[Cu(L^{11})][ClO_4]_2$ exhibits a broad asymmetric peak at 665 nm (66 $M^{-1}cm^{-1}$). This is typical of low symmetry coordination geometries such as a distorted pseudo octahedron. For example, the distorted pseudo octahedron, $[Cu(spa)(H_2O)_2](ClO_4)_2$ complex characterised by van Koningsbruggen *et al.*,[44] shows an asymmetric band centred around 676 nm in its UV-Vis spectrum and is said to be typical of CuN_2O_4 chromophores. This suggests the copper complex is $[Cu(L^{11})(H_2O)_2][ClO_4]_2$ in solution.

The $[Ni(L^{11})][ClO_4]_2$ complex exhibits three peaks in the UV-vis spectrum, the bands are assigned as above assuming the complex is octahedral symmetry, 824 nm (15 $M^{-1}cm^{-1}$), 515 nm (16 $M^{-1}cm^{-1}$) and 297 nm (13200 $M^{-1}cm^{-1}$). Unusually high Δ = 12,135 cm^{-1} and B = 956 cm^{-1} values are obtained. From previous discussions on similar complexes, it can be concluded that this complex is heavily distorted from a regular octahedral symmetry.[20,39]

The UV-vis spectrum of $[Fe(L^{11})][ClO_4]_2$ show no d-d bands in the visible region of the spectrum however they may be hidden under the MLCT band seen at 505 nm (1125 $M^{-1}cm^{-1}$). This is typical of octahedral Fe(II) bipy complexes.[21]

5.3.4.2 Crystallographic data

Suitable crystals could not be obtained for the complexes of L^{11}.

5.3.4.3 Electrochemistry

The CV measurement of the Cu complex produced two reversible reduction processes, –0.449 and –0.785 V vs Fc/Fc^+, the former value is typical of Cu^{II}/Cu^{I} couple and the latter reduction is likely to be caused by the coordinated pyridyl ligand rather than the bipyridyl. From previous reports we know that bipyridyl reductions typically occur between –1.06 V (when coordinated to M(II)) to –1.96 V (in free bipy) vs Fc/Fc^+, in $[Cu(bipy)_2(OH)]$, a reversible one electron Cu^{II}/Cu^{I} reductions is seen at +0.144 V and an irreversible bipy reduction is seen at –1.06 V vs Fc/Fc^+.[36] The Fe complex gave a reversible oxidation process at + 0.663 V (75 mV) vs Fc/Fc^+ (74 mV) typical of the one electron Fe^{II}/Fe^{III} redox couple. This oxidation is very similar to that observed in $[Fe(bipy)_2(CH_3CN)_2]^{2+}$, where a reversible one electron oxidation couple is seen at + 0.69 V vs Fc/Fc^+ suggesting the complexes are of similar nature.[38]

5.3.5 $[M(L^{12})][ClO_4]_2$

All transition metal complexes were obtained in reasonable yields (46-70%). Their IR correlations are illustrated in Table 5.13. Again the same shifts in stretching frequency are also observed here as discussed above for L^{10} and L^{11}.

	IR, wave number (cm^{-1})		
	O-H	**C=N (bipy)**	**Cl-O**
L^{12}	3322mb	1580s, 1429s	—
$[Cu(L^{12})][ClO_4]_2$	3423mb	1605m, 1457m	1087s
$[Ni(L^{12})][ClO_4]_2$	3406mb	1600s, 1465s	1090s
$[Zn(L^{12})][ClO_4]_2$	3398mb	1595s, 1454s	1091s
$[Fe(L^{12})][ClO_4]_2$	3426mb	1654s, 1452m	1089s

Table 5.13 Correlation of IR spectra of L^{12}, and complexes $[M(L^{12})][ClO_4]_2$.

Accurate masses were obtained for all the complexes except $[Cu(L^{12})][ClO_4]_2$. The masses obtained for Ni, Zn and Fe complexes were consistent with the IR data, it gave the $[M(L^{12})+ClO_4]^+$ ion suggesting a 1:1 metal to ligand ratio with at least a perchlorate counter-ion. The mass spectrum of $[Cu(L^{12})][ClO_4]_2$ indicated the presence of the $[Cu(L^{12})+H]^+$ ion also suggesting a 1:1 ratio.

A ^1H NMR spectrum was obtained for the zinc complex in DMSO-d_6, Table 5.14 compares the spectra of the free ligand and $[Zn(L^{12})][ClO_4]_2$.**ffdainfdf** Again the same trend is observed as before, protons become less shielded upon coordination. All three bipy units are equivalent suggesting they all coordinate to the zinc centre in the same fashion.

	^1H NMR (DMSO-d_6) *ppm*						
	$H^{3'}$	**$H^{4'}$**	**$H^{5'}$**	**$H^{3''}$**	**$H^{4''}$**	**$H^{5''}$**	**$H^{6''}$**
L^{12}	7.50	8.52	7.96	8.52	7.68	7.13	8.60
$[Zn(L^{12})][ClO_4]_2$	7.55	8.56	8.02	8.57	7.72	7.17	8.69

Table 5.14 Comparison of ^1H NMR spectra for L^{12} and $[Zn(L^{12})][ClO_4]_2$.

5.3.5.1 Electronic spectra

The UV-vis spectrum of $[Cu(L^{12})][ClO_4]_2$ exhibits an asymmetric broad peak at 622 nm (37 $M^{-1}cm^{-1}$). This shape is typical of distorted octahedral symmetry.[17]

The $[Ni(L^{12})][ClO_4]_2$ complex exhibits two bands in the d-d region (see Figure 5.15), we can again assume octahedral symmetry and assign the bands accordingly. The peak at 940 nm (20 $M^{-1}cm^{-1}$) has a shoulder at 838 nm (14) and is the ν_1 transition ($^3A_{2g} \rightarrow {}^3T_{2g}$), the second band seen at 531 nm (20 $M^{-1}cm^{-1}$) is ν_2 ($^3A_{2g} \rightarrow {}^3T_{1g}(F)$). From this, Δ_o is 11,933 cm^{-1} and B is 880 cm^{-1}. One would expect a ligand of this shape to possess a

trigonal prismatic geometry like it analogous Zn(II) complex. Comparison of UV-vis spectra with similar complexes seen in previous literature are $[Ni(bipy)_3)][ClO_4]_2$ and $[NiP(bipy)_3)][ClO_4]_2$ where, $P(bipy)_3$ = tris(6(2,2'-bipyridyl))phosphine, the former octahedral complex has a Δ of 12,800 cm^{-1} and B = 710 cm^{-1} and is quite different from the $[Ni(L^{12})][ClO_4]_2$ spectrum.[20,41] The latter complex has similar Δ_o of 11,904 cm^{-1} (17 $M^{-1}cm^{-1}$) and B value of 785 cm^{-1} and also display other d-d absorption bands at 926 nm (10,800 cm^{-1}, (20 $M^{-1}cm^{-1}$)) and 540 nm (18,500 cm^{-1} (18 $M^{-1}cm^{-1}$)), these bands strongly resemble the spectrum of $[Ni(L^{12})][ClO_4]_2$ suggesting that electronically the ligands have similar field strengths and cause similar delocalisation within the complex. One would expect both facially capping hexadentate ligands ($P(bipy)_3$ and L^{12}) to have similar coordination geometries. Severe distortion from a regular octahedron is expected due to the rigidity of the ligand caused by the bridgehead tertiary alcohol group.

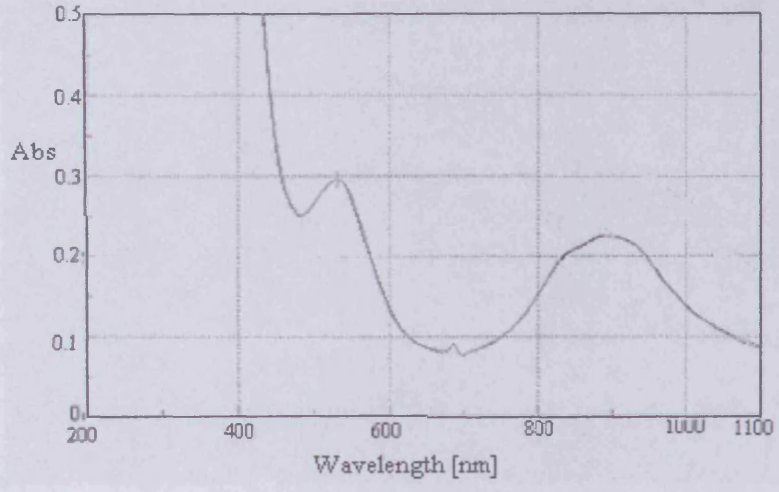

Figure 5.15 UV/Vis spectrum of $[Ni(L^{12})][ClO_4]_2$ in CH_3CN.

The $[Fe(L^{12})][ClO_4]_2$ complex exhibits a ligand to metal charge transfer (LMCT) peak at 544 nm (497 $M^{-1}cm^{-1}$). This is typical of Fe(II) complexes, as discussed

previously, octahedral $[Fe(bipy)_3]^{2+}$ species exhibits a MLCT band at 521 nm under the same Experimental conditions.[19]

5.3.5.2 Crystallographic data

$[Zn(L^{12})]_2[ClO_4]_4$

A white precipitate was obtained (68%) and recrystallised by slow diffusion of ether into a methanolic solution. Transparent single crystals were isolated for $[Zn(L^{12})]_2[ClO_4]_4$ (46%). The structure is depicted in Figure 5.16. Table 5.15 lists the selected bond lengths and angles.

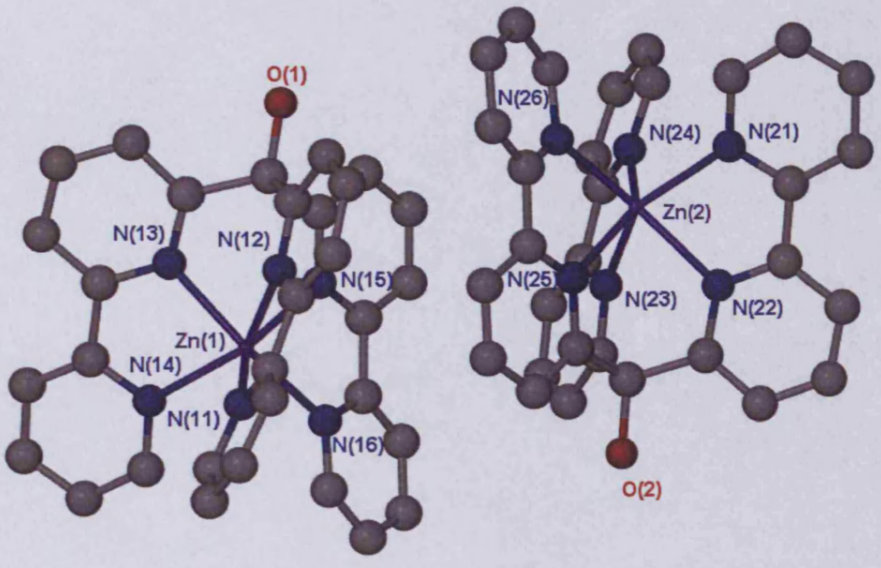

Figure 5.16 Crystal structure of $[Zn(L^{12})]_2[ClO_4]_4$. Hydrogen atoms omitted for clarity.

Table 5.15 Bond distance (Å) and angles (°) for $[Zn(L^{12})]_2[ClO_4]_4$.

N(11)-Zn(1)	2.207(3)	N(14)-Zn(1)	2.168(3)
N(12)-Zn(1)	2.183(3)	N(15)-Zn(1)	2.181(3)
N(13)-Zn(1)	2.162(3)	N(16)-Zn(1)	2.160(3)
N(16)-Zn(1)-N(13)	142.38(12)	N(14)-Zn(1)-N(12)	142.84(11)
N(16)-Zn(1)-N(14)	94.65(12)	N(15)-Zn(1)-N(12)	81.01(11)
N(13)-Zn(1)-N(14)	75.04(11)	N(16)-Zn(1)-N(11)	93.42(12)
N(16)-Zn(1)-N(15)	74.80(11)	N(13)-Zn(1)-N(11)	123.07(12)
N(13)-Zn(1)-N(15)	80.26(11)	N(14)-Zn(1)-N(11)	94.94(12)
N(14)-Zn(1)-N(15)	121.71(11)	N(15)-Zn(1)-N(11)	141.84(12)
N(16)-Zn(1)-N(12)	120.99(11)	N(12)-Zn(1)-N(11)	74.32(12)
N(13)-Zn(1)-N(12)	81.42(12)		

The are two crystallographically symmetrical independent molecules in the unit cell of $[Zn(L^{12})][ClO_4]_2$. The two molecules show only slight differences in bond lengths and angles, thus, only data for Zn(1) ion will be discussed. The most obvious feature of the structure is the hexacoordination of the zinc, which is caused entirely by the $[N_6]$-donor set of the hexadentate ligand. The coordination polyhedron is described best as a slightly tapered trigonal prism (TP), this is indicated by the torsional angles around the three bidentate arms (which should be zero in a perfect TP): C(110)-N(12)-Zn(1)-N(11) = 5.1°, C(122)-N(15)-Zn(1)-N(16) = 9.9°, C(112)-N(13)-Zn(1)-N(14) = 4.4°, C(222)-N(25)-Zn(2)-N(26) = 11.1°, C(210)-N(22)-Zn(2)-N(21) = 8.6°, C(212)-N(23)-Zn(2)-N(24) = 4.5° (Figure 5.17 shows the ORTEP diagram of the molecules). Another interesting feature of the structure are the trans –donor atom angles, these are expected to be 180° for octahedral coordination. The average value for both molecules (12 angles) is 132(11)°, which is in good accordance to the geometry of an ideal trigonal prism.[45]

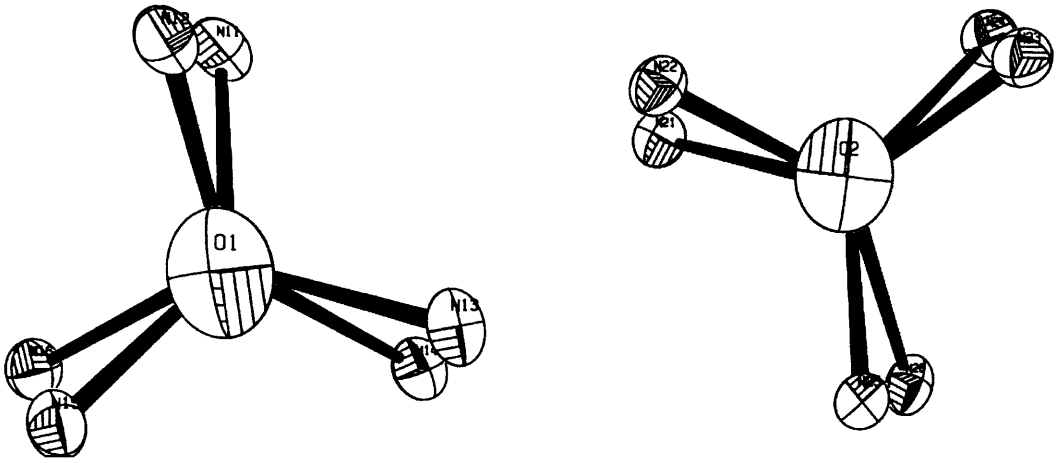

Figure 5.17. ORTEP diagram along the O(1)-C(111-Zn1 (left) and Zn2- C211-O2 vector (right).

The rigid nature of this ligand means that if a monomeric species is to be formed then it would be trigonal prismatic or a severe distortion of the ligand from typically expected bond angles would be required to give an octahedral complex. While the rigidity of the ligand is an important factor in the formation of trigonal prismatic complexes (for example Wentworth[46,47] has clearly shown that the rotational barrier in the C=N bond in tris(pyridine-2-carboxyaldimino) cyclohexane is responsible for the isolation of trigonal complexes), rigid ligands are still capable of forming multinuclear octahedral complexes so long as the steric energies associated with it are favourable with respect to the ligand field stabilisation energies which result from the structure, i.e. the formation of an octahedral complex could occur so long as the extra ligand field stabilisation energy from octahedral geometry (versus trigonal prismatic) outweighs any steric repulsion which might result from the structures. It is clear that for this ligand, even the large ligand field stabilisation energy associated with low spin octahedral d^6 does not allow the formation of an octahedral complex.

Comparison of metal donor bond lengths to similar complexes with N_6 donor sets,

where N is a bipyridine show that the Zn-N bond lengths (average 2.177(3) Å) are slightly longer than typical Zn(II) complexes seen in previous literature. For example, the octahedral $[Zn(II)(2,2'\text{-bipy})_3][CrO_4^{2-}][H_2O]$ complex has an average Zn-N bond length of 2.150(3) Å.[48] However, the Zn-N bond lengths are more similar to the average Zn-N bond length seen in the heavily distorted octahedral $[Zn(L^9)]_2[ClO_4]_2$ complex discussed earlier in this Chapter where the average Zn-N is 2.163 Å.

5.3.5.3 Electrochemistry

Cyclic voltammetry measurements were performed on the Cu, Ni and Fe compounds. Again these analyses were performed using the same solvent and reference compound as used above. The $[Cu(L^{12})][ClO_4]_2$ complex produced one irreversible reduction (-0.250 V vs Fc/Fc^+) which can be attributed to either the one electron Cu^{II}/Cu^{I} redox and one reversible reduction (-0.486 V vs Fc/Fc^+) which may be caused by the one electron Cu^{II}/Cu^{I} redox in the $[Cu(L^{12})]^{2+}$ complex. Unlike the electrochemical scan for $[Cu(bipy)_3]^{2+}$ reported previously,[36] it does not produce a reversible one electron Cu^{II}/Cu^{I} reduction process at + 0.444 V vs Fc/Fc^+ and an irreversible bipy reduction process at – 1.06 V Vs Fc/Fc^+ . Figure 5.18 illustrates the CV sweep of the $[Ni(L^{12})][ClO_4]_2$ complex, two reversible reductions are seen, a quasi-reversible wave at -1.378 V and a reversible one electron wave at –1.757 V vs Fc/Fc^+, both of which can be assigned to the bipyridyl ligands bonded to the Ni(II).

The CV sweep for the $[Fe(L^{12})][ClO_4]_2$ complex is shown in Figures 5.19 and 5.20. One reversible oxidation process is seen at + 0.695 V vs Fc/Fc^+ and characteristic the one electron Fe^{II}/Fe^{III} redox couple and one quasi-reversible bipy reduction process is

seen at -1.421 vs Fc/Fc^+. This cyclic voltammogram can be compared to $[Fe(bipy)_3][ClO_4]_2$ where a reversible one electron Fe^{II}/Fe^{III} oxidation is seen at a higher potential + 0.76 V vs Fc/Fc^+ suggesting that it is more stable than $[Fe(L^{12})][ClO_4]_2$. Also three reversible ligand centred reduction processes are seen at the following potentials, –1.06 V, -1.26 V and –1.46 vs Fc/Fc^+ all of which can be attributed to the coordinated bipy ligands.[36]

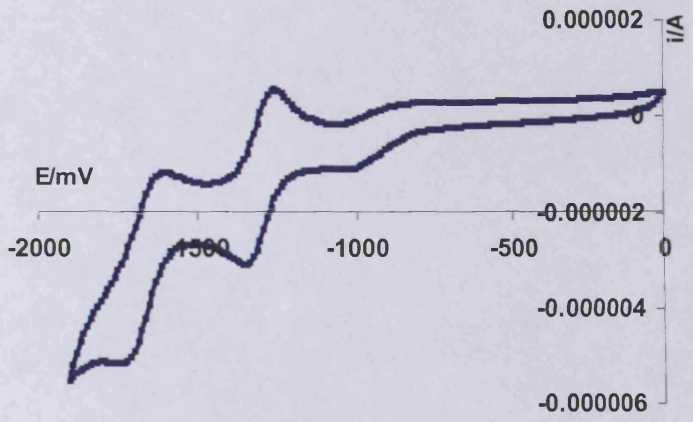

Figure 5.18 Cyclic Voltammogram of $[Ni(L^{12})][ClO_4]_2$ in CH_3CN + 0.1M Bu_4NPF_6 at 20 °C vs.Fc/Fc^+ reference standard.

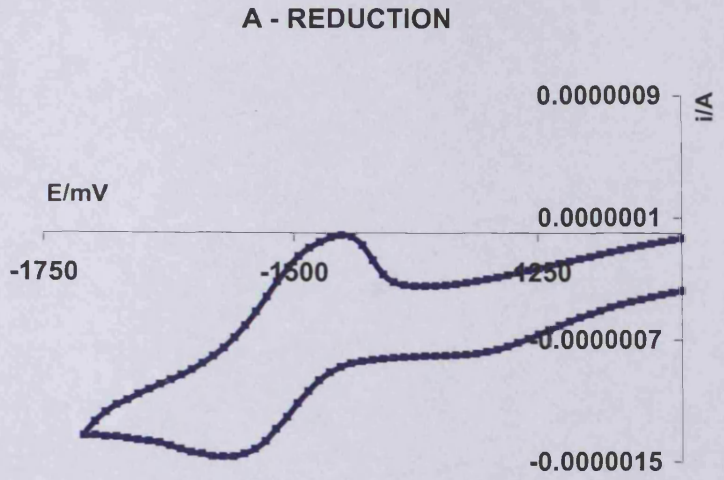

Figure 5.19 Cyclic Voltammogram of $[Fe(L^{12})][ClO_4]_2$ in CH_3CN + 0.1M Bu_4NPF_6 at 20 °C vs.Fc/Fc^+. **A**- Reduction process.

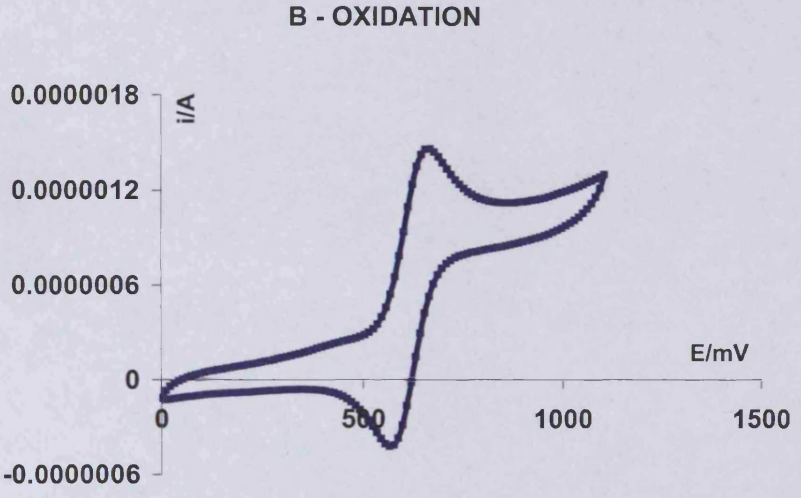

Figure 5.20 Cyclic Voltammogram of $[Fe(L^{12})][ClO_4]_2$ in CH_3CN + 0.1M Bu_4NPF_6 at 20 °C vs.Fc/Fc^+. **B**- Oxidation process.

5.4 Conclusions and suggestions for further research

The preparation of the Cu, Ni, Zn and Fe complexes with L^9 were successful. The following monomeric species were synthesised and characterised by X-Ray crystallography, $[Cu(L^9)][ClO_4]_2$ and $[Ni(L^9)(H_2O)_2][ClO_4]_2$ both gave pseudo octahedral geometries. Complexation of L^9 with Zn or Fe in the presence of methanol resulted in the formation of a hemiacetal (as shown earlier in Scheme 5.2) but not when reacted with Cu or Ni. An explanation for this may be due to stronger acidity of Zn^{2+} / Fe^{2+} ions which help to catalyse the formation of hemiacetals. The following dimeric species, $[Zn(L^9{+}OCH_3)]_2[ClO_4]_2$ and $[Fe(L^9{+}OCH_3)]_2[ClO_4]_2$ are best described as heavily distorted octahedrons. Other crystal structures obtained were $[Cu(L^{10})(H_2O)][ClO_4]_2$ and $[ZnL^{12}]_2[ClO_4]_4$, their X-ray data also confirmed the existence of these novel ligands along with their preferred geometries, with Cu(II) the ligand coordinates in a trigonal bipyramidal fashion and with Zn(II), L^{12} coordinates in a very unusual trigonal prismatic geometry.

The geometries of all Cu, Ni and Fe complexes were also investigated in solution using UV-vis spectroscopy. $[Cu(L^9)][ClO_4]_2$ exhibits a typical distorted octahedral Cu(II) spectrum, [14] an asymmetric band is seen at 612 nm. We can eliminate square planar geometry as they typically occur at higher energies (500-588 nm). With L^{10} a five coordinate square pyramidal pattern is observed, this geometry probably interchanges between square pyramidal and trigonal bipyramidal in solution as the latter geometry is observed in the solid-state. Copper complexes with L^{11} and L^{12} in solution is likely to be distorted octahedrons; the typical asymmetric broad peak that is seen in their spectra around 650 nm indicates this.

Ni(II) complex	ν (nm) / ε ($M^{-1}cm^{-1}$)	Δ (cm^{-1})	B (cm^{-1})	β
$[Ni(L^9)(H_2O)_2]^{2+}$	788(7), 561(9)	12 690	507	0.469
$[Ni(L^{10})]^{2+}$	813(10), 523(6)	12 392	976	0.902
$[Ni(L^{11}]^{2+}$	876(16), 538(18)	11 416	956	0.884
$[Ni(L^{12})]^{2+}$	823(12), 524(10)	11 933	880	0.813

Table 3.18 UV-vis spectra for Nickel complexes (assuming octahedral symmetry).

Racah B and Δ_o values were calculated for all Ni(II) complexes assuming octahedral symmetry. The pseudo-octahedral $[Ni(L^9)(H_2O)_2]$ complex in solution produces a low B value (507 cm^{-1}) and may be due to the electron withdrawing group of the carbonyl bridgehead, low B value (641 cm^{-1}) was also seen in $[Ni(L^2)(H_2O)_2]$ suggesting that it is typical of Ni(II) octahedral complexes containing ketone ligands. The other three Ni(II) complexes have unusually high B values 976 cm^{-1}, 956 cm^{-1} and 877 $cm^{-1}$and is an indication of severe distortion from a regular octahedron. One would expect the Δ and B values of the Ni(II) complexes to decrease upon the addition of a pyridine ring (from $L^{10}\rightarrow L^{12}$), as the ligands become more rigid you are likely to observe distorted octahedral or near TP geometries. TP geometries yield weaker fields than octahedral complexes due to poorer overlap. The UV-vis spectra for all iron complexes possess CT bands, this behaviour is typically seen in Fe(II) bipy complexes with octahedral coordination.

^1H NMR studies of the zinc complexes, $[ZnL^{10}](ClO_4)_2$ and $[ZnL^{11}](ClO_4)_2$ suggests a 1:1 ligand to metal coordination whereby, the zinc coordinates to all nitrogen donors. Further NMR experiments are required to support the oxidation states of the Fe(II) / Fe(III) complexes.

We can also conclude that these complexes prefer to be in the +II oxidation state as all positive charges were balanced with perchlorate counter-ions. The cyclic

voltammograms obtained show typical ligand cantered reductions (bipy→bipy$^-$) between -1.06 V to –1.76 V vs Fc/Fc^+. Other reductions are seen in the copper complexes with L^9, L^{11} and L^{12} and are assigned to the Cu^{II}/Cu^I couple that typically occur between –0.35 V and –0.49 V vs Fc/Fc^+. The only oxidations that are seen are for the Fe complexes (Fe^{II}/Fe^{III} couple) with L^{10} (+0.850 V), L^{11} (+0.663 V) and L^{12} (+0.695 V). From these values we can conclude either that $[FeL^{10}]^{2+}$ is more stable than the other two complexes (harder to oxidise) however, $[FeL^{12}]^{2+}$ is only slightly more stable than $[FeL^{11}]^{2+}$.

It may prove interesting to also prepare lanthanide or ruthenium complexes with the above ligands, thus further investigations may involve the following studies; luminescence spectroscopy for future tagging devices and relaxtivity measurements of the gadolinium complexes for possible uses as MRI contrast agents.

5.5 Experimental

5.5.1 Preparation of transition metal complexes

N.B. The instrumentation used for the characterisation and the Experimental conditions for the preparation of the metal complexes is the same as for Chapter 3. Single-crystals were obtained for some of the complexes; the yields were between 46 – 58%.

N.B. M = Cu, Ni, Zn, Fe.

5.5.2 *Spectroscopic data for* $[M(L^9)]\,[ClO_4]_2$

$[Cu^{II}(L^9)]\,[ClO_4]_2$

Blue crystals collected, 47%. IR (KBr disc, cm^{-1}), ν = 1689s, 1606s, 1576w, 1492m, 1449m, 1341m, 1244m, 1090s, 956m, 846w; Accurate ESMS (m/z): = 401.0458

$[Cu(L^9)+H]^+$; UV-vis (CH_3CN): λmax (nm), ε (M^{-1} cm^{-1}) 286 (8549), 316(6220), 612 (48). (Found: C, 41.59; H, 2.15; N, 8.86%. $C_{21}H_{14}Cl_2CuN_4O_9$ requires C, 41.98; H, 2.35; N, 9.33);

$[Ni^{II}(L^9)(H_2O)_2]$ $[ClO_4]_2$

Purple / grey crystals were obtained (53%). IR (KBr disc, cm^{-1}), ν = 3377sb, 1678s, 1636w, 1604s, 1595s, 1488m, 1448s, 1335s, 1241s, 1135s, 1025m, 1089s, 954s, 845w; Accurate ESMS (m/z): = 495.0004 $[Ni(L^9)+ClO_4]^+$; UV-vis (CH_3CN): λmax (nm), ε (M^{-1} cm^{-1}): 358 (27915), 561 (9), 788 (7). (Found: C, 42.68; H, 2.21; N, 9.19%. $C_{21}H_{14}Cl_2NiN_4O_9.2H_2O$ requires: C, 42.32; H, 2.37; N, 9.40%);

$[Zn^{II}(L^9+OCH_3)]_2$ $[ClO_4]_2$

White clear crystal collected (55%). ^1H NMR (400MHz d_6-DMSO): 3.24 (s, 3H, $-OCH_3$), 7.12 (dd, 2H, J = 7.1, 5.0 Hz, $H^{5''}$), 7.45 (d, 2H, J = 7.6 Hz, $H^{3'}$), 7.66 (t, 2H, J = 7.5, 5.2 Hz, $H^{4''}$), 7.96 (t, 2H, J = 7.7 Hz, $H^{5'}$), 8.51 (m, 4H, $H^{4'}$, $H^{3''}$), 8.55 (d, 2H, J = 7.3 Hz, $H^{6''}$); IR (KBr disc, cm^{-1}), ν = 1590s, 1447s, 1402w, 1300w, 1095s, 1015w, 771m; MS (m/z): 968.1741 $[(ZnL^9)_2+ClO_4]^+$. (Found: C, 48.08; H, 3.05; N, 9.98%. $C_{44}H_{34}Cl_2Zn_2N_8O_{12}$ requires C, 49.46; H, 3.21; N, 10.49%).

$[Fe^{II}(L^9+OCH_3)]_2$ $[ClO_4]_2$

Bright red crystals were formed (49%). IR (KBr disc, cm^{-1}), ν = 1596s, 1450m, 1410w, 1306w, 1097s, 1019w, 778m; Accurate ESMS (m/z): 949.0878 $[(FeL^9)_2+ClO_4]^+$; UV-vis

(CH_3CN): λmax (nm), ε (M^{-1} cm^{-1}) 236 (14878), 288 (14173), 532 (1265). (Found: C, 49.98; H, 3.20; N, 10.29%. $C_{44}H_{34}Cl_2Fe_2N_8O_{12}$ requires C, 50.36; H, 3.27; N, 10.68%).

5.5.3 *Spectroscopic data for* $[M(L^{10})]$ $[ClO_4]_2$

$[Cu^{II}(L^{10})(H_2O)][ClO_4]_2.H_2O$

Blue crystals were collected (47%). IR (KBr disc, cm^{-1}), ν = 3447mb, 1589s, 1491w, 1452m, 1306w, 1256w, 1087s, 774m; ESMS (m/z): = 502.1 $[Cu(L^{10})+ClO_4]^+$; UV-vis (CH_3CN): λmax (nm), ε (M^{-1} cm^{-1}) 256 (12562), 303 (9156), 685 (93), 919 (73). (Found: C, 41.48; H, 2.31; N, 9.11%. $C_{21}H_{16}Cl_2CuN_4O_9$ requires C, 41.84; H, 2.68; N, 9.29%).

$[Ni^{II}(L^{10})][ClO_4]_2$

Purple precipitate was obtained (53%). IR (KBr disc, cm^{-1}), ν = 3394mb, 1624s, 1598m, 1567w, 1450s, 1307w, 1090s, 941w, 768m; ESMS (m/z): = 497.2 $[Ni(L^{10})+ClO_4]^+$; UV-vis (CH_3CN): λmax (nm), ε (M^{-1} cm^{-1}): 254 (10356), 309 (8412), 504 (9), 807 (8).

$[Zn^{II}(L^{10})][ClO_4]_2$

White precipitate collected (65%). ^1H NMR (400MHz d_6-DMSO): 7.19 (dd, 1H, J = 6.9, 5.4 Hz, $H^{5''}$), 7.47 (t, 2H, J = 6.9 Hz, H^5), 7.51 (d, 1H, J = 7.1 Hz, $H^{3'}$), 7.69 (t, 1H, J = 5.4 Hz $H^{4''}$), 7.78 (d, 2H, J = 7.0 Hz, H^3), 7.99 (dd, 1H, J = 7.1, 5.0 Hz, $H^{5'}$), 8.11 (dd, 2H, J = 7.2, 6.9 Hz, H^4), 8.55 (m, 2H, $H^{4'}$, $H^{3''}$) 8.67 (d, 1H, J = 7.0 Hz, $H^{6''}$), 8.74 (d, 2H, J = 7.0Hz, H^6); IR (KBr disc, cm^{-1}), ν = 3399mb, 1610s, 1447s, 1402w, 1300w, 1087s, 1015w, 771m; MS (m/z): 335 $[Zn(L^{10})+H]^+$

$[Fe^{II}(L^{10})][ClO_4]_2$

A bright orange / red precipitate was formed (59%). IR (KBr disc, cm^{-1}), ν = 3412mb, 1604m, 1522w, 1451m, 1305w, 1257w, 1088s, 879w, 745m; ESMS (m/z): 497.2 $[Fe(L^{10})+ClO_4]^+$; UV-vis (CH_3CN): λmax (nm), ε (M^{-1} cm^{-1}) 253 (12463), 303 (8262), 341 (3088), 421 (860), 569 (60).

5.5.4 *Spectroscopic data for* $[M(L^{11})]$ $[ClO_4]_2$

$[Cu^{II}(L^{11})]$ $[ClO_4]_2$

Blue precipitate collected, 47%. IR (KBr disc, cm^{-1}), ν = 3413mb, 1594m, 1489w, 1452m, 1257w, 1085s, 781m; ESMS (m/z): = 580.1 $[Cu(L^{11})+ClO_4]^+$; UV-vis (DMF): λmax (nm), ε (M^{-1} cm^{-1}) 257 (12486), 297 (9087), 665 (66).

$[Ni^{II}(L^{11})][ClO_4]_2$

Purple precipitate was formed and collected (53%). IR (KBr disc, cm^{-1}), ν = 3394mb, 1678w, 1601s, 1450s, 1336w, 1243w, 1083s, 762m; ESMS (m/z): = 575.2 $[Ni(L^{11})+ClO_4]^+$; UV-vis (CH_3CN): λmax (nm), ε (M^{-1} cm^{-1}): 260 (15647), 297 (13200), 515 (16), 824 (15).

$[Zn^{II}(L^{11})][ClO_4]_2$

White precipitate collected (67%). ^1H NMR (400MHz d_6-DMSO): 7.19 (dd, 2H, *J* = 6.9, 5.4 Hz, H5''), 7.45 (t, 1H, *J* = 6.9 Hz, H^5), 7.53 (d, 2H, *J* = 7.1 Hz, $H^{3'}$), 7.70 (t, 2H, *J* = 5.4 Hz, $H^{4''}$), 7.79 (d, 1H, *J* = 7.0 Hz, H^3), 7.99 (dd, 2H, *J* = 7.1, 5.0 Hz, $H^{5'}$), 8.08 (dd, 1H, *J* = 7.2, 6.9 Hz, H^4), 8.56 (m, 4H, $H^{4'}$, $H^{3''}$) 8.65 (d, 2H, *J* = 7.0 Hz, $H^{6''}$), 8.72 (d, 1H,

J = 7.0Hz, H^6); IR (KBr disc, cm^{-1}), ν = 3395mb, 1607s, 1450m, 1338w, 1241w, 1087s, 760m; ESMS (m/z): 581 $[Zn(L^{11})+ClO_4]^+$

$[Fe^{II}(L^{11})][ClO_4]_2$

Bright orange / red precipitate was obtained (49%). IR (KBr disc, cm^{-1}), ν = 3447mb, 1603m, 1450m, 1338w, 1242w, 1090s, 774m; ESMS (m/z): 572 $[Fe(L^{11})+ClO_4]^+$; UV-vis (CH_3CN): λmax (nm), ε (M^{-1} cm^{-1}): 505 (1125).

5.5.5 *Spectroscopic data for* $[M(L^{12})][ClO_4]_2$

$[Cu^{II}(L^{12})][ClO_4]_2$

Blue precipitate collected (70%). IR (KBr disc, cm^{-1}), ν = 3423mb, 1605s, 1567m, 1492w, 1457m, 1301w, 1259m, 1090s, 1015w, 829w, 774s; ESMS (m/z): = 558 $[Cu(L^{12})+H]^+$; UV-vis (CH_3CN): λmax (nm), ε (M^{-1} cm^{-1}) 285 (7986), 333(6343), 622 (37).

$[Ni^{II}(L^{12})]$ $[ClO_4]_2$

Pink crystals obtained (55%). IR (KBr disc, cm^{-1}), ν = 3406mb, 1600s, 1560m, 1482w, 1465s, 1320w, 1090s, 906w, 773s; Accurate ESMS (m/z): = 651.0688 $[Ni(L^{12})+ClO_4]^+$; UV-vis (CH_3CN): λmax (nm), ε (M^{-1} cm^{-1}): 266 (21134), 290 (22402), 531 (20), 838 (20). (Found: C, 48.96; H, 2.53; N, 10.83%. $C_{31}H_{22}Cl_2NiN_6O_9$ requires C, 49.50; H, 2.95; N, 11.17%).

$[Zn^{II}(L^{12})]$ $[ClO_4]_2$

Clear white crystals collected (46%). ^1H NMR (400MHz d_6-DMSO) 7.17 (t, 3H, J = 7.5 Hz, $H^{5''}$), 7.55 (d, 3H, J = 7.8 Hz, $H^{3'}$), 7.72 (t, 3H, $H^{4''}$), 8.02 (t, 3H, J = 7.8 Hz, $H^{5'}$),

8.56-8.58 (m, 6H, $H^{4'}$, $H^{3''}$) 8.69 (d, 3H, J = 7.7 Hz, $H^{6''}$); IR (KBr disc, cm^{-1}), ν = 3398mb, 1595s, 1564m, 1488w, 1454s, 1303w, 1255m, 1091s, 1017w, 828w, 771s; Accurate ESMS (m/z): 658.6114 $[Zn(L^{12})+ClO_4]^+$. (Found: C, 48.90; H, 2.64; N, 10.67%. $C_{31}H_{22}Cl_2ZnN_6O_9$ requires C, 49.07; H, 2.92; N, 11.07%).

$[Fe^{II}(L^{12})]$ $[ClO_4]_2$

Dark red single crystals were isolated (49%). IR (KBr disc, cm^{-1}), ν = 3426mb, 1654s, 1522w, 1452m, 1305w, 1260m, 1089s, 879w, 795m; Accurate ESMS (m/z): 649.0684 $[Fe(L^{12})+ClO_4]^+$; UV-vis (CH_3CN): λmax (nm), ε (M^{-1} cm^{-1}) 290 (7234), 544 (497). (Found: C, 49.28; H, 2.46; N, 10.84%. $C_{31}H_{22}Cl_2FeN_6O_9$ requires C, 49.69; H, 2.96; N, 11.22%).

5.6 References

1. W.R. McWhinnie, J.D. Miller, *Adv. Inorg. Chem. Radiochem.,* 1969, **12**, 135.
2. L.F. Lindoy, S.E. Livingstone, *Coord. Chem. Rev.,* 1967, **2**, 173.
3. W.R. McWhinnie, *Coord. Chem. Rev.,* 1970, **5**, 293.
4. E. König, *Coord. Chem. Rev.,* 1968, **3**, 471.
5. J.H.Forsberg, *Coord. Chem. Rev.,* 1973, **10**, 195.
6. P. Gütlich, *Struc. Bonding (Berlin),* 1981, **44**, 83.
7. C. Creutz, M. Chou, T.L. Netzel, M. Okumura, N. Sutin, *J. Am. Chem. Soc.*, 1980, **102**, 1309.
8. W.H. Elfring, G.A. Crosby, *J. Am. Chem. Soc.*, 1981, **103**, 2683.
9. H. Smit, H. van der Goot, W.T. Nauta, P.J. Pijper, S. Balt, M.W.G. de Bolster, A.H. Stouthamer, H. Verheul, R.D. Vis, *Antimicrob. Agents Chemother.*, 1980, **18**, 249.
10. S.A. Bedell, A.E. Martell, *Inorg. Chem.*, 1983, **22**, 364.
11. J. Foley, S. Tyagi, B.J. Hathaway, *J. Chem. Soc. Dalton Trans.*, 1984, 1.
12. G.R. Newkome, V.K. Gupta, F.R. Fronczek, *Inorg. Chem.*, 1983, **22**, 171.
13. G.G. Mohamed, N.E.A. El-Gamel, *Spectrochemica Acta Part A,* 2005, **61**,1089.
14. E.V. Rybak-Akimova, A.Y. Nazarenko, L. Chen, P.W. Krieger, A.H. Herrera, V.V. Tarasov, P.D. Robinson, *Inorg. Chim. Acta,* 2001, **324**, 1.
15. For a review of the coordination chemistry of Cu(II) , see: B.J. Hathaway, G. Wilkinson, R.D. Gillard, J.A. McClevarty, "In Comprehensive Coordination Chemistry", Pergamon Press: Oxford, 1989, **5**, pp 533-750.
16. B.J.Hathaway, *Struct. Bond.,* 1973, **14**, 49.
17. D.E. Nickles, M.J. Powers, F.L. Urbach, *Inorg. Chem.*, 1983, **22**, 3210.

18. T. Pandiyan, M. Palaniandavar, M. Lakshminarayanan, H. Manohar, *J. Chem. Soc., Dalton Trans.,* 1992, 3377.

19. R.C. Holz, E.A. Evdokimov, F.T. Gobena, *Inorg. Chem.*, 1996, **35** (13), 3808

20. W.O.Gillum, R.A.D.Wentworth, R.F.Childers, *Inorg. Chem.*, 1970, **9**, 1829.

21. A. Ion, J-C. Moutet, E. Saint-Aman, G. Royal, S. Tingry, J. Pecaut, S. Menage, R. Ziessel, *Inorg. Chem.*, 2001, **40**, 3632.

22. P.Baret, D.Gaude, G.Gellon, J.P.Pierre, *New J. Chem.*, 1997, **21**, 1255.

23. Y. Bai, Y, Li, E. Wang, X. Wang, Y. Lu, L. Xu, *J. Mol. Struct.*, 2005, **752**, 54.

24. R.N. Patel, N. Singh, K.K. Shukla, J. Niclos-Gutierrez, A. Castineiras, V.G. Vaidyanathan, B.U. Nair, *Spectrochimica Acta Part A,* 2005, **62**, 261.

25. S. Midollini, A. Orlandini, A. Vacca, *Inorg. Chem. Commun.*, 2004, **7**, 1113.

26. R.N. Patel, N. Singh, K.K. Shukla, J. Niclos-Gutierrez, A. Castineiras, V.G. Vaidyanathan, B.U. Nair, *Spectrochimica Acta Part A,* 2005, **62**, 261.

27. S. Midollini, A. Orlandini, A. Vacca, *Inorg. Chem. Comm.*, 2004, **7**, 1113.

28. C. Ruiz-Pérez, P.A. Lorenzo Luis, F. Loret, M. Julve, *Inorg. Chim. Acta,* 2002, **336**, 131.

29. K.V. Langenberg, D.C.R. Hockless, B. Moubaraki, K.S. Murray, *Synth. Metals*, 2001, **122**, 573.

30. A.C. Deveson, S.L. Heath, C.L. Harding, A.K. Powell, *J. Chem. Soc., Dalton Trans.,* 1996, 3173.

31. C.G. Efthymiou, C.P. Raptopoulou, A. Terzis, R. Boca, M. Korabic, J. Mrozinski, S.P. Perlepes, E.G. Bakalbassis, *Eur. J. Inorg. Chem.,* 2006, 2236.

32. C.C. Evans, R. Masse, J-F. Nicoud, M. Bagieu-Beucher, *J. Mater. Chem.*, 2000, **10**, 1419.

33. C.J. Simmons, B.J. Hathaway, K. Amornjarusiri, B.D. Santarsiero, *J. Am. Chem. Soc.*, 1987, **109**, 1947.

34. E. Katsoulakou, N. Lalioti, C.P. Raptopoulou, A. Terzis, E. Manessi-Zoupa, S.P. Perlepes, *Inorg. Chem. Commun.,* 2002, **5,** 719.

35. M.E. Garcia Posse, M.A. Juri, P.J. Aymonino, O.E. Piro, H.A. Negri, E.E. Castellano, *Inorg. Chem.,* 1984, **23,** 948.

36. D.T. Swayer, *Inorg. Chim. Acta,* 1994, **226**, 99.

37. V. Lakshmanan, K.S. Nagaraja, M.R. Udupa, *Polyhedron,* 1993, **12**, 1487.

38. M.N. Collomb, A. Deronzier, K. Gorgy, J.C. Lepretre, *New J. Chem.,* 2000, **24**, 455.

39. A.B.P. Lever, *Inorganic Electronic Spectroscopy, Elsevier, Amsterdam*, p.1984

40. E. Larsen, G.N. La Mar, B.E. Wagner, J.E. Parks, R.H. Holm, *Inorg. Chem.,* 1972, **11**, 2652.

41. F. Huq, A.C. Shapski, *J. Chem. Soc.,* 1971, A, 1927.

42. S.P. Perlepes, J.C. Huffman, G. Christou, S. Paschalidou, *Polyhedron,* 1995, **14**, 1073.

43. S. Youngme, C. Chailuecha, G.A. van Albada, C. Pakawatchai, N. Chaichit, J. Reedijk, *Inorg. Chim. Acta.*, 2005, **358**, 1068.

44. P.J. van Koningsbruggen, J.G. Haasnoot, R.A.G. de Graaff, J. Reedijk, *Inorg. Chim. Acta.*, 1995, **234**, 87.

45. M.R. Churchill, A.H. Reis, *Inorg. Chem.*, 1973, **12**, 2280.